NASA CR-2002-211181

2002 RESEARCH REPORTS

NASA/ASEE SUMMER FACULTY FELLOWSHIP PROGRAM

JOHN F. KENNEDY SPACE CENTER
AND
UNIVERSITY OF CENTRAL FLORIDA

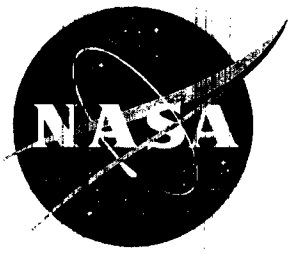

2002 RESEARCH REPORTS

NASA/ASEE FACULTY FELLOWSHIP PROGRAM

JOHN F. KENNEDY SPACE CENTER

UNIVERSITY OF CENTRAL FLORIDA

EDITORS:

Dr. Tim Kotnour, University Program Director
Department of Industrial Engineering & Management Systems
University of Central Florida

Ms. Cassandra Black, Program Management Specialist
Education Programs and University Research Division
John F. Kennedy Space Center

NASA Grant No. NAG10-315

Contractor Report No. CR-2002-211181

December 2002

PREFACE

This document is a collection of technical reports on research conducted by the participants in the 2002 NASA/ASEE Faculty Fellowship Program at the John F. Kennedy Space Center (KSC). This was the eighteenth year that a NASA/ASEE program has been conducted at KSC. The 2002 program was administered by the University of Central Florida (UCF) in cooperation with KSC. The program was operated under the auspices of the American Society for Engineering Education (ASEE) and the Education Division, NASA Headquarters, Washington, D.C. The KSC program was one of nine such Aeronautics and Space Research Programs funded by NASA Headquarters in 2002.

The basic common objectives of the NASA/ASEE Faculty Fellowship Program are:

a. To further the professional knowledge of qualified engineering and science faculty members;

b. To stimulate an exchange of ideas between teaching participants and employees of NASA;

c. To enrich and refresh the research and teaching activities of participants institutions; and,

d. To contribute to the research objectives of the NASA center.

The KSC Faculty Fellows spent ten weeks (May 20 through July 26, 2002) working with NASA scientists and engineers on research of mutual interest to the university faculty member and the NASA colleague. The editors of this document were responsible for selecting appropriately qualified faculty to address some of the many research areas of current interest to NASA/KSC. A separate document reports on the administrative aspects of the 2002 program. The NASA/ASEE program is intended to be a two-year program to allow in-depth research by the university faculty member. In many cases a faculty member has developed a close working relationship with a particular NASA group that had provided funding beyond the two-year limit.

TABLE OF CONTENTS

2002 NASA/ASEE SUMMER FACULTY FELLOWSHIP PROGRAM

JOHN F. KENNEDY SPACE CENTER
UNIVERSITY OF CENTRAL FLORIDA

DEVELOPMENT OF A HYDRAZINE/NITROGEN DIOXIDE FIBER OPTIC SENSOR

J. Clayton Baum
Associate Professor
Department of Chemistry
Florida Institute of Technology

KSC Colleague: Rebecca C. Young
Technology Implementation Branch
Spaceport Engineering & Technology

ABSTRACT

A simple, low cost fiber optic sensor is described for the simultaneous vapor phase detection of hydrazines and nitrogen dioxide. The device utilizes an acid-base indicator that undergoes color changes depending on which gas is present. The indicator is imbedded in a hydrogel matrix to aid long-term stability. The sensor responds in less than one minute to hydrazine (50 ppm) and nitrogen dioxide (400 ppm). Stability over times greater than several days remains to be tested. The sensor should be ideal for long-term detection of leaks in propulsion systems utilizing hypergolic propellants especially since explosion hazard due to spark is a concern.

DEVELOPMENT OF A HYDRAZINE/NITROGEN DIOXIDE FIBER OPTIC SENSOR

J. Clayton Baum

1. INTRODUCTION

Hydrazine and monomethylhydrazine (fuels) and dinitrogen tetroxide (oxidizer) are hypergolic propellants that are used in the Space Shuttle and other spacecraft guidance systems and several types of military missiles. These hypergols form hazardous gases that are toxic to humans at low concentrations and are flammable and explosive at higher concentrations. The recommended exposure limits are 0.01 ppm for hydrazine (HZ), 0.01 ppm for monomethylhydrazine (MMH) and 3 ppm for nitrogen dioxide (NO_2), the dissociation product of dinitrogen tetroxide.[1] The lower explosion limits in air at atmospheric pressure are 2.9% for HZ and 2.5% for MMH.[2,3] Therefore, leak detection of these chemicals is very important.

The ideal sensor for leak detection should meet the following requirements. To avoid the risk of explosion, electrical devices should not be used. The sensor should be capable of identifying which gas is leaking. Although high sensitivity is an attribute, for leaks in contained spaces where toxicity is not a concern (e.g., the interior of a missile), detection at higher concentrations is both necessary and sufficient. Especially for applications to missiles that are stored for periods of years, long-term stability of the sensor is critical. Finally, the ideal sensor should be simple, increasing its reliability, and low cost.

A variety of sensors are currently in use for the detection of hydrazines and nitrogen dioxide.[4] Electrochemical detection of hydrazines (ppb) and NO_2 (ppm) is a common method (e.g., Interscan Corporation). In addition to the electrical danger, however, a separate device is required for each gas, increasing the inherent cost and size. Simultaneous detection by solid-state devices such as gold-doped tungsten oxide and titanium dioxide has been suggested[5-8] but these detectors require elevated temperatures (100-800°C) and are therefore unsafe when combustible gases may be present. They also are unselective to a wide variety of gases. Other sensors for hydrazines are coulometric[9] (based on reaction with bromine) colorimetric (based on reaction of hydrazines with p-dimethylamino-benzaldehyde[10] or the reversible reaction with pH sensitive triphenylmethane dyes[11]) or fluorescent[12] (based on reaction with aromatic dicarbaldehdyes).

We describe the use of a fiber optic sensor, employing light rather than electricity to minimize explosion hazards. We take advantage of the acid-base properties of the hypergols using indicators that change color with pH to distinguish NO_2 from the hydrazines. The relevant chemical reactions are listed below. Dinitrogen tetroxide is in equilibrium with nitrogen dioxide:

$$N_2O_4 \rightleftharpoons 2\,NO_2 \qquad (1)$$

Nitrogen dioxide in turn reacts with water to form an acidic solution (nitric acid) and nitric oxide:

$$3\,NO_2 + H_2O \rightarrow 2\,H^+ + 2\,NO_3^- + NO \quad \text{(acid)} \qquad (2)$$

On the other hand, hydrazine forms a basic solution with water:

$$N_2H_4 + H_2O \rightarrow N_2H_5^+ + OH^- \quad \text{(base)} \qquad (3)$$

Incorporating the indicator in a hydrophilic polymer matrix (hydrogel) should inhibit evaporation of water and give stability to the sensor over a long period of time. Although commercial fiber optic pH sensors are available (Ocean Optics), these probes are expensive, involving a spectrophotometer and computer, and are designed for solution rather than gas phase measurements.

2. EXPERIMENTAL

A. Description of the First-Generation Prototype Sensor

This sensor was designed for measurements on solutions that had been exposed to gases but not as a direct gas probe. A jar (2.75 in diam, 3.5 in tall) with a flat mirror (30 mm diam) glued to the inside bottom contained the indicator (Figure 1). The optical sensor consisted of two 1 mm jacketed plastic fiber

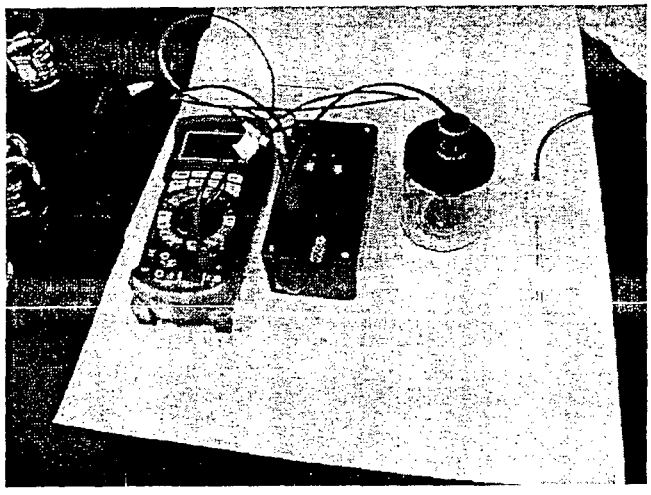

Figure 1. Sensor system (left to right: DMM, electronics box, first and second-generation sensors)

optic cables (Digi-Key A1700-5-ND) that passed through the top of the jar and were enclosed by heat shrink tubing with a 2 mm diameter wooden rod for rigidity. The sensor tip was positioned about 20 mm above the mirror. Light from a red LED (Industrial Fiber Optics IF-E97, peak wavelength 660 nm) was carried by one of the optical fibers. The reflected light was detected through the second fiber by a photodiode (Industrial Fiber Optics IF-D91, maximum photosensitivity 850 nm). The LED and photodiode were each contained in PVC housing with a cinch nut to hold the fiber optic cable in place. Schematics of the two electrical circuits are shown in Figure 2. The LED required a 360-ohm resistor with a 9-volt battery. The photodiode required a 1-mega ohm resistor between the output leads to the voltage meter along with a 9-volt battery. All the electronics were contained in a plastic box that was connected at some distance to the sensor solely by the fiber optic cables. The photodiode output was read with a Wavetek Model 235 digital multimeter (DMM).

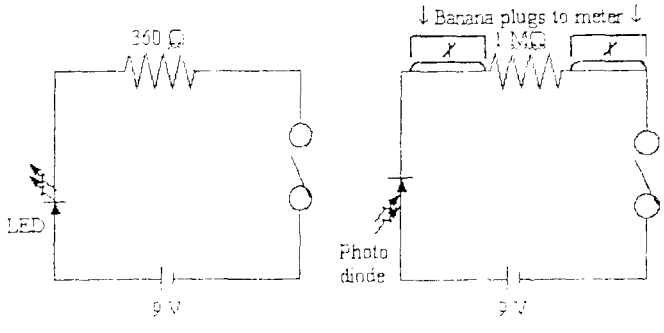

Figure 2. Circuit diagrams for LED and photodiode

B. Description of the Second-Generation Prototype Sensor

A fiber optic probe was constructed as shown in Figures 1 and 3. The reflecting surface in the Teflon cap was the backside of an aluminized 12.5 mm diam mirror, 2 mm thick (Edmund Industrial Optics NT32-942). The glass protected the aluminized surface and was flat (4-6 wave) so distortion of the beam was avoided. Two to three drops of the indicator/hydrogel mixture were placed on the mirror and allowed to flow evenly over the surface. The hydrogel sealed the edges of the mirror and provided additional protection of the aluminum surface from the corrosive gases. The same LED, photodiode, and associated electronics described above were connected to the probe by its fiber optic cables.

Coarse adjustment of the fiber position was made using the compression fitting at the top of the sensor with the cap screwed in about half way. The fiber distance from the mirror was optimized after each new sample was introduced by screwing the cap in or out to give the maximum signal. The mirror could be removed by tapping the cap on the bench or by inserting a small flat spatula along the edge of the mirror

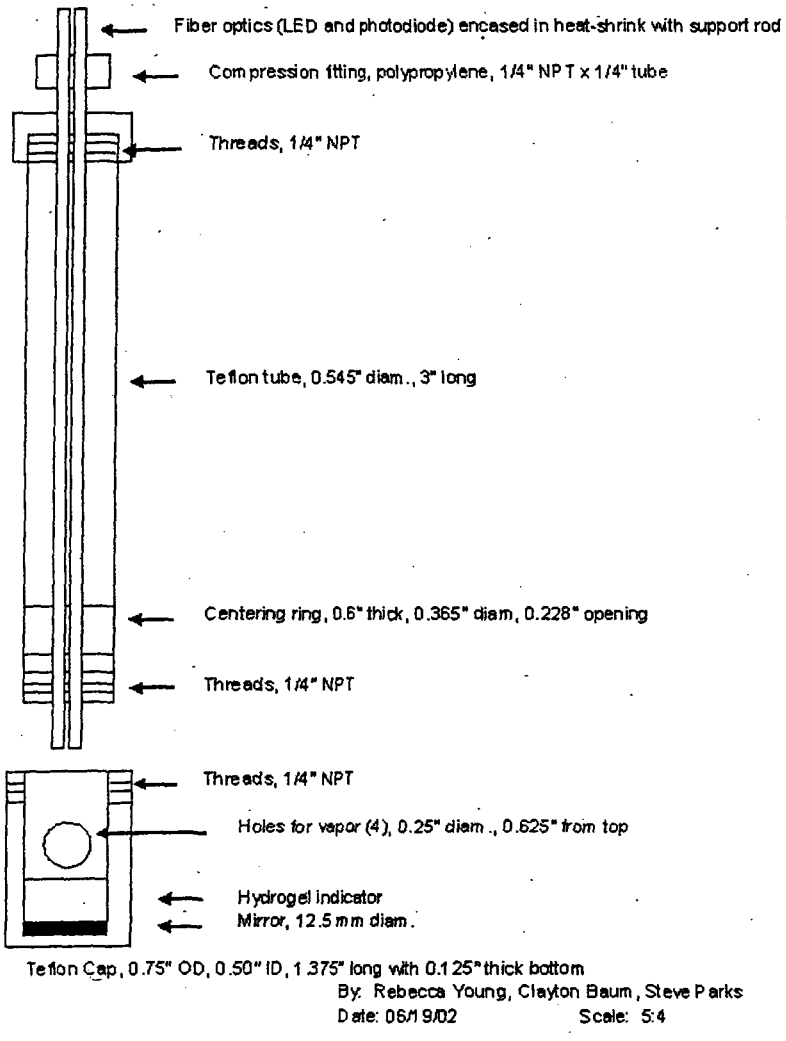

Figure 3. Fiber optic probe

C. Preparation of the Acid-Base Indicators

Preparation of the indicators (Figure 4) followed the instructions in the Handbook of Chemistry and Physics[13]. Specifically, 0.1 g Mallinckrodt indicator grade thymol blue (TB) was dissolved in 21.5 mL 0.01 M NaOH plus 228.5 mL water; 0.1 g Kodak reagent grade bromophenol blue (BP), sodium salt, was dissolved in 15 mL 0.01M NaOH plus 235 mL water; 0.1 g Aldrich A.C.S. reagent grade bromocresol green (BG), water soluble, was dissolved in 14 mL 0.01 M NaOH plus 236 mL water; 0.1 g Baker Analyzed Reagent bromothymol blue (BT), sodium salt, was dissolved in 16 mL 0.01 M NaOH plus 234 mL water. Universal Indicator Solution (UI) was purchased from Fisher Scientific and contains the following dyes: phenolphthalein, thymol blue, methyl red and bromothymol blue. Concentrations reported later are percent by volume of these standard solutions added to water or hydrogel.

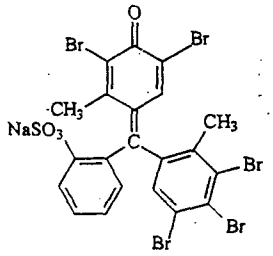

Bromocresol Green (BG)

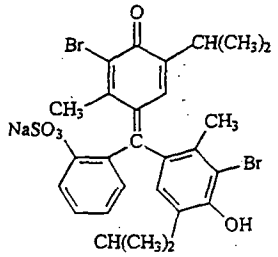

Bromothymol Blue (BT)

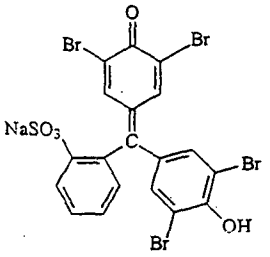

Bromophenol Blue (BP)

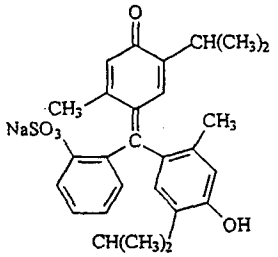

Thymol Blue (TB)

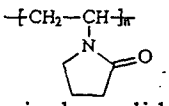

Polyvinylpyrrolidone (PVP)

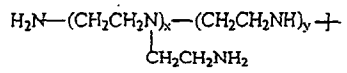

Polyethyleneimine (PEI)

Figure 4. Molecular structures of indicators and hydrogel components

D. Preparation of the Hydrogel Matrix

The hydrogel chosen because of its ease of preparation was Aquatrix II marketed by Hydromer, Inc. This hydrogel is a mixture of two polymers (Figure 4). Part A (Product Code 1CQA01) is polyvinylpyrrolidone (PVP) and Part B, High Tack (Product Code 1CQA07) is polyethyleneimine (PEI). Part B includes glycine as an additive to help retain water. The two components can be mixed in a variety of ratios. Ratios of Part A/Part B ranging from 4/1 to 1/3 were tested and the 1/1 ratio provided the best penetration of the hydrazines and NO_2.

The PEI has a pH of 9.2. Before mixing with Part A, Part B was neutralized by adding 1 drop of 1.76 M

sulfuric acid to approximately 4 mL of PEI. At a pH of 7, Part B is clear; excess or deficient acid results in a cloudy liquid. The pH was confirmed with Hydrion Paper, Micro Essential Laboratory (range of 1 to 11). The neutralized hydrogel initially was less viscous than the hydrogel without neutralization but thickened over time. The indicator solution generally was mixed with Part A before forming the hydrogel. Similar results were obtained, however, by adding the indicator to the hydrogel mixture. Aquatrix II sticks to most surfaces including glass and cannot be removed without distorting the gel; it does not stick to Teflon. After testing, the hydrogel was removed by flushing the cap with deionized water. If the hydrogel hardened, removal required soaking the cap in water for about 1 hour.

E. Generation of the Gases

Anhydrous HZ, MMH and NO_2 vapors were produced using Span Pac 361 Precision Standard Generators (Kin-Tek Laboratories, Inc.) that incorporate Teflon permeation tubes for the hydrazines and heated steel cylinders containing liquid N_2O_4 for the NO_2. Dry air was used as the carrier gas at a flow rate of 2 L/min. The calibrated concentrations were 52 ppm for HZ, 17 ppm for MMH and 56 ppm for NO_2. An Air Liquide cylinder of 4000 ppm NO_2 in N_2 was used for most of the NO_2 experiments. The flow rate was varied and the mixture could be diluted further with dry N_2. The CO_2 was standard grade.

3. RESULTS AND DISCUSSION

As the color of the indicator changes, the amount of red light transmitted by the indicator changes and the detector signal should change. If the indicator is red (absorption in the blue region) then more red light is reflected off the mirror and the detector voltage signal should be high. If the indicator is blue (absorption in the red region) less red light is reflected so the signal should be low.

A. First generation sensor

1. Opaque materials

Initial studies showed that the sensor responds to differences in the colors of opaque materials such as colored tape (yellow, 80 mV; red, 76 mV; green, 15 mV) and pH paper (air, orange, 74 mV; hydrazine, green, 40 mV; sulfuric acid, red, 73 mV). Note that yellow absorbs less of the LED light than red and that there is very little distinction between red and orange. Thus, the indicator in the pH paper would not be useful in distinguishing NO_2 from the CO_2 in air using the red LED.

2. Solutions

Samples in vials or beakers were exposed by placing them in a polypropylene container and directing the gas at the sample through tubing in the top of the container. There was good reproducibility (< 10% variation) when solutions filled the sensor jar to a level above the mirror. However, when solutions or hydrogels were kept in vials placed on the mirror the variation was sometimes greater than 100% depending on the position of vial. The reason is that the bottom of the container was not uniform, affecting the transmission of the light. Typically, a minimum of six trials was performed when using the vials, changing the position for each trial. Significant results were obtained as reported below.

An initial selection of indicators was based on the change in their wavelength of maximum absorption with pH[14]. Although the pH depends in part on the concentration of the dissolved gas, the approximate pH values are hydrazine 11, carbon dioxide 5, and nitric acid < 2. The indicator should absorb strongly at the wavelength of the LED for one gas (e.g., hydrazines) but not the other (e.g., nitrogen dioxide) and there should not be interference by other gases, specifically carbon dioxide. TB shifts from 596 nm to 430 nm as the pH goes from 9.6 to 8.0 and from 430 nm to 544 nm as the pH goes from 2.8 to 1.2. It gives a very rapid response (< 1 min) to both HZ and NO_2. However, TB is sensitive to CO_2, changing

from green to red/orange overnight. Thus, there is not much further change when TB is exposed to NO_2; in fact, there is a decrease in signal so it is hard to distinguish from exposure to HZ. Likewise, UI is affected by CO_2 so there is not much change (yellow to red) upon exposure to NO_2. BP shifts from 592 nm to 436 nm as the pH goes from 4.6 to 3.0, but its response to NO_2 is relatively slow and there is no response to HZ. BT shifts from 617 nm to 433 nm as the pH goes from 7.6 to 6.2. BT is already dark green at neutral pH so there is not much change with HZ, although it is rapid. However, BT is the indicator of choice to distinguish HZ if CO_2 is a problem because it is yellow below a pH of 6. BG shifts from 617 nm to 444 nm as the pH goes from 5.6 to 4.0. It shows rapid response and large color change (blue to yellow) when exposed to NO_2. A 10%TB/BG (3/1) solution was the best combination of indicators with the best indicator ratio and concentration for observing a relatively large (7 mV) change for both acid and base. It responds to HZ and MMH (1-2 mV/min) and NO_2 (13 mV/min at 4000 ppm, 2 mV/min at 400 ppm, 0.1 mV/min at 56 ppm). A summary of the indicator results is given in Table 1.

Indicator	HZ	NO_2	Disadvantage
Thymol blue	rapid	rapid	Sensitive to CO_2; no response to HZ in hydrogel
Bromophenol blue	none	slow	
Bromothymol blue	rapid	rapid	Sensitive to CO_2; small color change with HZ
Bromocresol green	none	rapid	

Table 1. Indicator response

3. Hydrogels

Although 10% TB in solution responds quickly to HZ, 12% TB in hydrogel (Part A/Part B, 1/1) showed no visual change after 10 min exposure to HZ. In contrast, 12% BT in hydrogel (1/1) turned blue to a depth of 1 mm below the surface after 1 min of HZ while the rest of the hydrogel mixture remained green. Thus BT is much better than TB in HZ response even though in solution TB gives a more dramatic color change. In hydrogel (4/1), 6% BT produced only a 0.5 mm depth of blue after 1 min exposure to HZ which darkened over 10 min of exposure. In hydrogel (1/3), 13% BT produced only a 0.5-1 mm depth of blue after exposure to HZ. Thus, a 1/1 ratio for hydrogel seems to be best for penetration of the gas although it is only to a depth of 1 mm. This implies that a thin film no more than 1 mm should be used. Several hours after exposure, the blue color diffused throughout the sample to give a darker green. Exposure of 16% BT in hydrogel (1/1) to NO_2 (4000 ppm) produced a 0.5 mm depth of pale green-yellow in 1 min extending to a 2 mm depth of yellow in 10 min of exposure. The sensor response was 22 ± 1 mV for the indicator alone, 18 ± 6 mV after 10 min exposure to HZ, and 48 ± 17 mV after 10 min exposure to NO_2. A 16% mixture of BT/BG (1/1) in hydrogel (1/1) also showed a change from blue to darker blue to a depth of 1 mm) in 1 min exposure to HZ and blue to pale blue-green to yellow (5 min) to a depth of 1 mm after 1 min exposure to NO_2 (4000 ppm).

B. Second generation sensor

1. Solutions

The development of the sensor probe allowed much more accurate measurements in a real time mode. The probe was placed through a hole cut in the top of a polypropylene container. The top also contained a tube through which the gas flowed into the container. After optimizing the distance between the optical fibers and the mirror, readings were taken with no gas flow to establish a baseline. BT alone (40%) with a solution depth about 2 mm gives very good response (Table 2). The readings and change in readings are higher than for the first generation sensor and the response time is faster. The sensor detects NO_2 at 10 ppm in less than 1 min and senses this gas even at 0.005 L/min (almost static conditions). It also

responds well to HZ. However, BT is sensitive to carbon dioxide.

Readings in mV					
Exposure	0 min	1 min	5 min	10 min	Average
No Gas	164	164	164		
Hydrazine, 52 ppm	164	164	155	125	4 mV/min
New Sample, No Gas	158	162	171	184	2 mV/min
NO_2, 4000 ppm, 0.005 L/min	186	188	217	288	10 mV/min
New sample, no gas	100	100	100		
NO_2, 40 ppm, 2.8 L/min	100	106	131	181	8 mV/min
New Sample, No Gas	120	120	120		
NO_2, 10 ppm, 2 L/min	120	129	149		5 mV/min

Table 2. Response of BT in Solution to HZ and NO_2

2. Hydrogels

In contrast to solution, BT in hydrogel senses NO_2 only at high concentration (4000 ppm but not 400 ppm) and high flow rate (> 0.1 L/min), but it is not as sensitive to CO_2. Blowing CO_2 on BT in solution turns the color to yellow in about 15 seconds; there is no visual effect on BT in hydrogel even after 30 min. Increasing the concentration of BT in hydrogel from 16% to 50% improves the response. The increased fluidity allows a thinner layer of indicator to be deposited on the mirror. No additional improvement occurs at still higher concentrations up to 84% BT. Solid BT dissolved in neutralized hydrogel (0.004g BT in 10 mL) giving a dark green color. However, the response of the sensor was not better than mixtures of the standard BT solution with hydrogel. The optimal sensor to date is a BT/BG (1/1) mixture, 50% in hydrogel, that is deposited in a very thin coat, less than 1 mm. The results are shown in Table 3. This sensor detects HZ at 52 ppm and NO_2 at 4000 ppm under near static conditions and 400 ppm at a flow rate close to that of HZ. The fact that the response increases as the flow rate increases suggests that there is a pressure buildup in the container housing the sensor that aids in diffusion of the gas into the hydrogel matrix. In solution, the response is fairly independent of the flow rate.

Readings in mV					
Exposure	0 min	1 min	5 min	10 min	Average
No Gas	359	358	352		
Hydrazine, 52 ppm	350	347	326	311	4 mV/min
New Sample, No Gas	376	378	381		
NO_2, 4000 ppm, 0.01 L/min	378	381	394		3 mV/min
NO_2, 4000 ppm, 0.1 L/min	364	369	380		3 mV/min
New Sample, No Gas	370	371	372		
NO_2, 400 ppm, 2.3 L/min	372	380	396		5 mV/min

Table 3. Response of BT/BG (1/1), 50% in Hydrogel to HZ and NO_2

CONCLUSIONS

We have developed a method for simultaneous detection of hydrazines and NO_2 in the vapor phase and have constructed a sensor prototype that gives promising results. The sensor is a simple fiber optic device composed of just a red LED light source, a photodiode detector, fiber optics and a mirror. There are no moving parts, increasing the long-term reliability. The cost, excluding labor, is under $100 so that these sensors can be expendable and used in multiple locations. There is no spark hazard and no electrical noise interference because of the fiber optics. Likewise, the sensor is light and compact, requires low power, and is amenable to remote control.

A range of acid-base indicators has been examined and 10% TB/BG (3/1) and 40% BT were found to provide the best response in solution, while 50% BT/BG (1/1) was best in hydrogel. In solution, the sensor detects HZ (52 ppm), MMH (17 ppm) and NO_2 (10) ppm in less than 1 min and senses NO_2 even at 0.005 L/min (almost static conditions). Diffusion of the gases through the hydrogel matrix is restricted to the top 1 mm reducing the response and leading to the use of films less than 1 mm. Nonetheless, with hydrogel the sensor still detects HZ (52 ppm) and NO_2 (400 ppm) at 2-3 L/min and NO_2 at 4000 ppm at 0.01 L/min. There is no interference from humidity.

Future development includes fine-tuning the indicator ratio and concentration. Other matrices may allow easier penetration of the gases and retain moisture better than the Aquatrix II. The major test is determining the stability of the sensor over time. The plastic fiber and optics must be replaced with silica for longer transmissions distances. An alarm will need to be incorporated set to detect a minimum voltage change per unit time in the positive (NO_2) or negative (hydrazines) direction rather than an absolute voltage. This would eliminate problems with voltage drift over time resulting from a variety of sources such as CO_2, or degradation of the LED, power source, indicator, hydrogel, and optics.

The short-term value to KSC is an increase in the ability to sense the hazardous gases associated with hypergolic propellants, reducing the response time for leak detection and identification and the cost of detection. The long-term value is increased safety at the spaceport and at other sites that make use of these propellants.

REFERENCES

[1] American Conference of Governmental Industrial Hygienists (ACGIH), "TLV's-Threshold Limit Values for Chemical Substances and Physical Agents in the Workroom Environment", American Conference of Governmental Industrial Hygienists (1991).

[2} Mallinckrodt Baker, Inc., Material Safety Data Sheet for Hydrazine (1999).

[3] Olin Corporation, Material Safety Data Sheet for Monomethylhydrazine (1991).

[4] Schmidt, E. C., *Hydrazine and Its Derivatives. Preparation, Properties, Applications*, Wiley (1984).

[5] Akiyama, M.; Tamaki, J.; Miura, N.; Yamazoe, N., "Tungsten Oxide-Based Semiconductor Sensor Highly Sensitive to NO_2", *Chem. Lett.* , 1611-1614 (1991).

[6] Maekawa, T.; Tamaki, J.; Miura, N.; Yamazoe, N., "Gold-Loaded Tungsten Oxide Sensor for Detection of Ammonia in Air", *Chem. Lett.*, 639-642 (1992).

[7] Moseley, P.T.; Williams, D.E., "Selective ammonia sensor", *Sens. Actuators B*, 1, 113-115 (1990).

[8] Moseley, P.T., "New trends and future prospects of thick- and thin-film gas sensors", *Sens. Actuators B*, 3, 167-174 (1991).

[9] Wyatt, J. R.; Rose-Pehrsson, S.L.; Cecil, T.L.; Crossman, K.P.; Mehta, N.K.; Young, R., "Coulometric Method for the Quantification of Low-Level Concentrations of Hydrazine and Monomethylhydrazine", *Am. Ind. Hyg. Assoc. J.*, 54, 285-292 (1983)

[10] Gojon, C.; Dureault, B., "Spectrophotometric Study of the Reaction between Hydrazine and p-dimethylaminobenzaldehyde", *J. Nucl. Sci. Tech.*, 33, 731-735 (1996).

[11] Carter, M. T.; Smith, J.R.; Mowry, D.R.; Patel, "Reversible evanescent wave sensors for hydrazine", J.G., *Proc. SPIE*, 3540, 123-133 (1998).

[12] Collins, G.E.; Rose-Pehrsson, S.L., "Fluorescent Detection of Hydrazine, Monomethylhydrazine, and 1,1-Dimethylhydrazine by Derivatization with Aromatic Dicarbaldehydes", *Analyst*, 119, 1907-1913 (1994).

[13] Lide, D.R., Editor, *Handbook of Chemistry and Physics*, 81st Ed., CRC Press, Boca Raton, FL, (2000). pp 8-16 to 8-18.

[14] Dean, J. A., *Lange's Handbook of Chemistry*, McGraw Hill, (1992). pp 8.115, 8.116.

2002 NASA/ASEE SUMMER FACULTY FELLOWSHIP PROGRAM

JOHN F. KENNEDY SPACE CENTER
UNIVERSITY OF CENTRAL FLORIDA

USEFUL LIFE PREDICTION FOR PAYLOAD CARRIER HARDWARE

David Ben-Arieh
Associate Professor
Department of Industrial & Manufacturing Systems Engineering
Kansas State University

ABSTRACT

The Space Shuttle has been identified for use through 2020. Payload carrier systems will be needed to support missions through the same time frame. To support the future decision making process with reliable systems, it is necessary to analyze design integrity, identify possible sources of undesirable risk and recognize required upgrades for carrier systems.

This project analyzed the information available regarding the carriers and developed the probability of becoming obsolete under different scenarios. In addition, this project resulted in a plan for an improved information system that will improve monitoring and control of the various carriers. The information collected throughout this project is presented in this report as process flow, historical records and statistical analysis.

USEFUL LIFE PREDICTION FOR PAYLOAD CARRIER HARDWARE

David Ben-Arieh

1. INTRODUCTION

The objectives of the project were defined before the project started in the following way:

> The Space Shuttle has been identified for use through 2020. Payload carrier systems will be needed to support missions through the same time frame. To support the future decision making process with reliable systems, it is necessary to analyze design integrity, identify possible sources of undesirable risk and recognize required upgrades for carrier systems.

Project Summary:

> The project resulted in a limited analysis of life expectancy of several carrier systems. Moreover, it established a basis for developing a centralized source of information related to the various payload carrier systems. This information system will be used to monitor and estimate the payload carrier systems ability to meet future mission requirements. While investigating the various carrier systems, the main processes that handle the carriers were analyzed, and a comprehensive historical record of the carriers were developed.

2. PROJECT DESCRIPTION

In order to perform the project, the following steps were identified:

Project Steps:

1. Identify the carrier system items at all locations (KSC, MSFC, GSFC, and JSC) and any commercial carriers (inventory).
2. Identify the various sources of information that describe the various carriers. In each such source the information contents stored has to be identified.
3. Identify the main processes that support the operation of the carriers. These processes include design, analytical integration, configuration management, etc.
4. Develop an integrated view of the information needs of the Payload Carriers Program (building on existing information). This step will lead to a design of a database/documentation system that will store all pertinent data. Based on the system's complexity, determine the level of detail necessary for a useful analysis.
5. For each carrier system, create a useful life profile that identifies expected service life. Historical data, by serial number, will include:
    a. Already assigned useful life
    b. Number of flights
    c. Any failures, damages, accidents
    d. Periods of storage and transportation

e. Test and checkout

f. Maintenance, scheduled or performed only prior to flight

g. Upgrades

Additional information items will be identified in step 3.

6. Using past mission manifests and any known future mission requirements, develop scenarios for more probable, probable, and least probable requirements though 2020.
7. Perform analysis for each system's profile and estimate each system's ability to meet mission requirements through 2020.

3. RESULTS

This section describes the main results of the project. The results are divided into three sections:

1. Analysis of carriers' flight history.
2. Analysis of the processes that handle the carriers.
3. Statistical analysis of probability to exceed the life span of the carriers.

3.1 Analysis of Carriers Flight History

This analysis was performed for the following main carrier types: MPESS, SLP (Space-Lab Pallet, LMC (Lightweight MPESS Carrier) and the Side-Wall carrier also termed Adapter Beam Assembly (handled by GSFC). The historical records of the SLP (also termed Pallet) carrier is presented in Table 1.

Table 1: Pallet Flight History

Table 1a: Flight # 1

Pallet			Flight 1		
Serial No.	Flight no.	Date	Orbiter	Payload	Time in space
F001/MD001	STS-9	28-Nov-83	Columbia	SL-1	11 days
F002/MD009	STS-35	02-Dec-90	Columbia	ASTRO-1(AFT)	8 days
F003/MD004	STS-51F	29-Jul-85	Challenger	SL-2(3)	9 days
F004/MD002	STS-51F	29-Jul-85	Challenger	SL-2(1)	9 days
F005/MD003	STS-51F	29-Jul-85	Challenger	SL-2(2)	9 days
F006/MD005	STS-41G	05-Oct-84	Challenger	OSTA-3	8 days
F007/MD006	STS-51A	Nov. 8, 1984	Discovery	SRM(WESTAR)	7 days 23 hours
F008/MD007	STS-51A	Nov. 8, 1984	Discovery	SRM(PALAPA)	7 days 23 hours
F009/MD010	STS-61	02-Dec-93	Endeavor	HST SM-01	11 days
F010/MD008	STS-35	02-Dec-90	Columbia	ASTRO-1(FWD)	8 days
E001					
E002	STS-2	12-Nov-81	Columbia	OSTA-1	2 days

E003	STS-2	12-Nov-81	Columbia	OSTA-1	2 days
E004					
E005					

Table 1b: Flight # 2

Pallet			Flight # 2		
Serial No.	Flight no.	Date	Orbiter	Payload	Time in space
F001/MD001	STS-?	Future mission		HST SM-03A*	
F002/MD009	STS-67	02-Mar-95	Endeavor	ASTRO-2 (AFT)	16 days
F003/MD004	STS-46	31-Jul-92	Atlantis	TSS-1	9 days
F004/MD002	STS-45	24-Mar-92	Atlantis	ATLAS-1(Fwd)	10 days
F005/MD003	STS-45	24-Mar-92	Atlantis	ATLAS-1(Aft)	10 days
F006/MD005	STS-59	09-Apr-94	Endeavor	SRL-1	11 days
F007/MD006	STS-64	09-Sep-94	Discovery	LITE-1	11 days
F008/MD007	STS-56	08-Apr-93	Discovery	ATLAS-2	11 days
F009/MD010	STS-82	11-Feb-97	Discovery	HST SM-02	10 days
	STS-67	02-Mar-95	Endeavor	ASTRO-2 (FWD)	16 days

Table 1c: Flight # 3

			Flight # 3		
	Flight no.	Date	Orbiter	Payload	Time in space
F002/MD009	STS-104	12-Jul-01	Atlantis	ISS-7A (airlock)	12 days, 18 hours
F003/MD004	STS-75	22-Feb-96	Columbia	TSS-1R	17 days
F004/MD002	STS-100	19-Apr-01	Endeavor	ISS-6A	11 days, 21 hours
F005/MD003	STS-92	11-Oct-00	Discovery	ISS-03-3A	12 days
F006/MD005	STS-68	30-Sep-94	Endeavor	SRL-2	11 days
F008/MD007	STS-66	03-Nov-94	Atlantis	ATLAS-3	11 days
F009/MD010	STS-*	Future mission		HST SM-03	
F010/MD008	STS-104	24-Jul-01	Atlantis	7A(FWD)	12 days, 18 hours

Table 1d: Flight # 4

			Flight # 4		
	Flight no.	Date	Orbiter	Payload	Time in space
F006/MD005	STS-99	11-Feb-00	Endeavor	SRTM	11 days

From Table 1 it is evident that only one pallet flew four missions. The life expectancy of the pallet carrier is fifty missions, thus, there are enough remaining flights within the ten available pallets.

The flight history of the MPESS Carrier is more succinctly represented by Table 2.

Table 2: Flight History of MPESS Fleet

Flight		MPESS F001	MPESS F002	MPESS F003	MPESS F004	MPESS F006
1	Payload	OSTA -2	LFC/ORS	SL-3	OAST-1	MSL-2
	Flight	STS-7	STS-41G	STS-51B	STS-41D	STS 61-C
	Orbiter	Challenger	Challenger	Challenger	Discovery	Columbia
	Date	18-Jun-83	5-Oct-84	29-Apr-85	20-Aug-84	12-Jan-86
	Days is Space	6 days	8 days	8 days	6 days	6 days
2	Payload		USMP-1 (Aft)	EOIM-III	EASE/ACCESS	USMP-1 (Fwd)
	Flight		STS-52	STS-46	STS-61B	STS-52
	Orbiter		Columbia	Atlantis	Atlantis	Columbia
	Date		22-Oct-92	31-Jul-92	26-Nov-85	22-Oct-92
	Days is Space		11 days	9 days	8 days	11 days
3	Payload		USMP-2 (Aft)	SRL-1	TSS-1	USMP-2 (Fwd)
	Flight		STS-62	STS-59	STS-46	STS-62
	Orbiter		Columbia	Endeavor	Atlantis	Columbia
	Date		4-Mar-94	09-Apr-94	31-Jul-92	04-Mar-94
	Days is Space		14 days	11 days	9 days	14 days
4	Payload		USMP-3 (Aft)	SRL-2	TSS-1R	USMP -3 (Fwd)
	Flight		STS-75	STS-68	STS-75	STS-75
	Orbiter		Columbia	Endeavor	Columbia	Columbia
	Date		22-Feb-96	30-Sep-94	22-Feb-96	22-Feb-96
	Days is Space		17 days	12 days	17 days	17 days
5	Payload		USMP-4 (Aft)		MFD	USMP-4 (Fwd)
	Flight		STS-87		STS-85	STS-87
	Orbiter		Columbia		Discovery	Columbia
	Date		19-Nov-97		07-Aug-97	19-Nov-97
	Days is Space		17 days		12 days	17 days

Flight		MPESS F001	MPESS F002	MPESS F003	MPESS F004	MPESS F006
6	**Payload**		MSP-1 (Aft)			MSP-1 (Fwd)
	Flight		?			?
	Orbiter		?			?
	Date		?			?
	Days is Space		?			?

The table shows that the MPESS carrier have flown up to six flights. Currently, there are 3 MPESS in existence with a life expectancy of 10 flights. Thus, the fleet of MPESS carriers has a higher chance of becoming obsolete within the planning horizon. This point is further discussed in section 3.3.

3.2 Processes Involved with Carrier Flights

In addition to the discovery of the historical data, the project analyzed several processes that deal with the carriers. The most relevant processes are the general preparation process shown in Figure 1, the Logistic process and Configuration Management process. The later two processes are not described in this report due to lack of space.

The main process of handling the KSC carriers is performed by at least three parties. The design and sustaining engineering is currently performed by a contract supervised by Marshall SFC. The payload ground operations is performed by a contract to Boeing at KSC, while the management of the carrier program is performed by the NASA program. This analysis does not cover the actual loading of the carrier with the payload and loading into the shuttle.

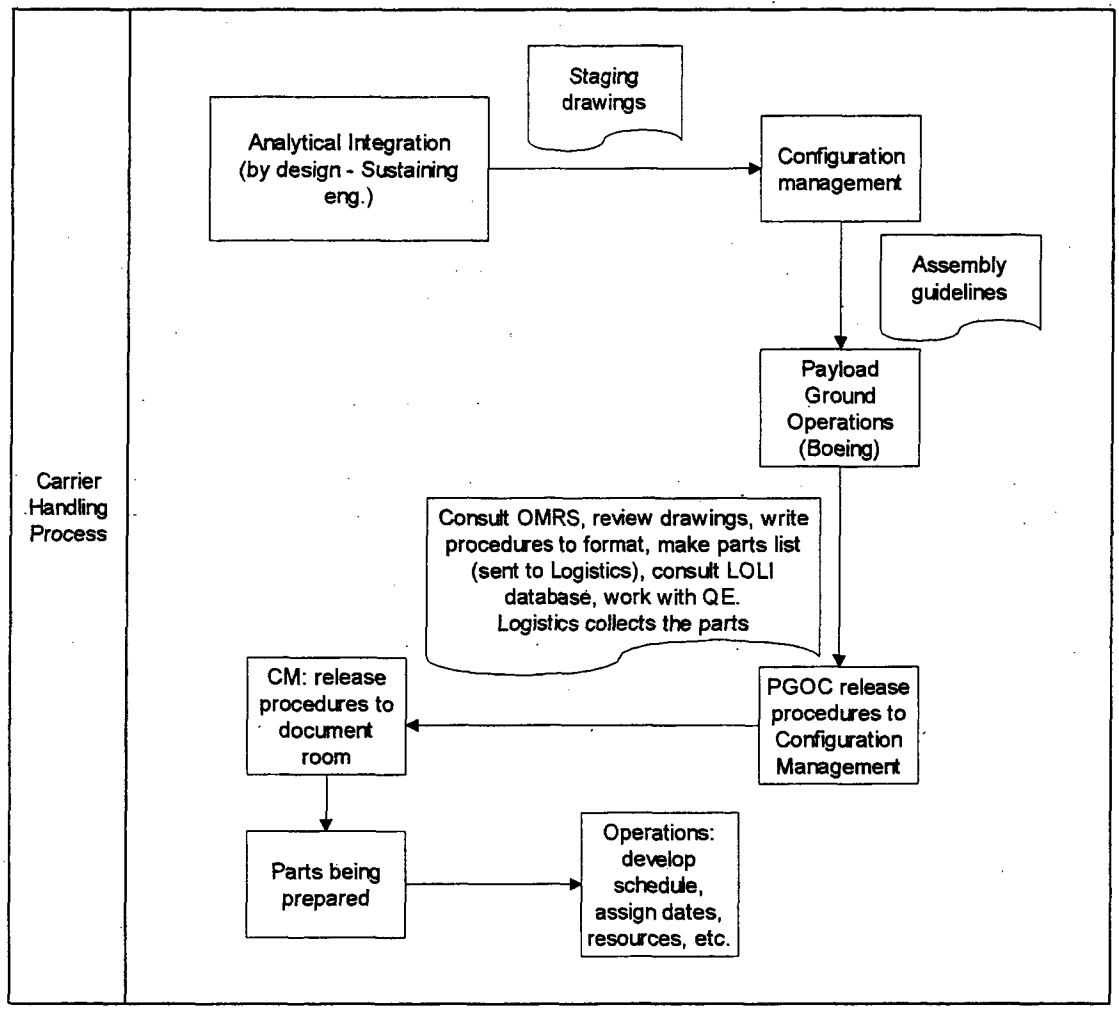

Figure 1: Basic Process of Preparing KSC Carriers

3.3 Statistical Analysis of Carriers Life Expectancy

The statistical analysis of the KSC carriers consists of two parts. The first part considers the "weakest link" within each carrier type. This is the specific carrier (serial number) with the most flights, thus having the shortest expected life span. The second type of analysis is fleet-wide considering al the flights remaining within the entire fleet of each specific carrier type.

The statistical analysis uses the Poisson distribution to model the probability of a given number of flights per year. The Poisson distribution was chosen for the following reasons:

1. It is a discrete distribution very suitable to model a discrete phenomenon such as number of flights per year.
2. The distribution has a moderate variability built-in (the variance is proportional to the mean). This property provides sufficient coverage and safety for the decision maker without exaggerating the range of the results.

The calculations used considered the complement to the cumulative probability expressed as:

$$P(x > K) = 1 - \sum_{k=0}^{K} \frac{e^{-\lambda} \cdot \lambda^{k}}{k!}$$

Where x is the assumed number of flights and K is the given life span of the carrier. Thus the expression above calculates the probability of the cumulative number of flights *(x)* to exceed the life span of the carrier *(K)*.

The results of the analysis of the first type are presented in figures 2, and 3. The "fleet-wide" analysis is presented in Figures 4, and 5.

3.3.1 "Weakest Line Analysis"

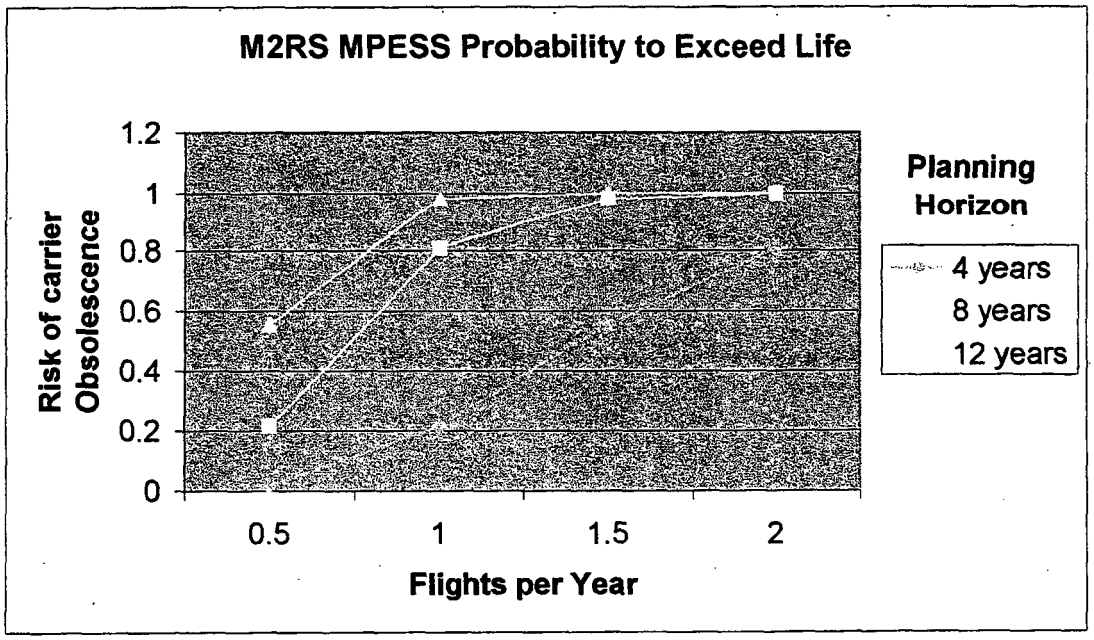

Figure 2: Probability of M2RS MPESS to Exceed Life Span

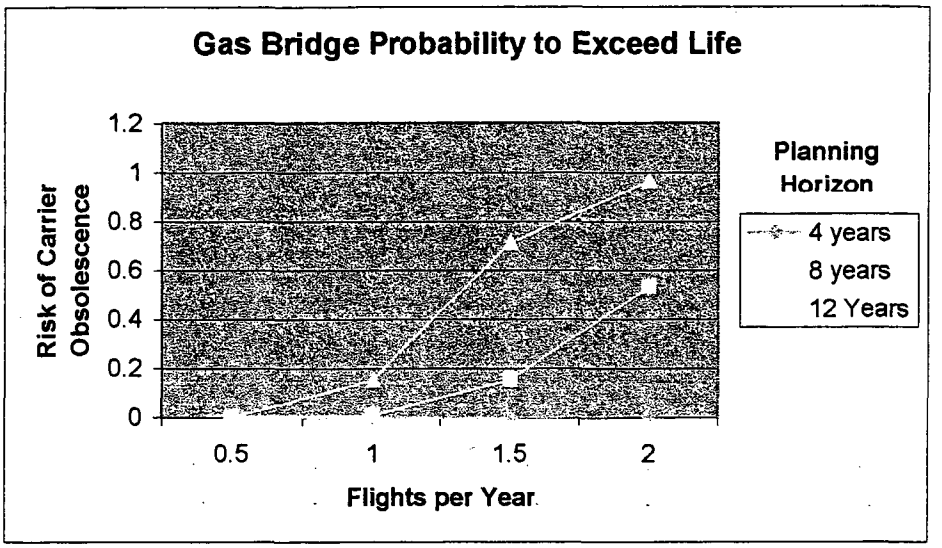

Figure 3: Probability of Gas Bridge to Exceed Life Span

3.3.2 Fleet-Wide Analysis

This analysis is based on the cumulative number of flights that the entire fleet of carriers still has. The figures below show the probability to exceed the life span of the entire fleet. Due to limited space only selected carrier fleets are presented.

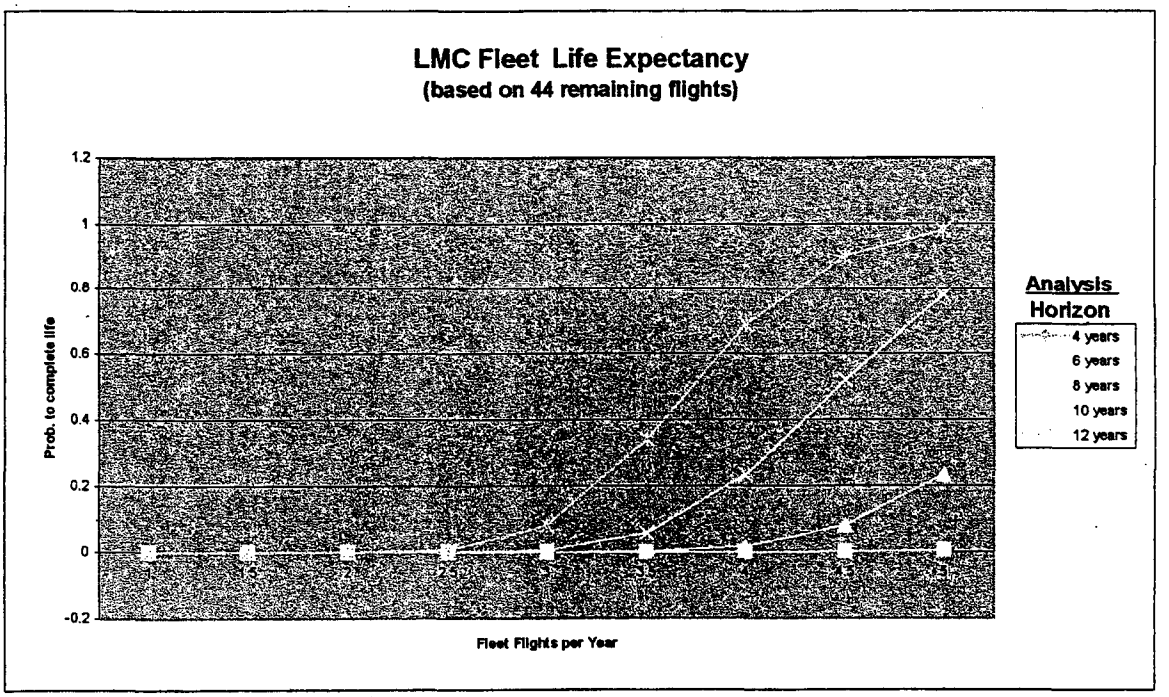

Figure 4: Life Expectancy of the LMC Fleet (three carriers)

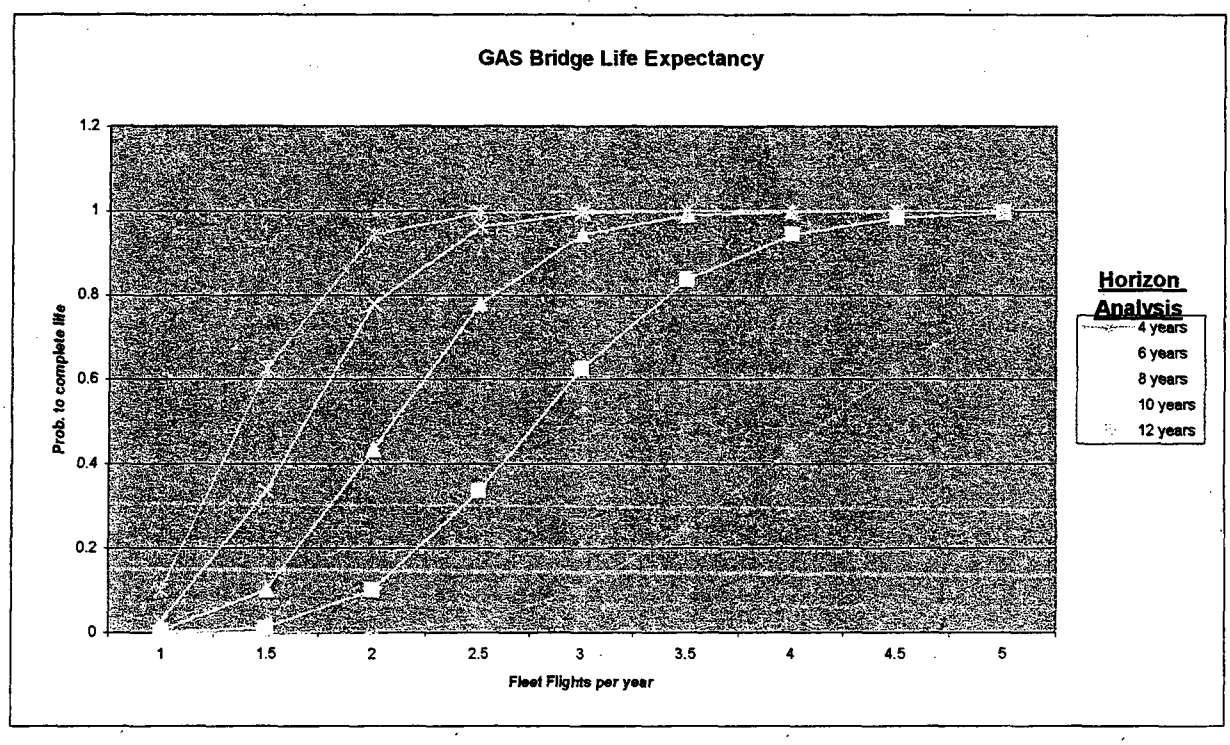

Figure 5: Life Expectancy of the Gas Bridge Fleet (one carrier)

4. SUMMARY

The management of the payload carriers is an intensive activity involving groups across the various NASA centers and dealing with a variety of contractors' organizations. The project identified the main carriers under the Payload Carriers Program responsibility. The only carriers missing so far are the HST (Hubble Space Telescope) and the Side-Wall carriers handled by JSC.

The project was able to achieve four main objectives. First, record the history of the main carriers. This history includes the flight history as well as major modifications performed on the carrier.
The second accomplishment of the project is the analysis of the main processes pertinent to the carriers.
The third benefit from the project is a statistical evaluation of the probability to exceed the life span of the various carriers, given the assumption that the Space Shuttle will be used until the year 2020.
The fourth accomplishment of the project is the development of a skeleton web-based information system that will allow better monitoring and management of the various carriers. This system was developed and demonstrated to the program management.

2002 NASA/ASEE SUMMER FACULTY FELLOWSHIP PROGRAM

JOHN F. KENNEDY SPACE CENTER
UNIVERSITY OF CENTRAL FLORIDA

INTEGRATED GLOBAL POSITIONING SYSTEMS (GPS) LABORATORY

Dr. Dewayne Randolph Brown
Assistant Professor
Electronics and Computer Technology (ECT) Department
North Carolina A & T State University
NASA/KSC Colleague: Dr. Jim Simpson

ABSTRACT

The purpose of this research is to develop a user-friendly Integrated GPS lab manual. This manual will help range engineers at NASA to integrate the use of GPS Simulators, GPS receivers, computers, MATLAB software, FUGAWI software and SATELLITE TOOL KIT software. The lab manual will be used in an effort to help NASA engineers predict GPS Coverage of planned operations and analyze GPS coverage of operation post mission.

The Integrated GPS Laboratory was used to do GPS Coverage for two extensive case studies. The first scenario was an airplane trajectory in which an aircraft flew from Cape Canaveral to Los Angeles, California. In the second scenario, a rocket trajectory was done whereas a rocket was launched from Cape Canaveral to one thousand kilo-meters due east in the Atlantic Ocean.

INTEGRATED GPS LABORATORY

Dewayne R. Brown

1. INTRODUCTION

In this research an integrated user-friendly GPS lab manual was produced. NASA engineers will use this lab manual in their efforts to estimate trajectories of future Shuttle Launches. The manual is an integration of the use of GPS Simulators, GPS receivers, computers, MATLAB software, FUGAWI software and SATELLITE TOOL KIT (STK) software.

MATLAB Version 6.5 is a high performance software tool for technical computing [1]. This software was used in the research to integrate and differentiate post Shuttle launch data. The data was from the STS103 Shuttle Launch in December 1999. The goal of this part of the research was to examine the accuracy of MATLAB's differentiation and integration capabilities. MATLAB was used to integrate the Shuttle's velocity in order to obtain position. MATLAB was used to differentiate the Shuttle's position in order to get velocity. MATLAB produced errors on the order of 0.0125 % during the test runs.

The CAST –1000 GPS Simulator is a portable satellite simulator [2]. It can simulate 10 GPS satellites simultaneously. It simulates Coarse/Acquisition (C/A) and P codes. It can generate both L1 and L2 frequencies. L1 frequency is 1575.42 MHz and L2 is 1227.60 MHz. It was used in this research to simulate up to 8 satellites on the L1 frequency.

The ASHTECH G12 GPS receiver is a portable hardware device that processes signals from the GPS satellite constellation [3]. This receiver uses twelve discrete parallel channels for C/A code-phase (pseudo-range) measurements and carrier phase measurements on the L1 (1575.42 MHz) band. The receiver was used in this research to provide real-time position, velocity, and time measurements.

SATELLITE TOOL KIT Version 4.3 is a hands-on software tool designed to provide the skills necessary to perform basic aerospace analysis [4]. It can generate paths for a variety of space-, air-, sea-, and land-based objects, such as satellites, aircraft, ships and ground vehicles. It can be used to calculate and visualize a satellite's position and attitude. STK provides 3D animation capabilities and a 2D map background for visualizing the path of these vehicles over time. Ephemeris data from the STS103 's December 1999 Shuttle Launch was loaded into STK from a text file. STK used the data to simulate the trajectory of this Shuttle Launch.

FUGAWI Version 3.0 is a comprehensive program for integrating bit-mapped charts or maps with a GPS receiver [5]. The FUGAWI software is used for visualization of the trajectory of a moving vehicle. The software was used in this research to visualize the ground tracks of an airplane and a rocket.

2. EXPERIMENTAL WORK

2.1 LOADING EPHEMERIS DATA INTO STK

In order to load Ephemeris data into STK, first create a new Scenario by clicking the Scenario icon upon

opening STK. Second in the browser menu select the missile icon. The missile object will be created. Click on the missile object so that it will be highlighted in blue. Third click on Properties in the main menu. Fourth select Basics. The Basics menu appears. Fifth under the Propagator drop-down menu select STK External. Sixth browse through the External Ephemeris File to find the STS103 Shuttle Launch data file. Seventh click the apply button. Eighth click the ok button. STK displayed the trajectory of the shuttle launch as orbit tracks in the 3-D visualization window. STK displayed the trajectory of the shuttle launch as ground tracks in the 2-D map window. The plot of the trajectory is shown in the Results section.

2.2 MATLAB COMPUTATIONS

The STS103 Shuttle was launched in December 1999. The Ephemeris report showed the output data for velocity in meters per second and position in meters and time in seconds. The velocity was integrated by MATLAB in order to retrieve the position. The percent errors were less than 0.0125 %. The position was differentiated by MATLAB in order to get the velocity. The percent errors were less than 0.0125 %. MATLAB is an excellent tool to use in integrating and differentiating space data. The MATLAB recipe for differentiation of the Ephemeris data is given in Appendix A. The MATLAB recipe for integration of the Ephemeris data is given in Appendix B. MATLAB outputs used in this research for integration and differentiation are shown in the Results Section.

2.3 TRAJECTORIES PRODUCED FROM INTEGRATED GPS LABORATORY

Two scenarios were created for producing trajectories. The CAST –1000 GPS Simulator, ASHTECH G12 GPS receiver and the FUGAWI 3.0 software were used for these scenarios. An airplane was the vehicle used in the first scenario. A rocket was the vehicle used in the second scenario.

In the first scenario, the aircraft will be stationary for five minutes. Second, the aircraft changed terminal speed to 500 m/s and changed maximum acceleration to 100 m/s^2. Third, the airplane reached a terminal height of 10,000 m. It will climb at a maximum angle of 40°. It reached a maximum climb acceleration of 80 m/s^2. Fourth it cruised for 180 minutes. The airplane traveled from Cape Canaveral, Florida to Los Angeles, California. The latitude setting was 28° and the longitude was -81°. The true initial heading was 290° from the North. The GPS receiver locked onto 7 satellites. The FUGAWI software showed the airplane trajectory. A plot of the airplane trajectory is shown in the Results Section. The lab manual for set-up of the airplane trajectory is given in Appendix C.

In the second scenario, a very fast helicopter was used to simulate the rocket scenario. First the helicopter was stationary for thirty minutes. Second it took off at a terminal velocity of 1000 m/s, at a maximum acceleration of 50 m/s^2. During the takeoff, the course heading was 90° and the course climb angle was 90°. Third it pitched up at a climb angle of 60° at a maximum acceleration of 100 m/s^2. Fourth the helicopter reached a terminal speed of 2000 m/s at a maximum acceleration of 100 m/s^2. Fifth the helicopter cruised for 30 minutes. The GPS receiver locked onto five satellites for the second scenario. The FUGAWI software showed the rocket trajectory. A plot of the rocket trajectory is shown in the Results Section. The lab manual for set-up of the rocket trajectory is given in Appendix D.

3. RESULTS

In Figure 1, the trajectory of the STS103 Shuttle Launch is shown. The STK software produced the trajectory.

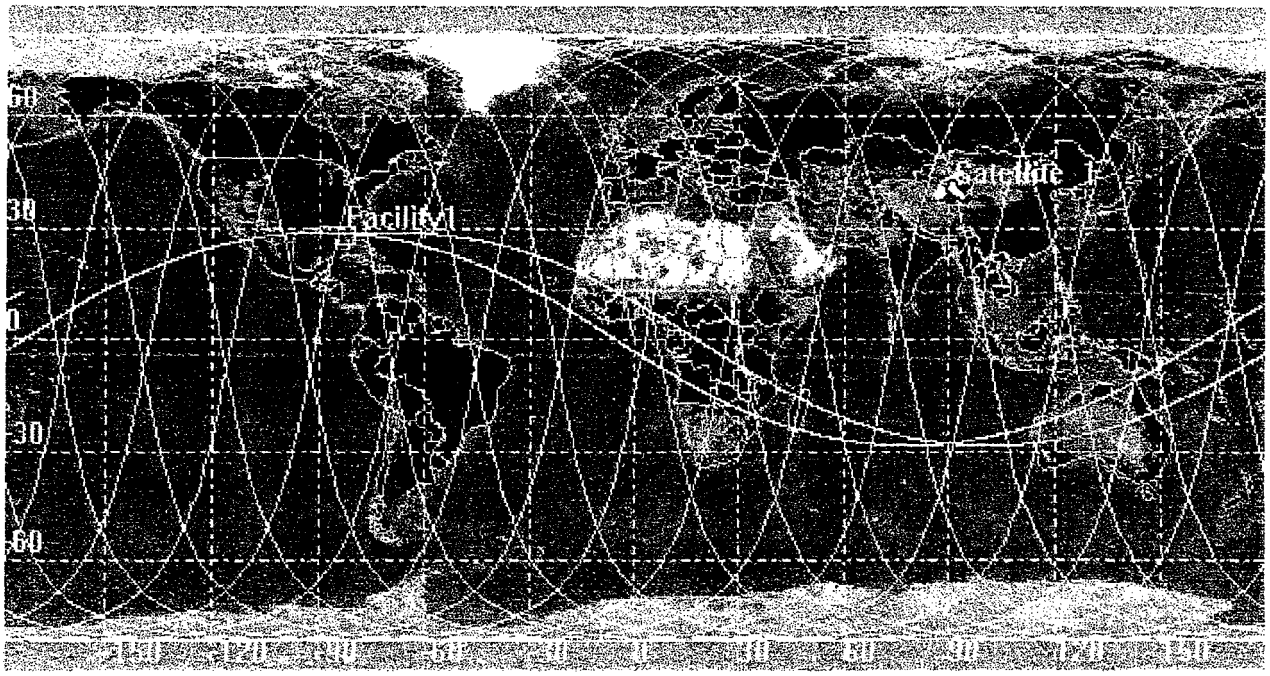

Figure 1: SHUTTLE LAUNCH TRAJECTORY PRODUCED BY STK SOFTWARE

MATLAB was used to produce the waveform in Figure 2. The waveform represents the velocity trajectory of the Shuttle launch STS103 in orbit. The trajectory was produced by the differentiation of the position vector in the x-direction. This output waveform is the velocity vector in the x-direction. Trajectories representing the y-direction and z-direction for velocity were similarly.

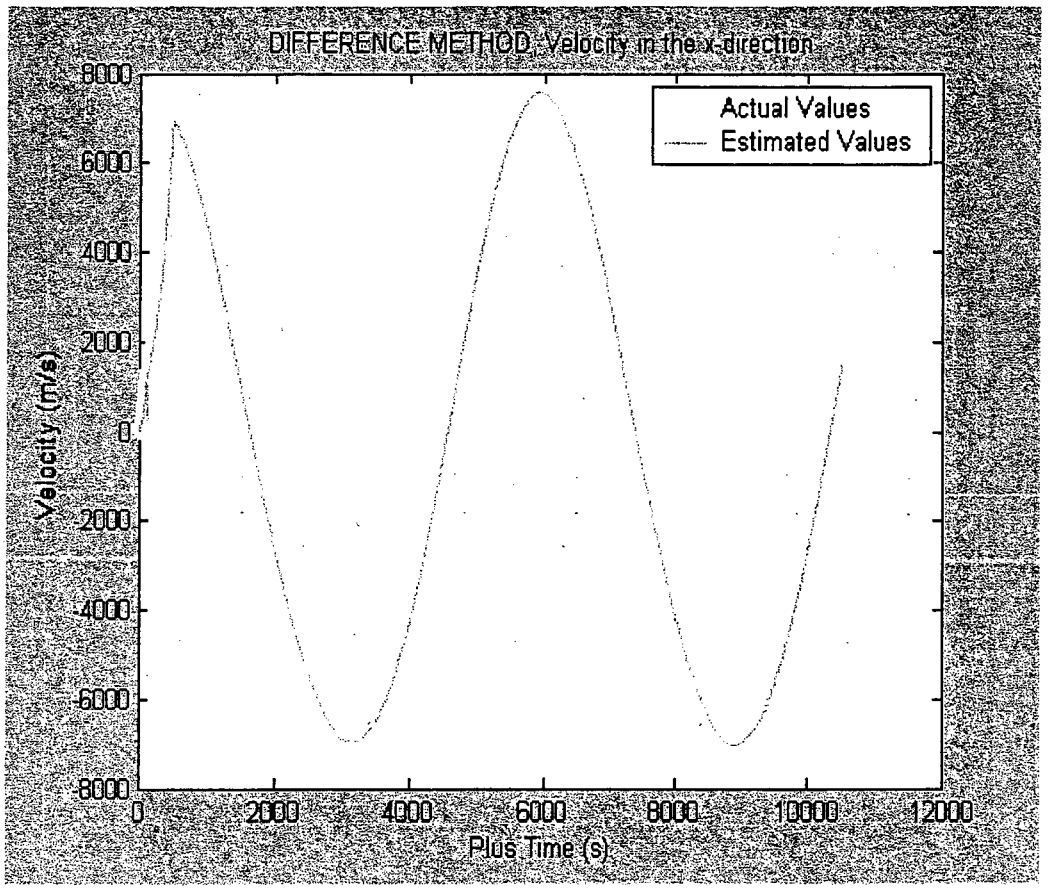

FIGURE 2: VELOCITY TRAJECTORY PRODUCED BY MATLAB

MATLAB was used to produce the waveforms in Figure 3 and Figure 4. The waveform represents the position trajectory of the Shuttle launch STS103 in orbit. The trajectory was produced by the integration of the velocity vector in the y-direction. These output waveforms are the position vectors in the y-direction. Trajectories representing the x-direction and z-directions for position were similarly. MATLAB used the Cumulative Trapezoidal Numerical Integration (CTNI) Method to integrate the velocity data. There is a shift in the two waveforms because CTNI Method started its numerical integration at zero. A MATLAB recipe was written to include a correction factor (CF) to add to the estimated values of the position vectors. Figure 3 shows the integration without CF. Figure 4 shows the integration with CF.

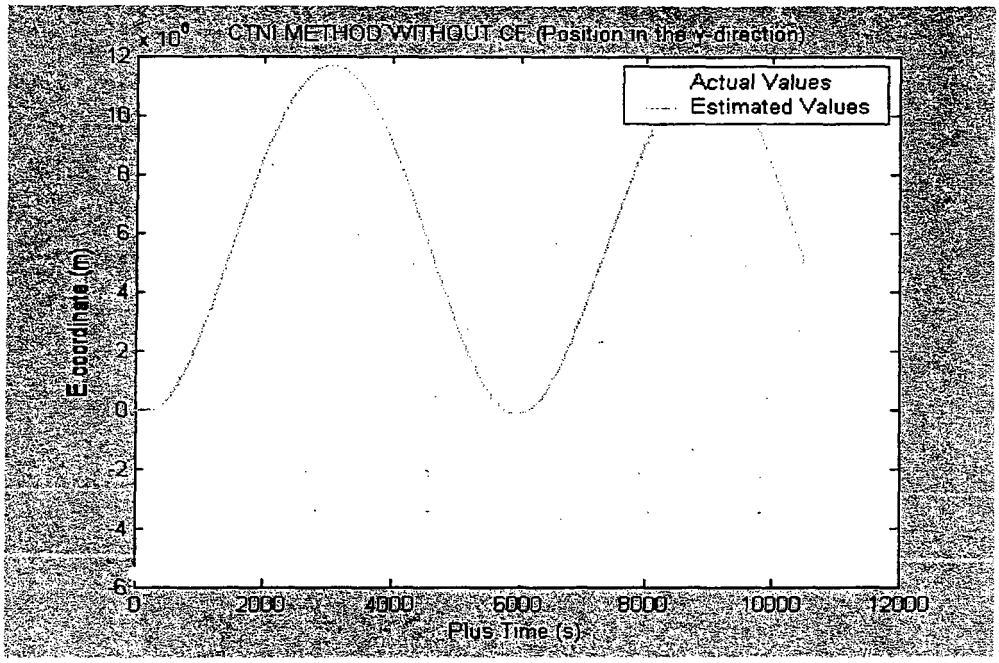

FIGURE 3: POSITION TRAJECTORY WITHOUT CF PRODUCED BY MATLAB

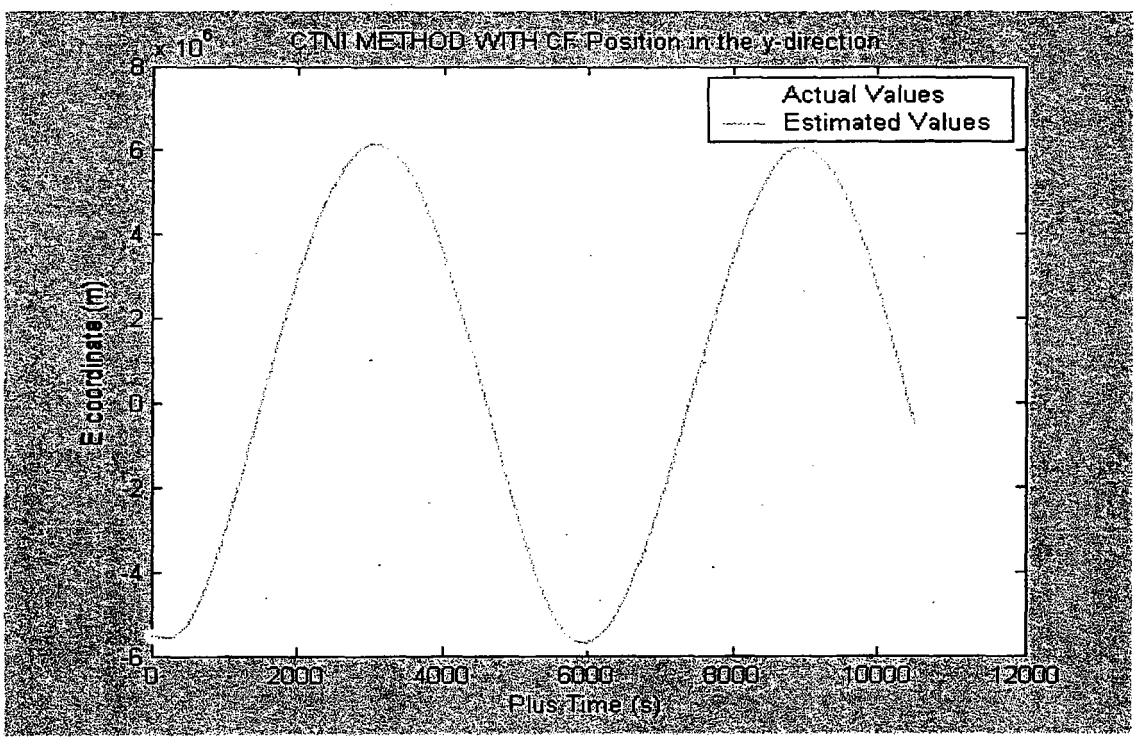

FIGURE 4: POSITION TRAJECTORY WITH CF PRODUCED BY MATLAB

Figure 5 shows the trajectory of the airplane scenario. The airplane started its flight at Cape Canaveral. The final destination was at Los Angeles, California. The trajectory was created by the integrated use of the GPS Simulator, GPS Receiver and the FUGAWI software.

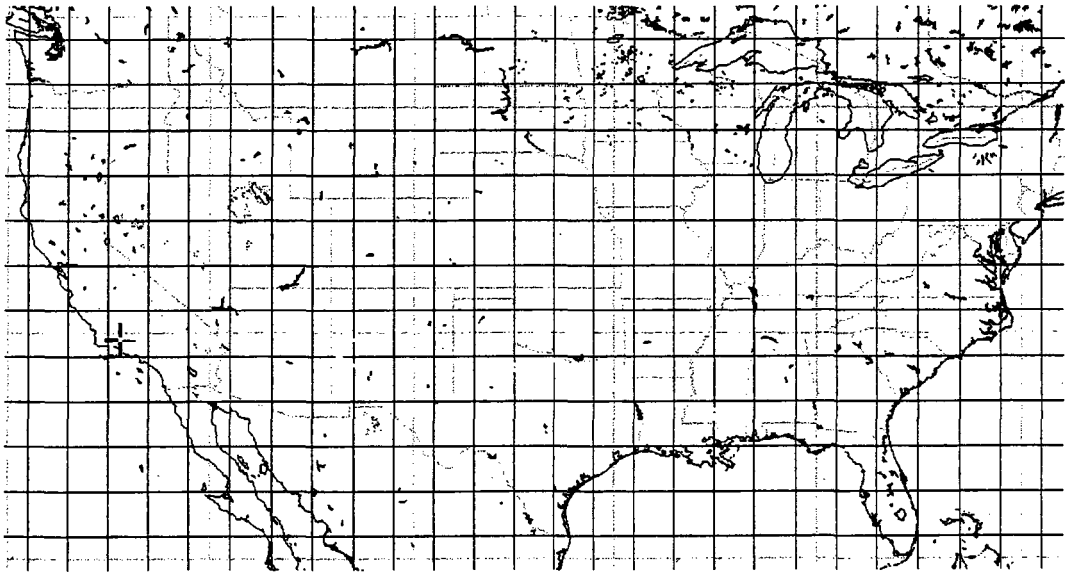

FIGURE 5: AIRPLANE TRAJECTORY

Figure 6 shows the trajectory of the rocket scenario. The rocket started its launch at Cape Canaveral. The final destination of the rocket was 1009.486 km due east in the Atlantic Ocean. The trajectory was created by the integrated use of the GPS Simulator, GPS Receiver and the FUGAWI software.

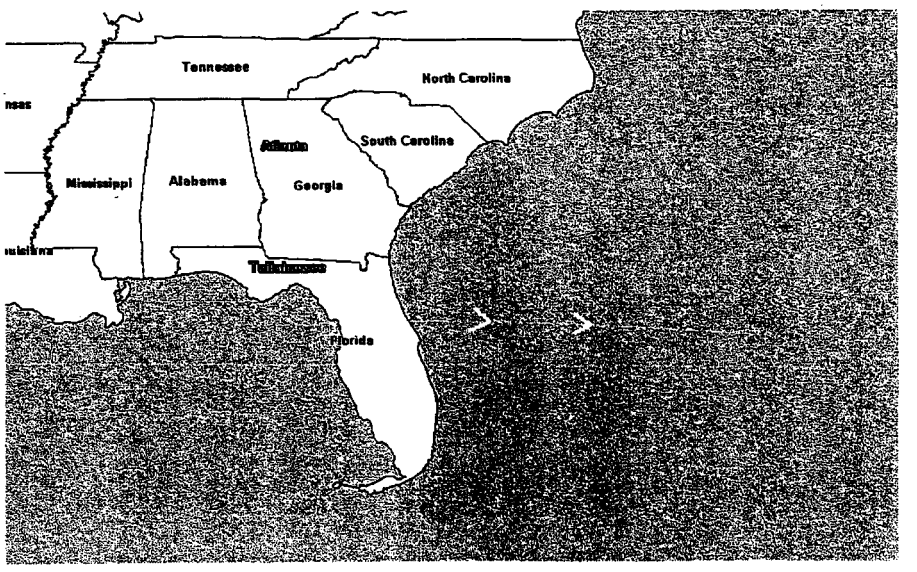

FIGURE 6: ROCKET TRAJECTORY

4. CONCLUSION

A user-friendly GPS lab manual was developed that integrates the use of STK, MATLAB, GPS Simulator, GPS Receiver and Visualization software. Two MATLAB recipes were written to help aid the integration and differentiation. The manual will be used to predict GPS coverage of planned operation. The Integrated GPS Laboratory was used to create two scenarios. One scenario created an airplane trajectory and the second scenario created a rocket scenario. The ability to predict GPS Coverage for future vehicles is the short-term value to NASA/KSC. Reduction in cost of future launch systems and increased flexibility are the long-term values to NASA/KSC.

5. REFERENCES

1. Dabney James B., and Harman Thomas L., Mastering MATLAB 5, Prentice-Hall, Inc., Upper Saddle River, New Jersey 07458 June 1998.

2. CAST CCSG Users Manual CS100145, CAST Inc, Billerica, MA 01821, July 23, 2001.

3. ASHTECH Evaluate 5.0, Magellan Corporation, Santa Clara, California, December 1997.

4. STK Training Manual 4.3, Analytical Graphics, Incorporated, Malvern, PA 19355, June 2001.

5. FUGAWI Navigator's Manual 3.3, Northport Systems Inc., Toronto, Ontario M4T1W5 Canada, January 2002.

2002 NASA/ASEE SUMMER FACULTY FELLOWSHIP PROGRAM

JOHN F. KENNEDY SPACE CENTER
UNIVERSITY OF CENTRAL FLORIDA

PROGRAM AND PROJECT MANAGEMENT FRAMEWORK

Cassandra D. Butler
Program Coordinator
Department of Computer and Information Sciences
Miles College

Tracey Fredrickson - KSC Colleague

ABSTRACT

The primary objective of this project was to develop a framework and system architecture for integrating program and project management tools that may be applied consistently throughout Kennedy Space Center (KSC) to optimize planning, cost estimating, risk management, and project control. Project management methodology used in building interactive systems to accommodate the needs of the project managers is applied as a key component in assessing the usefulness and applicability of the framework and tools developed. Research for the project included investigation and analysis of industrial practices, KSC standards, policies, and techniques, Systems Management Office (SMO) personnel, and other documented experiences of project management experts. In addition, this project documents best practices derived from the literature as well as new or developing project management models, practices, and techniques.

1. INTRODUCTION

The purpose of this work was to develop a framework for integrating project management tools being used at KSC so that they may be easily accessed and efficiently used from a central system architecture, as administered through KSC's Systems Management Office (SMO) under the Directorate of Safety, Health and Independent Assessment. The goal this project management framework was to reveal proven principles that establish the basis for project management success and methods for integrating those principles to form a reliable system.

The National Aeronautics and Space Administration (NASA) and KSC have designed a thorough system of well-defined policies and procedures based on traditional project management techniques. Investigation and analysis of project management strategies revealed that many different software applications are being used to generate project management tools. However, there is no integrated system to assist project managers in completing the compliance requirements while using these applications. Such a system would provide opportunities for project teams to collaboratively share project responsibilities and allow project managers to spend more time managing project requirements rather than learning new project management systems.

KSC SMO, based on research and development prior to commencement of this project, had determined that project success would likely be improved by providing a consistent means for project managers and team members to access and complete project requirements as delineated by policies and standards. According to most project management authorities, more projects are unsuccessful than successful (Levine, 2002; Walker, 2000). Researchers also agree that prior to deciding on a project management tool, organizations must carefully evaluate the reliability of internal policies, procedures, and practices (Trepper, 2000). Thus, initial tasks included investigation of applicable policies, procedures, tools, and techniques.

Due to competition for limited project resources, successful project management requires the use of tools to access scope, time, cost, risk, and quality (Project Management Institute, 2000). Tools used for these purposes are most often computerized today, although they come in numerous forms. While many project management tools and techniques are integrated into project management software applications, many are also developed using other software such as Microsoft Access, Excel, Outlook, PowerPoint, and Word.

Project management software generally makes available tools such as work breakdown structure (WBS), task list, Gantt chart, calendar plan, task usage chart, network diagram or PERT chart, critical path analysis, and earned value analysis that are used to help project managers and project team members in accomplishing scope, time, cost, and quality management (Schwalbe, 2002; Barkley and Saylor, 2001). However, Barkley and Saylor (2001) indicate that quality is actually the fundamental goal of project success leading to successful integration of cost and schedule. The integral relationship between managing quality and managing metrics necessitates evaluation of the metrics used by SMO as well (TenStep, 2002). The KSC SMO uses a diverse network of rationale-based metrics with specific goals based on its mission.

This research project used the trials of industry and academia to develop a project management architecture for integrating software applications used at NASA KSC that will promote effective management of scope, time, cost, and quality via access to an integrated web-based system designed for that purpose.

More specifically, project managers at NASA KSC need the following capabilities:

- To use project management software and systems without the necessity of being an expert in the framework of the project management system and how it works.
- To access the project management system at any time from any place while maintaining organizational security.
- To have instantaneous, automatic notification to team members that task requirements or action items have changed.

Furthermore, the author determined and documented an architecture for a system that will eliminate redundancy by automating project team tasks to allow the transfer of data from forms, templates, and other required documentation into a knowledge base for integrated and distributed project management. To accomplish this end, project management experiences in aerospace industry and public sector as well as review of the literature led the author to explore basic questions regarding integrated project management. Based on project management methods, theory, and years of project management experience of the author, desirable characteristics for integrated project management in a web-based environment include, but are not limited to:

1. Simple processes
2. Powerful processes
3. Form-based interfaces for easy connection to existing data sources, input and modification by non-project management personnel
4. Well-organized, consistent data
5. Quick-scan dashboards
6. In-depth reports
7. Consistent and reliable security

2. INVESTIGATION AND RESEARCH

Project work initiated with an investigation into the policies and operations of the NASA KSC Program and Project Management organization; the Systems Management Office (SMO). The Systems Management Office acts as an agent for the KSC Center Director, KSC's CFO and the NASA Chief Engineer (Code AE) to assure that development efforts and mission operations are being planned and conducted based on a sound engineering and project management basis with appropriate controls and management of technical risks. The Systems Management Office also houses KSC'S Chief Engineer who ensures engineering excellence in the execution of Programs and Projects. The SMO Organization Structure web page provides member names, position descriptions, and other contact information.

The SMO website is based on sound principals of using project management tools which have been characterized according to the principal project management phases and activities. These tools provide a basis for enforcing the use of standards, review processes, and foremost to define quality in terms of deliverables (Trepper, 2000). While project management methodology has remained constant for almost 20 years, research revealed two fairly new method improvements that warrant mention: 1) Total Project Control (TPC) (Devaux, 1999) and Critical Chain Analysis (Newbold, 1998). Although not a project management method, TQM or Total Quality Management programs, popular in the 1980s, should have been included in project management methodology according to both Devaux (1999) and Newbold (1998. In addition, many organizations are modifying project management systems and developing internal applications to address specific project management issues. For example, the United States Air Force

(USAF) has developed PAPIE, a Visual Basic 6 program that links to a SQL 7 database to track requirements and provide standardized process management and more (Personal Communication, Henry D. Akin, July 1, 2002). The Hampton Group (http://www.4pm.com) uses an "achievement-driven project management methodology" which includes a measured achievement in addition to a budget, schedule, and completion date for each component of the project plan.

While not included in this document, a gap analysis of NPG 7120.5, the primary document governing the operation of SMO against the SMO website was done to determine if all policy requirements are handled in the SMO website. Additional information regarding Center documentation including program/project management reports was gathered from the NASA/KSC TechDoc 2.0 System Document Manager and Search Manager User's Guide (KSC-TD-01005) and website (http://tdsearch.ksc.nasa.gov/). The SMO website, organized into three categories: SMO/Resource, Functional Areas, and SMO Services was approximately 20 percent complete with policies, procedures, tools, techniques, responsibilities, and reference documents at the beginning of this project. During the course of this project, Tracey Fredrickson has consistently applied improvements and modifications to the SMO site, expediting its release on July 19, 2002. Therefore, the SMO site is ready to initiate an integrated architecture prototype, as detailed in the Conclusions section of this report. Figure 1 illustrates the basic framework for this system.

2.1 Project Management Applications

Research revealed that several project management applications and support systems for project management have been previously investigated and selected for use at the Center. Although the real-time sharing offered by some applications is attractive, they are not feasible for large project management teams unless they include a collaborative infrastructure (Penã-Mora and Dwivedi, 2002). Telelogic DOORS (http://www2.telelogic.com/products/doorsers/doors/index.cfm), SAP R/3 Project System, and Scitor PS8 incorporate interaction protocols, information policies, and meeting structures that are much more appropriate for large organizations like NASA KSC. Distributed database technology offers potential for integrating project management requirements through common functional tasks and reporting requirements and is readily accomplished using Java programming. Java has been shown to be an excellent programming language for designing interfaces for web-based applications as well as distributed systems incorporating such tools. The following website contains links for companion products for Microsoft Project http://www.projectmanagement.com/tools.htm. Such applications demonstrate how Microsoft Project can be the focal point of a web-based application for integrating project management tools.

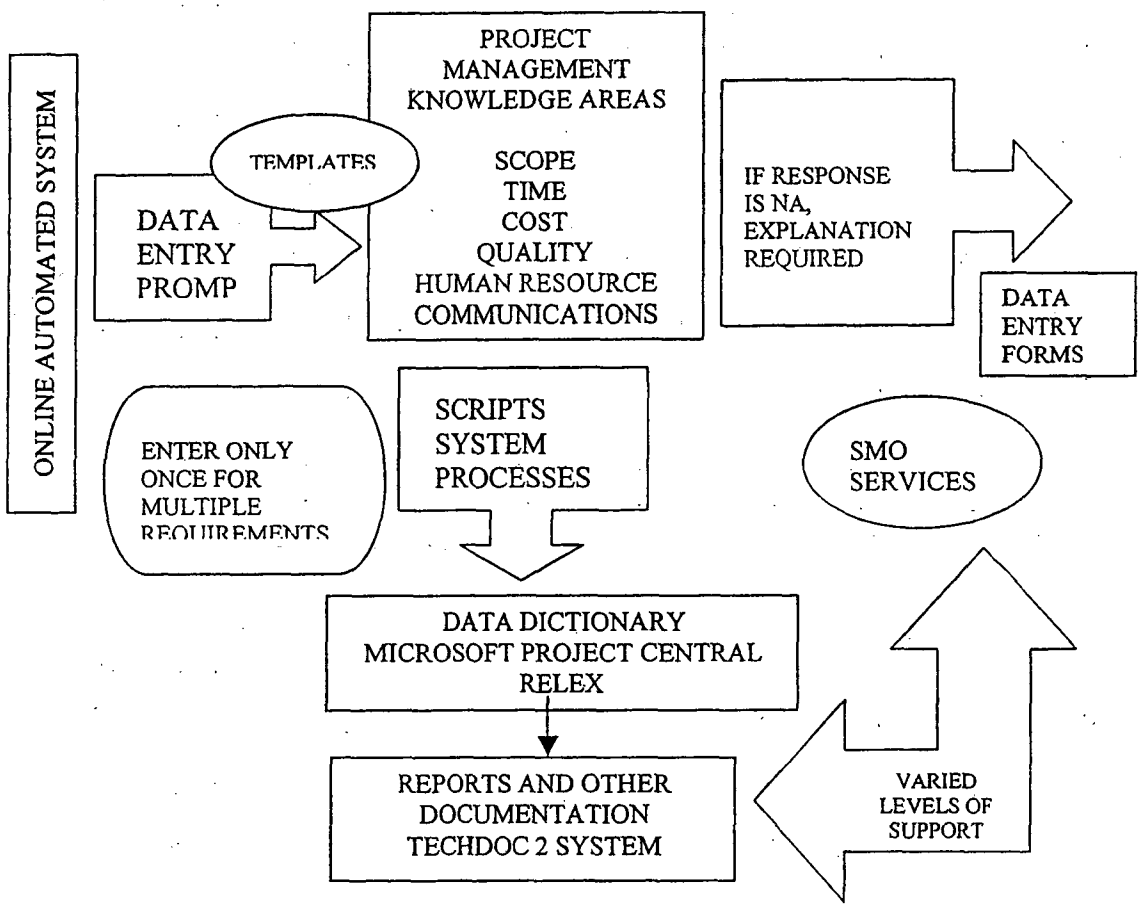

Figure 1. Prospective SMO Web-based Intranet Architecture

2.2 Project Management Document System

The Tech Doc 2.0 System (http://tdsearch.ksc.nasa.gov/) uses a graphical user interface type interface similar to Windows Explorer to provide access to NASA documents including those specific to KSC. In doing so, the system provides electronic access to a limited number of project management reports. This system should also be integrated into the Project Management Integration System so that project managers and team members have a central location for the most current project management reports, thereby retaining consistency for the TechDoc System objectives. A Project Management Tools Questionnaire was developed, however, not completed as part of this project.

3. RESULTS

While the NASA KSC SMO has access to several effective project management tools, use of these tools by project managers appeared to be less than optimal. Therefore, a major objective was determined to be the optimal participation of project managers in project management activities (Levine, 2002). A system designed to comply with guidelines while offering consistent support to assure project managers that they and their team members have entered data required to retain an accurate picture of project status and direction is essential to optimal participation. An additional impediment to the implementation of a

feasible project management system, according to Levine, is that program management is usually complex in its requirements and execution. Therefore the author proposes the development of an architecture based on what may be referred to as the three Es of project management: efficient, effective, and easy. The proposed architecture is based on these features. Equally as important is the development of a framework designed to encourage a proactive method rather than a cycle of problem solving (Penã-Mora and Dwivedi, 2002). Of course, to achieve efficiency, project management software along with the structural framework for processing data must be supported by the implementation of real-time analysis capabilities, as corroborated by Penã-Mora and Dwivedi.

As true with most of the project management methods used today, the current design is inefficient for adequately handling all sources of change (Petrie, Goldmann, and Raquet, 2000). The large number of projects and responsibilities involved in project management at KSC requires a system to eliminate duplication and assure both the project schedule and required changes are instantaneous and automatic. Based on the assessed requirements and the current system capabilities, the author determined that an investigation of processes and techniques to automate project management software requirements using tasks, reports, and activities commonly executed by project managers and their team members on a daily basis was the best methodology for investigating solutions. This decision led to the investigation of several methodologies including Distributed Integrated Project Management (DPIM), Customer Relationship Management (CRM), and Enterprise Resource Planning (ERP). An integrated system designed based on each of these methods would be optimal. However, based on funding and organizational requirements, it may not be practical to integrate all into the system initially.

3.1 Short-term Versus Long Range Plans for the SMO Site Functionality

Short-term considerations for improving the SMO site function include using process plans, flow charts such as KDP-KSC-P-2603 to make completing requirements more intuitive for project managers by automating the flowchart contained in the template. For example by clicking the Start link in the automated version of a KDP-KSC-P 2602 template would appear on the screen so that it could be completed online or printed. Ultimately, the systems would be designed to track the user's status in the project implementation process thereby revealing where the project manager stopped during the last session. While ERP software is very effective for incorporating the information used by many different functional areas into one computer-based system, it is also very expensive, difficult to deploy, high maintenance, and takes a great deal of time to implement (Mello, 2002). CRM software, if properly implemented, has been proven to produce invigorating savings. However, the software is extremely complex and time consuming because of all of the customer relationships that must be integrated (Baldwin, 2002). Therefore, the author recommends further investigation of the benefits and cost of ERP and CRM technologies, while incorporating a common graphical interface to access the applications already deployed at KSC.

3.2 Distributed Project Management (DPM): A Solution with Promise

For large complex organizations such as KSC, DPIM is the most feasible of the methods reviewed for integrated project management. Petrie, Goldmann, and Raquet (2000) describe DPIM as an intense form of "Process Coordination" that infuses design, planning, scheduling, execution through distributed institutions and engineering disciplines as well as computer tools. Distributed project management offers the most versatile and effective solution to integration and automation for project management. This technology, while continuing to advance as a result of research and development in varied work sectors, has shown significant benefits (Ly, 1997; Matsutsaka and Hara, 2000; Collaborative Strategies, 2001).

4. CONCLUSIONS

Research into the organizational structure, practices, and procedures has lead to a determination by the author that the project management deficiency experienced at KSC is a result, in part, of lacking a system to streamline the processes required to meet internal and external standards relative to project management and to eliminate redundancy imposed when program and project managers must enter data for documents that are a normal part of their functional activities and again as a part of project management procedures.

4.1 Overall Infrastructure for Integrating Project Management Information Technology

Research during the course of this project indicates trends from data-focused project management to people-focused distributed project management support the framework proposed herein (Collaborative Strategies LLC, 2001). This framework of automated tasks incorporated from templates, standards, procedures, and techniques is based on computer-aided interactions of individuals throughout the organization. Thus, such interactions will result in automated entry within the Program Management Information System (PMIS). The proposed PMIS may be deployed using a web-based graphical interfaced to integrate commercial off-the-shelf (COTS) software, application service providers (ASP), custom designed software, or a combination of these. For example, Project Insight Project Management Software (http://www.project-management-software.org/) is an enterprise web-based project management software providing Gantt charts, calendars, tasks, risk, resource, time/billing discussions, files, security, Microsoft Project, Microsoft Project Central (Microsoft, 2000) integration and more. Figure 2 shows the system architecture of such an application. Review of the literature shows that Microsoft Project's custom programming language, Visual Basic for Applications (VBA) can be used to computerize recurrent tasks, interact with other Windows applications, and develop high-level custom reports quickly and easily. VBA can be used to create routines to dynamically adjust resource assignments and schedule information. This programming language is designed to develop macros to associate Microsoft Word documents, Excel workbooks, Access database applications, and PowerPoint presentations with specific tasks in the Microsoft Project application. Routines can also be designed to create and use "boilerplate" project templates. Probably most useful for designing systems to be used by individuals who do not specialize in using project management software is the capability to use VBA to create menus and toolbars to organize customized Microsoft Project functions on each user's desktop based on specified parameters.

4.2 System Resources Required for the PMIS

The primary resources required to design the proposed automated system are:

- Server w/Intel Pentium 75 MHz or higher or similar processor, 10–20 MB available hard disk space, and 16 MB RAM or more
- Windows 95 or 98, Windows NT 4.0 with Service Pack 3 or later, or Windows 2000
- Microsoft Internet Explorer 4.01 or later, or the Browser Module for Microsoft Project Central
- Appropriate number of Microsoft Project/Project Central 2000 licenses
- Microsoft Visual Basic for Applications
- The Microsoft Project 2000 Resource Kit
- The Microsoft Project 2000 Software Development Kit

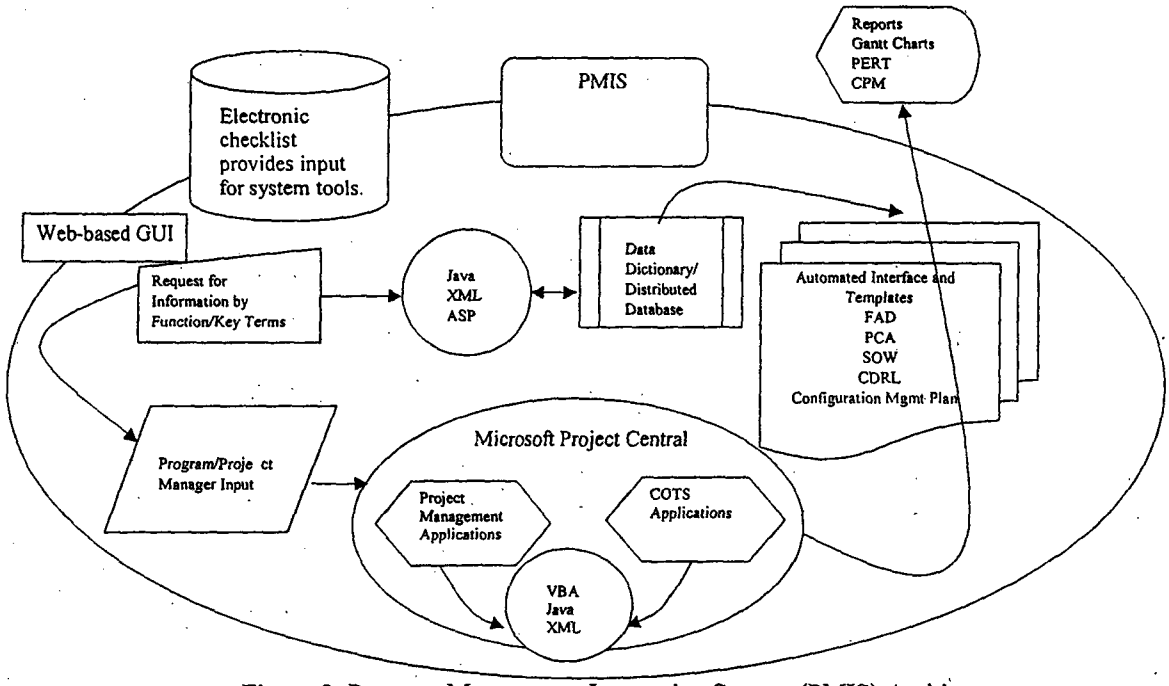

Figure 2. Program Management Integration System (PMIS) Architecture

Resource and Development Kits are free of charge and may be retrieved from the Microsoft World Wide Web site http://www.microsoft.com/office/project/prk/2000/appndx/toolbox.htm. Microsoft offers the Microsoft Project 2000 Software Development Kit http://msdn.microsoft.com/library/default.asp?URL=/library/sdkdoc/pr2ksdk/default.htm to assist developers in designing applications to interface Microsoft Project, Microsoft Project Central, and other applications. While a COTS application often will not meet all requirements, Resource Development Kits and programs like AsOne (http://www.as-one.com/ONE/SilverStream/Pages/pgAs1home.html) allow organizations to design custom interfaces and project management tools integration architectures without the need to redesign components of the software application that already exist and have demonstrated a record of success.

Unfortunately, research of the literature revealed that one of the most prevalent problems faced by organizations attempting to institute more efficient systems is the lack of implementation (Pfeffer and Sutton, 2000). However, because the SMO system of tools helps managers link performance metrics to budget formulation, thus enabling more focused and more effectively managed spending, the proposed PMIS holds greater prospects for implementation. Too often, research and development does not result in installation of recommended systems and approaches. Thus, organizations such as KSC should include in research and development projects such as this a requirement to evaluate and test the results within a specified period of time. A major component of that evaluation should be creating a KSC-wide project group to implement a prototype based on assessment of the results of this project.

5. REFERENCES

Baldwin, Howard (2002, March). Prescription for healthier CRM. Retrieved June 17, 2002 from the World Wide Web: http://www.zdnet.com/filters/printerfriendly/0,6061,2854592-92.html

Barkley, Bruce T. and Saylor, James H. (2001). *Customer-Driven Project Management: Building Quality into Project Processes*. (2nd ed.). New York, NY: McGraw-Hill.

Collaborative Strategies LCC. (2001). Executive summary: Distributed project management: Update 2001(Volume 1). Retrieved June 11, 2002 from the World Wide Web: http://www.collaborate.com/news/dpm2001vles.html

Devaux, Stephen A. (1999). *Total Project Control: A Manager's Guide to Integrated Project Planning Measuring and Tracking*. New York, NY: John Wiley & Sons, Inc.

Doyle, W. (n.d.). CLI project management. Implementation of scheduling and contract management software using the CLI project management implementation system. Retrieved May 22, 2002 from the World Wide Web: http://www.clipm.com/

Levine, Harvey A. (2002). Why project management implementation programs fail. Retrieved May 22, 2002 from the World Wide Web: http://www.myplanview.com/expert69.asp

Ly, Eric. (1997). Distributed java applets for project management on the web. IEEE Internet Computing. May-June, Industry Report. P. 21-26.

Marin Research (1998). Project observatory: Connecting your project community. Retrieved April 4, 2002 from the World Wide Web: http://www.marinres.com/pg5doc/admin/admin01_PG5_System_Administration_Manual_Contents.pdf

Mello, Andrian (2002, February). ERP fundamentals. Retrieved June 17, 2002 from the World Wide Web: http://www.zdnet.com/filters.printerfriendly/0,6061,28844319-92,00.html

Microsoft (2000). Microsoft Project 2000 enterprise project planning workbook deployment tool. Retrieved June 11, 2002 from the World Wide Web: http://www.microsoft.com/office/previous/project/workbooks/ProjWB.asp

Neroda, Edward. (1990, Fall). Uses and benefits of microcomputer project management software. Cause/Effect, 13(3). Retrieved June 14, 2002 from the World Wide Web: http://www.educause.edu/ir/library/text/CEM9037.txt.

Newbold, Robert C. (1998). *Project Management in the Fast Lane: Applying the Theory of Constraints*. Boca Raton, FL: St. Lucie Press.

Paradigm (n.d.). Project management implementation. Retrieved May 22, 2002 from the World Wide Web: http://www.paradigmmanagement.com/Mentor/PMI.htm

Penã-Mora F. and Dwivedi, G. (2002, January). Multiple device collaborative and real time analysis system for project management in civil engineering. *Journal of Computing in Civil Engineering.*

Okubo, Takao, Matsutsuka, Hara, Hirotaka. (2000, December). System for distributed project management over the Internet: PI-CEE. FUJITSU Science Technology Journal, 36(2), pp. 193-200.

Petrie, C., Goldmann, S., & Raquet, A. (2000). Agent-based project management. Stanford Center for Design Research. Retrieved June 7, 2002 from the World Wide Web: http://www-cdr.stanford.edu/ProcessLink/papers DPM/dpm.html

Project Management Institute. (2000). A Guide to the Project Management Body of Knowledge: PMBOK® Guide. 2000 ed. v1.2. CD-ROM

Schwalbe, K. (2002). *Information Technology Project Management.* (2nd ed.). Boston, MA: Course Technology.

TenStep (2002). 10.0 Manage Metrics.Retrieved May 28, 2002 from the World Wide Web: http://www.tenstep.com/10.0%20Manage%20Metrics.htm

The Hampton Group (2002). Out training provides skills for success. Retrieved May 21, 2002 from the World Wide Web: http://www.4pm.com/adpm/adpmslid/sld010.htm

The Hampton Group (2002). The project office: High-flying PM aces & TV weather people. Retrieved May 21, 2002 from the World Wide Web: http://www.4pm.com/articles/control.html

Trepper, C. H. (2000). Application Development Trends. A project management primer. Retrieved June 14, 2002 from the World Wide Web: http://www.artemisintl.com/lang_en/press_room/in_the_news/adtMag_August01.pdf

Walker, E. D. (2000). An introduction to critical chain project management. Retrieved May 31, 2002 from the World Wide Web: http://sapittoolbox/documents/asp?I=1209

2002 NASA/ASEE SUMMER FACULTY FELLOWSHIP PROGRAM

JOHN F. KENNEDY SPACE CENTER
UNIVERSITY OF CENTRAL FLORIDA

INSTRUMENTATION AND METHODOLOGY DEVELOPMENT FOR MARS MISSION

Yuan-Liang Albert Chen
Professor of Physics
Division of Natural Science and Mathematics
Oklahoma Baptist University
500 West University Drive
Shawnee, OK 74804

KSC Colleague: Dr. Carlos I. Calle

ABSTRACT

The Mars environment comprises a dry, cold and low air pressure atmosphere with low gravity (0.38g) and high resistivity soil. The global dust storms that cover a large portion of Mars were observed often from Earth. This environment provides an idea condition for triboelectric charging. The extremely dry conditions on the Martian surface have raised concerns that electrostatic charge buildup will not be dissipated easily. If triboelectrically generated charge cannot be dissipated or avoided, then dust will accumulate on charged surfaces and electrostatic discharge may cause hazards for future exploration missions. The low surface temperature on Mars helps to prolong the charge decay on the dust particles and soil. To better understand the physics of Martian charged dust particles is essential to future Mars missions. We research and design two sensors, velocity/charge sensor and PZT momentum sensors, to detect the velocity distribution, charge distribution and mass distribution of Martian charged dust particles. These sensors are fabricated at NASA Kenney Space Center, Electromagnetic Physics Testbed. The sensors will be tested and calibrated for simulated Mars atmosphere condition with JSC MARS-1 Martian Regolith simulant in this NASA laboratory.

INSTRUMENTATION AND METHODOLOGY DEVELOPMENT FOR MARS MISSION

Yuan-Liang Albert Chen

1. INTRODUCTION

Mars has a very high resistivity soil and an extremely dry atmosphere. The water concentration in the atmosphere is in the range of 210 PPM [1],[2]. Martian air density is close to 0.02 kg/m^3 and an average dust concentration of 1 mg/m^3 suspended in the Martian air equivalent to 13.4 times the amount of dust in normal air in manufacturing plants on Earth [3]. The local dust cyclone and global dust storm on Mars has a dust loading of 30 mg/m^3, which is 402 times of dust in normal air in manufacturing plants on Earth. The Martian dust storm has these properties; (1) Martian Dust Storms can occur at any time of the year, (2) Typical storms cover areas of one million square kilometers, (3) Storms contain particles having speeds of 25-65 m/s. This environment provides an idea condition for triboelectric charging. [4],[5]. The extremely arid conditions on the Martian surface have raised concerns that electrostatic charge buildup will not be dissipated easily. If triboelectrically generated charge cannot be dissipated or avoided, then dust will accumulate on charged surfaces and electrostatic discharge may cause hazards for future exploration missions. The low surface temperature on Mars helps to prolong the charge decay on the dust particles and soil [6].

Martian dust plays a major role in all of the surface interactions considered. Space systems affected by Martian dust and electrostatic charging on Mars are (1) solar cells and viewing ports, (2) thermal radiators, (3) moving parts on vehicles and machines, (4) space suits and life support systems, (5) communication systems, and (6) fuel production and storage systems.

Kolecki et al. at NASA Glenn Research Center reported that 350 volts was observed in their WAE experiment [7]. It is also believed that an article moving on Mars may charge more strongly than the wheel did in the laboratory. Pathfinder wheel charging was observed nearly independent of the rotation speed and wheel slip. It is suggested that charge generation may have resulted from triboelectric effects in the dust when compacted by the wheel.

The dust particles behave as a dielectric medium in Martian atmosphere. These charged dielectric particles accumulate space charges and generate a reverse electric field, which terminates the corona discharge. It is possible to produce highly active plasma without sparking [8]. The plasma generated has a high electron temperature and low gas temperature that is able to enhance chemical reactions. This partial (silent) discharge behavior is also possibly helping insulation [9] and increasing the total charges on the soil surface.

When strong surface winds and a resulting large dust mass loading in the course of large dust storms occurring on Mars, there is possible to produce large electrical discharge - lightning on Mars [10].

To characterize the dust charge and speed in the Martian atmosphere, two sensors are designed to perform these tasks. The design and tests of new sensors are described and presented in the following sections. We conclude with a discussion of the results of the experiments, and present conclusions about the new sensors.

2. Sensors Design

The design and development two sensors, (1) charge and velocity sensor, and (2) mass/momentum sensor, are presented in this section.

2.1 Velocity/Charge Sensor

The purpose of this sensor is to measure the amount of electric charge and airborne dust particle velocity. It is based on the fact that when a charged particle passes through the center of a cylindrical capacitor, an equal amount of opposite charge will be induced on the capacitor. By measuring the induced voltage on this capacitor and knowing the capacitance of this cylinder, we can compute the original charge on the passing particle. Setting two cylindrical capacitors at a pre-determined distance and measuring the time that takes the charged particle to pass through, the particle speed can be calculated. Figure 1 shows a two cylindrical capacitors system that was constructed to perform the experiments. The cylinder is a brass tubing of 0.1875 cm OD, 0.1595 ID and 1.0 cm in length. Each cylinder is supported by a 0.5 cm long Teflon spacer and housed inside a 0.347 ID brass tube. This outside tube serves as an integrated housing and insulator to shield the external noises. Two cylinders are separated by 2.0 cm in the housing tube. The effective separation distance "d" is 3.0 cm. In front of the first cylindrical capacitor, there are three collimator disks to filter and align the dust particles. The collimator has a small hole, diameter 0.033 cm, at the center of the disk. The charged dust particles must pass through three collimator plates to reach the capacitor sensors.

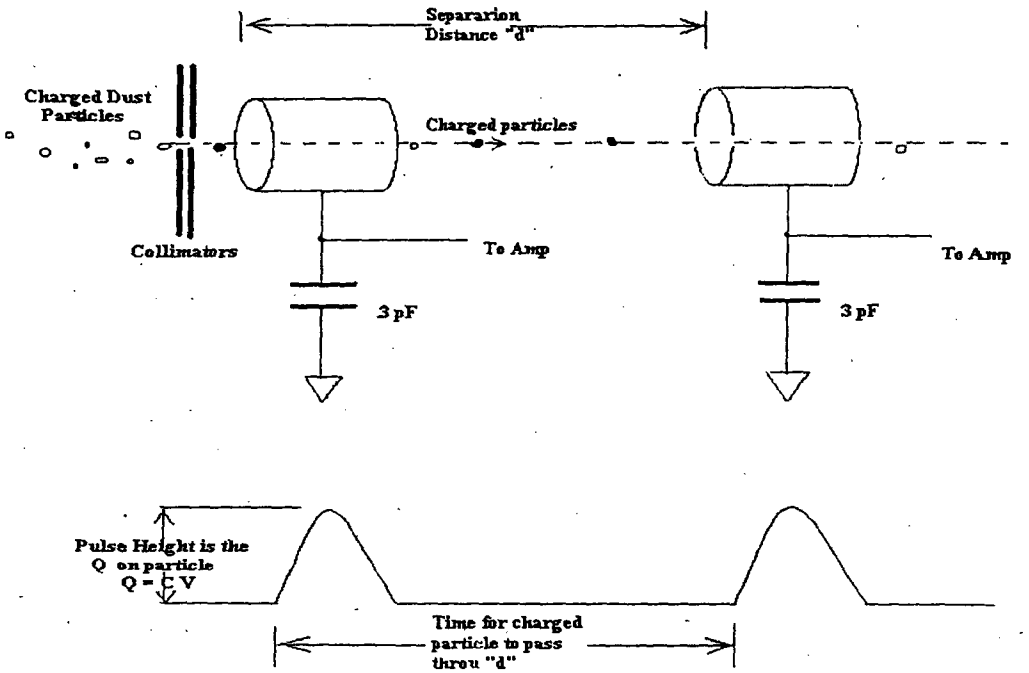

Figure 1. Velocity Sensor Design

The capacitance of the sensing tubing is 4.5 pF. This capacitor in series with a fixed external capacitor, 3.0 pF, forms a voltage divider. The induced voltage is measured through an amplifier with a 50 times gain. Figure 2 shows the basic electronics of the amplifier. The amplifier is using a LMC6044 chip, which has four identical OP-Amps. Two OP-Amps are used to form a complete amplifier for each cylindrical sensor. The total gain of the amplifier is determined by the ratio of two external resisters R_1, R_2, and the voltage divider.

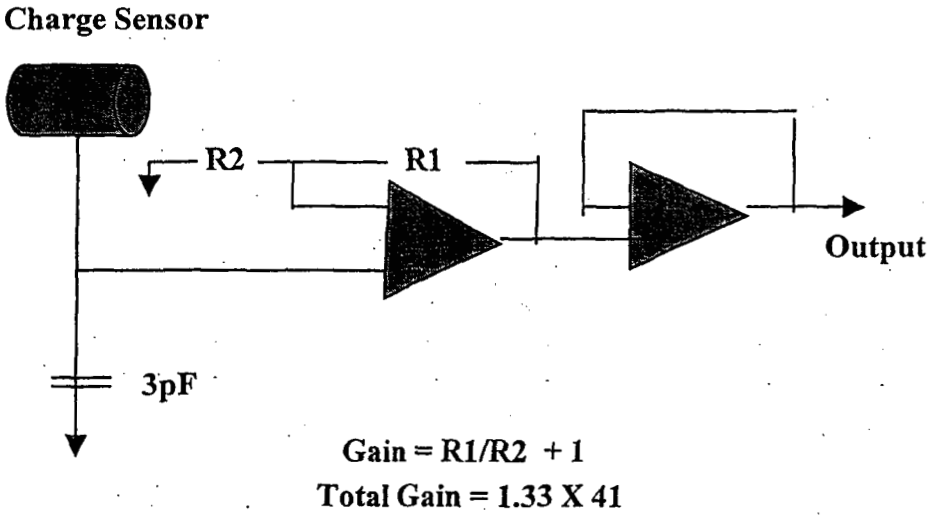

Figure 2. Velocity Sensor Amplifier Circuit

The amplifier circuitry is derived from MECA electrometer, a proven flight instrument designed and developed by NASA KSC Electromagnetic Physics Testbed Team and NASA JPL scientists [11],[12],[13]. We use this circuit to simplify the design and to cut down the hardware cost. A Tektronix Digital Phosphor Oscilloscope (DPO) model DPO3052 (500MHz, 5GS/sec, 2 channels) was used to collect the data. A DPO probe type P6139A (10 MOhm, 8 pF, 500 MHz, 10:1) was used to pick up the output voltage coming from the sensor amplifiers in the vacuum chamber.

Martian dust storms will be simulated in a vacuum chamber using an impeller fan to propel dust particles to the velocity sensor. When the impeller fan is turned on the dust particles moving in the chamber will be charged triboelectrically. The Martian soil simulant is propelled towards the velocity/charge sensor. The charged dust particles passed through collimators will enter the cylindrical capacitor sensors as shown in figure 3.

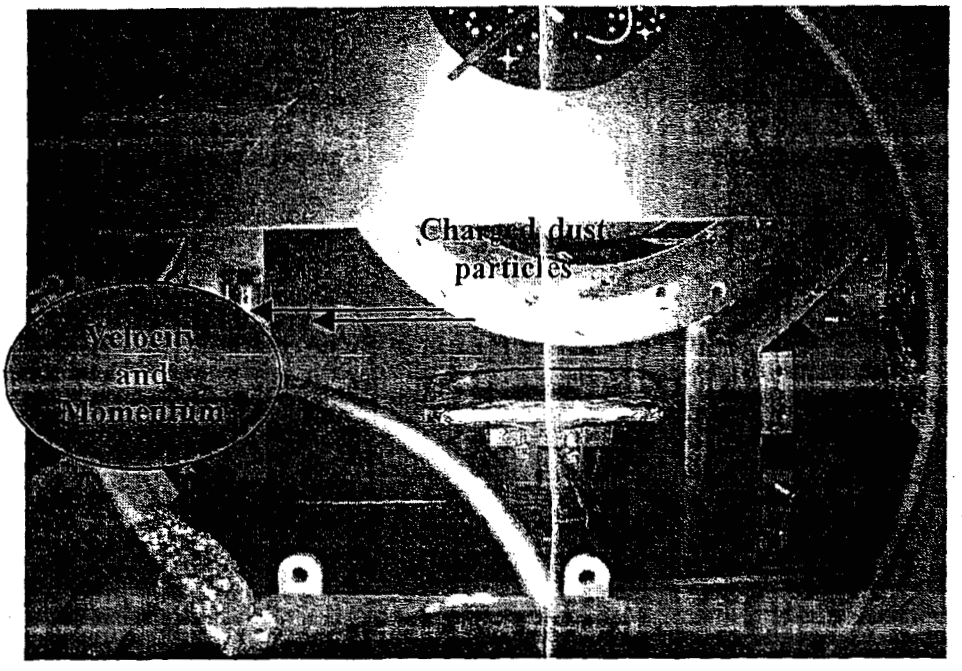

Figure 3. The velocity/charge sensor and dust impeller apparatus shown in the small vacuum chamber where experiments will be performed.

The windborne dust particles would pass through the sensor detecting cylinders. Data will be taken with the velocity sensor under conditions that attempt to simulate a Martian dust storm.

2.1 Momentum Sensor

Momentum sensor is utilizing the property of Piezoelectric Transducer (PZT) that changes the mechanical energy (crystal distortion due to stress applied) into electrical voltage. Figure 4 shows an incident particle with a momentum **P**. The particle impacted on the top plate of PZT produces a voltage output. By calibrating the momentum/voltage output, the voltage is translated into the impact momentum of the incident particle.

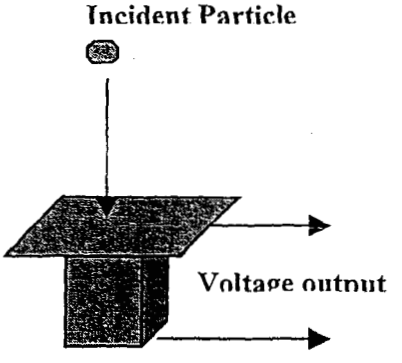

Figure 4. PZT Transducer

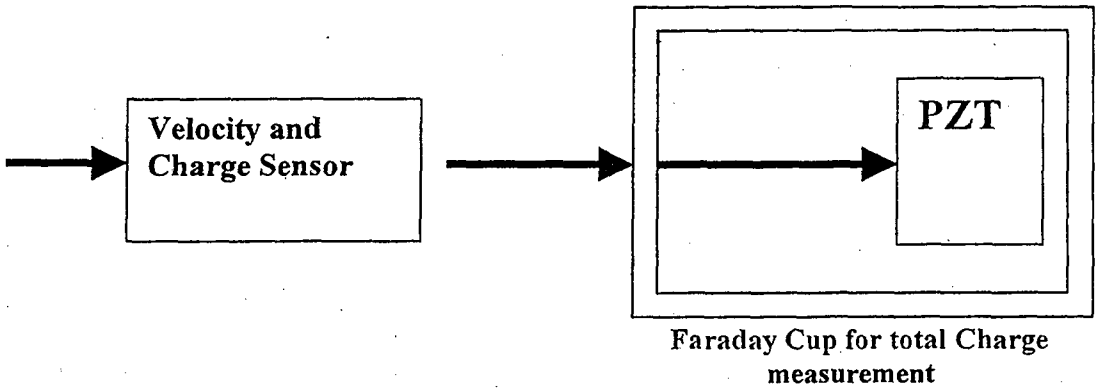

Figure 5. Charged dust particles pass through velocity/charge sensor will be collected by a Faraday Cup for total charge counts. The momentum of each particles is measured by a PZT sensor.

Knowing the momentum, $\mathbf{P = mV}$, we can calculate the mass of the incident particle. The PZT momentum sensor and the velocity/charge sensor are integrated into one unit for the dust particle mass, charge and velocity measurement.

3. DISCUSSION

The velocity/charge sensor is very simple, inexpensive to build and can be fabricated into a very small instrument to measure the velocity vector and charging of charged dust particles on Mars. The small cylindrical capacitor configuration with the amplifier has high input impedance. It is necessary to take extra care for noise reduction. A single dust particle source is needed to calibrate the velocity/charge sensor.

In the Earth atmosphere environment, the lower velocity limit for this design is around 4 to 5 m/s. Slower particles detection can be achieved by shortening the distance between the cylindrical capacitors, and/or increase the diameter of the cylinders. In the Martian atmosphere condition, due to a 0.38 g of Mars gravity, the lower limit of particle speed is approximately 1.5 m/s to 2.0 m/s. The upper limit of the particle velocity is controlled by the speed of electronics. The current design is capable to measure charged particle speed up to a few km/s. This sensor is designed to collect the information of speed distribution and charge distribution of Martian charged dust particles.

The Quartz Crystal Microbalance (QCM) has been widely used for micro-scale mass detection. The QCM is reliable and able to detect very small mass; however, the electrostatic adhesion of dust particles require an extra efforts to clean the detector. The PZT can be made very small. It has a fast response, simple design and very inexpensive. The PZT needs to calibrate for temperature and momentum/voltage sensitivity. We selected the PZT over QCM for the reasons that PZT handles the dust adhesion with better single response for single dust particle, and smaller physical size. The PZT sensor is capable of measuring the individual particle mass to collect the mass distribution of Martian dust particles and total charges over a given period of time.

4. CONCLUSIONS AND FUTURE WORKS

We designed the velocity/charge sensor with a few targets in mind (1) simple, (2) inexpensive to build, (3) the size can be very small, and (4) less problem of dust cleaning. Two

velocity/charge sensors have been fabricated for our laboratory analysis. The current tasks to improve these sensors are (1) electronic noise reduction, (2) miniaturize the sensor, and (3) improve collimation for single particle detection. A Grid Correction circuit to improve the single particle selection can be used. We are also doing research to select the best PZT to improve temperature drifting and momentum/voltage sensitivity.

We are planning to combine the velocity/charge sensor and the PZT sensor to form an integrated unit. The small size and expense of these two sensor type makes this unit easily form a detector array for better Martian dust characteristic study.

ACKNOWLEDGMENTS

I would like to thank Dr. Carlos Calle for inviting me to work with him on this project, and for all of the assistance and support he provided during my stay at NASA Kennedy Space Center. I would also like to thank Dr. James Mantovani, Dr. Charles Buhler, Andrew Nowicki, and Ellen Groop for their assistance during the course of the research. Finally, I would like to express gratitude to Dr. Tim Kotnour and Cassie Spears of the University of Central Florida for organizing the summer faculty program at KSC.

REFERENCES

[1] D. I. Kaplan, Environment of Mars, 1988, NASA Technical Memorandum 100470, 1988.

[2] J. Kolecki, and G. Hillard, Overview of Mars System-Environment Interactions, 27th AIAA Plasmadynamics and Lasers Conference, June 17-20, 1996, New Orleans, LA.

[3] A. Eugene, A. Avallance, and T. Baumeister, Sources and Control of Air Pollution, Mark's Standard Handbook for Mechanical Engineers, 9th edition.

[4] J. Gaiser, and M. Perez-Davis, Effects of Martian Dust on Power System Components, Sand and Dust on Mars, NASA CP-10074, 1991.

[5] D. Sentman, Electrostatic Fields in a Dust Martian Environment, Sand and Dust on Mars, NASA CP-10074, 1991.

[6] C. Buhler, and C. Calle, et al., Charge Decay Characteristics of the JSC Mars-1 Martian Regolith Simulant, 33rd Lunar and Planetary Science Conference. Houston, Texas, 2002.

[7] M. Siebert, and J. Kolecki, Electrostatic Charging of the Pathfinder Rover, AIAA 96-0486, 34th Aerospace Sciences Mtg & Exhibit, Jan 1996, Reno, NV.

[8] J. Chang, et al., Handbook of Electrostatic Processes, Chap. 9, 1995 by Marcel Dekker.

[9] H. Blennow, et al., Active High Voltage Insulation, J. of Electrostatics 55 (2002).

[10] O. Melnik and M. Parrot, Electrostatic Discharge in Martian Dust Storms, J. of Geophysical Research, VOL 103, NO. A12, December 1998.

[11] M. Buehler, L.-J. Cheng, O. Orient, M. Thelen, R. Gompf, J. Bayliss, J.Rauwerdink, "MECA Electrometer: Initial Calibration Experiments", Inst. Phys. Conf., Ser. No. 163, pp. 189-196, Proceedings of the 10th Int. Conf., Cambridge, 28-31 March 1999.

[12] M.G. Buehler, et al., "From Order to Flight in Eighteen Months: The MECA/Electrometer Case Study", IEEE Aerospace Conference, March 2000.

[13] J.G. Mantovani, "Evaluation of the Performance of the Mars Environmental Compatibility Assessment Electrometer", 2000 NASA/ASEE Summer Faculty Fellowship Program Final Report, July 2000.

2002 NASA/ASEE SUMMER FACULTY FELLOWSHIP PROGRAM

JOHN F. KENNEDY SPACE CENTER
UNIVERSITY OF CENTRAL FLORIDA

REMOTE LEAK DETECTION: INDIRECT THERMAL TECHNIQUE

Dr. Sandra Clements
Visiting Assistant Professor
Physics and Space Sciences
Florida Institute of Technology
Dr. Robert Youngquist

ABSTRACT

Remote sensing technologies are being considered for efficient, low cost gas leak detection. Eleven specific techniques have been identified for further study and evaluation of several of these is underway. The Indirect Thermal Technique is one of the techniques that is being explored. For this technique, an infrared camera is used to detect the temperature change of a pipe or fitting at the site of a gas leak. This temperature change is caused by the change in temperature of the gas expanding from the leak site. During the 10-week NFFP program, the theory behind the technique was further developed, experiments were performed to determine the conditions for which the technique might be viable, and a proof-of-concept system was developed and tested in the laboratory.

REMOTE LEAK DETECTION: INDIRECT THERMAL TECHNIQUE

Sandra Clements

1. INTRODUCTION

As currently performed, locating a gas leak is a time consuming, labor-intensive process. The Remote Leak Detection Project grew out of the desire to vastly improve the efficiency of this process. The project's goal is to reduce the cost of detecting hydrogen and helium leaks into air by at least an order of magnitude. To achieve this goal, several remote sensing techniques are being considered by NASA for application to gas leak detection [1]. The Indirect Thermal Technique is one such technique being considered. With this technique, an infrared camera would be used to detect the temperature change in a pipe or fitting at the site of a leak caused by the change in temperature of the gas as it expands from the site. The specific goals for the 10-week 2002 NASA/ASEE Summer Faculty Fellowship Program were to increase the Technology Readiness Level (TRL) for the Indirect Thermal Technique and to develop a proof of concept that would be demonstrated in a laboratory setting. To increase the TRL, it was necessary to further develop the theory behind the technique as applied to remote leak detection, to test and refine the theory via experiments, and to determine the range of conditions for which the technique is viable. Progress has been made toward each of these goals, though further work is needed.

2. THEORY

With the Indirect Thermal Technique, an infrared camera is used to detect the temperature change of a container at the site of a gas leak caused by the change in temperature of the gas as it expands during the leak. Thus, the theory underlying the technique involves thermodynamics and gas dynamics of the leaking gas as well as heat transfer between the gas, container, and detector.

Thermodynamics

A gas leak can be considered a thermodynamic process involving a system (the leaking gas) and its environment (the container and the ambient air into which the gas leaks). The variables that describe the state of the system are called the state variables. These include the pressure (P), volume (V), density (ρ), absolute temperature (T), internal energy (E_{int}), enthalpy (H), and entropy (S). Equations of state such as the perfect gas law PV = nRT (discussed later) describe the relationship between the state variables. Other variables are involved in transitions between thermodynamic states, but are not state variables. Heat (Q) and work (W) are two such variables. The three laws of thermodynamics governing thermodynamic processes [ref.2, Ch.1] are given below.

0^{th} Law: If systems A and B are in thermal contact and $T_A = T_B$, then the two systems are in equilibrium.

1^{st} Law: $dE_{int} = dQ + dW = dQ - PdV$ (1)

In this equation, dE_{int} is the change in internal energy of the system, dQ is the heat transferred to the system from the environment, and dW is the work done on the system by the environment.

$$2^{nd}\text{ Law: } \Delta S = S_B - S_A \geq \int_A^B \frac{dQ}{T} \tag{2}$$

The entropy S is a measure of the disorder in a system, Q is the heat, and T is the absolute temperature.

The first law indicates that if heat is added or removed from a system and/or work is done on or by the system, the internal energy of the system will change. This simply means that energy is conserved when a system changes from one state to another during a thermodynamic process. The first law does not say anything about the direction of thermodynamic processes. However, the second law does, limiting natural or spontaneous processes to those for which entropy is conserved or increases. Entropy is a measure of the level of randomness in a system. In a gas leak, order is converted to disorder as organized gas flow is impeded by viscosity and turbulence resulting in an increase in the entropy of the system.

It is often appropriate to consider a gas to be a perfect or ideal gas. For such a gas, the size of the gas molecules is negligible, collisions between gas molecules and with container walls are perfectly elastic (that is, no energy goes into deforming the molecules), and the molecules do not interact with each other. For such a gas, the perfect gas law is a valid equation of state [3].

Perfect Gas Law: $PV = nRT$ (3)

Here, P is the pressure of the gas, V is its volume, n is the number of moles of gas, R is the Universal Gas Constant (8.314 J/mol·K), and T is the absolute temperature in Kelvin.

However, at high pressures and low temperatures or at low pressures and high temperatures, gases deviate from the perfect gas law. In the low pressure, high temperature regime, molecules are subject to dissociation. In the high pressure, low temperature regime, intermolecular forces become important [ref.2, p.34]. The van der Waal equation [3] is an approximation often used for gases in the low temperature, high pressure regime.

van der Waal equation of state: $\left(P + a\left(\frac{n}{V}\right)^2\right)(V - nb) = nRT$ (4)

In this equation, a is related to the intermolecular attractive force between molecules and b is related to the size of each molecule. The intermolecular attractive force reduces the gas pressure for a given volume and temperature. The finite size of the molecules effectively reduces the volume in which the molecules move.

Of relevance to the problem of a leaking gas is the process followed as the gas goes from one state to another. The polytropic equation of state can be used to describe the thermodynamic process that a system follows in going from state A to state B [ref.4, pp.77-79].

Polytropic equation of state: $PV^n = const$ (5)

Here, n is the polytropic exponent. Many types of processes are possible. A constant temperature (isothermal) process, for example, has $n = 1$. A constant entropy (isentropic) process has $n = \gamma$ with γ being the adiabatic index. Combining the perfect gas law (3) and the polytropic equation of state (5), relationships between pairs of state variables can be formed. Of interest for this project is the relationship between the temperature and the pressure.

$$T_2 = T_1\left(\frac{P_2}{P_1}\right)^{\left(\frac{n-1}{n}\right)} \qquad (6)$$

The polytropic exponent in these equations depends on the type of process as well as on whether the process is reversible or irreversible. A reversible process is one in which equilibrium exists throughout the process. Equilibrium exists if there are no currents of heat, mass, or momentum. In such processes, entropy is conserved. Spontaneous processes are irreversible and in such processes entropy increases due to the currents of heat, mass, or momentum in the process [ref.2, pp.6-7].

A gas leak can be considered an adiabatic process. An adiabatic process is one for which no heat is transferred between the system and environment ($Q = 0$). An adiabatic process can occur when the system is insulated from its environment or when the process occurs too quickly for heat transfer to occur. With a gas leak, the process occurs too quickly for heat to be transferred. If the process were reversible, the polytropic equation $PV^{\gamma} = constant$ would apply with the adiabatic index γ depending on the gas. For diatomic gases such as nitrogen and hydrogen, $\gamma \cong 1.4$. For a monatomic gas such as helium, $\gamma \cong 1.67$ [ref.4, p.724]. Note that a reversible adiabatic process is an isentropic process ($n = \gamma$). When a perfect gas undergoes a reversible adiabatic expansion, its temperature will always decrease. For example, consider the expansion of nitrogen gas at $T_1 = 300K$ from $P_1 = 54.7psi$ to $P_2 = 14.7psi$. The temperature of the gas from equation (6) after expansion is $T_2 = 206K$ for a change in temperature of $\Delta T = -94K = -94°C$!

A gas leak, however, is a spontaneous, and thus irreversible, expansion process. For an irreversible adiabatic expansion, the polytropic index lies between 1 and γ. The more irreversible the process (i.e. the more entropy is generated), the closer the index is to 1, and the more closely the process resembles an isothermal (constant temperature) process.

Gas leaking through an orifice can be considered a throttling process in which the gas flow is impeded by a resistance. Because this process involves fluid flow, it is more appropriate to consider the enthalpy of the gas instead of the internal energy. The enthalpy of the gas is given by the following equation [ref.2, Ch.2].

Enthalpy: $H = Q + PV$ (7)

Like internal energy, enthalpy has units of energy.

Gas Dynamics

Because the gas flows through an orifice or crack when it leaks from its container, the state variables will vary throughout the flow and thus gas dynamics are important. The general equations that govern steady fluid flow are given below [ref.2, Ch.2]. Here, steady flow means that the masses of fluid passing any two cross-sections in the flow are equal.

Continuity Equation: $\rho u A = const$ (8)

Energy Equation: $q = h_2 - h_1 + \frac{1}{2}u_2^2 - \frac{1}{2}u_1^2$ (9)

Momentum Equation: $\rho_2 u_2^2 A_2 - \rho_1 u_1^2 A_1 = (p_1 A_1 - p_2 A_2) + p_m (A_2 - A_1)$ (10)

In the above equations, A is the cross-sectional area of the flow, u is the fluid speed, and p_m is the mean pressure.

For an adiabatic flow process, the energy equation (9) becomes $h + \frac{1}{2}u^2 = constant$. For a perfect gas, the equation relating the temperature in the upstream reservoir to the temperature in the orifice (throat) is $c_p T_2 + \frac{1}{2}u^2 = c_p T_1$. Using the sound speed of N_2 (353m/s at 300K) as the gas speed in the orifice, the temperature of the gas flowing through the nozzle is computed to be 240K for a temperature drop of 60K = 60°C from the upstream reservoir temperature of 300K! Again however, real gases are not ideal and the fluid flowing in the leak is not at equilibrium due to viscosity and turbulence.

The throttling process or Joule-Thomson process is an adiabatic process in which enthalpy is conserved as gas flows from one reservoir (where $u = 0$) into another [ref.2, pp43-44]. For a perfect gas, the enthalpy is a function of temperature only and $h = c_p T$. Thus, when a perfect gas undergoes a throttling process, enthalpy conservation ($h_1 = h_2$) implies temperature conservation ($T_1 = T_2$). However, real gases change temperature as a result of the throttling process. The Joule-Thomson coefficient μ can be used to relate the change in temperature to the change in pressure [ref.5, p.1-33].

Joule-Thomson coefficient: $\mu = -\frac{1}{c_p}\left(\frac{\partial H}{\partial P}\right)_T = \left(\frac{\partial T}{\partial P}\right)_H$ (11)

Note that if $\mu > 0$, the gas will cool upon expansion and if $\mu < 0$, the gas will become warmer upon expansion. Each gas has a characteristic temperature, the inversion temperature, below which the gas will cool upon expansion and below which the gas warms upon expansion.

Using thermophysical data published by the National Bureau of Standards (now the National Institute of Standards and Technology), the relationship between the change in gas temperature as a function of the pressure change experienced by a gas as it passes through an orifice (a throttle) was determined. Specifically, tabulated data for the enthalpy as a function of pressure at T = 300K were used to compute the Joule-Thomson coefficient (equation 11) for several gases [5, 6, 7, 8]. From this, the change in gas temperature ΔT as a function of pressure change ΔP experienced by the gas was computed. Empirically determined relationships were computed for nitrogen, oxygen, helium, and hydrogen. Nitrogen and oxygen are predicted to cool as they expand (N_2: ~-0.0143°C/psi, O_2: ~-0.0185°C/psi), while helium and hydrogen are expected to become warmer (He: ~+0.0043°C/psi, H_2: ~+0.0005°C/psi). At 300K, nitrogen and oxygen are below their Joule-Thomas inversion temperatures, whereas helium and hydrogen are above their inversion temperatures.

Note that the Joule-Thomson process relates gas properties in two reservoirs, yet reservoir conditions (flow speed equal zero) will not be met close to the site of the leak. In addition, a real gas leak will not be a truly adiabatic process since heat will be transferred between the gas and the walls of the orifice or

crack. Since the gas properties will vary as the gas flows through the orifice or crack, gas dynamics should be considered in more detail.

Heat Transfer

For the temperature of the container at the site of the leak to change, energy transfer must take place. The transferred energy is called heat. There are three forms of heat transfer – conduction, radiation, and convection. Conduction is the transfer of heat from molecule to molecule as kinetic energy is transferred via collisions. Radiation is heat transfer in the form of electromagnetic waves. Convection is the transfer of heat via motion of a group of molecules [ref.9, pp.1.1-1.6]. In a natural process, heat is always transferred from a region of high temperature to a region of low temperature.

Conduction

The general equation describing heat transfer via conduction and that describing the temperature as a function of position and time are given below [ref.10, pp.7 and 11].

General heat conduction: $$dQ = -kdA\frac{\partial T}{\partial n} \tag{12}$$

Here, dQ is the heat transferred to the surface element dA, T is the temperature, k is the thermal conductivity of the material, and n is the vector normal to dA. Good thermal conductors, such as metals, have high values for thermal conductivity. Poor conductors, such as gases and insulating materials, have low thermal conductivities.

General temperature relation: $$\frac{\partial T}{\partial t} = \alpha\nabla^2 T \tag{13}$$

In this equation, $\alpha = k/\rho c_p$ is the thermal diffusivity of the material, k is the thermal conductivity (assumed independent of temperature for this equation to be valid), ρ is the density, and c_p is the specific heat at constant pressure. This equation assumes no heat is generated within the material. Some special cases of interest are described below [ref.9, Ch.3].

Slab:

A slab of thickness l with walls at T_1 and T_2 approximates a container wall (or the insulation covering a container) having different inside and outside wall temperatures.

Half-Space:

A material of semi-infinite extent with an infinite planar surface is at an initial temperature T_{amb} considered to be the ambient room temperature. At time $t = 0$, the temperature of the planar surface is set to the constant value T_f. This case is an approximation to a leak from an approximately planar crack. When the leak begins, the temperature of the crack's wall is considered to suddenly change to the temperature of the gas flowing through the crack. Of course, more realistically, the wall temperature would vary with time.

Cylindrical hole:

Another relevant case is the cylindrical hole through a material of infinite extent. Again the initial temperature of the material is considered to be the ambient room temperature T_{amb}. At time $t = 0$, the temperature of the cylinder walls is set to T_f. This is an approximation for a leak through a circular orifice.

Equations for these special cases [ref.9, Ch.3] for the fractional temperature change with time and distance from the leak site were solved. It was found that the temperature changes much more quickly with time for a half-space (linear crack) than for a cylindrical hole. Also, a temperature gradient with distance exists near the leak site. The temperature gradient is steeper for the cylindrical hole than for the half-space.

Radiation

A blackbody is an ideal object that absorbs all radiation incident upon it and reradiates in all over a range of wavelengths according to Planck's equation [ref.9, pp.7.1-7.12].

Planck's equation: $$W_\lambda = \frac{2\pi hc^2}{\lambda^5 (e^{hc/\lambda kT} - 1)} \times 10^{-6} \left[Watt / m^2 \mu m \right] \quad (14)$$

In this equation, W_λ is the radiant emittance at wavelength λ (in meters), c is the speed of light (3×10^8 m/s), h is the Planck constant ($h = 6.6 \times 10^{-34}$ *J·s*), k is Boltzmann's constant ($k = 1.4 \times 10^{-23}$ *J/K*), and T is the absolute temperature in Kelvin. Integrating Panck's equation over all wavelengths yields the total emittance.

Total emittance: $$W = \sigma T^4 \quad (15)$$

Here, σ is the Stefan-Boltzmann constant ($\sigma = 5.7 \times 10^{-8}$ *Watt/m*^{2}). The wavelength at which the maximum emission occurs decreases as the temperature increases according to Wien's Law ($\lambda_{max} = 2898/T$ *microns*). (The shorter wavelength blue part of a flame is hotter than the longer wavelength yellow part of the flame.) Objects that are at room temperature emit most of their radiation at infrared wavelengths. Also, the hotter the object, the more radiation is emitted at all wavelengths. These factors indicate that small changes in temperature will result in large changes in the emittance over a specific wavelength regime.

Real objects are not perfect blackbodies. Instead they can be considered graybodies that are described by the equation below.

Total Emittance: $$W = \varepsilon \sigma T^4 \quad (16)$$

The emissivity ε varies with material ($0 \le \varepsilon \le 1$). Metals have very low emissivities and very high reflectivities ρ. For opaque objects like metals, $\varepsilon + \rho = 1$.

Convection

Natural convection occurs when a collection of molecules with relatively higher kinetic energy (and thus higher temperature) are buoyed to regions of relatively lower kinetic energy (and thus lower temperatures), transferring their energy in the process. Forced convection is the transfer of energy that occurs when there is forced fluid flow. Such would be the case within the orifice or crack for a gas leak unless the gas leak is extremely slow. The equation describing the convection of heat involving high-speed flows is given below [ref.9, pp1.4-1.6].

Convection: $$Q = hA(T_w - T_{aw}) \quad (17)$$

Here h is the convective heat transfer coefficient, T_w is the temperature of the surface (the wall of the orifice or crack), T_{aw} ($= T_f + ru^2/2c_p$) is the adiabatic wall or recovery temperature of the flowing gas, T_f is the gas (fluid) temperature, u is the speed of the gas, c_p is its specific heat, and r is the recovery factor (a number between 0.8 and 1 for most gases). Note that this equation is from the gas dynamic energy equation relating the temperature of a perfect gas in a reservoir to that in a flowing fluid. The value of h depends on the geometry, the temperatures of the gas and wall, as well as the temperature gradient within the gas.

In real processes, all three forms of heat transfer will occur. The temperature at each point within the material will no longer change once equilibrium is reached. Once equilibrium is reached, the net flow of heat across a surface equals zero. That is, $Q_{conduction} + Q_{radiation} + Q_{convection} = 0$. This equation will govern the final equilibrium temperature of the leak site. If convection can be neglected, much more heat is transferred initially via conduction than via radiation. When equilibrium is reached, conduction and radiation will balance.

3. EXPERIMENTS AND RESULTS

Camera Specifications

A FLIR Systems ThermaVision IRVM™ 320M infrared camera that is planned for deployment at the Shuttle Launch Complex was used. The camera is sensitive over wavelengths between 7.5μm and 13μm. The image is formed on a 320 × 240 pixel detector and has a field of view of 24° × 18°. To determine if a leak will be detectable with this camera, the minimum temperature change detectable is needed along with the camera's resolution. The manufacturer indicates that temperature differences of 0.1°C are resolved by the camera. Experiments were carried out that suggest that smaller temperature differences can sometimes, though not always, be detected using a technique described later.

The relationship, $d = 1.851\times10^{-3}x$ gives the minimum diameter d of the feature as viewed from a distance x. The constant ($\theta = 3.7\times10^{-3} radians$) is the angular size of an object that subtends a 2 × 2 square pixel section of the detector. A 2 × 2 square pixel region was chosen as the minimum area covered by an object that can be reliably detected. A single bright or dark pixel in an image may be due to a bad pixel, not an actual feature. (Of course, if the feature seen in only one pixel moves across the image as the camera is scanned, it can be considered a real feature and not a bad pixel.) From a distance of 0.5m (the camera's closest range), the camera would be able to detect features as small as ~2mm. From 100m, the camera would be able to detect features ~40cm across.

Proof-of-Concept System

In order to detect very small temperature differences, a procedure borrowed from astronomical image analysis was employed. Notice that the two images in Figures 1 and 2 appear practically identical. Both images show two fittings. One is connected via a hose and regulator to a K-bottle of gas. The other is sitting isolated on a plastic stand. Other metal posts are seen as well. Note that the metal appears very bright despite its low emissivity because it has such a high reflectivity and thus reflects nearby thermal sources (including the researcher). One image was made prior to a gas leak and the other during the gas leak. It is not possible to determine which fitting has the leak from a comparison of these two raw images. By producing difference images, very small temperature changes can be detected. Two images are subtracted pixel by pixel to produce a difference image. If all objects in the image maintain a constant temperature between the two images, the difference image will appear featureless. All objects will vanish.

If instead an object cools between the two images, the object will appear darker in the difference image than objects that have not changed temperature. If the object warms between images, it will appear brighter in the difference image than objects that have not changed temperature. Figure 3 shows the difference image made by subtracting a pre-leak image from an image made during the leak. Inspection of the difference image shows that only the fitting on the right experienced a change of temperature, cooling during the leak. All other objects remained at their pre-leak values and thus they do not show up in the difference image.

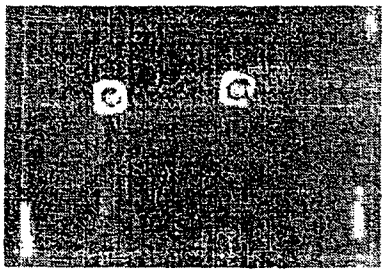

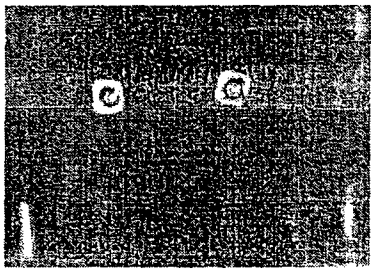

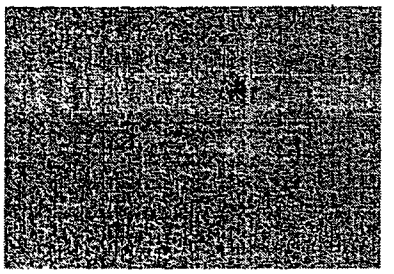

Figure 1 – Raw pre-leak image. Figure 2 – Raw image during leak. Figure 3 – Difference image.
(Leaking – Pre-leak)

Numerous steps were involved in producing the difference images. The camera was connected to a monitor that, in turn, was connected to a DVD recorder. DVD recordings of experiments were made. Images were grabbed off of the DVD recorder and saved as bitmap files using a National Instruments® LabVIEW program written by Dr. Christopher Immer of Dynacs. Off-site, these bitmap files were converted to FITS file format and analyzed using the Axiom Research® Mira AP_{TM} image analysis software. In the field, the system would need to be much less labor intensive and should work in real time. For this reason, Dr. Christopher Immer was asked to write a LabVIEW program that would produce difference images in real-time by subtracting images being acquired from the camera (or DVD) from a stored reference image of the scene made in the absence of leaks. The reference image is displayed along with continuously updated raw acquired images and difference images. This LabVIEW program would need some minor adjustments to perfect it for use in the field. It was, however, used and shown to be effective on recorded images acquired from the DVD.

Experiments

A number of experiments were carried out using K-bottles of pressurized gas. Two different fittings were used in these experiments. One fitting had a small (0.010in diameter) hole drilled in the center of a metal plate at its end. This *end-hole fitting* was attached to the end of the hose from the regulator and impeded the flow of gas through the hose. Another fitting had a somewhat larger hole (0.025in diameter) drilled into its side. This *side-hole fitting* connected a small section of pipe to the hose, extending the length of the hose.

Nitrogen

In one experiment, nitrogen gas was allowed to flow under pressure through the end-hole fitting. Experiments were run for various pressure differences. The change in temperature as a function of time near the site of a leak was measured using a thermoelectric temperature probe. The temperature decreased with time as expected for heat conduction associated with a cylindrical hole.

In addition, the temperature change of the metal near the leak site varied as a function of pressure change, decreasing by less than a degree even with $\Delta P = 50$psi. The observed results for the metal are in fairly good agreement with the predicted results for the gas obtained using the Joule-Thomson coefficient and assuming a throttling process. Certainly, the observed results are in much better agreement with the throttling process predictions than they are with the predictions made assuming static, reversible, adiabatic expansion ($\Delta T \sim -100°C$) or with predictions made by equating reservoir enthalpy with enthalpy plus kinetic energy of the flow within the orifice ($\Delta T \sim -60°C$).

Because a real gas leak will likely have gas in the pipe flowing perpendicular to the gas flowing from the leak site, the side-hole fitting was used. The gas flowed from the hose through the fitting into the pipe. The gas was allowed to flow freely within the pipe and some leaked out of the hole. The temperature of the metal near the orifice (~1-2mm away) was measured. The change in temperature that was measured was comparable to that observed using the end-hole fitting.

The end-hole fitting was used to direct a leak toward the back (unseen) side of External Tank Insulation. A temperature change was noted where the gas flowed around the edges of the insulation. When a hole was pierced through the insulation and the gas directed into the hole, the results were unexpected. A hot spot would appear in raw images when the leak first started. Occasionally the hot spot was absent entirely. Usually, it appeared, sometimes persisting and sometimes quickly dissipating. A 4.2°C temperature rise was observed at one point (as measured by the infrared camera). This hot spot is likely caused by a shock front where the high speed gas from the orifice is drastically slowed and compressed within the hole in the insulation. After the hot spot dissipated, the insulation cooled off at the site of the leak as discovered examining difference images.

Because insulation has a much lower thermal conductivity than metal, the temperature gradients from the leak site are steeper for insulation than for metal. Thus hot or cold features appear much more compact on insulation than on metal.

Additional experiments were carried out using the boil-off from liquid nitrogen as a source of very cold gas. When a hole was pierced into a piece of insulation with cold gas behind it, the hole would appear darker as the cold gas flowed into the hole, cooling the insulation at that spot. Another experiment was performed to see if a cold gas impinging on the back of a slab of insulation would be detectable from the other side of the insulation. A weak flow of cold nitrogen gas boil-off was directed toward the back of a piece of ET insulation and observed with the IR camera from the other side. The leak was detectable through 3cm thick ET insulation even without using the difference imaging technique. The leak was not detectable through 3inch thick ET insulation despite using the difference imaging technique. However, leaks of colder gases may be detectable even through thicker insulation.

Helium

The experiments using the end-hole fitting were performed using helium as the leaking gas. The temperature was measured to decrease. This observation conflicts with predictions of a temperature increase based on the conservation of enthalpy in an adiabatic throttling process. When the leak was from the side-hole fitting, the temperature near the fitting (~1 – 2 mm) was observed to increase ($\Delta T < 1°C$). The observed temperature change as a function of pressure change is in fair agreement with the predicted values using the Joule-Thomson coefficent and assuming a throttling process. However, different images of these experiments show a cold spot at the site of the leak, not a hot spot as was measured by the temperature probe. The temperature of the pipe was measured to increase and is seen to become brighter

during the leak process. Perhaps this heating is due to the friction between the gas and the pipe walls. Or, perhaps it is due to heating caused by expansion of the gas from the high pressure side of the regulator to the low pressure side ($\Delta P \sim 1500$psi).

The temperature probe was placed in the path of the flow near the end-hole fitting. When the flow is impeded by the temperature probe, the stagnation temperature is measured. That is, the temperature inside the reservoir where the flow rate is zero is measured because the gas is compressed to its reservoir conditions. The temperature increased very slightly for the gas leaking from the end-hole fitting (~0.2°C). In contrast, the measured temperature decreased dramatically (~6 - 8°C within a few seconds) when the temperature probe was placed in the flow escaping from the side-hole fitting. These results suggest that the stagnation temperature for the freely flowing gas is lower than for the gas impeded by the end-hole fitting. The gas dynamic energy equation (9) indicates that enthalpy is reduced from its reservoir conditions when gas is flowing. Perhaps the reduced enthalpy corresponds to a decrease in temperature below reservoir conditions for the flowing gas. Indeed this would be the case for a perfect gas.

More theoretical work is needed to better understand the temperature behavior of a gas expanding from a leak site. Specifically, the thermodynamics and gas dynamics of the flow through the orifice or crack need to be more thoroughly investigated.

4. CONCLUSIONS

Theoretical progress was made toward describing the temperature of the leaking gas via the laws of thermodynamics and gas dynamics. A gas leak is considered a throttling process with the non-ideal gas flowing through a resistance from one reservoir into another. Depending on the gas, the temperature of the gas can increase or decrease with expansion. Experiments are in fairly good agreement with theory, though there are still some perplexing issues to be addressed. To make further progress toward understanding the temperature within the flow through the leak site, gas dynamics need to be considered more carefully. The theory describing the heat transfer between the gas and the container wall was considered. Neglecting convection, conduction is a far more important heat transfer mechanism than radiation when the leak first begins, though over time equilibrium will be approached for which there will be balance between conduction and radiation. The convection will be forced convection of the fluid flow and should be considered in more detail. It was not considered in detail here because of the uncertainly of the value for the convective heat transfer coefficient. This coefficient is experimentally determined for specific situations.

The image analysis technique of difference imaging was applied to images from the infrared camera, allowing detection of temperature changes that would otherwise be lost in the background noise. A prototype system was developed that uses LabVIEW to generate these difference images in real time. Such a system should allow for on-the-spot detection of small temperature changes caused by a leaking gas. (This LabVIEW application was written by Dr. Chris Immer of Dynacs.)

Experiments suggest that the Infrared Thermal technique would be viable when large leaks are present through an uninsulated metal pipe or fitting. These leaks however would likely make their presence known in other, more obvious ways. Leaks of cryogenic material may be detectable when the leak site is covered with insulation. If the leaking gas flows through a hole or crack in the insulation, the hole or crack will appear much cooler at the leak site. Even without a hole or crack in the insulation, the insulation near the leak site may cool by a detectable amount. The thinner the insulation, the more likely it

will be to detect the leak. Also, leaks of cooler cryogens are more likely to be detected through thicker insulation.

REFERENCES

[1] Seller, R. Glenn and Wang, Danli, "Assessment of Remote Sensing Technologies for Location of Hydrogen and Helium Leaks. Phase 1 Final Report", NAG10-0290, 2001.

[2] Liepmann, H. W. and Roshko, A., "Elements of Gasdynamics", Dover Publications, Inc., New York, 1985.

[3] Vawter, Richard, "Van der Waal's Equation of State", http://www.ac.wwu.edu/~vawter/PhysicsNet/Topics/Thermal/vdWaalEquatOfState.html, 2002.

[4] Black, William Z. and Hartley, James G., "Thermodynamics", Harper and Row, Publishers, New York, 1985.

[5] McCarty, R. D., Hord, J., and Roder, H. M., "Selected Properties of Hydrogen (Engineering Design Data). NBS Monograph 168", U. S. Department of Commerce/National Bureau of Standards, 1981.

[6] Strobridge, Thomas R., "The Thermodynamic Properties of Nitrogen from 114 to 540°R Between 1.0 and 3000 PSIA. Supplement A (British Units). NBS Technical Note 129A", U.S. Department of Commerce/National Bureau of Standards, 1963.

[7] McCarty, Robert D., "Thermophysical Properties of Helium-4 from 4 to 3000 R with Pressures to 15000 PSIA.NBS Technical Note 622", U.S. Department of Commerce/National Bureau of Standards, 1972.

[8] Roder, Hans M. and Weber, Lloyd A., "ASRDI Oxygen Technology Survey. Volume 1: Thermophysical Properties", NASA SP-3071, 1972.

[9] Rohsenow, Warren M., Hartnett, James P., and Cho, Young I., "Handbook of Heat Transfer, 3rd. Edition", McGraw-Hill, New York, 1998.

[10] Eckert, E. R. G. and Drake, Jr., Robert M., "Analysis of Heat and Mass Transfer", Hemisphere Publishing Corporation, New York, 1987.

2002 NASA/ASEE SUMMER FACULTY FELLOWSHIP PROGRAM

JOHN F. KENNEDY SPACE CENTER
UNIVERSITY OF CENTRAL FLORIDA

IMPLEMENTATION OF AUTONOMOUS CONTROL TECHNOLOGY FOR PLANT GROWTH CHAMBERS

Thomas A. Costello
Associate Professor
Biological and Agricultural Engineering Department
University of Arkansas

John C. Sager
Agricultural Engineer, NASA-KSC

Valdis Krumins
Biological Engineer, Dynamac Corp.

Raymond M. Wheeler
Plant Physiologist, NASA-KSC

ABSTRACT

The Kennedy Space Center has significant infrastructure for research using controlled environment plant growth chambers. Such research supports development of bioregenerative life support technology for long-term space missions. Most of the existing chambers in Hangar L and Little L will be moved to the new Space Experiment Research and Processing Laboratory (SERPL) in the summer of 2003. The impending move has created an opportunity to update the control system technologies to allow for greater flexibility, less labor for set-up and maintenance, better diagnostics, better reliability and easier data retrieval. Part of these improvements can be realized using hardware which communicates through an ethernet connection to a central computer for supervisory control but can be operated independently of the computer during routine run-time. Both the hardware and software functionality of an envisioned system were tested on a prototype plant growth chamber (CEC-4) in Hangar L. Based upon these tests, recommendations for hardware and software selection and system design for implementation in SERPL are included.

IMPLEMENTATION OF AUTONOMOUS CONTROL TECHNOLOGY FOR PLANT GROWTH CHAMBERS

Thomas A. Costello
John C. Sager
Valdis Krumins
Raymond M. Wheeler

1. INTRODUCTION

1.1 Background

Human space missions require facilities for ongoing supply of clean water, oxygen and food (and the removal of carbon dioxide). Although these resources can be Earth supplied on short duration and/or short distance missions, the high cost of re-supply during longer, more distant missions will require other options such as bio-regeneration or manufacture from local planetary material. Bioregeneration involves use of living systems (crop plants, algae, small animals, microbes) to provide net photosynthesis to maintain oxygen and carbon dioxide balance for the crew, as well as providing clean water, food and nutrient recycling to offset needs for resupply. Wheeler (1996) estimated that plant growth chamber facilities having 40 m^2 of planted crop per crew member could provide major food requirements and provide oxygen for human needs as well as oxidation of all organic waste (and potential for nutrient recycling). Drysdale and Finger (1997) provided a conceptual basis for considering bioregeneration with only partial closure of the food, oxidation and recycling loops. Decisions regarding overall system design and the need and cost of re-supply can be analyzed using an equivalent system mass approach (Levri et al., 2000).

Continued research is needed to quantify the mass balances of food crop production grown in enclosed chambers to simulate long-term space missions. The efficiency and rate of biomass accumulation and the fraction of biomass that is edible will directly impact the size of bioregenerative systems and the need and cost of partial resupply from Earth or local planetary resources. Methods of nutrient recovery and re-use need to be tested as well to identify microbes and plants which optimize these processes (e.g., Garland et al., 1993; Mackowiak et al., 1996).

On-going research in bioregenerative life support involves operating controlled biological reactors for plant growth, aerobic solids decomposition (in-vessel composting), aerobic liquid waste decomposition (membrane and other bioreactors) and other specialized systems. In such systems, not only is it necessary to control environmental process variables in order to express reproducible treatment effects, but often the environmental variables are targetted at levels intended to simulate some space-based system (shuttle, space station, planetary outpost). For example, light spectral quality and flux density as well as atmospheric pressure may be adjusted to investigate possible plant growth characteristics in a Martian greenhouse environment.

Biologists and engineers who develop bioregenerative life support experiments may be constrained by the level of complexity required to configure, control and monitor living systems in the laboratory. Hardware and software are used to process electronic signals from various sensors, compare existing conditions to some predefined standard and then make decisions to adjust/operate/deactivate various control devices (such as pumps, fans, valves, relays, etc.). In the past, these functions required significant design effort from a biological engineer and on-going support from an instrument technician. Newer hardware and software options can decrease the technical overhead so that an engineer and technician can provide

support for more experiments and investigators can take a more direct role in designing an experimental methodology and subsequent data recording. More powerful, customized software may empower a scientist to conceive and implement an experimental protocol that was previously passed over due to technical constraints. A new generation of control and data recording hardware and software has the potential to decrease costs, increase reliability, improve information quality and potentially lead to new discoveries.

At NASA-KSC, the Bioregenerative Life Support research programs are operated as part of the Biological Sciences Office under the Spaceport Technology Center. Existing plant growth chambers (and other experimental biological systems) function under the direct control of a central work station computer, using NASA-written custom software (Universal Data Acquisition and Control Engine, UNDACE). The established procedures for replication of routine experiments using UNDACE operate efficiently and reliably. However, the intellectual property that UNDACE represents is rapidly becoming devalued because of attrition of technical staff who had the specialized knowledge required to maintain the software and hardware. New configurations and control suites are not attempted due to this uncertainty. The expected move of the growth chamber complex to SERPL in 2003 underscores the need to replace UNDACE and the associated hardware with an alternative system which requires less specialized technical support that can be maintained over the next decade of biological research.

Concepts for an improved control and data recording methodology include the following features:

1) Use of autonomous control modules which do not require continuous interaction with the supervisory computer (in order to better maintain control during periods of disrupted communication).
2) Backup control capability existant in commercial chambers, which can take over to prevent catastrophic experiment failure (death of plants or microbes in a reactor) should the customized, external control fail.
3) Communications using ethernet connections to provide simplicity in wiring and extend possibilities for better process monitoring by investigators from any workstation.
4) Capturing and making real time data available for web-based applications using XML or other technologies which are platform independent. These capabilities will increase the efficiency of data analysis and increase the extraction of knowledge from the research. It will also promote potential utilization of research results by clientele outside NASA, including potential educational web-sites for K-12 students interested in following on-going space-based biological experiments.
6) Providing a suite of software tools that allow rapid configuration and interfacing between chamber equipment and control modules so that a biologist with minimal technical support can devise and implement innovative experimental protocols.
7) Supplementing the graphical interface associated with UNDACE with improved visual displays that promote on-going human observations of experimental conditions. Better visualization means more power to detect irregularities associated with equipment malfunctions. Moreover, scientists often extend their systemic knowledge when interesting phenomena become visible. There is real potential to pull more knowledge from each experiment using an improved human-machine interface.

Specifically, a proposed strategy would include the use of programmable logic controllers (PLC's; model SNAP-B3000-ENET and associated modules, OPTO 22, Temecula CA) connected through an ethernet connection to a PC running supervisory software developed using a graphical programming language (LabVIEW, National Instruments, Austin, TX). The PLC's can operate independently with periodic

communication with the PC for data recording and to provide the human-machine interface. The SNAP hardware had been used to control and monitor other experiments in Hangar L, but the specific module needed for temperature control in a plant growth chamber (SNAP PID Module) and interfacing using LabVIEW had not been attempted.

1.2 Objective

The objective of this research was to test the functionality of SNAP-B3000-ENET hardware and a LabVIEW-based user-interface for controlling and monitoring advanced life support experiments, specifically by testing a protoype system for a plant growth chamber. Following development and testing, results and recommendations will be made to NASA regarding future system development for the SERPL facilities.

2. METHODS

2.1 Hardware System Prototype

The prototype growth chamber (Figure 1) was located in Room 210 of Hangar L at KSC and designated 'Controlled Environment Chamber 4' (CEC4). The chamber (model M-12, EGC, Inc., Chagrin Falls, OH) is a reach-in chamber having a growing area of 1.4 m x 0.9 m to accommodate 8 hydroponic trays, each 80 cm x 13 cm. The chamber is currently set up to handle nutrients solutions for 4 treatments separately. Nutrient solution pH is monitored using pH probes and controlled through the addition of acid (HNO_3) using commercial pH controllers (model PHCN-37, Omega Engineering, Stamford, CT). There are 3 lighting banks that can be selected: "1/3FL" consisting of 7 fluorescent tubes (F48/T12/VHO/CWF), "2/3FL" consisting of 13 of the same tubes, and "HPS" consisting of 4 high pressure sodium lamps (400 W, G.E. Lucalux). The banks can be used individually or in combination on a selected diurnal time schedule. Current studies have used the HPS lights only with a typical photoperiod of 18 hours of light per day with an average intensity of 350 $\mu mol\ m^{-2}\ s^{-1}$ PPF. An integrated heating/cooling refrigeration unit was used to circulate conditioned air through the chamber to maintain the desired chamber air temperature, with supply air temperature regulated by a hot gas bypass valve (Barber-Coleman) which was actuated with a 6-9 VDC analog control signal. Separate units for dehumidification and humidification were actuated using on/off relay control as needed to maintain a desired humidity level. The CO_2 concentration in the chamber was monitored and controlled to a target level using the existing UNDACE system.

The integral controller (model TC2) provided by the manufacturer of CEC4 uses a proprietary algorithm for proportional-integral-derivative (PID) control and usually controls chamber temperature with a ripple of about 0.3 °C amplitude. External control using UNDACE (and later using SNAP-B3000-ENET or "PLC" modules) was effected using a bank of double-throw relays to re-route control signals to the equipment via either the EGC controller or the PLC modules. A selector switch was installed to allow the operators to manually revert to EGC control if the computer or PLC's needed servicing. The wiring panel (Figure 2) used with the PLC's housed the power supply (24 VDC), thermocouple transmitter (to convert thermocouple output to a linear 2-10 VDC output roughly calibrated to a temperature of 0-100 °C) and a bus containing the individual PLC modules. For CEC4, we used the SNAP-B3000-ENET brain module, two SNAP-ODC-SNK digital output modules, two SNAP-AIV-4 analog input modules, and one SNAP-PID module. The wiring panel was connected to the chamber using multiconductor cable terminated with DB-25 connectors. A cable drop (Category 5, 4-twisted pair) was connected to the brain for ethernet communications. All of the control equipment was powered through an uninterruptable power supply. The chamber equipment was wired on a special panel which coulld be powered by emergency generator if

local power was interrupted.

After installation of the SNAP hardware and connection of sensors and control wires to the chamber, the parameters of the control algorithm PID module were adjusted to attain the 'best' control response. The adjustment procedure, called 'tuning' followed the so-called Ziegler-Nichols Closed Loop Method which involves a directed sequence of trials in which parameters were varied, response was observed, measurements made of the response and then a new set of parameters was tried. Due to poor documentation from the PID module manufacturer, this process was tedious and time consuming (required about 60 hours).

2.2 Software System Prototype

A limited user-interface for the CEC4 was programmed using LabVIEW (Full Development System). The functions that were included in the interface included: a) real time visual display of data (individual digital and analog indicators for key variables, banks of switches and lights for digital outputs and logical states), b) a time-moving strip chart graph that can display multiple traces (for multiple variables) on the chart, and c) dialog boxes to display/change/update the various setpoints for the control logic. The software product, a virtual instrument (VI) named MainOPTOMonitorChange.VI called several sub-VI's, as shown in Figure 3. The strip chart recorder display and other indicators were configured from control elements included in the LabVIEW package, as were various dialog boxes associated with the main VI.

Communication between the VI and the PLC's was accomplished using two methods. To get data, a VI was configured to poll an XML data file that had been uploaded to and serviced by the PLC brain module. Individual data items were extracted using an XML parser (an Active-X class of procedures named MSXML2.IXMLDOMDocument2, available free from microsoft.com). Unfortunately, the existing PLC firmware did not support memory-write capability using XML, so parameter updates were written to the brain's memory using another Active-X class, named OptoSnapIoMemMapXLib.IO22SnapIoMemMapX, which was supplied by the PLC manufacturer.

Due to time constraints, it was not feasible to attempt to program functions for configuring the PLC's and to record data. These functions were accomplished using existing OPTO-22 configuration web-pages and an exisitng custom data recording program (written using Visual Basic, collected data from the brain using a streaming data socket and stored data in a text file), respectively. Additional capabilities are still required to implement a fully automatic supervisory control, including error-checking, alarming, and integrated achival of quality-checked data.

3. RESULTS AND DISCUSSION

3.1 Autonomous Control

In general, results from these tests, combined with earlier experience using the OPTO SNAP-B3000-ENET in other experiments in Hangar L, indicated that the hardware was robust in terms of extended periods of autonomous operation in the laboratory environment, with modules operating as expected. However, the PID module performance was disappointing.

Under nominal conditions, UNDACE and the EGC controller were able to control chamber temperature with a deviation of about $\pm$ 0.5 °C and $\pm$ 0.3 °C, respectively. With the OPTO-SNAP-PID module, control was more variable sometimes ranging $\pm$ 0.5 °C and then unexpectedly shifting to a different waveform having a range of $\pm$ 1.0 °C, see Figure 4. Other times, the OPTO module was observed to control at $\pm$ 0.2 °C for a short period of time (data not shown), but this desired behavior would disappear

following some routine perturbation (like lights coming on or the door being opened).

It is not clear that the tuning procedure attained the optimal set of PID parameters. The module documentation and accompanying software tools contained conflicting terminology, units, errors and a great deal of ambiguity. A normally straight-forward tuning procedure actually became more of a trial and error procedure, because of these uncertainties, with infinite possible combinations of the PID parameters potentially to test. There is a major concern about the reliability of the module's internal program, particularly relating to implementation of the derivative control parameter in the PID algorithm. These concerns were shared by another NASA engineer who tested the module independently and urged caution about using the SNAP-PID module (Curtis Ihlefeld, electrical engineer, NASA-KSC, personal communication, July, 2002). These deficiencies seemed to be purely analytic (involving the internally programmed logic, documentation and interface software) and did not seem to involve hardware/instrumentation; therefore, it is possible that a future firmware/software upgrade could provide a remedy.

The SNAP-B3000-ENET brain uses Digital Events, Alarms and Timers as formal structures to define the control logic. Defining, coding and documenting logic using these structures is very tedious and prone to error, which leads to the need for significant debugging. In general, the SNAP system provided flexibility to perform the desired control functions. However, there is no provision for control events to be triggered by PC clock-time (events can be triggered only by elapsed time referenced to some previous event). This requires a tedious process to synchronize control cycles to clock time and human work schedules. This can be done manually on a periodic basis or it could be programmed to occur automatically within the supervisory software.

3.2 Supervisory Software

A limited software system that provides the human-machine interface was developed using LabVIEW. Analog, digital and strip chart displays were developed which provide adequate visual representation of the chamber processes to a scientist, engineer or technician. A sample of the real time display is shown in Figure 5. The displays utilize visual control components from the LabVIEW package and provide a distinct improvement in visual quality of the display, compared to the UNDACE system. These controls are easy to include in an interface; however, customizing the controls is difficult because most object properties are poorly documented in LabVIEW. An experienced LabVIEW programmer will gradually learn to adjust the controls as needed, but only through significant investment in a trial and error process. This may not be an issue if the interface is designed and maintained by an experienced LabVIEW programmer; however, if future modifications are intended to be made by in-house technical staff then special training may be required.

The interface was developed in about 80 hours by an engineer with considerable conventional programming experience (including Visual Basic) and some prior exposure to another graphical programming environment (but with no direct LabVIEW experience). Understanding the basic LabVIEW scheme and implementing simple single-process programs (or virtual instruments, VI's) was accomplished fairly quickly. Programming a more complex system (with multiple sub-VI's) was tedious and frustrating due to poor documentation of methods and properties. The system includes multiple examples but they are not linked directly to the context-sensitive help. Progress in development often occurred by guessing how it might be accomplished and then trying multiple alternatives until one actually worked.

The LabVIEW system seems particularly unsuited to building a user-interface for on-going

monitoring/data-recording of a process. Since processing in LabVIEW is data driven, and there can be multiple threads of code running in parallel, it is difficult to coordinate and respond to user input with predictable and satisfactory results. For example, a menu editor can be used to develop a menu structure, but the events triggered as the user navigates the menu are difficult to control. Sub-VI's that pop-up in response to mouse-clicks won't always stay or disappear as needed. Clicking a button in a sub-VI may not be processed in a sequence as expected. Again, a more experienced LabVIEW programmer may be able to work this out, but it is not a natural consequence of the LabVIEW architecture. A programmer using Visual C or Visual Basic could accomplish the functionality of responding to user mouse-clicks much quicker and more reliably.

The LabVIEW interface worked well in interacting with external program libraries (Active-X classes of sub-programs). Establishing a reference to the class, performing methods and changing properties were straight-forward. The LabVIEW documentation suggested that VI's could be compiled, packaged as Active-X components, and able to be called by other software. This was not tested because the Full Development package did not support creating a stand-alone file version of a VI. Assuming this was possible, one might use Visaul Basic to develop the user-response framework (menus and dialog boxes) to call LabVIEW VI's to display data within various windows on the screen.

Because of the extended development time required for the real-time display and parameter change functions, other functionality that should be included in a supervisory control package was not attempted. The functions not tested included: a) the process of configuring PLC modules and control regimes for a new experiment, b) the ability to define and implement a data recording session, c) the process of checking data for errors in case of failure in the chamber equipment or PLC's, and d) a method for archiving error-checked data in a format easily accessible by the scientists.

4. CONCLUSIONS

General comments regarding the performance and suitability of both OPTO-SNAP hardware and LabVIEW for this application, based on these tests, were listed in the discussion above. Specific recommendations for monitoring/control/data-recording in SERPL are listed here.

1) Further testing is needed to insure that the OPTO-SNAP-PID Module is a reliable controller for experiments in which cost of temperature control failure is high. Efforts should be made to work with the manufacturer to establish the accuracy of the PID algorithm. Alternatively, another PLC manufacturer may be sought, but this would necessitate movement to a completely new hardware system which would negate the expertise already established within Hangar L staff in supporting the OPTO modules. In its present configuration, the OPTO-PID module is not recommended.

2) Testing of prototype systems is needed to apply PID modules to the control of CO_2 and humidity. The CO_2 control actuation could be identical to that used at present with UNDACE with gas valves controlled by a PID module in time-proportional mode. Time proportional control could also work to control humidity. The current control algorithm for humidity is a simple on/off control with set points and an arbitrary on-time and subsequent wait-time. Time-proportional control would be more stable. In addition, because of the impact of the dehumidification processes on the sensible heat of the air mass, and because sensible heating lowers the relative humidity, the controls for air temperature and relative humidity appear to sometimes work against each other. A more stable control for humidity might be obtained using

a set point for absolute humidity (or vapor pressure) associated with the set point temperature, rather than targeting a specific relative humidity. This would require calculation of the vapor pressure based on dry bulb temperature and relative humidity (or by selecting a different sensor which provides a direct indicator of absolute humidity, such as a dew point hygrometer). At present, there is no direct way to use the SNAP hardware to make these calculations in an autonomous mode to provide a dynamic measure of the process variable (vapor pressure). Alternate hardware might have the capability to perform user-specified and uploaded calculations within the PID algorithm.

3) It is recommended that OPTO upgrades be sought that will provide support of XML communications with the brain in both the read and write modes. This would simplify the communications and increase the access to the data and machines in the future.

4) A dedicated work station will be needed to provide continuous supervisory control and to record and archive data. For best operator performance, it is suggested that a large screen be installed to provide real time display, located near the chambers themselves. Because of the ethernet connection, investigators can monitor and adjust processes from other locations on the network by running the software on a local PC.

5) User interface design should build on the successful results using UNDACE. Users are generally satisfied with the interface. Changes should be carefully considered to insure that an improvement is actually made. Changes that increase the flexibility and ease of use without sacrificing any current functions should be sought.

6) Data recording processes should include not only the dynamic chamber variables, but should also provide a log of the current control parameters and indicate when changes are made.

7) There is a need to develop a formal protocol for sensor maintenance and calibration, with appropriate staff assignments and budget to get this done.

8) It is suggested that a comprehensive documentation library be developed, including inventories of equipment, wiring diagrams, software source code (with comments) operating procedures, trouble-shooting guides and maintenance schedules and procedures.

9) It is recommended that LabVIEW product upgrades or alternative software be selected for development of the permanent user-interface. LabVIEW seems to be valuable for developing screen displays, but other programs might be more efficient in controlling user interaction (menus, dialog boxes). Experienced consultants may provide guidance for the most efficient combination of software development tools.

10) Permanent user-interface design should be preceded by a detailed definition of the flexibility needed by users in configuring future systems, in terms of new hardware, new control schemes and new data recording schedules. It should be decided if the interface will provide for these changes or if new source code will be required. Also, it should be defined how much technical expertise will be required to make future modifications to start a new suite of experiments. These decisions will impact greatly the architecture of the new software.

REFERENCES

[1] Wheeler, Raymond M. Gas balance in plant-based CELSS. In: H. Suge (ed.) Plants in Space Biology, pp. 207-216. Institute of Genetic Ecology, Tohoku University. 1996.

[2] Drysdale, Alan E. and Barry W. Finger. Waste processing for advanced life support:influences on operational strategies and design. SAE Technical Paper No. 972292. Soc. Automotive Eng., Warrendale, PA, USA. 1997.

[3] Levri, Julie A., David A. Vaccari and Alan E. Drysdale. Theory and application of the equivalent system mass metric. SAE Technical Paper 2000-01-2395. Soc. Automotive Eng., Warrendale, PA, USA. 2000.

[4] Garland, Jay, Cheryl L. Mackowiak and John C. Sager. Hydroponic crop production using recycled nutrients from inedible crop residues. SAE Technical Paper No. 932173. Soc. Automotive Eng., Warrendale, PA, USA. 1993.

[5] Mackowiak, C. L., J. L. Garland, R. F. Strayer, B. W. Finger and R. M. Wheeler. Comparison of aerobically-treated and untreated crop residue as a source of recycled nutrients in a recirculating system. Adv. Space Res. 18(1/2):281-287. 1996.

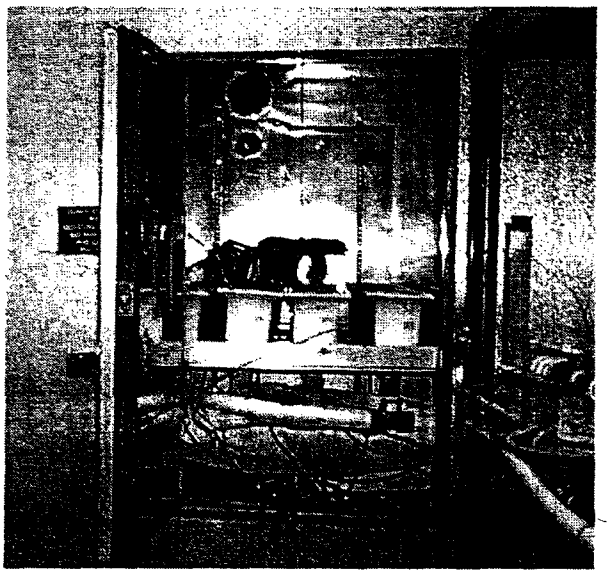

Figure 1. Plant growth chamber used to perform testing of the prototype control system.

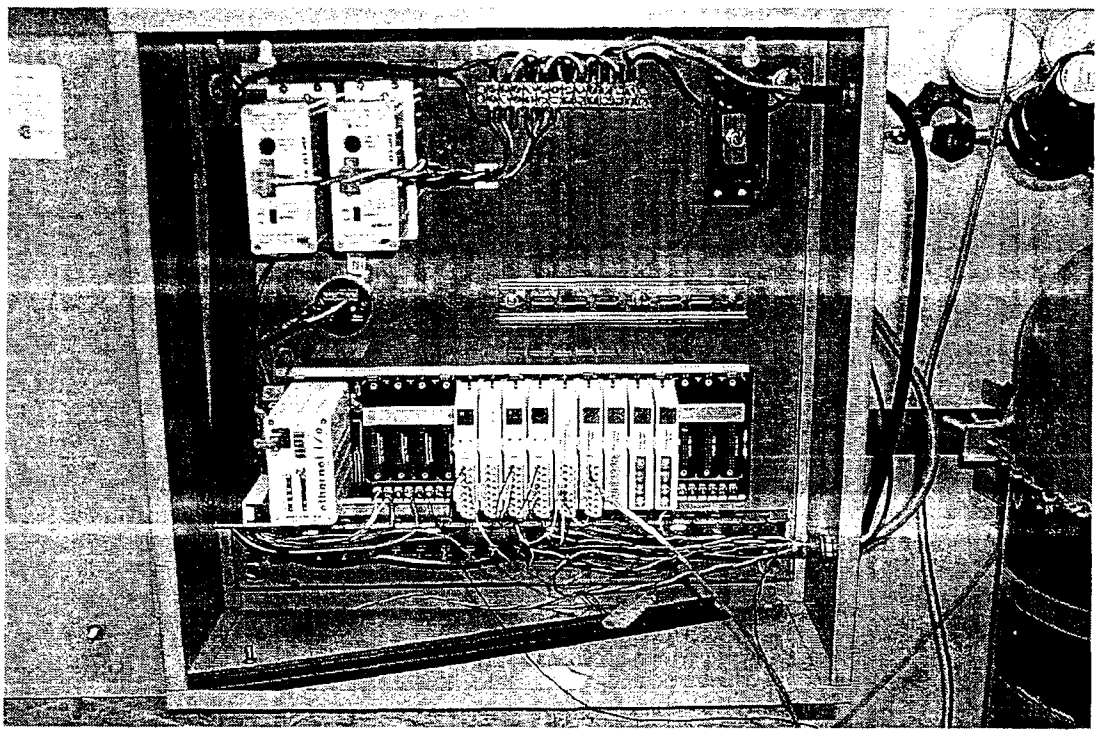

Figure 2. Wiring panel that housed the PLC modules.

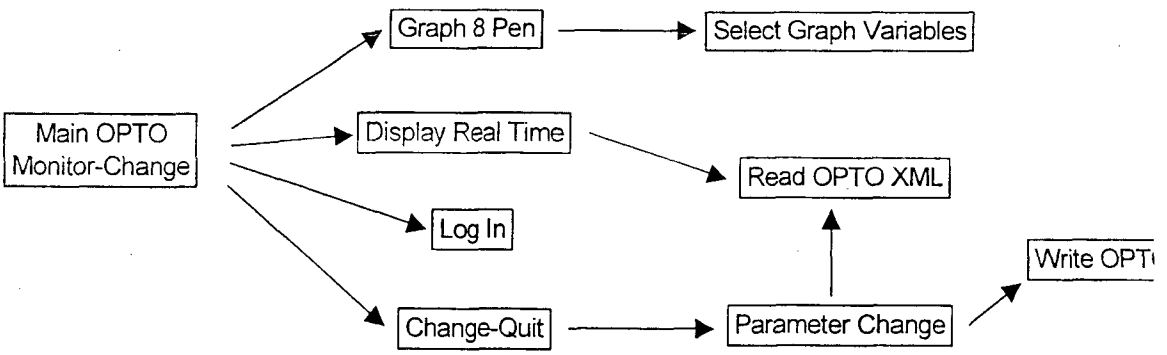

Figure 3. Structure of the LabVIEW interface showing the sub-VI's.

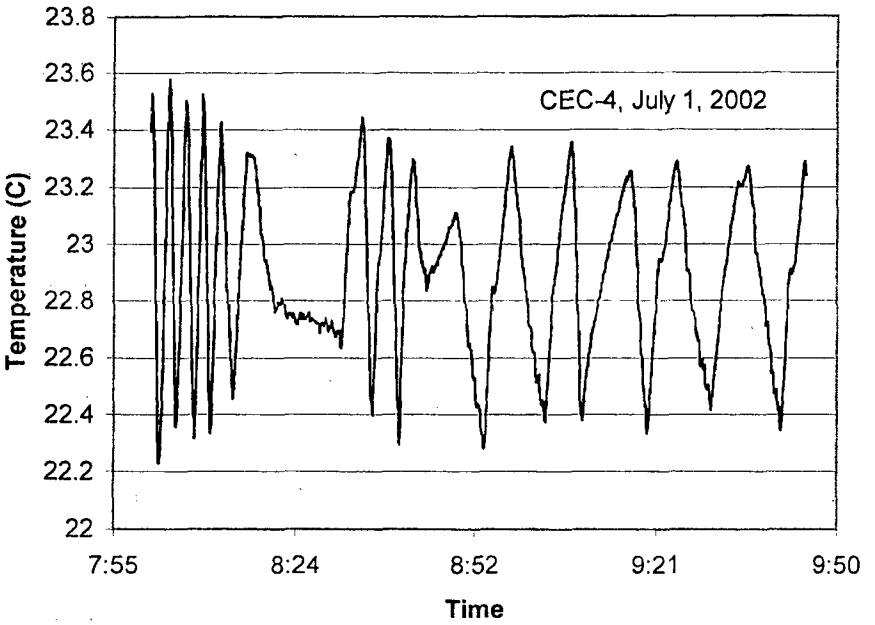

Figure 4. Typical temperature fluctuations in the growth chamber under autonomous control.

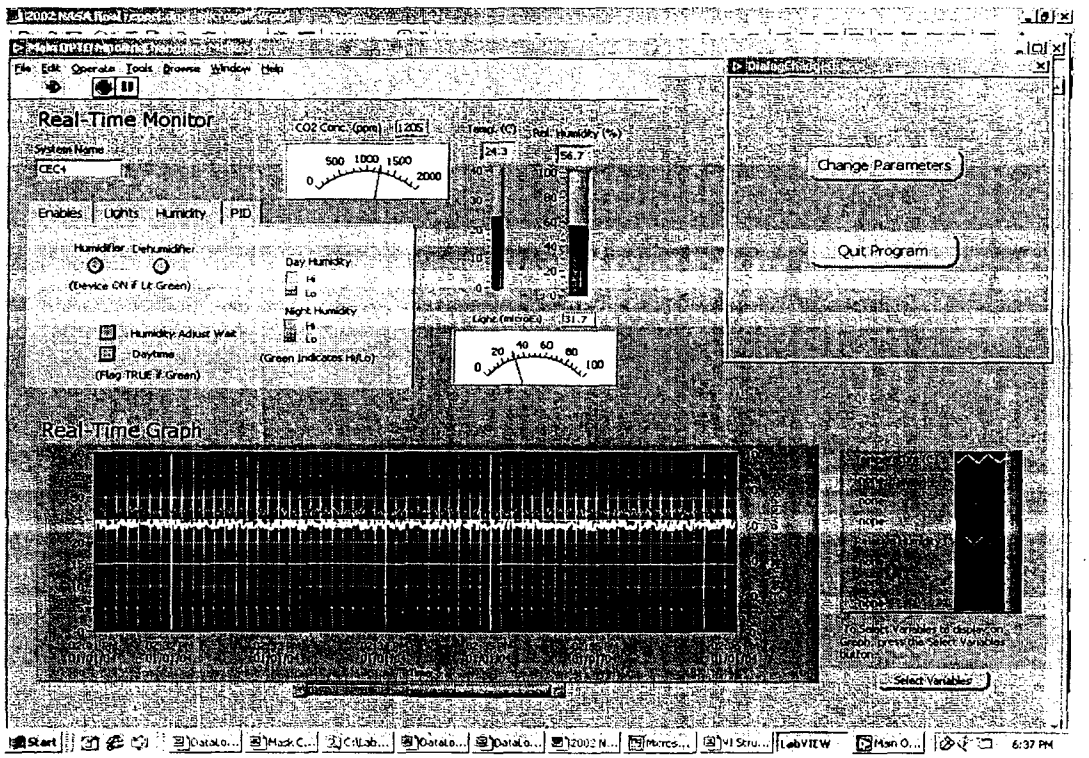

Figure 5. Real time display using the LabVIEW software.

2002 NASA/ASEE SUMMER FACULTY FELLOWSHIP PROGRAM

JOHN F. KENNEDY SPACE CENTER
UNIVERSITY OF CENTRAL FLORIDA

COLLAPSIBLE CRYOGENIC STORAGE VESSEL PROJECT

David C. Fleming
Associate Professor
Mechanical & Aerospace Engineering Department
Florida Institute of Technology

KSC Colleague: Eric A. Thaxton
Spaceport Engineering & Technology Directorate

ABSTRACT

Collapsible cryogenic storage vessels may be useful for future space exploration missions by providing long-term storage capability using a lightweight system that can be compactly packaged for launch. Previous development efforts have identified an "inflatable" concept as most promising. In the inflatable tank concept, the cryogen is contained within a flexible pressure wall comprised of a flexible bladder to contain the cryogen and a fabric reinforcement layer for structural strength. A flexible, high-performance insulation jacket surrounds the vessel. The weight of the tank and the cryogen is supported by rigid support structures. This design concept is developed through physical testing of a scaled pressure wall, and through development of tests for a flexible Layered Composite Insulation (LCI) insulation jacket. A demonstration pressure wall is fabricated using Spectra fabric for reinforcement, and burst tested under noncryogenic conditions. An insulation test specimens is prepared to demonstrate the effectiveness of the insulation when subject to folding effects, and to examine the effect of compression of the insulation under compressive loading to simulate the pressure effect in a nonrigid insulation blanket under the action of atmospheric pressure, such as would be seen in application on the surface of Mars. Although pressure testing did not meet the design goals, the concept shows promise for the design. The testing program provides direction for future development of the collapsible cryogenic vessel concept.

COLLAPSIBLE CRYOGENIC STORAGE VESSEL PROJECT

David C. Fleming

1. INTRODUCTION

Future exploration missions may take advantage of in situ resource production (ISRP) to increase mission effectiveness by allowing resources to be collected remotely rather than transporting them from Earth. For example, missions to Mars may use oxygen obtained from the predominantly carbon dioxide atmosphere for rocket fuel or for life support [1,2]. Such missions require the long-term storage of substantial quantities of oxygen. From volume considerations, the oxygen will be stored as a liquid. If the liquid oxygen is to be used primarily for rocket fuel, and if the flight vehicle arrives on site at the same time as the ISRP equipment, it may be reasonable to use the flight tanks as storage tanks. For other purposes or different mission scenarios, however, a dedicated cryogenic storage vessel would be required. Because of the inefficiency of launching a large, empty storage tank, a collapsible cryogenic storage vessel is desirable for this application.

Fleming and Hegab [3-5] evaluated preliminary design concepts for a collapsible liquid oxygen storage tank for use on Mars. The most promising design concept was an "inflatable" design, as illustrated in Figure 1, from Reference 3. In this design, the cryogen is contained within a flexible pressure wall comprised of a flexible bladder supported by external fabric reinforcement. A flexible, high performance insulation material is contained within a flexible vacuum barrier surrounding the pressure wall. High vacuum conditions are maintained in the insulation space by getter materials. Because the outer barrier of the insulation material is flexible, the small atmospheric pressure of Mars (approximately 7 torr) must be reacted by the insulation material. External to the insulation, additional flexible materials (not shown in Figure 1) for impact protection and abrasion resistance to the Mars dust must be added. The flexible pressure wall, insulation, and environmental protection systems are supported by rigid structure on the lower end of the tank. The tank collapses by folding along the vertical axis of the tank and is deployed by initial pressurization with gaseous oxygen prior to the introduction of the cryogen. This report describes ongoing development of this collapsible cryogenic tank concept and physical testing in support of the development of this concept.

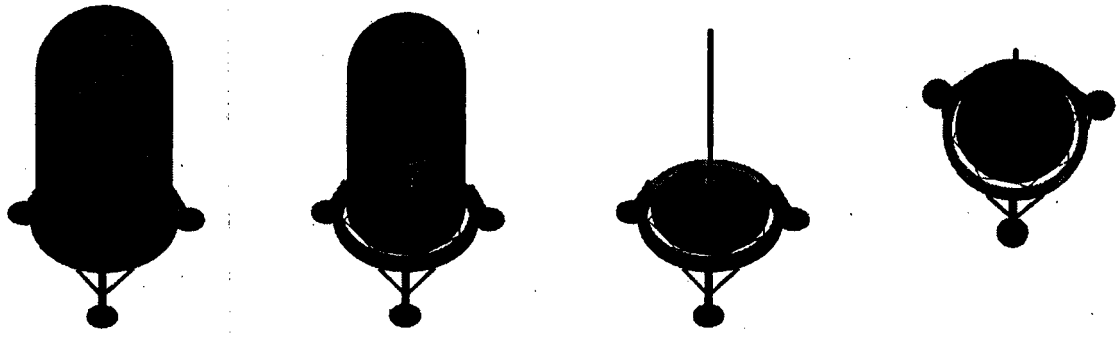

Figure 1 Schematic of the inflatable tank concept emphasizing (a) the flexible insulation jacket, (b) the pressure membrane, (c) the support structure including a rigid end cap, external support structure and legs, and (d) the suspension system (dark lines connecting the endcap to the external ring) (from Reference 3)

2. EXPERIMENTAL TESTING

Development and testing is done for two primary components of the collapsible cryogenic storage vessel: the pressure wall (comprising the cryogen containment bladder and the reinforcement material) and the flexible insulation material.

2.1. Pressure Wall

The flexible pressure wall is comprised of two main components: a bladder that serves to contain the cryogen, and which acts as the inner vacuum barrier for the insulation space; and a fabric reinforcement to resist the primary loading. A demonstration pressure wall is fabricated to verify the suitability of this approach. The full-scale design in References 3 and 4 is for a large manned mission, and the tank was sized to a capacity of 110,000 lb_m using a cylindrical tank with a 10 foot inside diameter. The concept is evaluated using an 18-inch diameter vessel. The basic design of the pressure wall is evaluated by burst testing the demonstration vessel. For scaling, the pressure wall is sized to resist the loading that would be experienced in the full-scale design article at a design burst pressure of 20 psi. Thus, the scaled demonstration pressure wall is designed to a burst pressure of 133 psi.

2.1.1. Bladder

The bladder contains the cryogen. As described in Reference 3, perhaps the only material that meets the combined requirements of oxygen compatibility, low-temperature performance and flexibility is Teflon. FEP Teflon offers somewhat better performance than other grades of Teflon. Teflon has poor oxygen permeability and thus the bladder must be metalized to prevent the rapid degradation of the vacuum in the sealed insulation space bounded on one side by the bladder. Metalized FEP film, a specialized material, was cost prohibitive for the current project. Because the function of the metal layer is not structural it was decided to use nonmetalized bladders. External fabrication of the Teflon bladder was pursued, however this option was also cost prohibitive, and difficult to implement in the limited time period of the project. Thus, it was decided to fabricate the necessary bladders in-house for the current project. FEP Teflon materials were secured for this purpose. However, difficulty in working with this material prevented its use. As a substitute for the current structural testing bladders were fabricated from a Mylar barrier material described below in Section 2.2.

Teflon and other polymer films can be fabricated in various ways including heat sealing, thermoplastic welding, and thermoforming [6]. Among these methods, the one judged most practical for the current project was heat sealing. In heat sealing, pieces of material to be joined are locally heated under the application of pressure. The material melts and fuses. Equipment for heat sealing materials is widely used for packaging and food handling. Heat sealers designed to reach sufficient temperature for Teflon are less common, but available. A variety of heat sealing equipment was purchased for use in this project including a foot-operated double impulse heat sealer that produces a linear seam up to 18 inches long. To fabricate a cylindrical bladder with hemispherical ends using this sealer, the bladder was assembled from gore segments extending along the entire axial length of the bladder, except for small openings left at each end. Simple geometrical relationships were used to determine the approximate shape of the gore segments. The curved shape of the gore segments was further approximated by straight lines because only linear seams can be produced by the heat sealer. Twelve gore segments were used to produce the bladder.

To produce the bladder, pieces of material were cut to a rectangular shape, and markings for the various seams were transferred to the material using paper patterns produced for each of the seams. Adjoining rectangles were then tacked together in the scrap portion of the material using the handheld sealing iron to keep the segments in position during the sealing operation. One side of each pair of

adjoining gore segments was then sealed using the foot-operated heat sealer. As each gore was assembled, the already-assembled gores were folded out of the way, taking care to avoid creasing of the material (though in practice this was impossible to avoid entirely). On the last seam initially only one or both of the seams of the dome ends of the gore were sealed, and the cylindrical seam left open. This permitted access to the interior of the bladder. At this point, circular openings remained on the domes of the bladder. These were closed using discs of material that were hand-sealed using the hand-held iron. This was a difficult operation, as the dome ends needed to be stretched open to prevent wrinkling while simultaneously applying pressure and heat using the sealing iron. It is unlikely that a near perfect air tight seal could be made by this process, and leakage of the bladder is most likely due to imperfect closure of the dome end pieces. An opening was left on one of the dome ends, and a fitting passed through it. Then, the remaining gore segments seams were closed, completing the bladder assembly. Bladders were checked for gross leaks by inflation and slight pressurization with gaseous nitrogen. Figure 2 illustrates the bladder fabrication procedure.

Two bladders made of the Mylar barrier film material were produced. Because the intent is to keep the bladders from being fully strained, they were designed to be approximately 10% oversize, as compared with the fabric reinforcement. The elongation of the Spectra reinforcement is approximately 4%, and deformation of the seams is likely to increase the average value of deformation to failure beyond this amount. The first Mylar bladder was found to have imprecisely shaped ends (much shallower than intended) which was attributed to the nature of the approximation of the gore segments used in this bladder. The total length of the first bladder was only about 4% greater than the nominal reinforcement bag length. The pattern was modified for the second bladder producing a closer approximation of the intended gore shape and an increase in the cylinder length of two inches. This resulted in an improved shape of the end domes. Because of the nature of the construction technique, the bladder collapses very efficiently in the circumferential direction.

2.1.2. Reinforcement

The bladder material alone is not sufficiently strong to resist the pressure and weight loading of the vessel. Therefore, it must be reinforced. For a high strength, flexible reinforcement, fabric

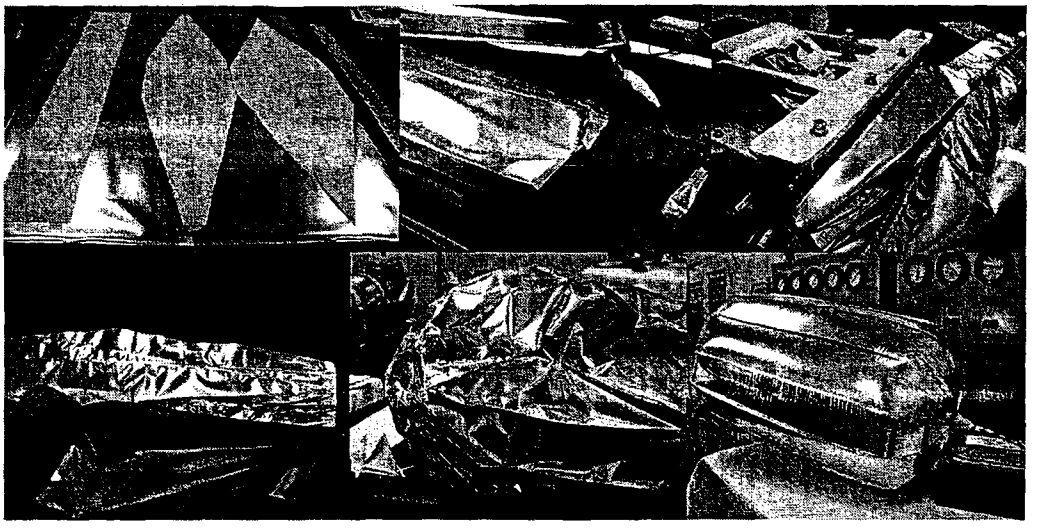

Figure 2 Fabrication of Mylar bladder illustrating (left to right starting from top): a) layout of pattern on Mylar, b) taking of adjoining gore segments, c) heat sealing of gore segments, d) partially assembled bladder showing seam pattern, e) end closure added by hand sealing, f) complete bladder

construction is a logical choice. Fabric materials have relatively high strength, and by their construction can flex and fold without damaging the material. Initial evaluation of materials for the reinforcement layer [3] called for fiberglass fabric to be used. This was selected based on oxygen compatibility requirements. However, because the fabric will be exterior to the containment bladder, and therefore in the insulation space, the reinforcement will not be exposed to significant concentrations of oxygen except in the event of bladder failure. Because bladder failure can be considered a system failure, the requirement for an oxygen compatible reinforcement material was relaxed. For a full-scale tank, the design burst pressure was estimated to be 20 psi. Hoop stress in the cylindrical portion is the critical load. For a 10-foot diameter, this results in a peak line loading of 1200 lb_f/in. This is within the range of commonly produced commercial glass fabrics. However, superior strength-to-weight properties can be obtained for other fabric types, such as Kevlar or Spectra. Based on availability of material, and working experience with the material by the KSC Parachute Refurbishment Facility, which was to fabricate the reinforcement bag, Spectra fiber fabric was selected for the demonstration article. The fabric used has breaking strength of greater than 400 lb_f/in, for a specimen containing a seam. Thus, three layers of material are necessary to fabricate the reinforcement bag.

The reinforcement bag was comprised of three main pieces: a central cylindrical portion, and two hemispherical end domes. The cylinder was fabricated from a single triple layer of Spectra with a single longitudinal seam. Domes were fabricated from eighteen identical gore segments. Longitudinal seams between gore segments were reinforced with Kevlar webbing. This Kevlar webbing passed from equator-to-equator in a single piece. Kevlar reinforcement was also placed at intervals in the latitudinal direction. The domes were connected to the cylindrical portion of the reinforcement bag through doubler material in the cylinder. There were six rows of stitching attaching the gore pieces to the cylinder. Kevlar stitching was used for all seams.

An inlet for the vessel was provided by a ½" Polypropylene bulkhead fitting which was included in the center of one dome on the bladder. Because the bladder material cannot resist the full pressure loading of the vessel, hard reinforcement is necessary around the fitting. In the full-scale design, a rigid lower endcap structure will serve this function. For the test article, a simple flat circular plate was used for this purpose. A circular bulkhead of 8 inches in diameter was fabricated in the KSC Prototype Shop, and a hole cut out to accept the fitting. Because the bulkhead is not representative of the actual full scale design, it was designed to a higher design pressure to ensure that it would not be the critical part during the burst test. The minimum required thickness for an Aluminum 6061-T6 bulkhead was calculated to be 5/16 inch. Based on material availability, a thickness of ½ inch was used. A radius was machined around the edge of the bulkhead to eliminate sharp edges that might damage either the reinforcement bag or the bladder material. Assembly of the dome with the fitting was completed with the bladder and bulkhead inside the reinforcement bag. An opening of 6-inch diameter was left in the end of the reinforcement dome where the fitting was placed. Seams near this opening were made such that the width of the gores was reduced near the end to account for the flat end. The Kevlar webbing was fabricated with loops extending into the space of the opening. Kevlar cord was placed through the loops, cinched tight and tied. Figure 3 shows the complete pressure wall.

The complete pressure barrier was checked out by lightly pressurization (½ psi gage pressure) with gaseous nitrogen. At this pressure, it was found that complete engagement of the Mylar to the reinforcement was obtained, and no obvious gas leak was observed. The vessel was then burst tested, as described in Section 3. A second vessel was fabricated for demonstration purposes.

2.2. Flexible Insulation

One of the most critical components of the proposed collapsible cryogenic storage vessel concept is the insulation. The insulation must be sufficiently flexible to permit folding for deployment, yet retain its performance after being folded then deployed. Salerno and Kittel [7] describe considerations for

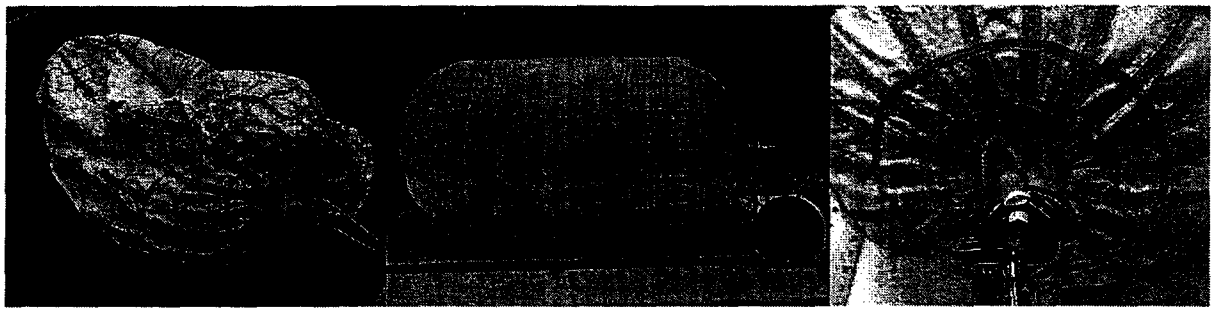

Figure 3 Complete reinforcement wall showing (from left to right): a) reinforcement with no inflation, b) under light inflation, c) detail of reinforcement around inlet fitting

cryogenic storage systems on Mars. Minimum mass systems are obtained when cryocoolers are used with effective passive insulation systems. Hegab [4] examined candidate insulation systems for a proposed collapsible liquid oxygen tank and found that optimum system mass required a high-performance insulation system, such as the NASA KSC-developed Layered Composite Insulation (LCI) systems [8] operating under high vacuum conditions. LCI insulation is similar to conventional multi-layer insulation (MLI), in that it combines reflective materials with nonconductive spacers, but the spacer materials are unconventional and the overall system is more effective under soft vacuum conditions than other insulations and is expected to be more robust under mechanical loading effects [8].

The proposed tank design calls for the layered composite insulation to be contained within a vacuum jacket surrounding the pressure wall of the collapsible tank. Although LCI was developed in part to give good insulation performance at soft vacuum conditions, such as would be experienced if the vacuum space were vented to the Mars atmosphere, high vacuum conditions are required in the insulation of the collapsible cryogenic tank to avoid prohibitive insulation mass [4]. Vacuum will be maintained in the insulation space by sealing the insulation space and using getters, or LCI materials that act as getters to absorb particles in the insulation volume that either permeate through the barriers, or that outgas from the insulation materials. This approach is the same as that used in vacuum insulation panels.

Although the ideal performance of various LCI systems is known (see, for example, Reference 8), the use of the material in the proposed fashion raises some concerns. In particular: 1) It is not known to what degree folding and unfolding the material will degrade the performance; and 2) because the insulation is in a flexible vacuum jacket, the local atmospheric pressure will be reacted by the insulation medium. For a MLI system, Black et al [9] showed that even small compressive loads of 10 torr were sufficient to seriously degrade the thermal performance. Although it is expected to be more robust, the LCI insulation may observe a similar response. Sufficient funding and time was not available to do an in-depth study of the problems of the insulation system for the proposed Mars liquid oxygen storage tank. However, because the feasibility of the proposed insulation system is a major driver of the proposed tank design, it is important to address these issues, at least in a preliminary fashion. Thus, a brief series of tests on the most promising LCI candidate material is proposed to obtain an initial impression of the seriousness of the issues identified above with respect to the use of a flexible LCI insulation jacket for the tank. A series of four tests using a single insulation specimen will be conducted as described below. The test specimen for the insulation tests has been fabricated, and a testing program established. Due to scheduling issues, the insulation testing will not be completed until after the term of the NASA Faculty Fellowship Program.

Based on consultation with Dr. James Fesmire, Lead Engineer, Cryogenic Systems, NASA Kennedy Space Center, and considering available materials, the LCI system chosen for the insulation tests was a modified version of LCI type C115 [8]. The system used for the insulation test specimen uses Hollingsworth & Vose Grade TR2402B polyester non-woven blanket material with wrinkled double

aluminized Mylar as the radiation barrier. Cab-O-Sil 530 silica powder is placed between the Mylar and the polyester. Because the vacuum in the insulation must be independent from the surrounding volume, the insulation is sealed within a barrier film. The test specimen uses Mylar 350SBL300 vacuum barrier film to contain the insulation. This is a nonmetallic film with excellent vacuum barrier properties. One problem with metalized barrier films is that folding of the material can cause pinholing of the metal that adversely affects the overall permeability of the system. It is expected that the nonmetallic nature of the film might avoid this problem, and thus permit better barrier performance after folding and unfolding. On this topic, it should be noted that this is the same material that was used for fabrication of the bladder described in Section 2.1.1. As an unavoidable part of the bladder fabrication process used, the material was subject to considerable amounts of handling. The complete bladder showed numerous visual defects resembling scratches or creases on the surface. It is not known to what extent, if any, this affects the barrier properties of the film. The specimen is fabricated to fit over a cylindrical cold mass 6.57 inches in diameter. The insulation has a total length of approximately 36 inches, with additional length in the barrier layers for sealing.

The insulation specimen was produced by wrapping the materials around a mandrel shaped to the size to fit in the cylindrical cryostat cold mass. A cylinder of barrier material is first fabricated to slide over the mandrel. Next, the insulation materials are wrapped around the inner barrier layer in a process as described in Reference 10. Silica powder is sprinkled over the Mylar film from a mechanical shaker container during the wrapping process. Ten layers of insulation, forming a total insulation thickness of approximately ½ inch were used for the test specimen. After the insulation is applied, an outer cylinder of barrier material is placed over the assembly, and the ends of the two barrier layers are sealed together using a linear heat-sealing machine and a handheld sealing iron. Before sealing, a small vacuum fitting is placed in the outer barrier layer to allow vacuum to be drawn in the insulation specimen. Figure 4 illustrates the insulation specimen fabrication process.

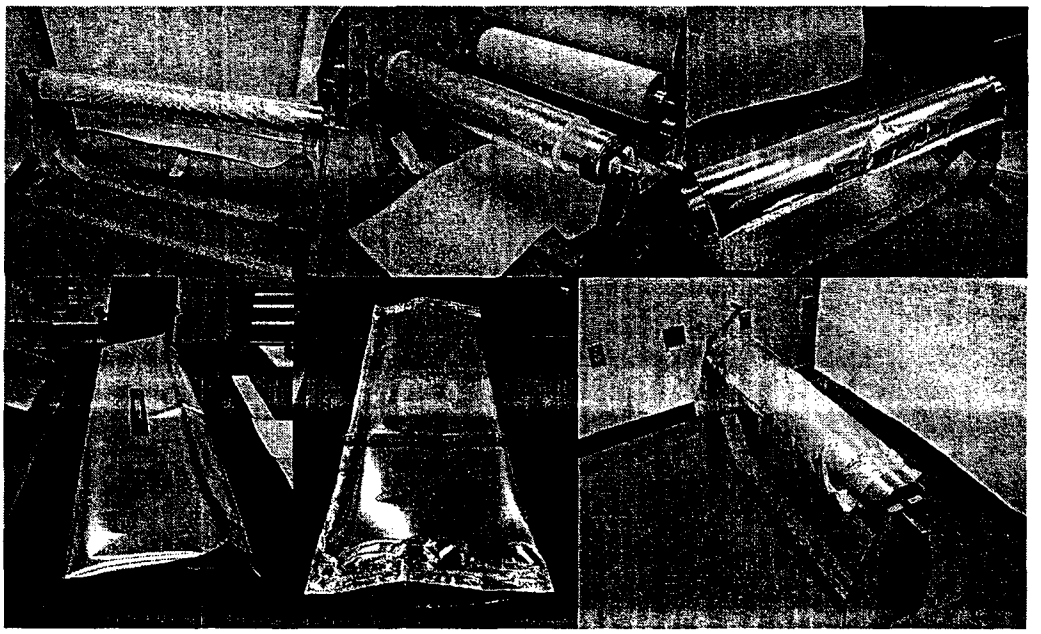

Figure 4 Fabrication of insulation specimen showing (left to right from top) a) Placement of inner barrier cylinder on mandrel b) Wrapping of insulation materials around mandrel (powder not shown in this photograph) c) placement of outer barrier cylinder containing vacuum fitting over the assembly d) assembly removed from mandrel prior to sealing the ends e) specimen with sealed ends f) complete specimen returned to mandrel

A series of four tests is proposed using the given insulation system. The first test will use the insulation specimen in it original manufactured condition. Apparent thermal conductivity, k_{app}, will first be determined for the specimen when equal high vacuum conditions are drawn in the specimen and in the vacuum vessel. This will provide a baseline value for the conductivity of the specimen. For the second test, high vacuum will be maintained in the specimen, while a pressure of 7 torr will be maintained in the outer vessel. Thus, the insulation will be subject to a compression effect due to the external pressure. Following this test, the insulation specimen will be removed from the cryostat, folded, and held in the folded state under light compression for a period of time. The specimen will then be unfolded and reinstalled in the cryostat. The specimen will then be tested under equal vacuum conditions, and under 7 torr of external compression, as before.

3. RESULTS AND DISCUSSION

3.1. Pressure Wall

The pressure wall described in Section 2.1 was tested to failure in a burst test cell. The initial intent was to test the vessel under hydrostatic pressure, though gaseous nitrogen was used for the final portion of pressurization. The available gages were not of a recording variety, so a video camera was used to film the gage throughout the test. An ordinary speed video camera filmed the test article during pressurization.

Because no rigid endcap or cradle structure was prepared for the test article, the specimen was tested in a horizontal orientation. Filling the vessel with water in preparation for the test was extremely time consuming due to the relatively large volume of the vessel and the lack of a vent. The tank was filled by placing a small water tube inside the bulkhead fitting with a loose seal to allow air to vent. The vessel started flat, and filled in a pillow fashion. This is not ideal because the weight of the water must tend to trap folds in the bladder material that may be difficult to remove in subsequent pressurization, perhaps overstressing the seams. During filling, it was attempted to manually extend the Mylar to prevent such folds, though it cannot be known to what degree this was successful. When the vessel was filled to the maximum extent possible, the vessel was connected to the pressurization system, and testing began. At the beginning of the test, the specimen still had a pronounced ovoid shape, and thus a substantial amount of time was required for the low-volume, high pressure pumping system to pump a sufficient volume of water into the tank such that the folds were removed and it began to take its intended shape. After a considerable time it was observed that the pressure was stable at a pressure of about 32 psi. Water was observed to be coming from under the vessel. The test was halted and the pressure observed. In a minute or two of observation no reduction in pressure was measured. The test was resumed, but no pressure increase could be maintained, and it became more apparent that water was leaking from the bladder. The rate of loss of water due to the leak had apparently equalized the rate of pumping from the low-volume system.

Because there was not enough time remaining in the program to disassemble the system and repair or remake the bladder, and because the leak was apparently small, it was decided to complete the testing using gaseous nitrogen as the pressurant (keeping as much of the existing water in the vessel as possible). For safety, all personnel were cleared from the test cell for the remainder of the test. The remainder of the test progressed rapidly. The test specimen quickly took the design shape, and almost immediately crackling noises (attributed to the breaking of threads) were heard, their frequency increasing toward the end of the test. At a pressure of about 60±10 psi, the vessel abruptly burst. Postmortem investigation showed that failure was concentrated in the upper dome, with separation of several of the longitudinal

Figure 5 Failure of upper dome in reinforcement bag showing (from left to right) a) failure in hoop-cylinder seam, b) failure of Kevlar webbing at the apex, c) separation of seams between gore segments

gore seams and about ¼ of the dome-cylinder seam evident. Figure 5 shows the failed pressure wall. The inner bladder burst all of the seams in this dome, resulting in a "banana peel" appearance. Portions of several other bladder seams throughout the bladder were also separated, though it is not known whether they failed during pressurization or at burst.

The pressure wall failed at a pressure well below the design burst pressure of 133 psi. This is attributed to a premature failure of seams in the fabric dome. Because of the compressed time frame of this project, verification testing of the seams used in the domes was not done. Furthermore, analysis of the fabric structure accounting for details of the construction such as the Kevlar webbing needs to be done to improve and verify the design. The bladder also requires improvements. It was observed that leakage occurred at relatively low pressure during testing. The fabrication technique used for the bladder, particularly the manual sealing of the end closures, is not ideal, and results in a large number of seams. Alternate fabrication techniques such as heat forming should be pursued.[1] Some other improvements to the bladder should be made: the bladder should be indexed to the reinforcement bag so that it maintains its position relative to the reinforcement after packing and unpacking. For ease of testing, a vent should be placed in the bladder.

3.2. Flexible Insulation

Because of delays in producing the insulation test specimen and because of scheduling of the cryostat, testing of the flexible insulation system is not yet complete. Interested parties may contact the author for results from the thermal insulation testing.

4. CONCLUSIONS

A demonstration article was produced to illustrate key portions of the collapsible cryogenic tank concept. A burst test of a scaled pressure wall was conducted and preparation of a test specimen to validate the performance of the insulation system was made. Burst testing showed that the pressure wall did not meet design goals. However, it is anticipated that redesign of the reinforcement seams will produce an adequate design.

Although redesign of some components is necessary to meet design goals, the testing supports additional development of the design concept. Further development of the collapsible cryogenic tank concept should include: redesign of the reinforcement, development of the bladder for oxygen compatible

[1] Heat forming of bladders for positive expulsion bladders was pursued by Pope and Penner [11], though difficulties in permeation were found and the process was abandoned.

materials and to improve its manufacturing method, verification of system performance and durability under cryogenic conditions, design of support structures, and design of plumbing and diffuser structures appropriate for the collapsible design concept.

ACKNOWLEDGEMENTS

There are many people at NASA Kennedy Space Center, across various organizations and from various contractors to thank for their generous support of time, resources and talent of this project. First, I would like to thank Dr. Eric A. Thaxton who originated this project, and has continued to provide direction throughout its progress. Thanks to Dr. Timothy Kotnour and Ms. Cassandra Spears for administering the NASA Faculty Fellowship Program at KSC, under which this project was conducted. Mr. Richard Peltzer of Dynacs provided program management, purchasing and facilities support always in a timely fashion and helped steer me thorough various organizations at KSC. I would greatly like to thank all of the people at the KSC Parachute Refurbishment Facility especially Ms. Carol Ball, Ms. Michel Frey, Mr. Dave Hillebrandt, and Mr. Terry McGugin of United Space Alliance for their enthusiastic support and for fabrication of the reinforcement bag. Support of the insulation testing effort was provided through the Cryogenics Testbed. Dr. James Fesmire of NASA, and Dr. Stan Augustynowicz of Dynacs, Inc., provided much help in understanding cryogenic insulation systems, and Mr. Wayne Heckle of Dynacs supported fabrication of the insulation specimen. Support from the KSC Prototype Shop, especially testing support from Mr. Charles Conley during the burst test is greatly appreciated. Thanks also to Mr. Terry Shipe of DuPont Teijin Films for providing the Mylar barrier film material used in this project.

REFERENCES

1. Hoffman, S. J., and D. I. Kaplan, eds., 1997. *Human Exploration of Mars: The Reference Mission of the NASA Mars Exploration Study Team*, NASA-SP-6107.
2. Drake, B. G., and D. R. Cooke, Eds., 1998. *Reference Mission Version 3.0 Addendum to the Human Exploration of Mars: The Reference Mission of the NASA Mars Exploration Study Team*, NASA Exploration Office Advanced Development Office, EX13-98-036, June 1998.
3. Fleming, D. C., 2001. "Evaluation of Design Concepts for Collapsible Cryogenic Storage Vessels," in *2001 Research Reports NASA/ASEE Summer Faculty Fellowship Program*, NASA CR-2001-210265, pp. 53-62.
4. Hegab, H., 2001. "Thermal Design of a Collapsible Cryogenic Vessel," in *2001 Research Reports NASA/ASEE Summer Faculty Fellowship Program*, NASA CR-2001-210265, pp. 85-94.
5. Fleming, D. C., and Hegab, H., 2002. "Design of a Collapsible Liquid Oxygen Storage Vessel for Mars," *Proceedings of the 3rd AIAA Gossamer Spacecraft Forum*, Denver, CO, 22-25 April 2002, AIAA paper 2002-1457.
6. Anon., 1996. "Techniques for Fabricating DuPont FEP Film," DuPont Technical Data 240667C, DuPont, Inc.
7. Salerno, L. J., and P. Kittel, 1999. "Cryogenics and the Human Exploration of Mars," *Cryogenics*, Vol. 39, pp. 381-388.
8. Augustynowicz, S. D., and J. E. Fesmire, 1999. "Cryogenic Insulation System for Soft Vacuum," *Advances in Cryogenic Engineering*, Vol. 45, Kluwer Academic/Plenum Publishers, New York, 2000, pp. 1683-1690.
9. Black, I. A., and P. E. Glaser, 1966. "Effects of Compressive Loads on the Heat Flux through Multilayer Insulations," in *Advances in Cryogenic Engineering*, Vol. 11, K. D. Timmerhaus, ed., Plenum Publishers, New York.
10. Fesmire, J. E., and S. D. Augustynowicz, 2000. "Insulation Testing using Cryostat Apparatus with Sleeve," *Advances in Cryogenic Engineering*, Vol. 45, Kluwer Academic/Plenum Publishers, New York, pp. 1683-1690.
11. Pope, D. H., and J. E. Penner, 1968. "Testing of Polymeric Materials for Use in Multiple-Ply Expulsion Bladders for Cryogenic Liquids," *Journal of Spacecraft*, Vol. 5, No. 3, pp. 259-264.

2002 NASA/ASEE SUMMER FACULTY FELLOWSHIP PROGRAM

JOHN F. KENNEDY SPACE CENTER
UNIVERSITY OF CENTRAL FLORIDA

NANOSCALE AND MICROSCALE IRON EMULSIONS FOR TREATING DNAPL

Cherie L. Geiger, Ph.D.
Associate Professor of Chemistry
University of Central Florida
Jacqueline Quinn, Ph.D.
Environmental Engineer
NASA, Kennedy Space Center

ABSTRACT

This study demonstrated the feasibility of using emulsified nanoscale and microscale iron particles to enhance dehalogenation of DNAPL free-phase. The emulsified system consisted of a surfactant-stabilized, biodegradable oil-in-water emulsion with nanoscale or microscale iron particles contained within the emulsion droplets. It was demonstrated that DNAPLs, such as TCE, diffuse through the oil membrane of the emulsion particle whereupon they reach an aqueous interior and the surface of an iron particle where dehalogenation takes place. The hydrocarbon reaction by-products of the dehalogenation reaction, primarily ethene (no chlorinated products detected), diffuse out of the emulsion droplet. This study also demonstrated that an iron-emulsion system could be delivered in-situ to the DNAPL pool in a soil matrix by using a simulated push well technique. Iron emulsions degraded pure TCE at a rate comparable to the degradation of dissolved phase TCE by iron particles, while pure iron had a very low degradation rate for free-phase TCE. The iron-emulsion systems can be injected into a sand matrix where they become immobilized and are not moved by flowing water. It has been documented that surfactant micelles possess the ability to pull pooled TCE into emulsion droplets where degradation of TCE takes place.

NANOSCALE AND MICROSCALE IRON EMULSIONS FOR TREATING DNAPL

Cherie L. Geiger

1. INTRODUCTION

Remediation of chlorinated solvents in ground water is most commonly addressed using pump and treat technology. It is now widely recognized that due to the slow dissolution of solvents from residual or pooled dense non-aqueous phase liquid (DNAPL) sources, pump and treat primarily provides containment, rather than remediation. Because of this slow dissolution, pump and treat systems will need to be operated for long periods of time (i.e. decades or longer) in order to maintain protection of human health and the environment, incurring high operation and maintenance costs over that period.

Currently, there are no available proven technologies that can treat 100% of DNAPL sources (free-phase, residual phase, and sorbed [matrix diffused] phases). Attempts have been made to remove the DNAPL sources through heating to enhance volatilization (steam injection and radio-frequency-heating). This approach is limited because of the energy costs associated with heating the groundwater, and the exponential volume of areas that will need to be treated to ensure that the entire DNAPL source is encountered and treated. An alternative approach is to flood the source area with surfactants or oxidizing agents. This approach is also limited because the agents will move primarily through the most permeable zones, but considerable DNAPL mass will penetrate into areas of low permeability and will also diffuse (matrix diffusion) into geological materials. DNAPLs that exist in the matrix are dissolved or sorbed (2) and oxidizing agents can diffuse into the matrix and treat the dissolved NAPLs. Thus the very nature of DNAPL sources prevents complete removal that is required to prevent the remaining DNAPL from re-contaminating the groundwater.

There is a critical need for technologies that can effectively treat DNAPL sources in the saturated zone and result in both their destruction and containment with reduced treatment times and lower costs. This project addresses this need.

Significant work has demonstrated that zero-valent metals will reductively dechlorinate chlorinated DNAPLs such as trichloroethene (TCE) to ethene (3, 4). Permeable reactive barriers (PRBs) composed of iron have been shown to be effective in treating dissolved plumes of chlorinated solvents. Although this technology is passive and requires no energy, it still relies on the DNAPL dissolution and transport of dissolved chlorinated solvents to the PTW for treatment. Thus, the length of the treatment is not shortened and there is still a requirement for long-term monitoring. Insertion of iron into source zones by use of soil mixing technologies has been attempted, but this approach is limited to accessible sources, and by the depth of soil treatment. This research project addresses these limitations through the demonstration of an innovative technique that can be applied to DNAPL pools located under existing, occupied facilities and demonstrates the feasibility of using emulsified nanoscale iron particles to enhance dehalogenation of DNAPL free-phase.

The emulsified system consists of a surfactant stabilized oil-in-water emulsion with the nanoscale iron particles contained within the emulsion droplets. The surfactant serves two purposes: 1) it makes the emulsion stable for injection into the DNAPL and 2) the micelles within the emulsion droplet aid in the delivery of TCE to the iron. DNAPLs, such as TCE, diffuse through the oil membrane of the emulsion particle whereupon they reach the surface of an iron particle where dehalogenation takes place. The hydrocarbon reaction by-products of the dehalogenation reaction diffuse out of the emulsion particle and vent to the ground surface. The iron-emulsion system can be delivered in-situ to a DNAPL pool through a series of push wells.

In the generation of the iron-emulsion system, it is desirable to use the smallest iron particles possible

because the small size produces a more stable and reactive emulsion that is capable of penetrating into the smallest of pore cavities between soil particles. Thus, it is desirable to use iron particles in the nanosize or microsize range. Microscale iron can be purchased from a variety of manufacturers. Nanoscale iron must be synthesized in the laboratory.

One of the methods used to synthesize nanoscale iron particles is to slowly add an aqueous solution of $NaBH_4$ to an aqueous solution of $FeCl_3.6H_2O$. The iron particles precipitate and can be readily separated from the solution (5). These chemicals are industrial chemicals produced in large quantities and are relatively inexpensive. A similar method for preparing nanoscale iron particles has been reported in the literature (6).

The nanoscale iron that has been prepared by this technique has a surface area between 15 and 25 m^2/g. This material has been demonstrated to be active in the dehalogenation of TCE in groundwater (7). Nanoscale iron could be mixed directly into water to form a slurry that could be injected into the ground to intercept or treat a plume of contaminated groundwater. However, if this aqueous slurry was to be used to directly treat a DNAPL pool, the hydrophobic pool would reject the hydrophilic slurry and thus the iron particles would not be delivered to the TCE molecules. Thus, it is necessary to make the iron particle slurry hydrophobic.

There is a large scientific basis for the production of what is known as liquid membranes (8, 9). These liquid membranes are emulsion droplets that can be made to have a spherical hydrophobic skin and an aqueous hydrophilic interior. The iron particles are contained in the aqueous interior phase. The exterior of the droplet is hydrophobic and would be able to penetrate into a separate DNAPL phase. The chlorinated solvent would dissolve in the hydrophobic emulsion membrane and then move by diffusion into the aqueous interior. The dehalogenation reaction would then rapidly take place at the surface of the iron. A graphic rendition of what this system looks like at the microscopic level is shown in Figure 1.

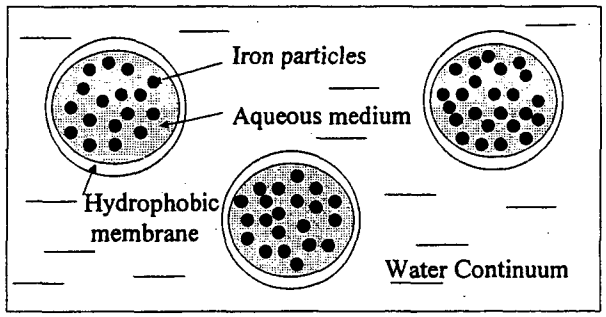

Figure 1. Nanoscale iron particles contained in emulsion droplet.

2. EXPERIMENTAL

Kinetic studies where performed to determine the degradation efficiency of the various emulsions made in the lab. In order to quantitate true destruction, ethene, the terminal product of the dehalogenation reaction, was measured by headspace analysis. Crimp-top, gas-tight vials were used for this work. All experimental work was carried out in an inert atmosphere (nitrogen) glove box. A measured amount

(based on weight of iron) of emulsion was added to the vial along with de-oxygenated, deionized water and 100-μL of TCE. Each vial had five-mL of headspace. Analysis was performed using a purge and trap concentrator and a Trimetrics gas chromatograph equipped with a flame ionization detector.

Pumping Studies

A column experiment was set-up using 2-inch o.d. x 2.0 ft. length acrylic tubing and soil obtained from a research site at launch complex 34, Cape Canaveral Air Station, Kennedy Space Center, FL. The soil used was from a lower (26-40-ft. below land surface) sandy unit of a contaminated shallow aquifer. The porosity of the column material after packing was 32%. Water and emulsion was pumped into the column (vertical up-flow) at a rate of 65-ml per hour and a water:emulsion ratio of 5:1.

3. RESULTS AND DISCUSSION

The liquid membrane emulsions can be made with nonionic, cationic or anionic surfactants. During this study, more than 200 different emulsions were made and tested for TCE degradation efficiency. Micrographs of a microscale iron emulsion (a) and a nanoscale iron emulsion (b) are shown in figure 2.The micrograph shown in Figure 2(a) was taken using a slide platform of depth approximately 200 μm so the emulsion droplet wasn't flattened. Because the droplet was still spherical, some of the micro-iron appeared in focus and the iron near the top appeared out of focus. A nanoscale iron emulsion Figure 2(b) was examined using a standard microscope slide and cover slip so the spherical shaped droplet was flattened by the cover slip. It was obvious from both micrographs that the iron was contained within the interior of the droplets. Since the oil layer was the outer-most layer of the droplet, hydrophobic TCE can dissolve through that layer and into the water/surfactant/iron phase where degradation takes place.

Tests narrowed the most effective emulsions to those made with three surfactants: Rhodapon LSB (anionic, sodium laurel sulfate), Span 80 (neutral, sorbitan monooleate), and Span 85 (neutral, sorbitan trioleate). These emulsions satisfied the practical need of being stable and flowable as well as being active. Emulsions were then made in the blends shown in Table I.

Table I. Composition of Emulsions Used in the Vial/Constant Headspace Kinetic Study.

Emulsion	*Nano Iron (wt%)*	*Corn Oil (wt%)*	*Water (wt%)*	*Surfactant (wt%)*
Blend #1	9.21	42.39	46.08	2.30
Blend #2	9.00	41.44	45.04	4.50
Blend #3	8.44	38.82	42.19	10.55
Blend #4	13.13	20.13	65.65	1.09
Blend #5	13.45	61.88	22.42	2.24
Blend #6	17.74	21.76	59.12	1.38

Experiments performed to test the efficiency of those blends for degradation of DNAPL TCE to ethene revealed that five emulsions gave the best results and those are shown in Table II. Rhodapon LSB (blend 4) and Span 85 (blend 5) showed the fastest reduction of TCE to ethene. Further long-term studies are needed to clarify the lifetime usefulness of the emulsions. However, these early results indicate that TCE mass in the DNAPL form can be reduced quickly using this methodology. Reduction of the source mass could significantly reduce plume remediation time and costs.

(a)

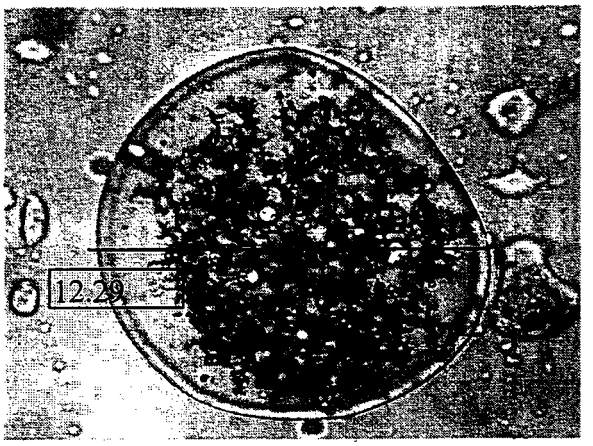

(b)

Figure 2. (a) Micrograph of a micro-iron emulsion dispersed in water. (b) Micrograph of nano-iron emulsion.

Table II. Ethene (ppm) Produced in the Constant Headspace Vials (5-mL samples) Over a 12-Day Period.

Emulsion Type	*Day 1*	*Day 2*	*Day 3*	*Day 7*	*Day 12*
Rhodapon LSB Blend #4	DL	6.15	8.91	19.32	38.06
Rhodapon LSB Blend #5	DL	2.38	2.49	5.47	13.08
Span 80 Blend #4	DL	4.03	6.21	10.29	14.69
Span 85 Blend #4	DL	3.04	4.82	6.21	9.87
Span 85 Blend #5	DL	7.04	9.92	28.94	33.88
Control	DL	DL	DL	DL	DL

Note: DL denotes concentration below detection limit.

None of the emulsions yielded concentrations of chlorinated by-products in solution above the detection limit (DL). The only product that could be measured was ethene and some small concentrations of other hydrocarbons. This indicates that TCE entered the emulsion and degradation occurred via proposed mechanisms (10). The chlorinated by-products produced during the degradation process (cis or trans-dichloroethene, vinyl chloride, etc.) remain in the emulsion and continue along the mechanistic pathways until ethene, a terminal product is formed. Ethene, which has a lower solubility in water, exits through the droplet wall where it then enters free phase water and the gaseous headspace. This is an important aspect of the use of such a potential technology since it won't contribute to the pollution problem by allowing partially de-chlorinated by-products to enter the groundwater.

Pumping Studies

In preparation for field scale tests, practical properties of the emulsions had to be determined. A primary concern was how the emulsion could be pumped into the subsurface. To investigate this concern, a column experiment was set-up using 2-inch o.d. x 2.0 ft. length acrylic tubing and soil obtained from a research site at launch complex 34, Cape Canaveral Air Station, Kennedy Space Center, FL. The soil used was from a lower (26-40-ft. bls) sandy unit of a contaminated shallow aquifer. The porosity of the column material after packing was 32%. Water and emulsion (micro iron formulation #5) was pumped into the column (vertical up-flow) at a rate of 65-ml per hour and a water:emulsion ratio of 5:1.

After a period of four hours, the emulsion had passed through the length of the column and began exiting in the effluent. Samples of the effluent emulsion were examined under a microscope and verified that the emulsion did not break down through the pumping process. The column was then dismantled by cutting it in half along its vertical length. The emulsion had saturated the bottom one-half of the column and then found preferential paths through the remainder of the soil matrix.

A similar column experiment was carried out with nano-scale iron emulsion using the same formulation as the micro-scale iron emulsion used in the previous column experiment. The nano-scale iron emulsion flowed into and through the column more effectively and saturated the entire length of the column material. The emulsion exiting in the effluent was examined and found to be in droplet form. Soil samples

containing emulsion were also examined and the structure of the emulsion was retained.

Field Studies

In preparation for deployment of the pilot-scale injection of the emulsion, 400-gallons of emulsion were prepared at LC-34. An industrial scale mixer was used to prepare approximately 35-40 gallons in 55-gallon drums. Nanoscale iron, covered in de-oxygenated water and a nitrogen head was obtained from Toda America, Inc. and shipped to KSC in 55-gallon drums. Oil and surfactant was also obtained in drums. Water used for the emulsion was potable water obtained on-site. The formulation used was 70-100-36-3 of oil-water-iron-surfactant on a gram-weight basis.

Tests were conducted to determine the best available injection technique for emplacing the emulsion into the subsurface at depths up to 24-ft. bls. The tests took place at Launch Complex-34, Cape Canaveral Air Station, Florida during July 2002. Wavefront, Inc. (Canada) is the injection company chosen by the NASA, GeoSyntec, UCF team for deployment of the emulsion. The technology used involves low flow, high pressure pulses of emulsion injected into the matrix material followed by a water flush using the same parameters. The purpose of the water is to enhance the distance that the pulse can push the emulsion. The initial test of the technology revealed some engineering and mechanical problems that Wavefront had to re-address. The injection required a 5.5-hp pump instead of a 1.0-hp pump and the design of the injector and well plugs had to be changed. Even with these obstacles, 20-gallons of emulsion injected over a 3-ft section of well casing moved at least 12-inches from the well. It is assumed that due to the well plug problem that the emulsion probably short-circuited around the plug and back into the well casing. This would greatly reduce the amount of emulsion available for distribution into the soil matrix. Figure 3 shows a soil coring taken at 21-24-feet bls.

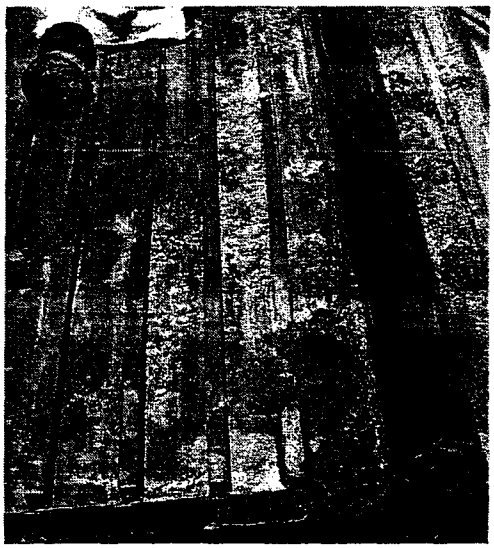

Figure 3. Core sample from 21 to 24 ft. bls. Distribution across end of core illustrates the distribution within soil matrix. Core tips (upper left) also show well-distributed emulsion droplets.

Micrographs of the emulsion recovered after injection show that the droplets withstood the pressure and shear forces of the injection process (Figure 4). This is important since the emulsion system is necessary

for DNAPL adsorption and degradation. If the droplets were destroyed in the injection process, only solubilized chlorinated hydrocarbons would be treated by this method.

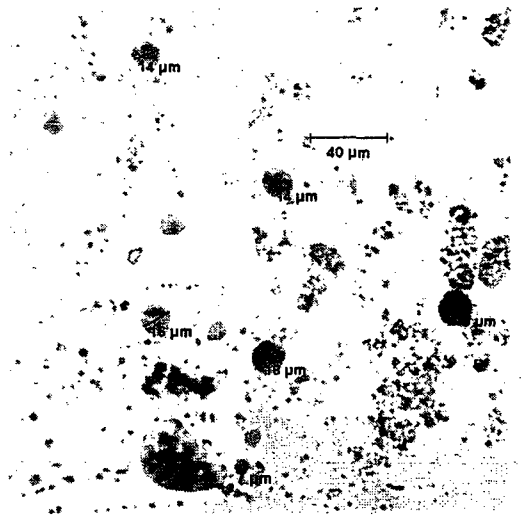

Figure 4. Micrographs of emulsion droplets from two different corings after field injection.

3. CONCLUSIONS

Emulsions containing microscale and nanoscale iron have been developed and tested at the University of Central Florida Chemistry Department. The components of the emulsion, corn or vegetable oil, food-grade surfactant, water and iron particles are biodegradable and/or harmless to the environment. These emulsions have been shown to encapsulate and degrade DNAPL in both water and soil matrices. Chlorinated by-products of the degradation of TCE are not released from the emulsion in measurable quantities. Ethene, a non-chlorinated product of the reaction, can be quantified and was used to follow the rate of the degradation reaction. The emulsion can be pumped at pressures of 160-psi in laboratory experiments through fine-grained or more coarse-grained materials. A field injection test showed that a direct push injection technology is not adequate for subsurface placement of the emulsion. Other technologies are being evaluated.

A field test that is being evaluated under the US EPA SITE (Superfund Innovative Technology Evaluation) Program is currently underway at Cape Canaveral Air Station, Launch Complex 34. This NASA cleanup site has been extensively characterized and it is estimated that over 40,000 kg of DNAPL (TCE and cis-DCE) lie beneath a former parts cleaning facility on the site.

REFERENCES

(1) Reilsma, S. and M. Marshall (1990) "Experimental Study of Oxidation of Pooled NAPL" in Chemical Oxidation and Reactive Barriers. Battelle Press, Columbus, Ohio.

(2) Gillham, R.W. and D.R. Burris (1992) "Recent Developments in Permeable In Situ Treatment Walls for Remediation of Contaminated Groundwater," In *Proceedings of Subsurface Restoration Conference*, June 21-24, 1992.

(3) Vogan, J. L., J.K. Ealberg, B. Gnabasik, and S. O'Hannesin (1994), "Evaluation of In Situ Groundwater Remediation by Metal Enhanced Reductive-Dehalogenation – Laboratory Column Studies and Groundwater Flow Modeling," presented at the 87th Annual Meeting and Exhibition of

the Air and Waste Management Association, Cincinnati, OH, June 19-24.
(4) Geiger, C. L., Ruiz, N. R., Clausen, C. A., Reinhart, D. R., Quinn, J. (2002), *Water Research.* Vol. 36, pp 1342-1350.
(5) Toy, P.C., Master's Thesis, University of Central Florida, Orlando, Florida, 1998.
(6) Wang, C.B. and Zhang, W.X., (1997). *Environ. Science Technol.*, Vol. 31, No. 7, p. 2154.
(7) Geiger, C. L., C. A. Clausen, D. Reinhart, N, Ruiz, P. Toy, N. Lau. (1998) "The Use of Ultrasonic Energy for Regeneration of Reactive Iron Used for In Situ Remediation." Proceedings of the Air and Waste Management 91st Annual Meeting, San Diego, CA. June 14-18.
(8) Cahn, R.P. and Li, N.N., (1974). *Separation Science*, Vol. 9, pp. 505-519.
(9) Kim, K.S., S. J. Choi, and S. K. Ihm, (1983). *Ind. Eng. Chem. Fundam.*, Vol. 22, pp. 167-172.
(10) Roberts, A. L., L. A. Totten, W. A. Arnold, D. R. Burris, T. J. Campbell. (1996) *Environ. Science Technol.*, 30,2654-2659.

2002 NASA/ASEE SUMMER FACULTY FELLOWHSIP PROGRAM

JOHN F. KENNEDY SPACE CENTER
UNIVERSITY OF CENTRAL FLORIDA

DEVELOPMENTS IN UNDERSTANDING STABILITY AS APPLIED TO MAGNETIC LEVITATED LAUNCH ASSIST

James A. Gering
Instructor and Director of Laboratories
Department of Physics and Space Sciences
Florida Institute of Technology

Frederick Adams
NASA KSC Colleague

ABSTRACT

Magnetic levitation is a promising technology, with the potential of constituting the first stage of a third generation space transportation system. Today, the Space Shuttle burns on the order of one million pounds of solid rocket propellant to bring the orbiter and external tank to nearly Mach 1 (1,000 kph). Imagine the reductions in launch vehicle weight, complexity and risk if an aerospace vehicle could be accelerated to the same speed utilizing about $1,000 of off-board electrical energy stored in flywheels. After over two decades of development, maglev trains travel on full-scale demonstration tracks in Germany and Japan reaching speeds approaching 500 kph. Encouraging as this may appear, the energy and power required to accelerate a 1 million pound launch vehicle to 1,000 kph would radically redefine the state-of-the-art in electrical energy storage and delivery. Reaching such a goal will require levitation with sufficient stability to withstand an operating environment fundamentally different from that of a high-speed train. Recently NASA let contracts for the construction of three maglev demonstration tracks. This construction and several associated trade studies represent a first-order investigation into the feasibility of maglev launch assist. This report provides a review of these efforts, other government sponsored maglev projects and additional technical literature pertinent to maglev stability. This review brings to light details and dimensions of the maglev stability problem which are not found in previous NASA-sponsored trade studies and which must be addressed in order to realize magnetic levitation as a launch assist technology.

DEVELOPMENTS IN UNDERSTANDING STABILITY AS APPLIED TO MAGNETIC LEVITATED LAUNCH ASSIST

James A. Gering

1. Historical Overview

First, Table 1 presents a very brief history of maglev developments. Then more recent events sponsored by the National Aeronautics and Space Administration (NASA), the Federal Department of Transportation (DOT) and the Department of Defense (DOD) will be briefly reviewed. Afterward, the focus will shift to the topic of levitation stability. It is the author's belief that this topic represents an unresolved, potential obstacle to realizing maglev as a space launch technology. Finally, this report will pose additional questions and suggest future paths NASA research and development.

- 1842 Earnshaw publishes theorem showing stable levitation of a magnet is impossible in a static magnetic field [1]
- 1910 – 1914 French émigré to Britain, Emile Bachelet, an electrician, builds and patents first prototype maglev vehicle the size of a toy train.
- 1956 Early paper on aspects of levitation, Philips Research Reports [2]
- 1966 Powell and Danby receive patent for null-flux coils for maglev
- 1972 Seminal work by researchers at Ford on electrodynamic lift and drag [3]
- 1970-75 M.I.T. Magnaplane project underway, funded by federal DOT.
- 1977 Eric Laithwaite's book on linear motors [4]
- 1991-94 National Maglev Initiative (NMI) underway
- 1997 articles on null-flux coils [5] and Rote's NASA Langley report [6].
- 1999 Thompson's dissertation on high T_c superconducting maglev
- 2002 Rote publishes review article on electrodynamic stability

To gain a historical perspective, the reader is referred to [4], [7] and, if one is pressed for time, [10]. Also useful is the final report of the National Maglev Initiative. A listing of websites, which index other maglev links, are found in this project's deliverables. Rather than cite individual sources for technical information, the reader is directed to the bibliographies found in [8] and [10].

NASA's interest in maglev dates from the Highly Reusable Space Transportation (HRST) concept studies conducted in the early 1990's. These studies paralleled renewed interest in American R&D sponsored by the DOT's NMI. In the late 1990's, NASA's Marshall Spaceflight Center (MSFC) let contracts for the design and construction of three maglev demonstration tracks. A separate contract was let to the Center for Electro-mechanics (CEM) at the University of Texas at Austin. CEM's report represents a thoughtful "order of magnitude" analysis of the feasibility of electromagnetic launch assist. CEM paid special attention to scaling laws and then applied them to estimate the requisite electric motor and flywheel technology.

The DOT's interest in maglev derives from the Inter-modal Surface Transportation and Efficiency Act of 1991 (ISTEA) and in 1998, the Transportation Equity Act for the 21st Century (TEA-21). The ISTEA funded the NMI and one deliverable from the NMI will be reviewed later in this report. TEA-21's impact on space launch assist has been indirect: active government funding helps to sustain maglev interest in certain R&D-oriented industry partners. As to ground

transportation, TEA-21 may begin construction of a commercial maglev rail line in the Northeast prior to its termination in 2006. Since American maglev technology was not developed during the late 1970's and 1980's, the DOT expects to purchase Germany's *Transrapid* technology. *Transrapid* is Thyssen-Krupp's brand name for their electromagnetically levitated, actively controlled maglev train. Siemens, a German company better known to the American public, is a division of Thyssen-Krupp.

During the mid and late 1990's a 100-ft.-long maglev modification was made to the Holloman Air Force Base High Speed Test Track (HSTT). Since the 1950's the HSTT has been the premier facility for testing ejection seats, near-ground hypersonics and the human limits to high-speed acceleration and jerk (the time rate of change of acceleration). Holloman's maglev modification relied on superconducting magnets, which suffered from repeated quenches (the magnetic equivalent of a melt-down). The industry partners (General Atomics, Boeing, Bechtel and Foster-Miller) redesigned the sled as funding expired. However, additional funds were not appropriated to build a redesigned sled.

The Navy's Electromagnetic Launch System (EMALS) is currently in its second phase of development. To date, the Navy has let two contracts each worth $60M to two competing industry teams (one lead by General Atomics and the other by Northrup-Grumman). An EMALS would not employ magnetic levitation but it must design a linear motor capable of accelerating a 100,000 lb. Aircraft to a speed of 67 m/sec (130 knots) on a short (330 ft.) aircraft carrier runway. This represents a vehicle 10% of the weight and 22% the proposed launch speed of a maglev first stage. The Navy's EMALS program will face similar challenges to store and deliver sufficient electrical energy to a linear motor just as an operational maglev train or launch assist system would. [11] The two EMALS teams are contracted to deliver a design study and scalable demonstration hardware by 2003. Installing an EMALS on an aircraft carrier must wait Congressional funding of a Next Generation Carrier. This is not expected until after 2006. Later in this report attention will return to these two DOD projects.

2. Recent NASA Development

The salient features of the three NASA demonstration tracks are summarized in Table 2. Note that EDL refers to ElectroDynamic Levitation and is often described as either 'repulsive' or 'passive' levitation, due to magnetic induction via Faraday's and Lenz's Laws. EML refers to ElectroMagnetic Levitation and relies on active feedback control of the "attractive" forces between electromagnets and ferrous metal rails. Accompanying the Foster-Miller Track was another "order of magnitude" analysis of the power requirements and scaling for electromagnetic launch assist. Both the CEM and Foster-Miller studies reach the conclusion that accelerating a 1 million pound (455,000 kg) vehicle to 0.85 Mach (300 m/sec) would require a track length of about 3 km. Such a 'Maglifter' vehicle program would redefine the state-of-the-art in flywheel energy storage (24 GJ) and pulsed power distribution (approximately 5 GW). Nevertheless, both studies believe this goal is eminently reachable given current technology: approximately 9 steel flywheels of the size used in electric generating plants (most of which would be located at the high-speed end of the track).

Prime Contractor	Type of Levitation	Disposition	Notable Features
Foster-Miller Inc.	EDL using permanent magnets and null-flux coils	Delivered to KSC, relocated to F.I.T.	Being outfitted with sensors.
Lawrence Livermore National Laboratory (LLNL)	EDL using Halbach arrays of permanent magnets and null-flux coils	Currenttly at LLNL	Communicated incorrect null-flux coil perimeter to manufacturer. Excessive magnetic drag.
PRT Advanced Maglev Inc.	EML using powered coils separate from propulsion	Located at MSFC	Flywheel delivers power to propulsion coils.

Table 2. Description of the Three NASA-sponsored Maglev Demonstration Tracks

These studies [11], [12] constitute only a first step, in terms of system design, sub-system scaling and modeling sophistication. For example, in both reports, aerodynamic drag is modeled by assuming a drag force of $F_d = \square\square C_d v^2$. Here, $\square$ is the mass density of air, A is a frontal cross-section area of a levitated vehicle, v is the vehicle's speed and the drag coefficient (C_d) is written as a function proportional to the square of velocity. As such, the power loss to aerodynamic drag is approximately equal to that required to overcome the payload's inertia. Power and energy requirements are obtained strictly from the equations of one-dimensional kinematics. Power loss from induced drag (also known as vortex shedding from an airfoil) is not included in either report. This would certainly be a contributor since all current second generation space shuttle concepts include one or more lifting bodies stacked piggy-back style or end-to-end. Aeroelasticity considerations are also beyond the scope of these 'first-pass' estimations. Also, the above expression for drag force does not take into account drag arising from the concrete guideway, in which the maglev carrier must ride. Both reports account for magnetic drag (also known as eddy-current drag) with lift and drag expressions equivalent to those derived in [3]. However, both reports do not contain a list of references to indicate the extent of the literature search performed as part of the studies.

3. Analytical Background of Magnetic Lift and Drag

Equations (1) and (2) are plotted in Figure 1. The inset drawing depicts the physical situation: a wire carries current, (I_0) into the plane of the page and moves with constant speed V_0 in the positive x direction over a conducting sheet of thickness $\square$ and conductivity $\square$. Note that $w = 2 / (\mu_0 \sigma \Delta)$ is a characteristic speed.

$$F_{lift} = \frac{\mu_0 L I^2}{4\pi h} \frac{V_0^2}{w^2 + V_0^2} \qquad (1)$$

$$F_{drag} = \frac{w}{V_0} F_{lift} \qquad (2)$$

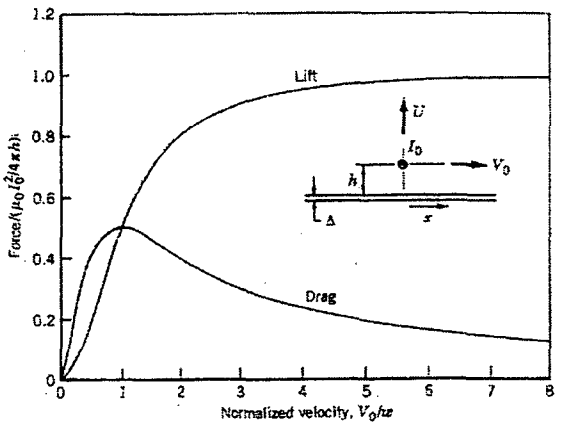

Figure 1. Lift and Drag as a Function of Speed (Moon 1994)

These equations arise by first combining Faraday's, Ohm's and Ampere's Laws, to show that $\boldsymbol{A}$, the magnetic vector potential, must satisfy Eqn. (3). $\boldsymbol{A}'$ is the vector

$$\frac{\partial\left(\vec{A}' + \vec{A}\right)}{\partial t} = w\frac{\partial \vec{A}}{\partial z} \qquad (3)$$

potential due to the source current and $\boldsymbol{A}$ is the vector potential due to the eddy currents. This is accomplished if $\boldsymbol{A}'$ is independent of time and $\boldsymbol{A}(x,y,z,t) = -\boldsymbol{f}_1(x,y,z+z_0+wt) + \boldsymbol{f}_2(x,y,z+z_0+wt)$. This allows a representation where the moving source current generates a 'trailing wake' of repeated image currents below the conductive sheet. The first image current is the same distance below the sheet as the source is above it. However additional images trail behind the first image and move down in the negative z direction at the *same* characteristic speed w as mentioned previously. Applying this representation, allows simpler, familiar expressions for the magnetic fields due to poles, dipoles and current loops to be modified by assuming equivalent image currents and then computing a magnetic field. The Lorentz Force Law ($\boldsymbol{F} = \boldsymbol{Il} \times \boldsymbol{B}$) then determines the forces on the source. Both lift and drag components arise from the vector cross product.

4. Analytical Background of Negative Damping

As mentioned above, both the CEM and Foster Miller studies accounted for magnetic drag. However, as early as 1974 [13] negative damping was recognized as a characteristic of EDL. Iwamoto considered negative damping in the context of a superconducting magnet and later in 1984, Moon showed this type of positive feedback was a general consequence of the eddy current distribution. Moon summarizes this paper in his 1994 book and states that a sinusoidal perturbation in the height of a current element moving over a conducting sheet results in negative damping.

Suppose the height of the current oscillates slightly. After performing a linear perturbation analysis of the resulting change in magnetic field, a perturbing lift force F'_{lift} is obtained. The first term in Eqn. (4) represents a spring-like restoring force however □ is velocity dependent. If the speed v is larger that the characteristic speed w, then the □ changes sign and negative damping results.

$$F'_{lift} = -\kappa \frac{z}{h_0} - \gamma \frac{dz}{dt} \tag{4}$$

$$\gamma = \frac{\mu_0 I^2 w}{4\pi h_0} \left(\frac{w^2 - v^2}{\left(w^2 + v^2\right)^2} \right) \tag{5}$$

This type of magnetic negative damping is of the same type of oscillatory instability as aeroelastic *flutter*. Flutter is technically distinct from resonance, which derives from an external, time dependent forcing function. Perhaps the best-known example of aeroelastic flutter is the Tacoma Narrows bridge collapse of 1940. This event is often characterized as resonance associated with a (Von Karmann) wake of vortices shed from the bridge span. However, further analysis showed the bridge collapsed due to a self-exciting, motion-induced train of vortices at a different frequency. This self-excitation is the fundamental difference between negative damping and traditional resonance in an undamped or under-damped oscillator. [14]

5. Time Dependence of Forces Due to Null-flux coils

The Foster-Miller maglev track and the Holloman HSTT upgrade used null-flux coils in the sidewalls of the guideway. A null-flux coil is a tight, closed-loop, figure eight winding of insulated wire. The sled's (or bogie's) magnets usually have a pole surface area as large (or larger) than the null-flux coil. When one of these magnets passes by the coil, it will induce a voltage (and hence a current flows) in the coil. If a current flows clockwise in the upper half of a closed figure eight loop of wire, the same current will necessarily flow counter-clockwise in the bottom half of the figure eight. If the bogie's magnet moves past a null-flux coil above the center of the coil (where the wires in the coil cross) more magnetic flux will link with the upper half of the coil and induce a larger current. Lenz's law dictates that the coil's induced current (and it's induced magnetic field) will oppose that of the bogie's magnet, thereby forcing the bogie down toward the center of the figure eight. The center of the coil is the null-flux position since this is where the magnet's motion induces zero net flux in the complete figure eight.

Null-flux coils are usually mounted vertically in the sidewalls of guideway. This has the added advantage of moving the levitation out from under the bogie, which opens that space for the linear motor. Also, adjacent (but separate) pairs of coils with rectangular windings can also be used in place of figure eight coils. To distinguish, this arrangement is called a flux-eliminating coil.

To summarize, null-flux coils have two advantages over a guideway made from a continuous sheet of aluminum or copper. First, null flux coils provide a built-in restoring (stabilizing) force. Powerful motivation when one recalls Earnshaw's theorem. Second, null flux coils provide significantly less drag than a continuous sheet guideway. However, it is equivalently true that null-flux coils provide only a minute amount of damping. The self and mutual inductance and the wire resistance are all very small. Hence, this stability only exists in an ideal, unperturbed scenario.

Moreover, the restoring force provided by a flux-eliminating coil has "spiky" time dependence. Thus, even when a maglev bogie moves past a long line of null-flux coils at a constant speed, an off-center magnet will experience a series of discrete, restoring impulses shaped (in time) much like a triangle wave [5]. Triangle waves have a Fourier representation of odd numbered frequency multiples: $A_1\sin(\omega t) - A_2\sin(3\omega t) + A_3\sin(5\omega t) \ldots$ This yields a spectrum, which peaks at a low fundamental frequency and has progressively smaller higher

frequency components.

Of course, the nominal operating mode for the launch of a space vehicle is acceleration not constant velocity (as in a maglev train). The net qualitative effect will be to re-shape the triangle waves and make them spikier. Simultaneously, the bogie will encounter an accelerated (compressed in time) sequence of these re-shaped restoring forces. This compression will distribute mechanical energy to higher frequency components. This has the potential of making available multiple resonant frequencies, which may be excited by various perturbations.

6. Efforts to Improve Magnetic Damping

The Holloman upgrade employed superconducting magnets wound from NbTi wire (cable in copper conduit construction was not used). Also, no method was used (pressurizing or on-board refrigeration) to reclaim the helium that boiled out of the cryostat. Loss of liquid helium was reported as no more than 30%. A year 2000 AIAA report on the Holloman effort listed the conclusion of a General Atomics investigation into the cause of the quenches. Apparently, impulses deriving from the null-flux coils (as mentioned previously) and impulses from the rocket engines imparted vibrations (at 2 KHz) to a magnetic damping plate built on the sled over the superconducting magnets. The heat from the vibrations warmed the magnets and triggered the quenches.

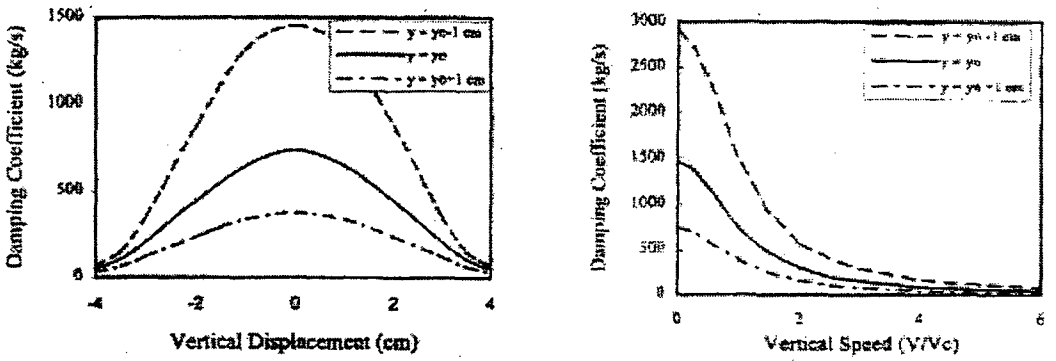

Figure 3. Damping decreases with vertical displacement (left) and vertical speed (right)

Holloman was conducting its tests in late 1997 and early 1998. At that time, two researchers at Argonne National Laboratory were on contract to Holloman AFB. They published a short paper [14] examining the magnetic characteristics of the damping plate. Their analysis is summarized in Figure 3. Here they calculate the damping coefficient as a function of vertical displacement from the null-flux position (zero on the horizontal axis). Ideally, one would prefer to see damping *increase* as the bogie moves away from equilibrium rather than decrease as a function of vertical displacement or vertical speed.

Moving along	Descriptor		Rotating about	Descriptor
X – axis	Forward		X – axis	Roll
Y – axis	Lateral or sway		Y – axis	Pitch
Z – axis	Vertical or heave		Z – axis	Sway

Table 3. Definitions of Terms Used in Maglev Vehicle Dynamics

7. Further Complications: Coupled Modes and Nonlinear Forces

Yet another challenge to designing a stable, EDL maglev system, which delivers good

'ride quality', is that the modes of oscillation of a generic maglev vehicle couple between differing degrees of freedom (DOF). Recall that for rigid bodies an object may move in six DOF's: translation along *and* rotation about the x, y and z axes. In general, analyzing the dynamics of a maglev vehicle involves solving Lagrange's equation and using magnetic circuit analysis as the input. An array of self and mutual inductance calculations must be a part of the circuit analysis. Reference [10] summarizes this approach and then focuses attention on a simplified vehicle constrained to just three degrees of freedom (±x, ±y, and rotations about the z axis). He shows (both analytically and with some experimental data) that such a vehicle is capable of coupled lateral-yaw oscillations that exhibit flutter. Table 3 defines common terminology. Coupling along four modes is possible as described in Table 4.

Coupling	Descriptor	Type of Instability
Lateral-roll	Listing to one side	Divergent (static)
Pitch-heave	Porpoising	Oscillatory
Lateral-yaw	Snaking	Oscillatory
Yaw-roll-pitch	Screw motion	Oscillatory

Table 4: Coupled Modes of Instability

Two other, non-coupled, modes of instability are possible: an oscillatory 'hunting' forward and backward along the x – axis and vertical or 'heave' oscillations along the z – axis. With sufficient x-acceleration and minimal motor slip, hunting may not be an issue for space launch assist. Vertical oscillations, however, must be damped out. Since magnetic forces are intrinsically non-linear, vertical perturbations can cause a departure from simple harmonic motion and generate chaotic oscillations [10]. One potential source of perturbations is flexure of the guideway due to theg weight of the vehicle. The oscillations may enter a limit cycle (an orbit in phase-space that does not close on itself). Collaboration between researchers at NASA-Langley and NASA-Ames has developed a Non-linear Generalized Predictive Control (NGPC) algorithm to actively control EML of an iron ball floating beneath an electromagnet. [16]. Though magnetic forces are intrinsically non-linear, the vast majority of stability studies employ linear approximations in EDL and linear control theory in EML. Simulated neural network may be especially well suited to EML.

8. Summary and Future Directions

The challenges of designing a stable maglev system based on electrodynamic repulsion using null-flux coils involves overcoming (i) near zero intrinsic damping, (ii) negative damping terms arising from eddy/image currents, (iii) spiky restoring forces, (iv) compression of restoring impulses when accelerating, (v) the effectiveness of passive damping plates/coils decreasing as a function of distance from the null-flux position, (vi) coupling of instability modes, (vii) the potential for chaotic dynamics.

Japan Railway (JR) has over twenty years of development experience in using superconducting magnets in EDL systems. Until recently, JR has exclusively relied upon passive damping from the generation of eddy currents in the cryostats, which house the superconducting electromagnet. More recently, JR has used modulated control of the power to the linear motor to reduce instabilities [17]. In a recent paper [9], Rote and Cai, review the history of individual and coupled modes of instability. The authors conclude with a call for those developing full-size maglev trains to fully address whether these instabilities exist or how they have been surmounted.

A group at M.I.T. proposed another avenue to maglev stability as part of the National Maglev Initiative. In their study and computational model, aerodynamic control and a secondary,

passive suspension system provided adequate system stability: on the order of ±2 cm of primary suspension displacement when control of vertical and lateral flaps on the winglets were assumed.

Also General Atomics of San Diego has constructed a six DOF dynamical, computer model to assess their wheel-based, limited DOF test apparatus. This model includes a passive secondary suspension and seems to be adequate to suppress instabilities [18]. However, General Atomics' urban maglev project is a low-speed application of maglev when compared to a 1,000 Km/hr. Maglifter concept.

Clearly, there is a constellation of challenges to stabilizing an EDL system. Options for further research and development include:

- Use superconducting magnets. They add complexity, but offer a mechanism for damping as well as larger and safer (7 to 10 cm) vehicle guideway gaps.
- Perform modeling on designs of null-flux coils, which include iron. This would remove stored energy in the coils, which is an impediment to damping.
- Investigate novel methods of damping in null-flux coils such as active magnetic damping with control coils between vehicle magnets and guideway coils.
- Perform a critical review of existing six DOF dynamical models to assess the efficacy of passive secondary suspensions in the environment of launch assist.
- Motivate developers of simulation software to integrate aerodynamics, aeroelasticity into their products.
- Investigate the use of high critical temperature superconductors, which tolerate A/C eddy current effects that were at the root of Holloman's quenching.

The author wishes to thank the NASA Summer Fellowship program team and Ric Adams, NASA colleague, for the opportunity to work on a most interesting topic.

9. References

1. Earnshaw, S. "On the nature of the molecular forces which regulate the constitution of the luminiferous ether", Transactions of the Cambridge Philosophical Society, Vol. 7, Part I, 1842, pp. 97 – 112.
2. Boerdijk, A. H., "Technical Aspects of Levitation," Philips Research Reports, vol. 11, 1956, pp. 45-56.
3. Reitz & Davis, "Forces on a Rectangular Coil Moving Above a Conducting Slab", *Journal of Applied Physics*, April 1972, p. 1547.
4. Laithwaite, Eric, editor, Transport Without Wheels, pub. by Elek Science, London, 1977.
5. Davey, Kent, "Designing with Null Flux Coils" *IEEE Transactions on Magnetics*, Sept 1997, vol. 33, no. 5, p. 4327. (Publishes two additional IEEE papers in '95 and '97 related to null-flux coils.)
6. Rote, Don M., Cai, Yigang. "Review of Dynamic Stability of Repulsive–Force Maglev Suspension Systems", *IEEE Transactions on Magnetics*, vol. 38, no. 2, pp. 1383-1390, March 2002.
7. Rhodes, R. G., and Mulhall, B. E., *Magnetic Levitation for Rail Transport*, Clarendon Press Oxford, 1981.
8. Thompson, Marc T. and Thornton, Richard D. "Flux-Canceling Electrodynamic Maglev Suspenion, Parts I and II, *IEEE Transactions on Magnetics*, vol 35, no. 3, pp. 1956-1963, May 1999.

9. Rote, Donald M., (Center for Transportation Research, Argonne National Laboratory, IL) "Magnetic Levitation and Propulsion Concepts of a New Wind Tunnel Design – A Feasibility Study" Report to the NASA Langley Research Center, 1997.
10. Moon, Francis C. (Cornell University) "Superconducting Levitation" John Wiley & Sons, Inc, New York.
11. Dill, J. and Meeker, D., NASA Report, NAS 98069-1362, December 2000.
12. Caprio, M. T., and Zowarka, R. C., NASA Report, "MAGLEV Launch Assist Technology Demonstrator: Task 1", RF-201, March 2001.
13. Iwamoto, M., Yamad, T., and Ohno, E. "Magnetic Damping Force in Electrodynamically Suspended Trains," *1974 Digest of Inter-Mag Conference of the IEEE*, Toronto, Canada, pp. 458-461.
14. Billah, K., Scanlan, Robert, H. American Journal of Physics, Vol. 59, No. 2, February 1991.
15. He, J. and Coffey, H., "Magnetic Damping Forces in Figure-Eight-Shaped Null- Flux Coil Suspension Systems", *IEEE Transactions on Magnetics*, vol 33, no. 5, pp. 4230-4233, September 1997.
16. Haley, P., Soloway, D., Gold, B. (1999) "Real-time Adaptive Control Using Neural Generalized Predictive Control" *Proceedings of the American Control Conference*, San Diego, California, June 1999
17. Rote, Don, private conversation with author, July, 2002.
18. Gurol, Sam, private conversation with author, July 2002.

2002 NASA/ASEE SUMMER FACULTY FELLOWSHIP PROGRAM

JOHN F. KENNEDY SPACE CENTER
UNIVERSITY OF CENTRAL FLORIDA

CORROSION ACTIVITIES AT THE NASA KENNEDY SPACE CENTER

Robert H. Heidersbach
California Polytechnic State University (retired)
KSC Colleague: Luz Marina Calle

ABSTRACT

This report documents summer faculty fellow efforts in the corrosion test bed at the NASA Kennedy Space Center. During the summer of 2002 efforts were concentrated on three activities: a short course on corrosion control for KSC personnel, evaluation of commercial wash additives used for corrosion control on Army aircraft, and improvements in the testing of a new cathodic protection system under development at KSC.

CORROSON ACTIVITIES AT THE NASA KENNEDY SPACE CENTER

Robert H. Heidersbach

1. INTRODUCTION

During the summer of 2002 efforts were concentrated on three activities: a short course on corrosion control for KSC personnel, evaluation of commercial wash additives used for corrosion control on Army aircraft, and improvements in the testing of a new cathodic protection system under development at KSC. These three projects will be discussed separately below.

2. CORROSION COURSE

A recent study placed the annual costs of corrosion in the United States at more than $275 billion—approximately 3.2% of the GDP. [1] NASA has millions of dollars in corrosion costs, and it is important that NASA personnel understand this multidisciplinary problem. The corrosion course held at KSC during the summer of 2002 was open to all KSC personnel. Approximately 12 participants would show up each week—the attendance varied depending on the topic. Figure 1, which shows corrosion on the nose of the Statue of Liberty, is one of a series of hundreds of slides used to

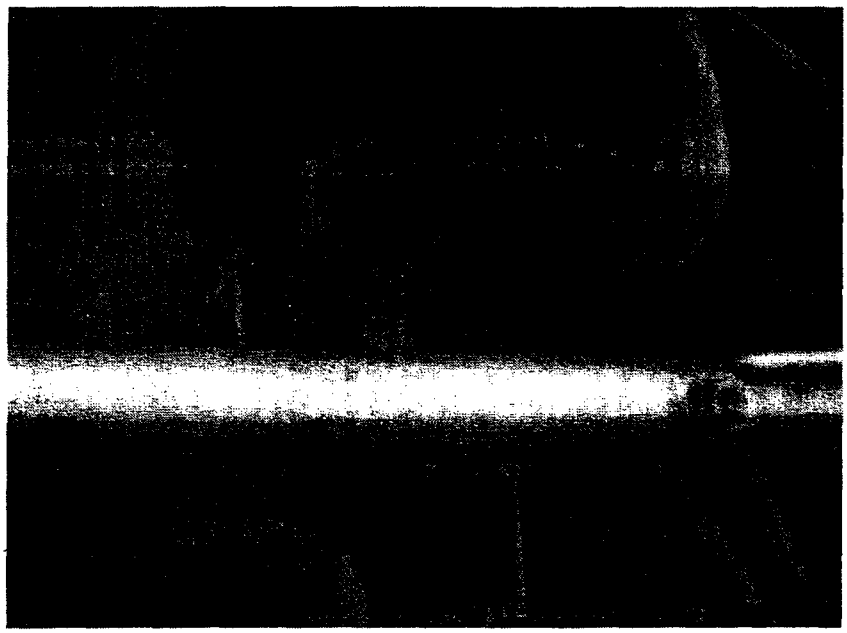

Figure 1: Corrosion on the nose of the Statue of Liberty caused by inadequate drainage of condensation forming on the inside of the statue.

discuss various aspects of corrosion control. Most participants in the course were chemists by training, so the course emphasized materials, a subject where most chemists have little or no formal training. Other subjects included in the course included basic electrochemistry, cathodic protection, and inspection techniques.

3. EVALUATION OF COMMERCIAL WASH ADDITIVES USED FOR CONTROL ON ARMY AIRCRAFT

Corrosion is a major problem facing the Army. Aircraft in use by the Army must be maintained for decades, and Army aircraft are frequently used and maintained under more

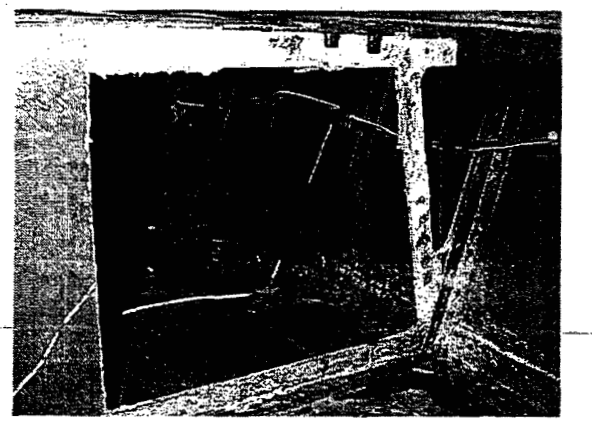

Figure 2: Helicopter corrosion due to the use of an improper cleaning compound

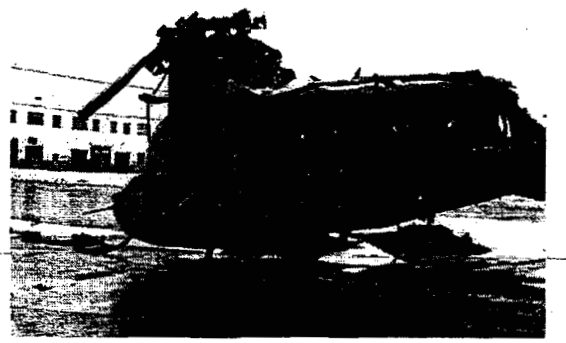

Figure 3: A crashed Chinook helicopter caused by hydrogen embrittlement due to the use of an improper cleaning compound.

corrosive circumstances than civilian aircraft. Figures 2 and 3 show the results of the use of improper cleaning compounds on Army aircraft. Excessive maintenance costs (Figure 2) are bad enough, but the loss of a $12 million helicopter (Figure 3) is even worse. Fortunately, no loss of life was associated with the crash shown in Figure 3. [2]

The Army has funded a multi-year exposure test at the Kennedy Space Center with the objective of determining the effectiveness of a variety of commercial products that are being promoted for washing helicopters and airplanes. Four commercial products are being tested and compared with three controls: washing with seawater, washing with demineralized water, and no washing. Table 1 shows the chemical analyses of the products under test.

Table 1

Chemical analysis of cleaning agents

	Concentration, ppm			
Sample ID	#1	#2	#3	#4
ANIONS				
Fluoride	nd	nd	3,477	nd
Chloride	110	60	nd	232
Nitrite	91	131	nd	314
Nitrate	94	nd	166	9,511
Phosphate	25,191	65	80	nd
Sulfate	1,152	92	227	529
CATIONS				
Sodium	7,930	2,367	1,453	nd
Ammonium	nd	1,919	134	36,053
Potassium	5,537	116	280	1,023
Magnesium	nd	nd	nd	nd
Calcium	48	56	60	nd

Three sets of identical panels are exposed on special racks at the KSC Atmospheric Test Facility. Six of the seven exposure programs require weekly washing with a liquid cleaner mixed according to the manufacturer's specifications. This is shown in Figure 4.

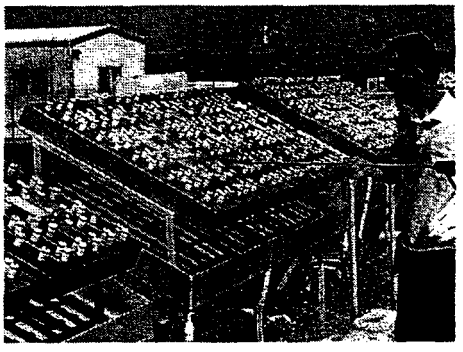

Figure 4: Weekly washing the top surfaces of exposure panels

After almost two years of exposure, some of the panels are corroding and some of them are in relatively better condition. Figure 5 shows exfoliation corrosion of 7075T6 aluminum panels washed with one of the commercial solutions. The condition of these

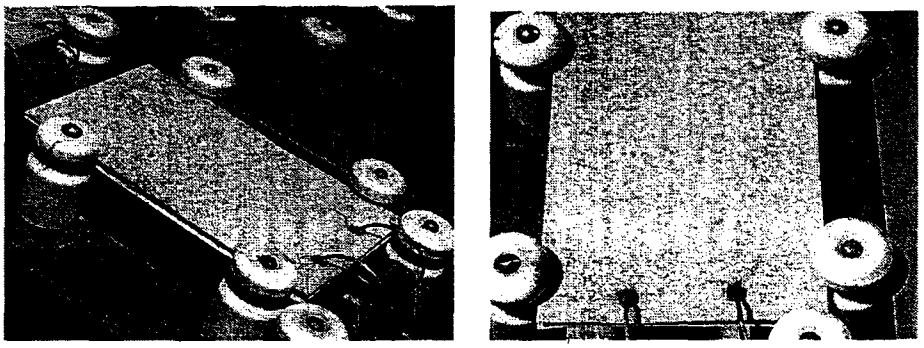

Figures 5a and 5b: Alternate views of Aluminum 7075T6 panel showing exfoliation corrosion.

panels appears worse than the control panels that were not washed or were washed with seawater. Two of the sets of panels being washed with commercial cleaners were showing exfoliation corrosion in July 2002. The other two sets of panels, washed with different cleaning solutions, seemed to show less corrosion, and no exfoliation was evident. The control exposures with demineralized water washing and with no washing seemed to produce better results than the two solutions that allowed exfoliation of the 7075T6 aluminum.

The samples are still under test, and they are not scheduled for removal from the beach until October 2002. Until this is done, it will be impossible to definitely rank the efficiency of the cleaning solutions, but one of the solutions may be doing better than the rest.
Figure 6 shows all of the alloys under test with one of the cleaning agents. The arrow points to a 6061T6 aluminum panel with a chromate conversion coating. The color of the chromate conversion coating was still apparent when this photo was taken in July 2002. The color was not apparent on similar panels of the same alloy/chemical treatment washed with any of the chemicals or on any of the control exposures.

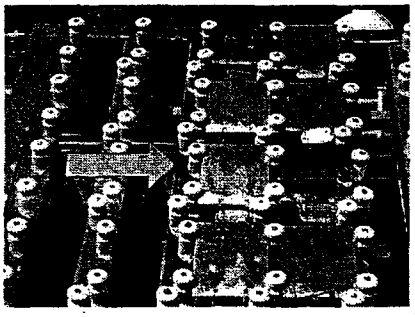

Figure 6: Effective wash additive with residual chromate color showing on middle aluminum panel.

A review of the results of the one-year test showed little weight loss and minimal pitting corrosion. Ranking of the exposure/washing conditions was very difficult.

Preliminary inspection during the summer of 2002 indicates that the extent of corrosion will be substantially greater after two years of exposure and that definite ranking of the exposure/washing conditions will be possible. The ASTM standards used for evaluating the alloys seem adequate for this purpose. Problems identified during the summer include a lack of documentation of how the one-year results were obtained. Photography to show the conditions

shown in Figure 4 will also be necessary.

4. CATHODIC PROTECTION OF REINFORCED CONCRETE STRUCTURES

Figures 7a and 7b show failures of reinforced concrete structures due to corrosion. Corrosion of reinforced concrete is a major problem on a variety of structures including buildings, highway bridges, and NASA KSC launch facilities. KSC has developed a new method of cathodically protecting concrete structures to limit/stop corrosion.

Figures 7a and 7b: Structural damage resulting from corrosion of reinforced concrete buildings [4-5]

The concrete samples with a developmental cathodic protection system are under test at the KSC corrosion test site. Review of the test procedure and the experimental setup has indicated that the following ideas should be incorporated into the KSC corrosion test plan:

1. Scanning electron microscopy should be added to the evaluation plan for all concrete corrosion tests at KSC. Concrete is a very inhomogeneous material, and the SEM can be used to determine migration paths, degradation mechanisms, etc. in concrete. Figure 8 shows how the X-ray spectroscopy capability of the SEM is being used by the Oregon Department of Transportation in their collaborative research with the U.S. Bureau of Mines laboratory in Albany, Oregon.

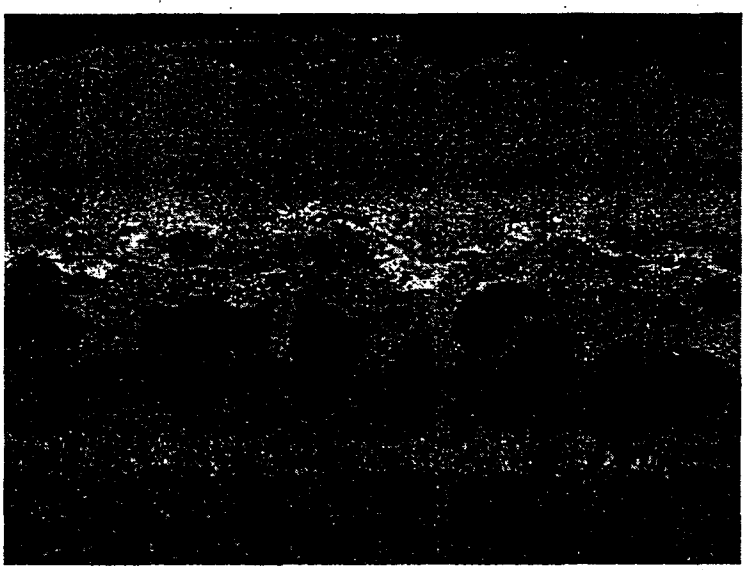

Figure 8: X-ray image map of chorine pattern in cathodically-protected concrete [6]

2. A technique for marking the depth of pH changes associated with either carbonation (reaction of the concrete with the CO2 in moist air) or with the effects of cathodic protection should be practiced and demonstrated. It should then be demonstrated on the initial samples at the start of the cathodic protection testing and at the end of the test.

3. Chloride analysis (ASTM total chloride testing) [7] should be started and documented. Initial efforts on this were underway during the week of 5 August. Wayne Marshall in the Chemistry group will conduct the test and coordinate with Prof. A. Sagues at the University of South Florida on these tests.

5. ACKNOWLEDGEMENTS

Dr. Luz Marina Calle was the NASA colleague whose original ideas started this project. She also obtained funding for its continuation. I thank her for her insight, ideas, and thoughtful contributions and encouragement. Louis McDowell is the NASA researcher most responsible for the continuing vitality of the Corrosion Test Bed efforts at Kennedy Space Center, and I thank him for his foresight and determination in keeping Kennedy Space Center as a major source of government expertise in corrosion research, engineering, and testing. Joe Curran from Dynacs insured that support was available whenever necessary. This work could not have been done without all of their help.

6. REFERENCES

[1] Cost of corrosion: In the U.S.A. $276 billion/yr, http://www.corrosioncost.com/home.html., August 6, 2002.

[2] Aircraft cleaners, http://www.chinook-helicopter.com/maintenance/issues/cleaners/cleaners.html)., August 6, 2002.

[3] Kennedy Space Center Corrosion Technology Test Bed, http://corrosion.ksc.nasa.gov/, August 6, 2002.

[4] Damage from chloride-based deicers, http://www.cryotech.com/imgs/garage.gif, August 6, 2002

[5]. R. Heidersbach, "Corrosion,' Chapter 3 in An Attorney's Guide to Engineering, 1. Kuperstein and N. Salters, eds., Matthew Bender & Company, New York, 1986.

[6] Photo image supplied courtesy of S.Cramer, U. S. Bureau of Mines Albany Research Center, June 2002.

[7] Chemical Analysis of Hydraulic Cement, ASTM Standard C114-00, ASTM, Philadelphia.

2002 NASA/ASEE SUMMER FACULTY FELLOWSHIP PROGRAM

JOHN F. KENNEDY SPACE CENTER
UNIVERSITY OF CENTRAL FLORIDA

KSC HISTORY PROJECT

Patrick K. Moore
Assistant Professor
Public History Program Director
Department of History
University of West Florida

Dr. Shannon Roberts, Ph.D.
Associate Director, XA
NASA KSC Colleague

ABSTRACT

The 2002 NASA/ASEE KSC History Project focused on a series of seven history initiatives designed to acquire, preserve, and interpret the history of Kennedy Space Center. These seven projects included the co-authoring of *Voices From the Cape,* historical work with NASA historian Roger Launius, the completion of a series of oral histories with key KSC personnel, a monograph on Public Affairs, the development of a Historical Concept Map (CMap) for history knowledge preservation, advice on KSC history database and web interface capabilities, the development of a KSC oral history program and guidelines of training and collection, and the development of collaborative relationships between Kennedy Space Center, the University of West Florida, and the University of Central Florida.

KSC HISTORY PROJECT

Patrick K. Moore

Introduction

Since July 24, 1950, with the launch of a modified German V-2 rocket called Bumper 8, the focus of the United States space program centered on the areas of Cape Canaveral and what would later become the Kennedy Space Center. In 1958, faced with a growing Cold War military threat, the United States Congress created the National Aeronautics and Space Administration to oversee the development of the nation's civilian space program. By the nature of that Act, Congress designed the agency to cultivate new avenues for space exploration and, in contrast to the Soviet Union, to keep the developments of the operations "open to public inspection." In keeping with that mission, NASA proceeded to face the challenges of exploring not only the earth's outer atmosphere, but also the other planets of the solar system and the cosmos beyond. In time, the obstacles facing NASA evolved from a Cold War mission to one of technical and scientific exploration. For KSC, despite the national and international issues surrounding the agency, they remained dedicated to safe and successful Spaceport operations. As part of that process, the American public, as well as much of the global population, focused their attention on the evolving activities and took ownership of the NASA program and the Kennedy Space Center in both its triumphs and its tragedies.

While the NASA operations encompass Centers and field operations across the country, for many people, Kennedy Space Center became the focal-point of the space program because of the highly visible launch and landing operations. Despite this international attention directed at the Center, the process of collecting and preserving its rich history was occasionally lost between the transition of programs and amidst the excitement of launches. Because of this, the KSC Public Affairs Office and the KSC Archives actively set out to create a formal history preservation program that would enable the Center to acquire, preserve, and interpret its history before the institution loses the pioneers of the many important programs and their personal papers and collection. As part of this endeavor, Public Affairs secured funding for a visiting faculty fellow to assist in the accomplishment of this monumental task. During the summer of 2002, the collaboration between Kennedy Space Center and the University of West Florida resulted a series of seven history initiatives for the ongoing mission of the KSC History Project. These projects included:

1. Co-author, with Dr. Roger Launius, *Voices From the Cape*.
2. Complete 4 oral histories of key KSC officials.
3. Complete historical monograph on KSC public relations.
4. Develop Concept Map prototype using UWF's Institute of Human and Machine Cognition's C-Map technology.
5. Advise KSC on development of KSC history database and web site interface capability.
6. Advise KSC on development of "KSC Training of Oral Historians" capability.

7. Develop collaborative framework for future history-related activities between KSC, the UWF Public History Program and Institute of Human and Machine Cognition, the University of Central Florida, and other universities and colleges, as appropriate.

Voices From the Cape

In 1999, the NASA History office published Glen Swanson's "*Before This Decade Is Out. . .": Personal Reflections on the Apollo Program*. This work that incorporates edited oral histories of fourteen prominent participants in the Apollo program including Center Directors, engineers, astronauts, and others. While the work was quite successful with readers, both NASA employees and the general public, its focus was strictly on the early lunar programs and the residual Skylab and Apollo Soyuz Test Project between 1961 and 1975. Although important, the Space Shuttle and International Space Station programs during the following twenty-five years offered an equally important aspect of the NASA story. Based on this, historians conducted a series of interviews between 2000 and 2002 that highlighted the entire scope of Kennedy Space Center History. Designed to celebrate the 40th Anniversary year of KSC, the project completed the final interviews for *Voices From the Cape* and began the initial development for publication in early 2003. Developed chronologically, with the earliest pioneers at the Cape and ending with the current Center Director, each chapter is a specific individual's story, an introductory essay, and a biography that provides a cohesive connection between sections. Potential interviews include key individuals Wernher von Braun and former Director Kurt Debus, but may also include the following:

Ike Rigell – Retired NASA engineer. First came to KSC as contractor to work on launches in 1953, worked on Redstone project and later came to KSC for the early Space Shuttle programs.

JoAnn Morgan – Engineer, Director of External Relations and Business Development. Started at the Cape in 1958 as one of first female engineers that paved the way for future women at the Center. Influence and experiences continue to the present.

Richard (Dick) Smith – Former KSC Center Director. Worked on the Redstone project, talks about working with Von Braun and Debus. Discussion of his career as aeronautical engineer, positions at other space centers, work before KSC on Space Shuttle programs.

Lee Solid – NASA engineer. First came to Cape in 1960. Previously worked as contractor with Rocketdyne and U.S. Air Force. Witnessed nearly every human launch. Covers Atlas, Mercury programs through to the present Shuttle program.

Gene Thomas – Retired NASA engineer. First came to the Cape in 1962. Covers his early background, changing nature of his career at KSC. Discusses Mercury through Space Shuttle programs and Challenger disaster.

George Page – Retired aeronautical engineer. Came to KSC in 1963 to work on Atlas program. Covers his early background, changing nature of his career at KSC. Addresses Atlas program through early Space Shuttle program.

Paul (Ernie) Reyes – Retired NASA engineer. Started with NASA during Mercury program and continued during Gemini, Apollo programs. Details Apollo 1 fire. Covers changing nature of his career at Kennedy from Gemini through Space Shuttle programs.

Hugh Harris – Former KSC Chief of Public Affairs. Started with NASA (Glenn Research Center) in 1963, came to KSC permanently in 1975. Covers his career in NASA media relations, and KSC's relationship with the press and public between Apollo and Shuttle programs.

Alan Parrish – Retired NASA engineer. Came to KSC in 1964 to work as a television systems engineer. Covers KSC's relationship with the outside press and discusses Apollo through Space Shuttle programs.

Bob Sieck –Medical engineer. Came to KSC in 1964. Covers his early background and changing nature of his career with KSC. Discusses Gemini through Space Shuttle programs.

Robert (Bobby) Bracken – NASA engineer. Came to KSC in 1966 out of college and discusses end of Gemini through the present. Covers the changing nature of his career at KSC.

John Straiton – NASA engineer. Came to KSC in 1968 right out of college. Went to Vandenberg briefly, then came back to KSC. Discusses pre-Space Shuttle, through the present. Covers the changing nature of his career at KSC.

General Forrest McCartney – Former KSC Center Director, long career in the U.S. Air Force. Came to Patrick AFB in 1971 and to KSC in 1986. Discusses differences and similarities between the military and NASA and the recovery from Challenger.

Lisa Malone – Deputy Director, External Relations and Business Development. Started at KSC as a journalism co-op student in 1982. Interview covers changing role and treatment of the press corps, nature of public relations and visitor interactions at KSC.

Roy Bridges, Current Center Director. Previous commander of Patrick Air Force Base, astronaut who flew aboard STS-51 F, and came to KSC in March, 1997. Covers career and experiences including the focusing of KSC into a Space Technology Center

In order to have the completed product of *Voices From the Cape* available for the concluding Celebration of the 40th Anniversary Celebration in July, the following represents the projected abbreviated timeline for the project:

September 30: Completed Selection of subjects, interview quotes, and draft intro essays.

November 15: Completed review of materials by KSC and NASA Headquarters.

December 31: Completed manuscript for publication. Submit for design and layout

February 28: NASA Headquarters send to print

KSC Oral Histories

Although the NASA/ASEE project agreement stipulated the completion of four (4) oral histories during the summer program, as a result of the demands for the historic monograph and *Voices From the Cape*, Dr. Moore completed eighteen (18) oral history interviews. Primarily focusing on Public Affairs media and visitor operations, completed interviews, with transcripts pending from KSC contractor, include the following:

Howard Benedict, AP Reporter, 1957-1990

Hugh Harris, KSC Public Affairs, NASA 1963-1998

Jim Ball, Visitor Complex, ISS Research Park, 1980-Present

Bill Harwood, CBS News, 1984-Present

Col. Kenneth Grine, CCAS Public Affairs Officer, 1956-1962

Barbara Grine, CCAS Employee, Contractor, 1956-1972

Jay Barbree, NBC News, 1959-Present

George English, KSC Executive Officer, 1960s-1990s

Larry Mauk, KSC Visitor Complex, 1965-Present

Arnold Richman, KSC Public Affairs, 1964-1995

Sue Butler, Independent Reporter, 1958-Present

Jack King, reporter, 1958-60; KSC Public Affairs, 1960-1970s

Manny Virata, KSC Public Affairs, 1974-Present

Dennis Armstrong, KSC Public Affairs, Web operations, 1986-Present

Kathy Hagood, Spaceport News, 1998-Present

Dan LeBlanc, Delaware North operations, 1996-Present

Bruce Buckingham, KSC News Chief, 1985-Present

Diana Boles, KSC Media Services, Coordinator, 1965-Present

Fueling the Fascination: Kennedy Space Center and the World's Spaceport Romance

Building on Dr. Moore's research specialization as a historian specializing in Cold War Culture, his monograph addressed the changing patterns in which Kennedy Space Center and its Public Affairs operations recognized the population's intrinsic interest and connection with the institution and worked, at varying levels, to cultivate their intrigue, communicate the intricacies of the operation, and capitalize upon this interest in furthering both the Center's and NASA's spaceflight mission. Originally expected to be forty pages in length, the final eighty page version charts Public Affairs' evolving press and visitor operations through three periods in KSC's history.

This begins with the Cold War years between 1957 and 1975 when the United States succeeded in its competitive quest for the Moon. During that period, press access evolved from the military denial of repeated missile launches to the NASA coordination of thousands of press and visitors attending the historic Apollo 11 and subsequent lunar missions. For curious visitors to the site, the process began with "drive-thru"car tours of the Cape in 1963 and later emerged into formal bus tours in 1966 and the opening of the Visitor Information Center in 1967.

During the next phase of KSC public operations from 1976 to 1986, the Center changed from a Cold War driven institution to one based in science and technological exploration. For the

press, they too began adjusting their views and celebrated the return of a human to space in 1981 with the successful launch of the orbiter *Columbia* on STS-1. For visitor operations, this too was a time of change. No longer could Public Affairs rely on guests arriving at the site simply to embrace the history of the operations. Following the opening of Walt Disney World in 1971 and of Epcot in 1983, suddenly guests expected better service and more captivating presentations. As a result, the Visitor Information Center began discarding the trade-show displays of the past and concentrating on maintaining the new market.

The final period between 1986 and the present marked the greatest transition for KSC from both an operational and a Public Affairs perspective. Following the terrible *Challenger* accident, relations between the Center and the press dramatically changed. Because of the lack of an agency-wide contingency plan, NASA failed to quickly respond to reporters' informational demands. Although relations improved during the later years, the era where the press accepted NASA operations as a given changed to a more inquisitive and questioning approach. Regardless of the change, KSC managed to develop new methods for disseminating information including the use of the Internet for broadcasting program updates and Shuttle launches and landings. For Public Affairs, the growing tourism market demands led KSC to select a new concessionaire for their Visitor Complex and responded to the guest expectations in opening a series of new facilities and shows with the cornerstone being the extraordinary Apollo Saturn V Center. Incorporating both the educational and entertainment approaches, KSC continued the quest of sharing the past, present, and future of the NASA program to a new young audience of future participants and leaders in the quest for space.

As a central aspect of the KSC operations, *Fueling the Fascination* marks the first scholarly evaluation on the subject of Public Affairs operations. Upon review, the work should be published as part of the NASA *Monographs in Aerospace History.*

Historical Concept Mapping (CMap) and the History Database

Working with the University of West Florida's Institute of Human and Machine Cognition (IHMC), Dr. Moore and the UWF Public History Program developed new and important research tools. Coined "concept mapping," these tools are based upon IHMC computer-driven models for acquiring, organizing, presenting, and preserving institutional knowledge. Unlike a book or report that reads from start to finish, these "cognitive prostheses" allow both researchers and audiences to identify and address materials through significant interrelating concepts rather than through the rigid, and often inflexible, framework of conventional publications. Since the original collaboration between the IHMC and UWF Public History Program to develop better knowledge acquisition techniques, we have applied these tools to several projects and realized the benefits of concept mapping to historical research and evaluation. As part of the history initiatives at Kennedy Space Center, Dr. Moore worked to create a CMap prototype to address the Center's history and create a cognitive tool for working with the various aspects of its development.

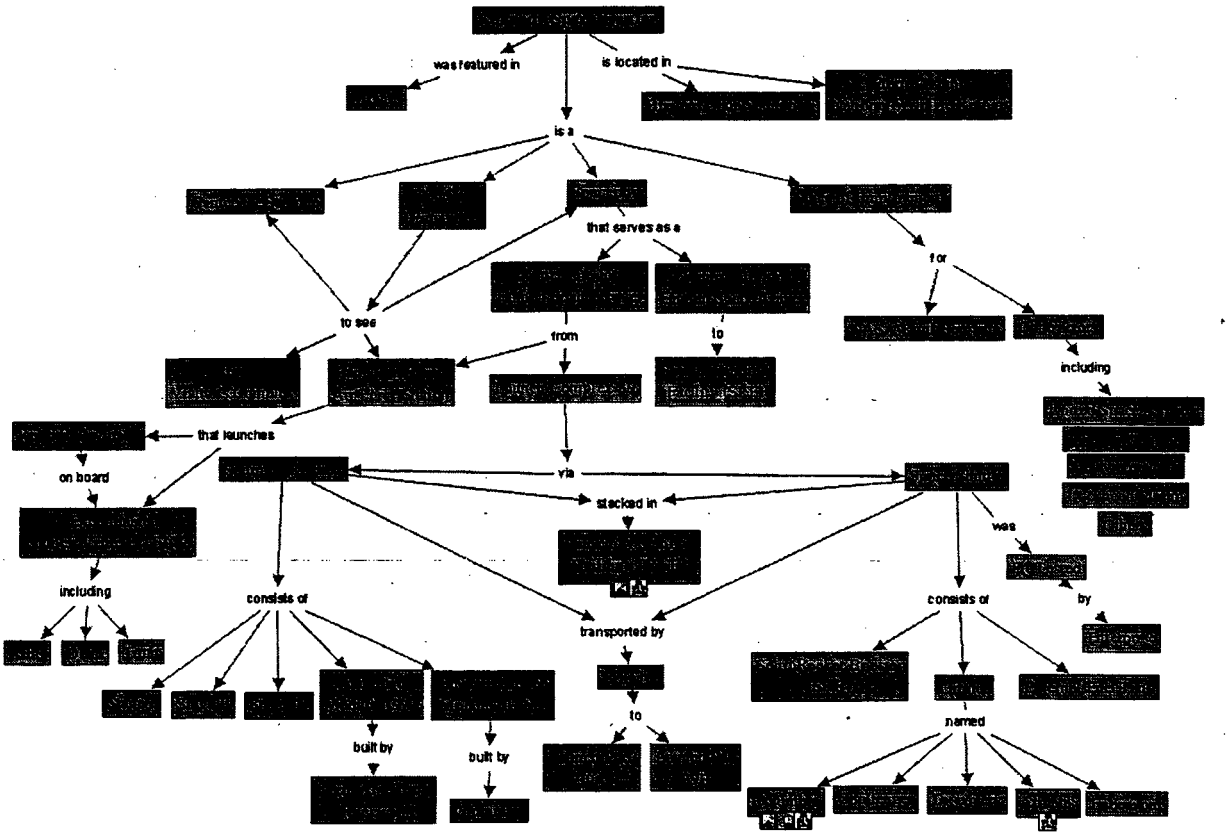

Figure 1.

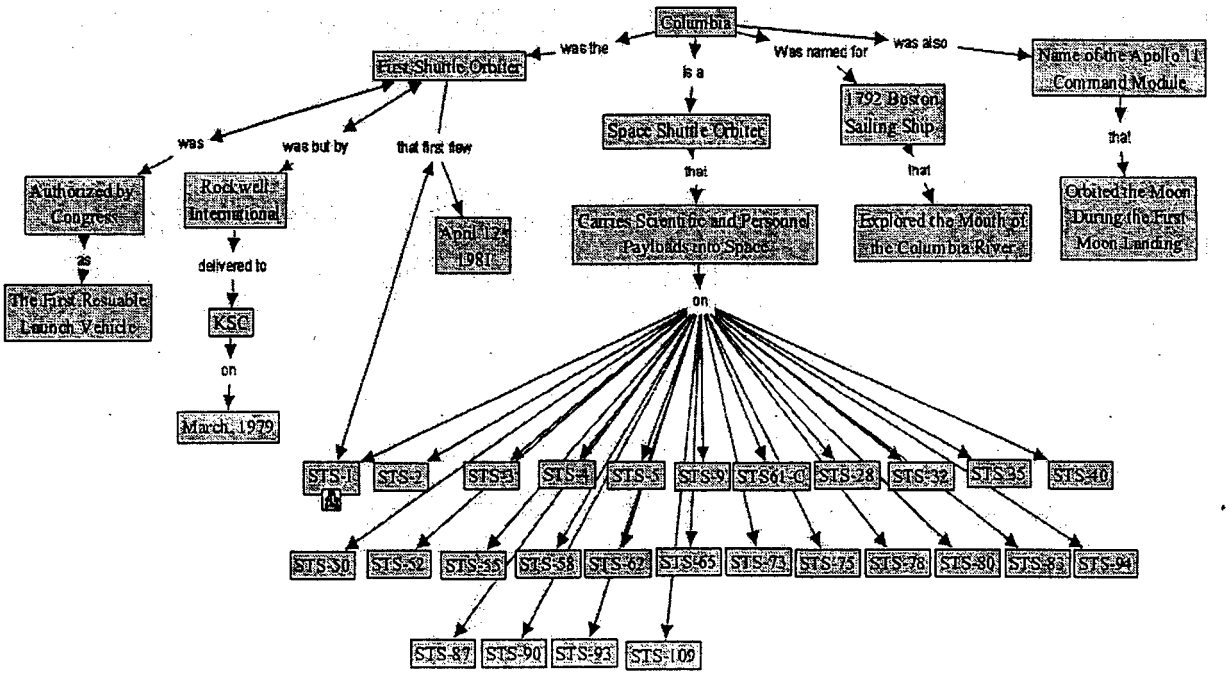

Figure 2.

Starting with the "KSC Master Map" (Figure 1) the structure provides key current and historic activities, or "concepts" connected by linking phrases. Once fully "populated" (containing icons for access to secondary maps and supporting materials), each of the concepts on the Master Map will contain specific key materials and maps. Examples of these are below the Concepts for the "Vehicle Assembly Building (VAB)," the "Columbia," and "Atlantis." Please note that these maps are explanatory prototypes and are far from fully populated. Users can either click on photographs, video clips, interviews, and other materials to explain the specifics of the concept. To explore the concept at a deeper level, users can then click on the secondary maps icon to open a new map.

Opening the secondary map under "Columbia" users find themselves at the "Orbiter Columbia Map" (Figure 2). In this map, users can explore the history of the specific orbiter as well as the purpose behind the vehicle and specific missions. Again, in a fully populated map this too would provide a spectrum of materials pertaining to the specific orbiter. For this exercise, however, the user would select the map under on the "STS-1" concept opening the "STS-1 Mission Map" (Figure 3). At this level, researchers and interested parties can work their way through the mission specific concepts. Once fully populated, additional materials, including yet another round of detailed photographs, video clips, oral history interviews, report selections, and others would provide detailed discussion of the mission, its crew, its successes, problems, and resolutions.

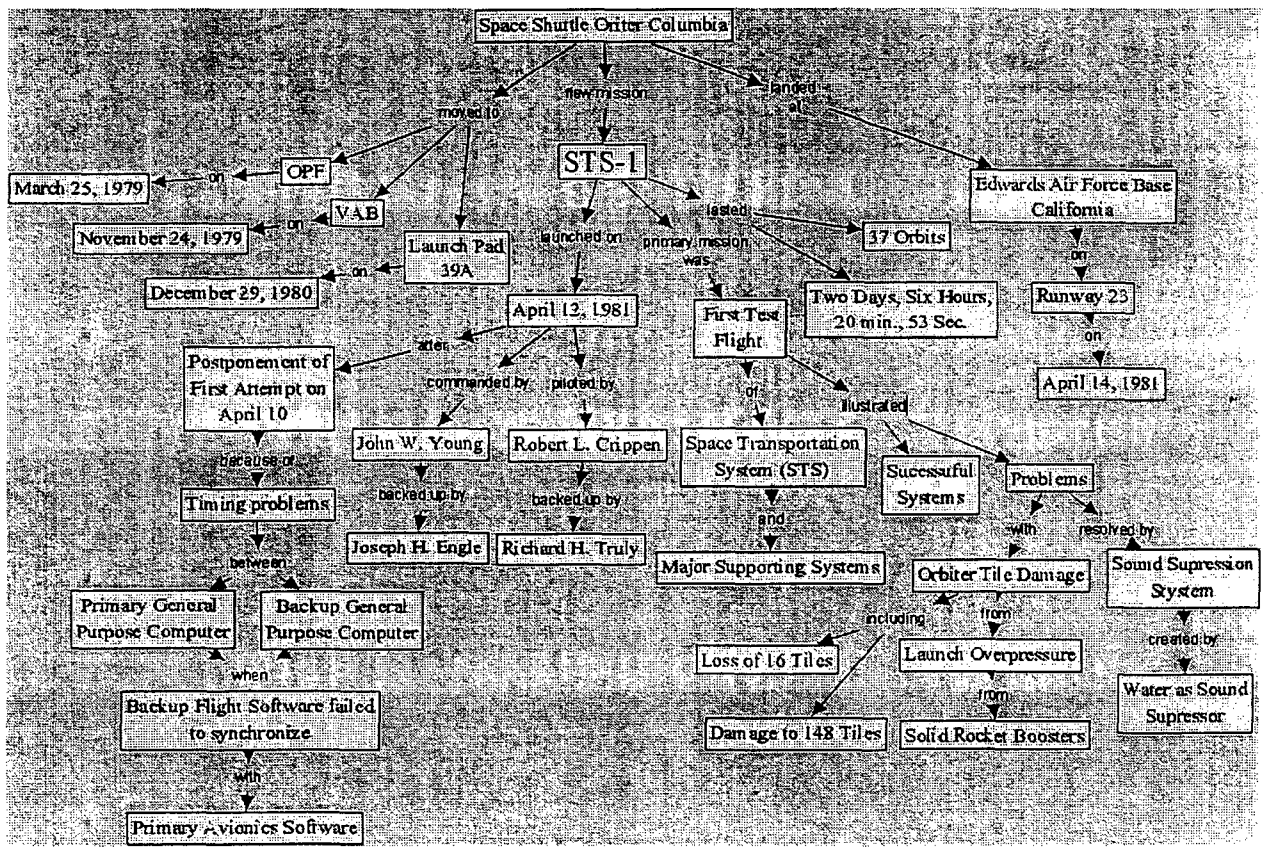

Figure 3.

By incorporating the existing KSC History Database into the CMap frame work, the tools will provide all interested parties, including researchers, policy planners, engineers, historians, and many others, with a conceptual framework for understanding all aspects of Kennedy Space Center. Further, by applying these tools to the existing Kennedy Space Center Website, Internet users all over the globe can access and understand the depth of the Center, its history, and its personnel.

KSC Oral History Program

As one of the most valuable and informative resources for collecting history, Kennedy Space Center began the task of collecting oral histories during previous programs and with the assistance of the NASA History Office. Building on this background, KSC desired additional focus to the collections process. From this, Dr. Moore, who previously served as Director of the Arizona Historical Society Oral History Program, prepared a framework for the KSC Oral History Program.

The Kennedy Space Center Oral History Program is dedicated to the recording and preservation of the memories and experiences of the Kennedy Space Center, Cape Canaveral Air Force Station and other locations as deemed appropriate. These memories and experiences include those of individuals of all ages, sexes, ethnic or national heritages, social and economic classes, education levels, and backgrounds.

Within this framework, Dr. Moore developed a set of materials that represent the proposed mission, focus, policies, procedures, and pertinent forms and documents associated with the National Aeronautics and Space Administration, Kennedy Space Center Oral History Program. The materials for this program are based on the most current approaches and methods of the discipline as accepted by professionals in the field and from the Oral History Association. These approaches, however, reflect current trends and, as with any program, should constantly evolve to reflect new approaches and accepted standards.

Collaborative Framework

As the final initiative of the summer KSC History Project, Dr. Moore, in conjunction with Dr. Shannon Roberts and Dr. Gregg Buckingham, created a series of opportunities for future collaboration between Kennedy Space Center, the University of West Florida, and the University of Central Florida.

For the UWF and KSC interaction, Dr. Moore identified a series of opportunities for the placement of interns with the UWF Public History graduate program. As part of the existing curriculum, students must complete a 200-hour internship during which time they complete a project within their area of Public History specialization. Working with the specific graduate program fields, Dr. Moore arranged the framework for students to work in three areas of the KSC operations. The first is within the KSC Archives where students can complete a variety of archival-management and history-focused projects as well as CMap development. The second is with Delaware North Park Services where students concentrating in museology (museum studies) can help develop exhibits, interpretive presentations, and other projects. The final area is working with the Webcast studio where students specializing in media and documentary production can develop historic pieces on KSC and program histories for broadcast over the Internet.

To fund these projects, the collaboration between UWF and KSC creates the unique opportunity for grant submissions to numerous humanities, history, and space related funding operations. Although as a federal agency guidelines prohibit NASA from applying for grants, the university relationship enables UWF to obtain funds for the completion of various projects. From this, the benefits extend to both the graduate students in the completion of their projects and to Kennedy Space Center for the furthering of their History preservation and interpretation goals. To formalize this agreement, upon return to the University of West Florida, Dr. Moore will work with UWF and KSC officials to craft a formal memorandum of understanding. This in turn will validate the ongoing cooperative venture between the two entities.

Beyond the KSC-UWF arrangement, Dr. Moore and Dr. Shannon Roberts also initiated communication with units at the University of Central Florida. Building upon the CMapping technology from the UWF Institute for Human and Machine Cognition, representatives tentatively explored the future collaboration opportunities with the UCF Institute for Simulation and Training. Upon completion of the first operational CMap from the materials obtained during the summer 2002 work, representatives from both organizations will meet to explore future interactive and funding opportunities. Also at the University of Central Florida, Dr. Moore and Dr. Roberts met with representatives from the UCF Department of History. Where working relations currently exist with the department for the collection and preservation of NASA's influence on Brevard County, further opportunities could well develop in the future. Following a comprehensive faculty search, the UCF Department of History will hire a new tenured historian to start a new Public History Program in the Fall of 2003. Based upon the focus of that new program, collaborative efforts between the ongoing UWF Public History Program activities and KSC could well provide a wealth of new opportunities.

Conclusion

As a result of the 2002 Summer KSC History Project through 2002 NASA/ASEE Summer Faculty Fellowship Program, the Kennedy Space Center has a number of valuable new resources. From this framework now exists continued history collection, preservation and interpretation through the creation of the CMap prototypes, the KSC Oral History Program Policies and Procedures, and the collaboration between the University of West Florida and Kennedy Space Center. Second, the Center now has the completion of a significant work on the history of the KSC press and visitor operations and a completed series of eighteen new oral history interviews. Finally, upon the completion of *Voices From the Cape*, Kennedy Space Center will have a significant historical publication in celebration of its 40th Anniversary.

2001 NASA/ASEE SUMMER FACULTY FELLOWSHIP PROGRAM

JOHN F. KENNEDY SPACE CENTER
UNIVERSITY OF CENTRAL FLORIDA

THE VIRTUAL TEST BED PROJECT[1,2,3]

Luis C. Rabelo, Ph.D.
NASA Fellow
lrabelo@mail.ucf.edu, lrabelo@alum.mit.edu
4000 Central Florida Boulevard
Industrial Engineering and Management Systems (ENG 2, Room 312)
University of Central Florida
Orlando, Florida 32816

ABSTRACT

This is a report of my activities as a NASA Fellow during the summer of 2002 at the NASA Kennedy Space Center (KSC). The core of these activities is the assigned project: the Virtual Test Bed (VTB) from the Spaceport Engineering and Technology Directorate. The VTB Project has its foundations in the NASA Ames Research Center (ARC) Intelligent Launch & Range Operations program. The objective of the VTB project is to develop a new and unique collaborative computing environment where simulation models can be hosted and integrated in a seamless fashion. This collaborative computing environment will be used to build a "Virtual" Range as well as a "Virtual" Spaceport. This project will work as a technology pipeline to research, develop, test and validate R&D efforts against real time operations without interfering with the actual operations or consuming the operational personnel's time. This report will also focus on the systems issues required to conceptualize and provide form to a systems' architecture capable of handling the different demands.

[1] This report will constitute the basis for future papers to be presented in conferences and submitted to journals. These papers will include my NASA colleagues as co-authors.

[2] Henry McCoy, Robert Turner, Jeppie Compton, and Darrin Skelly have contributed to this report.

[3] Robert Turner is the NASA-KSC Project Manager of the Virtual Test Bed Project. Jorge Bardina from NASA ARC is the associated NASA Researcher.

THE VIRTUAL TEST BED PROJECT

Luis C. Rabelo, Ph.D. - NASA Fellow

1. Introduction

The contributions to the Virtual Test Bed (VTB) Project during this fellowship are extensive. These contributions can be classified into the following areas: **(1)** systems architecting activities, **(2)** evaluations of models and processes, **(3)** evaluations of technologies, **(4)** systems design, **(5)** facilitation of technical meetings, **(6)** support to improve the communications of technical concepts and project management activities, **(7)** intellectual property consulting, **(8)** submission of proposals for funding, **(9)** documentation and technology transfer, and **(10)** liaison with Academic groups. Due to restrictions of space in this report, we will focus on the following four areas: systems architecting activities, evaluations of models and processes, evaluations of technologies, and systems design.

This report is organized in the following sections. Section 2 introduces general concepts. These concepts will be needed to understand the objectives of the project and its implications for the future of NASA. Systems Architecting contributions is the topic of Section 3. The systems architecting activities deal with the utilization of the House-of-Quality to translate the users' needs to the design requirements. Section 4 discusses the models and process evaluations activities accomplished during this fellowship. The CALPUFF model was reviewed from its computing characteristics viewpoint (operating system, hardware platform, computer programming language). In addition, Section 4 presents a process flow to determine the E_c based on the Blast Overpressure Assessment Model (BLASTX). The technology evaluations and recommendations are presented in Section 5. Section 5 presents a summary of different tools and technologies that can be used to develop the Virtual Test Bed. The last section is Section 6. Section 6 describes the systems design contributions to the project.

2. General Concepts

Virtual test bed environments are the next S-curve[1] of the computer-aided design (CAD) systems. These "advanced" CAD environments will combine not only the 3D solid modeling capabilities of the current CAD systems but also will integrate in a seamless fashion models that represent the different stages of the life-cycle of a system. Therefore, the 3D solid models of the mechanical/physical design will be integrated to the materials models, dynamics models, environmental models, operational models (including operators, crew members), safety models, and other type of models. These virtual environments will go beyond the virtual world attempts of the 90's. The virtual worlds of the 90's concentrated on the look and feel dimensions. However, a virtual environment will go beyond the former cosmetic approach with higher realism and fidelity, and more emphasis on engineering. Virtual test beds will create multi-disciplinary and collaborative design spaces.

From another viewpoint, the current CAD environments concentrated not only in a single dimensional view of a system but are also not adequate for complex systems design. One interesting characteristic of a complex system is that it is by default a system of systems. To be faithful to concurrent engineering principles, you have to study the interactions among the different systems that are elements of the complex systems. This system of systems is non-linear in nature and the interactions among the different components bring interesting emergent properties that are very difficult to visualize and/or study by using the traditional approach of decomposition.

A very interesting outcome of the current CAD systems is that the single view, which they display, have limited them to just being geometric design collaborative environments. For example, to develop a specific product, a CAD system will only serve as a collaborative environment to those

[1] S-curves are used to study the evolution path of technologies.

members of the design team that only need to know or use 3D Solid Modeling characteristics and/or geometric features. A virtual test bed environment is not only related to geometric design but also includes other properties such as materials, operational behavior, and interactions. A more comprehensive modeling environment such as a virtual test bed will need to have enhanced usability and connectivity capabilities to become an effective collaborative environment.

Spaceports are complex systems. According to Barth [1] "Spaceport technologies must employ a life-cycle "system of systems" concept in which major spaceport systems – launch vehicle processing systems, payload processing systems, landing and recovery systems, and range systems – are designed concurrently with flight vehicle systems and flight crew systems." Therefore, it seems logically to think that a virtual test bed can host the different

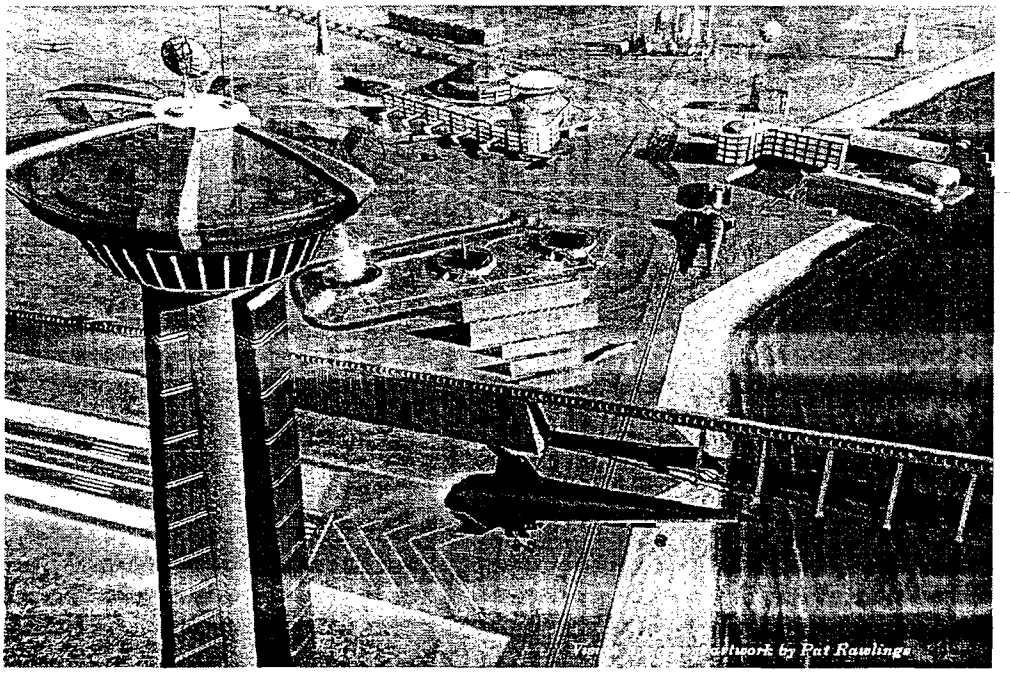

Figure 1. Conceptualization of a future spaceport.
(Vision Spaceport artwork by Pat Rawlings/SAIC)

models that represent different systems and elements of a spaceport. These models in the virtual test bed will work in an integrated fashion synthesizing in a holistic view and becoming together a Virtual Spaceport. This Virtual Spaceport can be utilized to test new technologies, new operational processes, the impact of new space vehicles in the spaceport supply chain, and the introduction of higher schemes of decision-making. A Virtual Spaceport will allow an intelligent visualization of the entire spaceport concept and the implementation of knowledge management strategies.

Another important and interesting system of the spaceport is the range. The range has different definitions depending on the NASA Center. In this report the range will follow the NASA-Kennedy Space Center (KSC) definition. According to KSC, the range is a "physical volume of space that opens during launch. It's used for vehicle tracking, telemetry, and communications, among other things." [1] The range encompasses many different operations. One of them, range safety has a high level of complexity. The Eastern Range (ER), with its launch base at Cape Canaveral Air Station, is under the observance of the 45th Space Wing (Patrick Air Force Base is the headquarters). The responsibilities of the safety offices at the ER and NASA-KSC include three areas [19]: (1) System safety reviews, (2) Flight safety, and (3) Ground safety. These responsibilities include the study, modeling, and analysis of the hazards from potential launch accidents and the corresponding calculations of E_c ("Casualty Expectation"). Toxic effects, debris, and blast overpressures and their effects in the population are the

primary hazards to be studied. The fuel of the vehicles may cause toxic effects. Vehicle explosions caused by system failures can produce debris. In addition, these explosions may also create blast overpressure. Modeling of these effects is required for launch safety. However, hosting the range models and vehicle models in the VTB will support the development of risk management and reduce risk avoidance approaches. A Virtual Range can be used to design and evaluate flight termination systems (FTS), to evaluate and implement a risk assessment scheme of legacy and new vehicles, and to develop emergency responses. A Virtual Range can help reduce the cycle time to certify legacy vehicles (change from one range to another, or when modifications have been performed) and new vehicles. These reductions of cycle times can have profound impacts on time and money.

The Intelligent Launch and Range Operations (ILRO) Program at NASA Ames Research Center (ARC) was started to perform initial studies of a test bed with a demonstration [5]. An evolution of the ILRO test bed is the Virtual Test Bed Project. The objective of the Virtual Test Bed (VTB) Project is to provide a collaborative computing environment to support simulation scenarios, reuse, and integration of multidisciplinary models that represent elements of the range and operations at spaceports. VTB will provide several benefits such as a risk management evaluation of legacy and new vehicles framework, a technology pipeline, and a knowledge management enabler. VTB will leverage current technological developments from NASA ARC in intelligent databases to present data and results as usable knowledge with associated security constraints (Developmental Aeronautics Revolutionizing Wind-tunnels with Intelligent Systems of NASA - DARWIN) and methodologies for remote access to research facilities employing interactive and virtual reality interfaces (Virtual Laboratory - VLAB).

3. Systems Architecting Activities

It is very well known that systems architecting integrates systems theory and systems engineering with architecting theory and practice of architecting [21,22]. Conceptualization is the keyword for architecting. System conceptualization involves creativity and the recognition of potential users and perceived needs. System architectures are driven by the function, instead of the form, of the system. Systems Engineering is the one that provides the form. We utilized in this project QFD (Quality Function Deployment) and in particular a modified house of qualities to guide our architecting activities.

QFD can be used to improve the process of introducing new ideas that translates the user requirements from concept to development and beyond [20,23]. In the application of QFD, the initial phase involves the creation of a matrix called the House-of-Quality matrix due to its roof-like format as shown in Figure 2. The House-of-Quality used here follows modifications of the matrix of change [4] (MOC). This House-of-Quality has a list of the user needs/benefits (organized on the left side of the House). This list of needs/benefits is translated into the features (technical) needed (design requirements of a solution to satisfy the needs and/or provide the benefits).

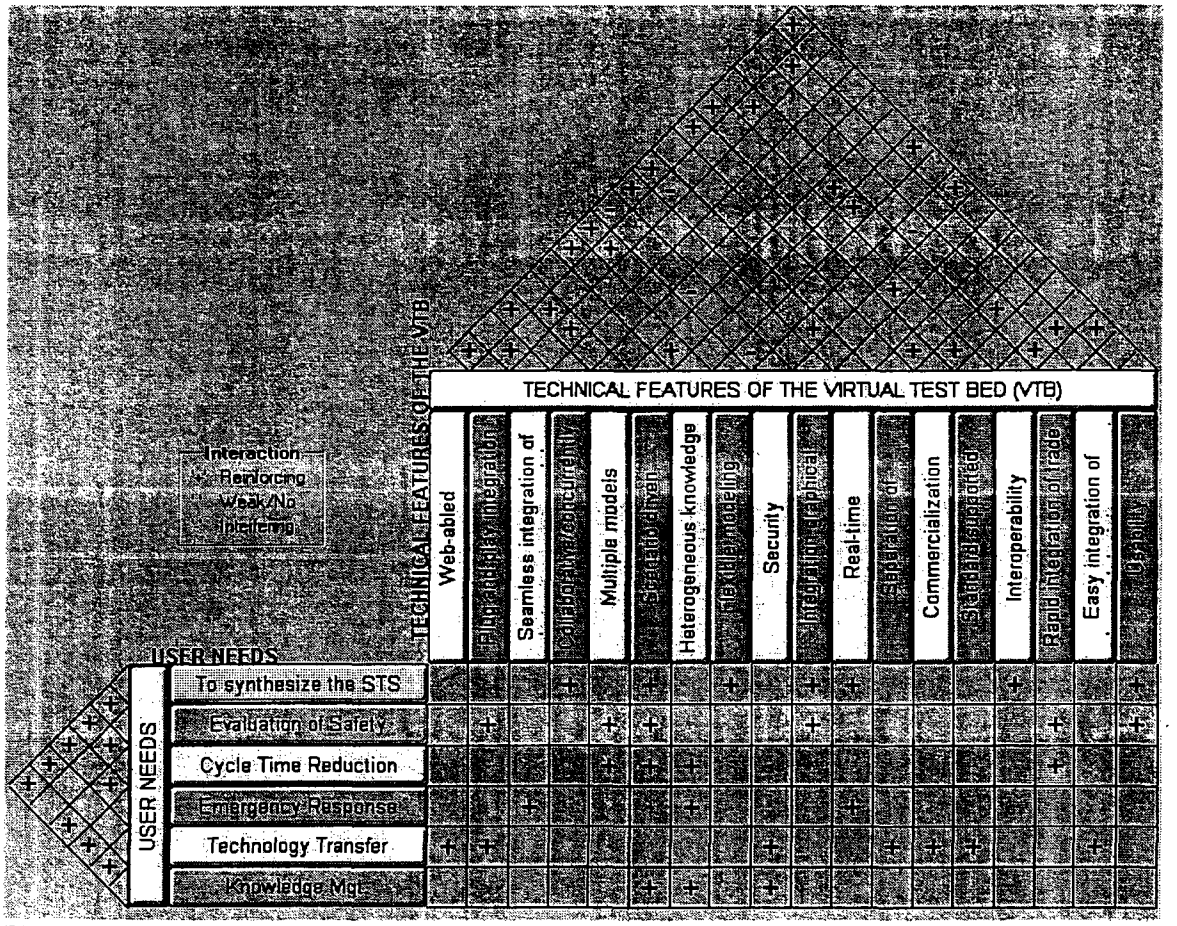

Figure 2. On going modified House-of-Quality for the VTB project. Look and feel adapted from MOC

Robert Turner, the project manager of the VTB project, facilitated several meetings with potential users (e.g., Federal Aviation Administration (FAA), NASA Wallops Flight Facility (WFF), NASA Range Safety, NASA-KSC Environmental Office, NASA-KSC Weather Office, Space Launch Initiative (SLI), NASA ARC Researchers and coordinators, the ER Range Operations Control Center (ROCC), and others). The potential users "verbalized" their needs and benefits desired. These "verbalized" needs and benefits were clustered in six areas:

1. *To decrease cycle time during the evaluation of vehicles and systems compliance to safety criteria.*
2. *To improve the evaluation of vehicles and systems compliance to safety criteria.*
3. *To synthesize in a single view the different elements of the Space Transportation System.*
4. *To develop precautions/emergency response measures to support range safety & security in a systematic manner.*
5. *To accelerate the introduction of new technologies (technology pipeline), new operational procedures, and help configure the current ones.*
6. *There is a need for a repository of knowledge and Knowledge Management strategies.*

The next step was to translate these needs/benefits to the desired design requirements/technical features of the VTB. The identification of the different features was the product of discussions with Henry McCoy. Henry is the Scientist assigned for this project by All Points Logistics. In addition, the different interactions among the needs, technical features, and between the needs/benefits and the technical features were carefully studied. I would like to say that this in an on-going process. The ranking of the

technical features is providing a guideline for the selection of a viable computing architecture for the VTB project. We understand that these technical features are very ambitious to obtain and some of them required trade-off to be implemented. The following is a listing of the technical features:

Web-Abled: The VTB must be able to use the Web and Internet resources. This will guarantee the distributed nature and user acceptance required for the different applications of the VTB.
Plug & Play Integration: The models should be able to be integrated without complications. Essentially, the models should not be re-written or reverse engineered to be integrated in the VTB.
Seamless Integration of Different Types of Models: A spaceport can only be represented using different types of models (sizes and nature). The VTB will have to be scaleable to support the growth in the size of the models. The nature of the models can differ. Examples of these models [8]: (1) Nonlinear first principles models of systems or subsystems that are based on the physics and chemistry of their underlying phenomena; (2) Linear regression models derived from analysis of steady-state system input/output data; (3) Fuzzy rules expressing a human expert's predictions of system behavior; (4) Linear state-space models developed by linearizing first-principles models; (5) Neural network models for inferring properties of a system; and (6) Discrete-event models.
Collaborative/Concurrently Environment: The computing environment should allow the implementation of collaborative design spaces (not limited by geographical constraints). This should be also implemented in a concurrent fashion.
Multi-Model: To represent the range and operations of a spaceport multiple models describing the different elements and processes will be integrated. In addition, scaleability (from the number of models to be hosted) is an important design requirement. The existence of scaleability allows for smooth growth of a computer system.
Scenario Driven: Scenarios representing impediments or lessons learned should be able to be executed and archived.
Extensive/Heterogeneous Knowledge Repository: The databases and knowledge bases should have enough capacity to handle large databases of numerical data, sounds, pictures, videos, and other media. In addition, knowledge integration of different forms is expected.
Flexible Modeling Environment: To satisfy the needs the VTB must provide a flexible modeling environment. This flexible modeling environment should be able to allow for queries and what-if scenarios. Ontologies could be used to provide the semantic primitives for a modeling language.
Real-Time Environment: There is a need in launch operations for real-time simulation and decision-making. It is important to have a real-time baseline and feedback.
Security Layers: Security has to be implemented in different manners and layers to provide the required level. Schemes based on SSL, Passwords, IP-addresses, and software agents could be designed to provide the required level of security.
Integrated Graphical Environment: Intelligent Visualization should be the result of this integration. The user should be able to see the output in different media and ways. The environment can be integrated with Visual Query Languages (VQLs).
Separation of Control/Application Logic/Architecture/Domain Knowledge: The VTB architecture should be independent of the domain knowledge. This will facilitate the technological products derived from the VTB platform. Maintenance and software life cycle assessment process can be easily implemented.
Commercialization (Business Development): One of the goals of NASA is to commercialize the technologies developed.
Standard Supported Protocols: Standardization is an important goal in the design. This will provide a cost-effective development process and user/industry acceptance.
Interoperability/Cross Platform Capabilities: Metadata mappings among different formats, common representations, reusability, and cross platform capabilities are envisioned capabilities.
Rapid Integration of Trade Studies: The rapid integration of trade studies for road mapping and technology transfer activities is a strong design requirement (in specific for groups such as ARTWG and

ASTWG).

Easy Integration of Advanced Decision Support Tools: One of the objectives of the VTB project is to advance the decision-making capabilities for range and operations (e.g., more risk management and less risk avoidance).

Usability (and User Friendliness): Human-centered computing principles taking into consideration the physical and cognitive models of the users must be implemented. The user should be able to configure the interface based on his/her needs.

4. Models and Process Evaluations

The CALPUFF model was reviewed from its computing characteristics (following the list of deliverables - The list of deliverables clearly stated the determination of computing characteristics as the only obligation for KSC). In addition, the subsection related to BLASTX explains the current flow of activities (operational and computational) to calculate the E_c.

4.1 The CALPUFF Model

CALPUFF is a Lagrangian puff dispersion model of the "plume segment" puff model family [6,7]. CALPUFF is applicable to complex terrain and coastal situations. This model is a multi-layer, multi-species non-steady state puff dispersion model. The user has to define a grid size for high-resolution simulation of episodes as well as for runs for one year or more with a one-hour time step. It can simulate the effects of time- and space-varying meteorological conditions on pollutant transport, transformation, and removal. This dispersion model is used for environmental impact assessments, and studies of air quality and pollutant transport on regional scales. Different forms of meteorological input can be used by CALPUFF. The time-dependent three-dimensional meteorological fields generated by the diagnostic meteorological model CALMET (which is a component of the CALPUFF modeling system), is the preferred form for regulatory application. The code has been used and reviewed by several different organizations for long-range transport distances, intermediate distances, and short to intermediate distances (e.g., EPA, NASA Marshall Space Flight Center).

The standard version of the code is Version 5. This version does not have the ability to accept and process changes in emission sources that occur over times shorter than one hour. However, the time-stepping algorithms within CALPUFF allow it to take very short time steps if necessary. NASA Marshall contracted the authors of CALPUFF, Earth Tech, Inc., to modify the code. Modifications were made to CALPUFF and CALPOST Version 5 to create Version 6. Version 6 has the following additions:

- The dispersion modeling system can accept emissions data with temporal variations as small as 1 second, and report average concentrations for intervals as short as 1 minute.
- The user can change the value of the variable EPSRAD via the CALPUFF control file. EPSRAD is the emissivity used in the radiative heat loss component of the energy equation of the numerical rise module for buoyant area sources.

These modifications contracted by NASA Marshall Research Flight Center (MRFC) were part of an effort to analyze PC-based modeling capabilities for the dispersion of hydrogen chloride from the catastrophic failure of a Space Shuttle early in flight [2,17]. The purpose of this initiative by NASA Marshall was to [2] *"support the development of a Launch Commit Criteria (LCC) and complimentary Emergency Response Planning for the launch of a Space Shuttle."* The source codes, executable codes, ancillary programs, and user manuals and reports for CALPUFF 5 and CALPUFF 6 were obtained. They were reviewed to obtain their computing characteristics as summarized in Table 1. These two programs were executed and tested with the example grids provided. We tried to translate from Fortran to either Java or C. The problem is that this required a better translator. In addition, we contacted Jeff Anderson and Joe Scire (from Earth Tech) to obtain more information about the modifications made to CALPUFF. The computer programs and the documentation were delivered to Jorge Bardina (NASA ARC on June 26,

2002). Jorge's group will take of the integration (with DARWIN) and modifications to the model.

4.2 Process Flow for Safety Risk Evaluation Taking into Consideration Blast-effect modeling.

Blast risks are estimated using BLASTX at the ER. BLASTX uses wind and temperature profiles to determine the risk of casualties. This process of calculating the Ec using BLASTX is a very interesting one. We have studied a process flow for the different activities. The activities can be in order, however, some of them can occur concurrently or be repeated [3]. We studied these activities and documented them with examples (due to restrictions of the length of this report, these activities are not included).

Table 1. Computing characteristics of CALPUFF [6,7,17]

Which machine it currently runs (Platform)	PC with WINDOWS (if GUI is used) or DOS
Specify language it is written in (Language)	FORTRAN (approximately 51K lines). There are no versions in C, C++, or Java.
Input	File containing the filename and path for each of the input and output (I/O) files used in the current run. Geophysical and hourly meteorological data. Source and emissions data for point sources with arbitrarily varying emission parameters.
Output	Unformatted data files containing gridded fields of time-averaged concentrations, time-averaged dry deposition fluxes, and time-averaged wet deposition fluxes are created with each run.
Size and storage requirements (Disk space requirements)	3 MB for unzipped files, 18 MB for installed system.
Run execution time and memory requirements	The memory required by CALPUFF is a strong function of the specified maximum array dimensions in the parameter file. For studies involving long-range transport, memory requirements will typically be at least 8 MB, with more required for simulations involving large numbers of sources. The run time of CALPUFF will vary considerably depending on the model application. Variations of factors of 10–20 are likely, depending on the size of the domain, the number of sources, selection of technical options, and meteorological variables such as the mean wind speed. From our own experience, and using CALPUFF 6, the execution is very fast for small grids. However, the execution time grows exponentially when the size of the grids increases.
Disclose and provide source code as well as executable code (Source & Executable)	Source Code and Executable Code was obtained and delivered for CALPUFF Version 5 and Version 6 to NASA ARC (Jorge Bardina).
Other Interface Issues	There are some interfaces/GUI developed with some minor graphics capabilities. However, these interfaces work in batch mode (and they are very primitive). In addition, NASA Marshall reports that in order to efficiently run CALPUFF for large sets a batching system was developed using a set of Visual Basic macros executed via Microsoft Excel.
Points of Contact	**Jeff Anderson, Ph.D.** B.J.Anderson@msfc.nasa.gov **Joe Scire, Ph.D.** Atmospheric Studies Group Internet: jss@src.com or EARTH TECH, 196 Baker Avenue telephone: (978) 371-4270 Concord, MA 01742 fax: (978) 371-2468 **Mark Bennett, Ph.D.** 619-208-7055. San Diego office of CH2MHill

5. Technologies, Techniques, and Information Tools Evaluations and Recommendations

This section will discuss several technologies, techniques, and information tools researched during this fellowship.

5.1 Leveraging Current NASA ARC Developments

Henry McCoy and I researched several of the developments of NASA ARC to see the suitability for the VTB project. Two technologies were found with good potential: DARWIN (an intelligent database) and VLAB (a virtual reality program that allows the user to configure his/her interface).

- **DARWIN.** DARWIN is based on a three-tier client/server/server architecture. The first server is the DARWIN Server. It runs a secure HTTP server, the executive server software, and the meta-database. The DReAM server, which is hosted in the aeronautics test area of choice, is the third tier server. The remote DReAM client system hosts the DARWIN Workspace environment that is composed of a secure HTTP browser, an executive, and a tool kit of additional visualization and collaboration software. Java or JavaScript are the programming environments of choice to implement the "small" remote applications. Implementation of larger applications, such as remote video tools are authorized and initiated through the DARWIN server (larger applications can be also initiated from the client site, however, knowledge of the middleware becomes even more critical for these applications). DARWIN can be used as an intelligent, distributed, and scaleable repository for the models, scenarios, and multi-media data used by the VTB.

- **VLAB.** VLAB is currently an environment programmed in the C language. It implements a virtual laboratory where the user can walk and select the different displays and databases that he/she wants to visualize in her/his desktop. It is currently used in NASA ARC to visualize the VMS. VLAB can be modified to serve as a way for the user of the VTB to configure his/her display and collaborate with other researchers (geographically distributed).

5.2 2D and 3D Graphics and Animation Environments

Several environments were researched. Among them, OpenGL, OpenFly, and Multigen Authoring Software.

- **OpenGL.** OpenGL [9,10,12,16] is the premier environment for developing portable, interactive 2D and 3D graphics applications. A low-level, vendor-neutral software interface, the OpenGL has often been called the "assembler language" of computer graphics. In addition to providing enormous flexibility and functionality, OpenGL applications enjoy the broadest platform accessibility in the industry. OpenGL has high visual quality and performance. Any visual computing application requiring maximum performance-from 3D animation to CAD to visual simulation-can exploit high-quality, high-performance OpenGL capabilities. There are various advantages of OpenGL: (1) An independent consortium, the OpenGL Architecture Review Board, guides the OpenGL specification; (2) Backward compatibility requirements ensure that existing applications do not become obsolete, (3) OpenGL API-based applications can run on systems ranging from consumer electronics to PCs, workstations, and supercomputers, and (4) numerous books have been published about OpenGL, and a great deal of sample code is readily available, making information about OpenGL inexpensive and easy to obtain.
- **OpenFly**. OpenFly [15] is an open source replacement game engine enabling designers of flight simulations created with Domark Flight Simulation Toolkit created by SIMIS Limited (Kuju Entertainment Limited) to take their simulations to the next level of graphical excellence.
- **Multigen Authoring Software [11,13,14].** A key requirement of any modeling system is the ability to import and export models from/to other CAD standards. **On July 1, 2002,** MultiGen-Paradigm, the leading developer of realtime 3D graphics software solutions, announced the availability of version

1.1 of SiteBuilder 3D, an extension to ESRI's popular ArcView® GIS desktop mapping program. SiteBuilder 3D provides users with a solution to quickly and easily transform 2D map data into realistic, fully interactive 3D scenes. In addition, the company is announcing the initial release of ModelBuilder 3D, an optional authoring software toolset that gives users the power to generate 3D models of real-world buildings, objects and vegetation for incorporation into 3D scenes generated by SiteBuilder 3D. Both products facilitate the simple creation of 3D scenes from GIS and geospatial data, without requiring a high-level of technical or 3D modeling experience. By giving users expanded functionality to create 3D terrain models from common GIS data, create paths and export them to digital movie files, SiteBuilder 3D v1.1 is the right choice for an affordable, easy to use 3D GIS application (currently used in the Control Tower application in NASA ARC).

5.3 Decision-Making Technologies

Several decision-making technologies were researched during this summer 2002. A simple example was developed for neural networks. However, due to the limitations of this report, we discuss three of them.

- **Bayesian Networks.** A method of reasoning using probabilities, called Bayesian Networks, has become popular in the artificial intelligence community. Bayesian networks are directed acyclic graphs (DAGs), where the nodes are random variables. The random variables can have two values (True and False), or several values (discrete or continuous). The arcs specify the independent assumptions that must hold between the random variables. These independent assumptions determine what probability information is required to specify the probability distribution among the random variables in the network. To specify the probability distribution of a Bayesian network, one must give the prior probabilities of all root nodes (nodes with no predecessors) and the conditional probabilities of all non-root nodes given all possible combinations of their direct predecessors. It is possible to appreciate that the concept of joint distributions plays a very important role in Bayesian networks. Bayesian networks allow one to calculate the conditional probabilities of the nodes in the network given that the values of some of the nodes have been observed.
- **Neural Networks.** There are two types of supervised neural networks researched this summer, which can be useful in for the VTB decision-making:
- Supervised neural networks based on minimizing errors
- Supervised neural networks based on forecasting by analogy.
- **Support Vector Machines.** Support Vector Machines (SVMs) are a new generation of algorithms in machine learning. SVMs are based on recent advances in statistical learning theory. There are two interesting features of SVMs:
- Complex Sructures. SVMs are able to generate structures that are complex enough to deal with practical applications. These structures contain classes of radial basis functions, neural networks, polynomials and splines-based functions as particular implementations.
- Mathematical Analysis. SVMs are able to generate complex structures but they are simple enough to be examined mathematically. SVMs can be conceptualized as a linear method in a high-dimensional feature space nonlinearly associated to input space.

6. System Design

Henry McCoy has developed a preliminary architecture ("form") of the VTB. Our contributions here were to validate his concept. We had many discussions about this architecture. We added some concepts to this architecture such as the utilization of Ontologies based on the Semantic Web Project. In addition, currently, we are developing a concept for a decision-making tool for safety evaluation/risk management of legacy and new vehicles.

6.1 Preliminary Concept

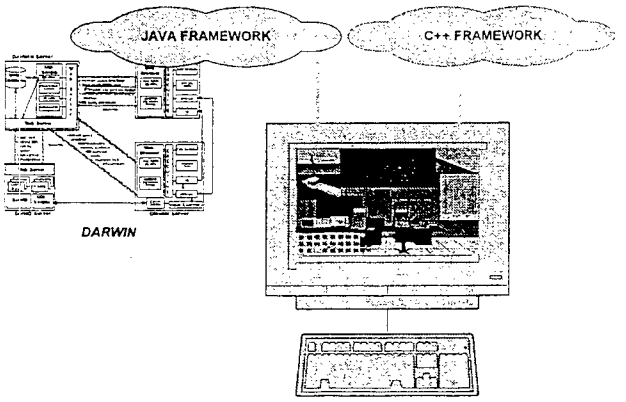

Figure 3. Preliminary architecture of the VTB.

There are intellectual properties issues. Therefore, we will sketch some of the concepts used in the preliminary architecture. The preliminary concept utilizes two frameworks: a C++ framework and a JAVA framework. The JAVA framework is used to provide the necessary services/handshakes with DARWIN. DARWIN is utilized as a repository of multi-media information, knowledge, and the models. The C++ framework is very important at the client side to implement the simulator and the client interfaces. VLAB will be modified (and translated to C++/object oriented) to operate in the client side. Ontologies will be used to develop a modeling language depending on the application. Kernels, security schemes (SSL, passwords, IP-addresses, and software agents), and innovative schemes of software re-configuration and data management are contemplated for this architecture.

6.2 Decision-Making Tool for Safety Evaluation/Risk Management

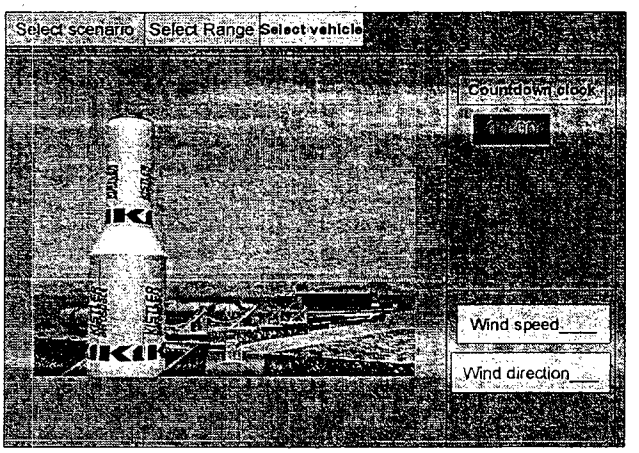

Figure 4. Look & Feel of a Decision Support Tool to evaluate safety/risk management.

The aerospace industry is developing commercial RLVs [18], some of which may someday operate from the ER. "The basic safety criteria for RLVs should be the same as for expendable launch vehicles in terms of E_c, P_c, and P_i. However, range safety processes for RLVs require special attention because RLV concepts will vary greatly in design and operational characteristics." [19] The development of a decision-making tool for safety evaluation/risk management of these new vehicles is very important. In addition, RLVs that carry human beings raise additional safety of flight issues, especially with respect to the acceptability of autonomous or semi-autonomous FTSs. [19] We have been supporting the conceptualization and providing form to this tool. The development of this tool will require the VTB to host different models:

- Vehicle component reliability
- Nominal trajectory and expected variations from nominal
- Vehicle failure modes, probabilities, and effects
- Wind modeling and debris-dispersion
- Population and geographical
- Debris
- Blast-effect
- Toxic-effect
- Impact limit lines
- Instantaneous impact point

- Destruct lines
- Collision avoidance

The VTB will have to host knowledge base systems containing knowledge and with capabilities of inferencing about:

- FAA regulations
- EWR 127-1
- Case Scenarios
- Tree analysis and interpretation
- Controllers/Schedulers of knowledge bases

In addition, optimization engines with capabilities to:

- Optimize trajectories
- Selection of Gates
- Compare scenarios (e.g., different fuel types, different ranges)
- Maximize or Minimize Objective Functions Provided by the Users

References

1. Barth, T., "Found in Space," IEE Solutions, April 2002.
2. Bennett, M., Technical Memorandum: Launch Commit Criteria Modeling Assistance, Analysis Summary, May 6, 2001.
3. Boyd, B., Harms, D., Rosati, P., Parks, C., and Overbeck, K., Wheather Support to Range Safety For Forecasting Atmospheric Sonic Propagation, Ninth Conference on Aviation, Range, and Aerospace Meteorology, 2000.
4. http://ccs.mit.edu/moc/.
5. Command Control Technologies Corporation, Intelligent Launch and Range Operations Testbed: Concept Paper, December 6, 2001.
6. Earth Tech, Addendum for CALPUFF Version 6, 2002.
7. Earth Tech, User Manuals for CALPUFF Version 5, 1997.
8. Godblole, D., Samad, T., and Gopal, V., "Active Multi-Model Control for Dynamic Maneuver Optimization of Unmanned Air Vehicles," Proceedings of the 2000 IEEE International Conference on Robotics & Automation, April 2000.
9. http://www.berkelium.com/OpenGL/
10. http://www.codeguru.com/opengl/index.shtml
11. http://www.dawnbreaker.com/navy_briefings/antiterror.html
12. http://www.frii.com/~martz/oglfaq/
13. http://www.multigen.com/news/pr/0701_02.shtml
14. http://www.multigen.com/news/pr/0309_00.shtml
15. http://www.openfly.org.uk/
16. http://www.opengl.org/
17. NASA MRFC Environmental Office Contacts.
18. National Research Council, Reusable Launch Vehicle, National Academy Press, 1995.
19. National Research Council, Streamlining Space Launch Range Safety, National Academy Press, 2000.
20. Portanova, P. and Tomei, E. Quality Function Deployment in Launch Operations, Aerospace Report No. TOR-0091 (6561-04)-1, November 1990.
21. Rechtin, E., Systems Architecting, Prentice Hall, 1991.
22. Rechtin, E. and Maier, M., The Art of Systems Architecting, CRC Press, 1997.
23. Zapata, E., " A Quality Function Deployment Method Applied to Highly Reusable Space Transportation," Space Technology & Applications International Forum in Albuquerque, NM, January 26-30, 1997.

2002 NASA/ASEE SUMMER FACULTY FELLOWSHIP PROGRAM

JOHN F. KENNEDY SPACE CENTER
UNIVERSITY OF CENTRAL FLORIDA

IN-VESSEL COMPOSTING OF SIMULATED LONG-TERM MISSIONS SPACE-RELATED SOLID WASTES

Abner A. Rodríguez-Carías
Associate Professor
Department of Animal Science, University of Puerto Rico

John Sager
Advanced Life Support Program, NASA - Kennedy Space Center

Valdis Krumins, Richard Strayer, Mary Hummerick,and Michael S. Roberts
Dynamac Corporation, NASA - Kennedy Space Center

ABSTRACT

Reduction and stabilization of solid wastes generated during space missions is a major concern for the Advanced Life Support – Resource Recovery program at the NASA, Kennedy Space Center. Solid wastes provide substrates for pathogen proliferation, produce strong odor, and increase storage requirements during space missions. A five periods experiment was conducted to evaluate the Space Operation Bioconverter (SOB), an *in vessel* composting system, as a biological processing technology to reduce and stabilize simulated long-term missions space related solid-wastes (SRSW). For all periods, SRSW were sorted into components with fast (FBD) and slow (SBD) biodegradability. Uneaten food and plastic were used as a major FBD and SBD components, respectively. Compost temperature (°C), CO2 production (%), mass reduction (%), and final pH were utilized as criteria to determine compost quality. In period 1, SOB was loaded with a 55% FBD: 45% SBD mixture and was allowed to compost for 7 days. An eleven day second composting period was conducted loading the SOB with 45% pre-composted SRSW and 55 % FBD. Period 3 and 4 evaluated the use of styrofoam as a bulking agent and the substitution of regular by degradable plastic on the composting characteristics of SRSW, respectively. The use of ceramic as a bulking agent and the relationship between initial FBD mass and heat production was investigated in period 5. Composting SRSW resulted in an acidic fermentation with a minor increase in compost temperature, low CO2 production, and slightly mass reduction. Addition of styrofoam as a bulking agent and substitution of regular by biodegradable plastic improved the composting characteristics of SRSW, as evidenced by higher pH, CO2 production, compost temperature and mass reduction. Ceramic as a bulking agent and increase the initial FBD mass (4.4 kg) did not improve the composting process. In summary, the SOB is a potential biological technology for reduction and stabilization of mission space-related solid wastes. However, the success of the composting process may depend of the physical characteristics (particle size, porosity, structure, texture) of the SBD components which would require pre-processing of solid wastes before placing them in the SOB.

IN-VESSEL COMPOSTING OF SIMULATED LONG -TERM MISSIONS SPACE-RELATED SOLID WASTES

Abner A. Rodríguez-Carías

INTRODUCTION

Evaluation of biological technologies to reduce and stabilize space related solid wastes has been the focus of different studies by the Advanced Life Support – Resource Recovery Program, National Aeronautics and Space Administration (NASA), at Kennedy Space Center (KSC). Solid wastes are substrates for pathogen proliferation, produce strong odor, and increase storage requirements during space missions. Previous experiments have shown the presence of *Escherichia coli, Bacillus spp., Salmonella spp, Klebsiella pneumoniae*, and other undesirable microorganisms in solid wastes generated in short-term space mission (Kish et al, 2002). For that reason, the biostability of solid wastes generated during space missions may represent a health issue for the crew. Because of storage limitations, space wastes produced on long-term and short-term mission will need to be reduced in volume as well. According to Maxwell and Drysdale (2001) a 6 men crew may produce 10 and 5 kg/d of solid wastes during long-term and short-term space missions, respectively. Therefore evaluation of alternatives to reduce and stabilize space-related solid wastes requires further evaluation.

Aerobic composting is a biological processing technology that has been identified as a possible mechanism to provide biochemical stabilization and mass reduction of solid wastes generated during space missions (Drysdale and Finger, 1997; Atkinson et al., 1998; Roberts et al, 2002, *In press*). Composting also has the potential to enable nutrient recycling, water reclamation, pathogen reduction, and to reduce storage requirements. For solid wastes composting, one design under evaluation is the Space Operations Bioconverter (SOB), a small scale, *in-vessel* composter that may potentially function as a sub-system within an integrated advanced life support recycling strategy (Drysdale and Finger 1997; Atkinson et al., 1998). In previous research, the SOB was utilized to evaluate the composting characteristics, and microbial community composition and diversity of alfalfa and aspen shavings composted at different temperatures and initial C/N ratios with excellent results (Roberts, et al., 2002, *In press*). However, the solid wastes of space-related missions include components with both low (trash, packaging material, tape, paper) and high biodegradability (inedible plant biomass, human feces). Because of differences in material composition, quantity, and degradability, we cannot extrapolate the composting characteristics of inedible biomass into wastes generated in space missions. Presently, not intent to compost space missions solid wastes have been performed. This research reported here was designed to evaluate the composting characteristics of solid wastes generated during simulated long-term space missions using the SOB.

EXPERIMENTAL PROCEDURE

A five periods experiment was performed in the Advanced Life Support -Resource Recovery – Integration Laboratory at KSC. The Space Operations Bioconverter (SOB; Figure 1), an *in -vessel* composting system with rotating drum, thermal control, gas monitoring, in *situ* mixing, leachate collection, and air recycle capability was used in the experiment. The *in-vessel* composting unit has been described and evaluated earlier with positive results (Roberts et al, 2002, *In press*). For all periods, a simulated long-term mission space-related solid waste (Maxwell and Dystdale, 2001) was prepared with components sorted for slow (SBD) and fast biodegradability (FBD, Table 1).

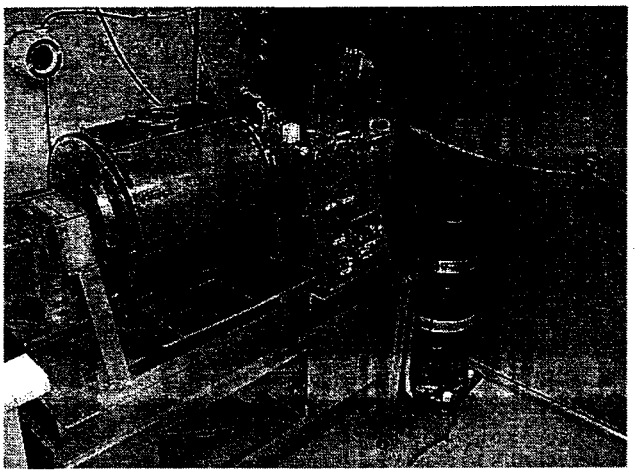

Figure 1. Space Operations Bioconverter – SOB

Table 1. Stimulated long-term mission space-related solid wastes

Fast Biodegradability	(55 %)	Slow Biodegradability	(45 %)
Carrots	7.69	Food Packaging Material	13.78
Tortillas	11.54	Paper	29.33
White Bread	15.38	Tape	6.22
Cream Spinach	7.69	Plastic	50.67
Turkey Ham	7.69		
Fruit Punch	15.38		
Celery	7.69		
Pitted Prunes	7.69		
Crackers	7.69		
Oranges	11.54		

For all periods, the composting materials were manually chopped into a 2.5 cm square pieces, adjusted to 55 % - 65 % initial moisture content with distilled water, and loaded into the SOB. After an initial 1 hour mixing period, the composter rotated for 4 min every 6 hours. During the entire composting process, compost temperature (°C), room temperature (°C), and CO_2 production, % (in line CO_2-sensor, GMP221 Probe, Vaisala Inc., Helsinki, Finlandia) were monitored at 5 min intervals, and averaged by the hour. Total mass reduction (%), calculated by difference between the initial and final compost mass weight, and final pH was determined at the end of each composting period.

In period 1, a simulated long-term mission space-related solid, 55-FBD: 45-SBD (w/w) proportions, was loaded into the SOB (± 4 kg) for 7 days. On day two, 15 g of soil (rear surface soil obtained from the Happy Hammock area of KSC) were added to the SOB as microbial inoculum. A second period *in-vessel* composting was conducted utilizing 45 % of the solid wastes composted in period 1, 55 % food wastes (total 4.2 kg), and 70 g of soil. The use of styrofoam as a bulking agent (to increase air flow through the pile) on the composting process was evaluated in period 3. The *In-vessel* composting unit was loaded for eleven days with 75% of pre-composted solid wastes (2 kg), 25% food wastes (1 kg), and 70 g of styrofoam. On day four, 0.58 kg of FBD components were added to the SOB. Using biodegradable plastic instead of regular plastic on the composting characteristics of SRSW was evaluated in period 4. The *In-vessel* composting unit was loaded for eleven days with 55% FBD (1.65 kg) and 45% SBD (1.29 kg) components. On day one, 50 g of styrofoam, and 300 g of previously composted SRWS were added as bulking agent and microbial inoculum. After 3 and 6 days of composting, 1 and 1.8 kg of FBD components were added to the composter, respectively. Period five evaluated the use of ceramic

(2.8 kg) as a bulking agent and the relationship between initial FBD mass (kg) and heat production on the composting of SRSW. The SOB was loaded for five days with a 55 % FBD (4.4 kg): 45% SBD (3.6 kg) mixture. Biodegradable plastic was utilized within the SBD components and 300 g of soil were added as microbial inoculum at the beginning of the composting process.

RESULTS AND DISCUSSION

Figure 2 shows the CO_2 production, compost temperature, and room temperature during the entire composting process. For each period, table 2 shows the compost components, final pH, total mass reduction, average CO_2 production, room temperature (RT), compost temperature (CT) and the difference between CT and RT. In period 1, composting SRWS resulted in an acid fermentation, with a minor increase in compost temperature, low CO_2 production, and only minor mass reduction. Similar to period 1, the period 2 reuse of SBD components in the compost mass did not increase the pH, CO_2 production, or compost temperature during the composting process. Total mass reduction was higher in period 2 than in period 1, but this difference in carbon loss may be due to the length of the composting process rather than the compost components (7 and 11 days for period 1 and 2, respectively). The acid pH observed in periods 1 and 2 could be an indicator of lack of oxygen in the compost mass, as a result of the presence of SBD components, especially plastic. The sticky properties of regular plastic might avoid the oxygen infiltration into the compost mass creating anaerobic conditions. Under anaerobic fermentation, the production of lactic acid and short chain volatile fatty acids by anaerobic or facultative microorganisms decrease the pH, affecting the metabolic activity and proliferation of heat producing microorganisms. These results show that it is not possible to use components with SBD as bulking agent during the composting process of SRSW. In both phases, an increase in CO_2 production, an indicator of microbial metabolic activity, was observed when adding soil as a microbial inoculum. This increase in food wastes degradation when added the microbial source may also indicate the beneficial effects of the addition of microbial starter for the composting process.

Addition of styrofoam as bulking agent (period 3) improved the composting characteristics of SRSW as evidenced by higher pH, CO2 production, compost temperature, and total mass reduction. The difference between compost temperature and room temperature was also higher in SRWS composted with styrofoam than in SRSW composted without the bulking agent. The presence of styrofoam may increase the aerobic conditions in the compost resulting in a shift in microbial populations in the compost mass. This change in microbial community maybe responsible by the lower acidity and greater heat production observed during this composting period. However, composting SRSW with stryfoam as a bulking agent did not reach 50-55°C/3 d, temperature necessary to destroy pathogen microorganisms.

Using biodegradable plastic on the *in vessel* composting of SRSW shows a slightly improvement in the compost characteristics as compared to the initial three periods. During the entire experiment, the highest compost temperature and average CO2 production were observed when biodegradable plastic was included in the compost mass. However, using biodegradable plastic did not increase the compost temperature to thermophillic conditions, and had similar total mass reduction and final pH relative to the SRSW composted without the biodegradable plastic. In this experiment, no attempt to calculate the percentage of bioplastic degrade during the composting process was made. However, the similar mass reduction observed in periods 3 and 4 might indicate that the effect of inclusion of biodegradable plastic on the composting characteristics of SRSW was more related to the particle size rather than its degradable properties.

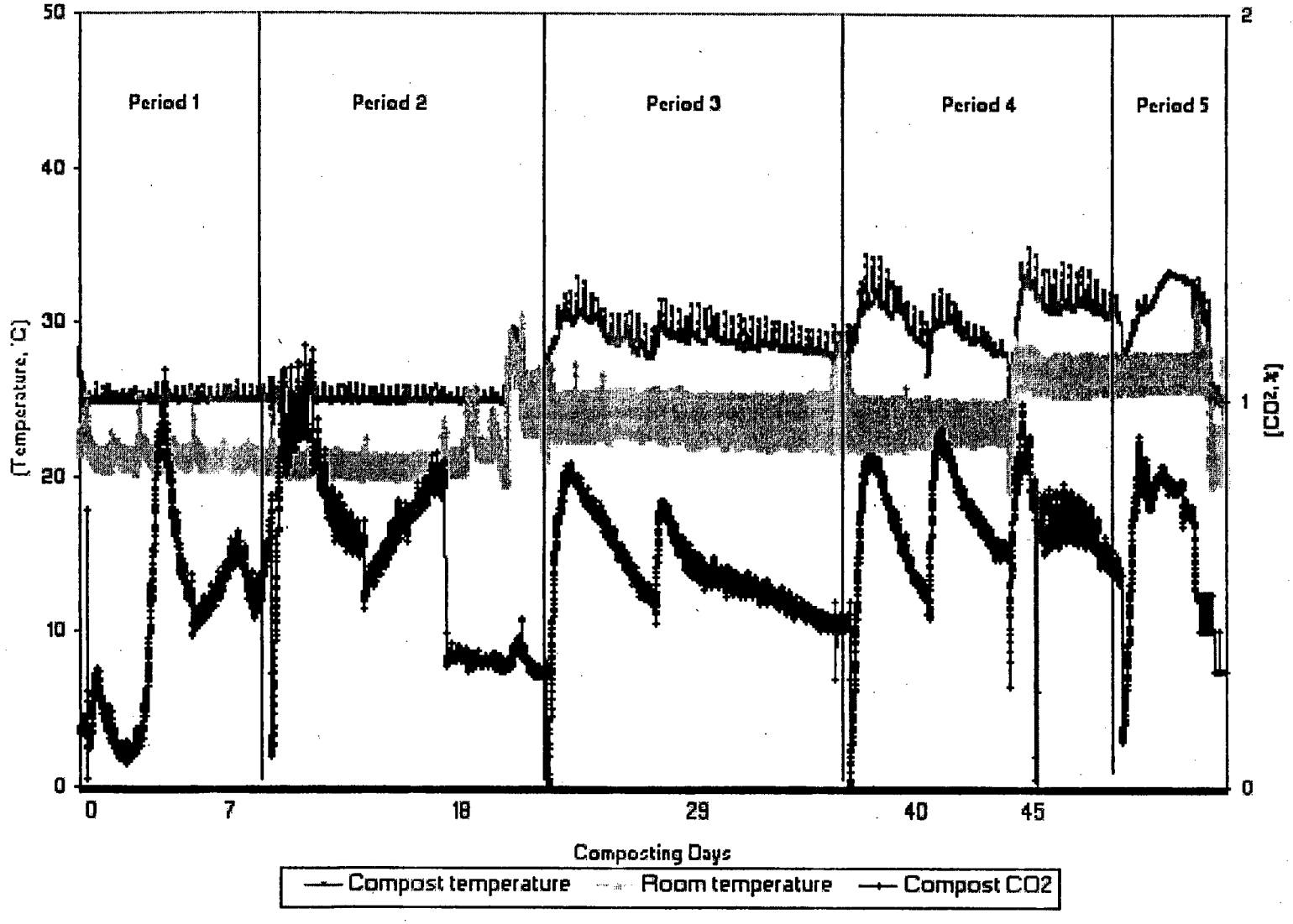

Figure 2. CO_2 production and compost temperature of simulated long-term mission space-related solid wastes using the SOB

Table 2. Composting characteristics of simulated long-term mission space-related solid wastes using the SOB

Period/Components	Composting days	Average				Final	
		CO2 (%)	CT (°C)[a]	RT (°C)[b]	CT-RT	Mass Reduction (%)	pH
1 55% FBD[c]: 45% SBD[d] Initial Mix = 4 kg 17 g Soil	7	0.42	24.9	21.5	3.4	8.2	4.40
2 55% FBD; 45% Pre-composted SRSW[e] Initial Mix = 4.2 kg 73 g Soil	11	0.66	25.3	21.8	3.7	15.8	4.59
3 75% Pre-composted SRSW; 25% FBD Initial Mix = 3 kg Added FBD;.58 kg on day 4 70 g Styrofoam	11	0.64	29.0	24.0	5.0	22.2	6.29
4 55% FBD; 45% SBD (22% Bio-plastic) Initial Mix = 3 kg Added FBD, 1 kg/d-3; 1.8kg/d-6 50 g Styrofoam 300 g pre-composted SRSW	11	0.73	30.1	24.7	5.5	17.7	6.20
5 55% FBD;45% SBD (22% Bio-plastic) Total Mix = 1k g Ceramic 300 g Soil	7	0.66	30.56	26.7	4.2	12.1	6.18

[a] Compost Temperature; [b] Room Temperature; [c] Fast biodegradability ;[d] Slow biodegradability; [e] Simulated long-term mission space-related solid wastes

A slight correlation between initial FBD components and heat production was observed in periods 1 to 4, however, in period 5 increasing the initial FBD mass to 4.4 kg did not result in better compost as compared to SRSW composted in previous periods. These results might indicate that higher amount of fast biodegradable components could be necessary to increase the compost temperature to thermophillic conditions during the composting of SRSW. Final pH, an indicator of aerobic conditions, was similar in SRSW composted with ceramic and styrofoam as a bulking agents. Therefore, these results indicate that ceramic represent a promising alternative to create and maintain aerobic conditions during the composting of SRSW.

Although a moderate thermophillic temperature was not obtained during the composting process in this experiment, composting still represents a potential biological processing technology for the reduction and stabilization of long-term and short-term mission space-related solid wastes. Future research should be undertaken because of the present and future requirements to reduce and stabilize SRSW. Experiments to determine the physical characteristics such as porosity, shape, structure, texture, and consistency of individual SBD components and their influence on the aeration process need to be performed. The optimum particle size of each SBD components and their effect on the composting process needs to be investigated. Biological alternatives to improve the composting process also need to be evaluated. Although solid wastes from space-related missions contain forms of inoculum from human sources, the development and evaluation of microbial products containing cellulose degrading (fungi, actinomycetes) and heat producing microbes on the composting process of SRSW should be studied. The determination of the optimum rate of microbial inoculation on the composting process would also be helpful.

CONCLUSIONS

On the basis of this study we concluded that the Space Operation Bioconverter (SOB) is a potential biological processing technology for the reduction and stabilization of simulated long-term mission space-related solid wastes. However, the success of the *in-vessel* composting process may depend on the physical, chemical, and biological characteristics (particle size, porosity, composition, structure, texture) of the SBD components. Additional work would be require to evaluate the necessary pre-processing steps, and their associated cost, to generate a suitable feed stock for composting in the SOB.

REFERENCES

Kish, A.L., M.P. Hummerick, M.S. Roberts, J.L.Garland, S. Maxwell, and A. Mills. Biostability and microbiological analysis of shuttle crew refuse. SAE Technical Paper N° 2002-01-2356

Maxwell, S. and Drysdale, A.E. 2001. Assessment of waste processing technologies for 3 missions. SAE Technical Paper N° 2001-01-2365.

Roberts, M.S., M. Klamer, C. Frazier, and J.L. Garland. 2002. Community profiling of fungi and bacteria in an In-Vessel composter for the NASA Advanced Life Support Program. Compost Science and Utilization. (*In press*).

2002 NASA/ASEE SUMMER FACULTY FELLOWSHIP PROGRAM

JOHN F. KENNEDY SPACE CENTER
UNIVERSITY OF CENTRAL FLORIDA

FLUID DYNAMICS OF SMALL, RUGGED VACUUM PUMPS OF VISCOUS-DRAG TYPE

JOHN M. RUSSELL
Associate Professor, Aerospace Engineering
Florida Institute of Technology
NASA colleague: FREDERICK W. ADAMS, YA-C3

ABSTRACT

The need to identify spikes in the concentration of hazardous gases during countdowns to space-shuttle launches has led Kennedy Space Center to acquire considerable expertise in the design, construction, and operation of special-purpose gas analyzers of mass-spectrometer type. If such devices could be miniaturized so as to fit in a small airborne package or backpack then their potential applications would include integrated vehicle health monitoring in later-generation space shuttles and in hazardous material detection in airports, to name two examples. The bulkiest components of such devices are vacuum pumps, particulary those that function in the low vacuum range. Now some pumps that operate in the high vacuum range (*e.g.* molecular-drag and turbomolecular pumps) are already small and rugged. The present work aims to determine whether, on physical grounds, one may or may not adapt the molecular-drag principle to the low-vacuum range (in which case *viscous-drag principle* is the appropriate term). The deliverable of the present effort is the derivation and justification of some key formulas and calculation methods for the preliminary design of a single-spool, spiral-channel viscous-drag pump.

FLUID DYNAMICS OF SMALL, RUGGED VACUUM PUMPS OF VISCOUS-DRAG TYPE

JOHN M. RUSSELL

1. INTRODUCTION

Consider the geometry illustrated in Fig. 1.1 nearby:

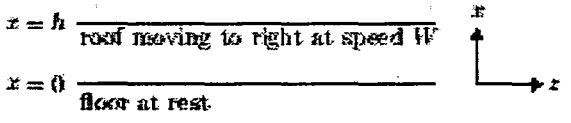

Fig. 1.1 Concept of a viscous-drag pump

The *no-slip* boundary condition of a viscous fluid asserts that a viscous fluid adheres to any solid with which it is in contact. The fluid that is in contact with the roof thus moves with the roof and the fluid in contact with the floor remains stationary. The distribution of longitudinal fluid velocity, w, with respect to the cross sectional coordinate, x, is an unknown of the problem. The no-slip condition furnishes boundary conditions for this w-distribution. If the channel is blocked at the ends then there can be no net mass transport through it. In this case the w-distribution must reverse sign at some value of x, as illustrated in Fig. 1.2.

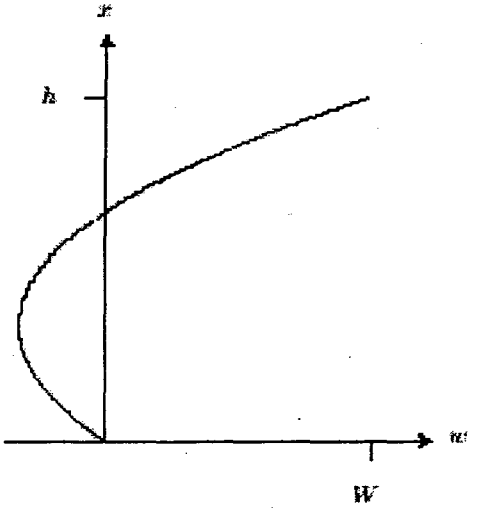

Fig. 1.2 Sample velocity profile with backflow

One may understand principle of operation of a viscous-flow pump by considering two extreme cases in turn. In the first case there is no imposed pressure difference between the two ends of the channel and the velocity distribution reduces to a simple linear interpolation between the boundary values. Following custom, I will refer to this case as COUETTE flow. In COUETTE flow there is nonzero mass transport in the direction of the wall motion but neither compression nor expansion. In the second extreme case there is a nonzero imposed pressure difference between the two ends of the channel (higher at the right end, say) but there is no wall motion. This latter case corresponds to capillary flow, in which the mass transport is nonzero and in direction from greater to lesser pressure (*i.e* in the negative z-direction in this example). In the capillary-flow case the fluid expands in the direction of its motion.

If, now, there is an imposed difference between the pressures at the ends of the channel and if there is wall motion in the direction of increasing pressure then the COUETTE mechanism—which favors mass transport in the direction of wall motion—and the capillary-flow mechanism—which favors mass transport in the opposite direction—are in competition. Whenever the COUETTE mechanism is the dominant of the two mechanisms (i.e. mass transport is in direction of wall motion), the moving-wall channel acts as a *compressor*. I will refer to such a compressor as a *viscous-drag pump*. A molecular-drag pump is, of course similar in concept, except that the channel width, h, in the latter case is large enough compared to the mean free path of the molecules to violate the usual continuum hypothesis of fluid mechanics.

One may imagine bending the straight channel illustrated in Fig. 1 into the shape of a corkscrew. One may produce such a channel by cutting a screw thread from the outer surface of an initially smooth cylindrical drum. By rotating such a drum within a smooth circular cylinder one may simulate, approximately, the conditions described in the foregoing paragraphs and thus generate a crude viscous-drag pump. In the following, I will provide detailed formulas for estimating the performance of a viscous-drag pump in according to such a model.

Consider a definite material point, $\mathcal{P}$, on the rotating drum situated at a some station along the channel. A observer fixed to $\mathcal{P}$ would report that

the outer cylinder is in motion and that the local velocity of the cylinder has nonzero components both tangent and perpendicular to the screw-thread. In the foregoing discussion I did not consider the effects of a nonzero component of wall motion perpendicular to the screw-thread. An interesting and important question, which I will address only partially in this report, is: *How does wall motion in the direction perpendicular to the screw thread affect the formulas for predicting of pump performance?* Further work to address this latter question is a fit topic for follow-on work.

2. METHODS EMPLOYED; CALCULATION EXAMPLES

Equations of motion. Typical scales. The operation of a viscous drag pump involves the physical effects of compressibility and viscosity, so I will begin by writing down the general form of the equations of motion of a viscous gas. I will suppose *a-priori*, that the coefficients of shear and bulk viscosity (denoted μ and κ, respectively) depend only upon the absolute temperature, T, and that the latter is uniform throughout the flow. Let ρ denote the mass density of the gas; let p denote the equilibrium (or thermodynamic) pressure as defined by the equation of state of an ideal gas, *i.e.*

$$p = \rho R T \ , \tag{2.1}$$

(in which R is the gas constant for the particular gas under consideration). Let $\mathbf{v}$ denote the fluid velocity vector and let $\mathbf{g}$ denote the local gravitational force-per-unit-mass. Then there are two equations of motion, namely the equation of *conservation of* mass,

$$\frac{\partial \rho}{\partial t} + \nabla \cdot (\rho \mathbf{v}) = 0 \ , \tag{2.2}$$

and the equation for the rate of change of translational momentum,

$$\underbrace{\rho \frac{\partial \mathbf{v}}{\partial t}}_{1} + \underbrace{\rho (\mathbf{v} \cdot \nabla)\mathbf{v}}_{2} = \underbrace{-\nabla p}_{3} + \underbrace{(\kappa + \tfrac{1}{3}\mu)\nabla(\nabla \cdot \mathbf{v})}_{4} + \underbrace{\mu \nabla^2 \mathbf{v}}_{5} + \underbrace{\rho \mathbf{g}}_{6} \ . \tag{2.3}$$

Equation (2.3) asserts that the mass (per unit volume) times the acceleration of an infinitesimal fluid element equals the force (per unit volume) exerted on the element by its surroundings. Term 1 is the due to unsteadiness of the velocity field (if present). Term 2 is due to acceleration of a fluid element as it passes through a region where the velocity field is nonuniform. Following custom, I will refer to terms 1 and 2 as *inertial reactions* due to unsteadiness and *advection*, respectively. Term 3 is the part of the force (per unit volume) due to unequal surface pressures on opposite faces of an element. Terms 4 and 5 are the parts of to the force (per unit volume) due to unequal *viscous stresses* on opposite faces of an element and Term 6 is the *weight* force (per unit volume) on the element.

I will apply certain idealizations in the sequel. First among these is the assumption that the velocity field is steady in time [so Term 1 in (2.3) is identically zero]. Following custom, I will express the remaining idealizations in terms of *typical dimensional scales* of the problem. To this end, let ℓ denote a scale typical of the channel length; let h denote a scale typical of the channel width; let U denote a scale typical of the fluid speed and let $g := |\mathbf{g}|$ denote the scalar acceleration due to gravity.

Then the following list furnishes estimates of the order of magnitude of the various terms in (2.3):

$$\left.\begin{array}{l} |\text{Term 2}| \sim \rho U^2 \ell^{-1} \ , \ |\text{Term 4}| \sim \mu U \ell^{-1} h^{-1} \ , \\ |\text{Term 5}| \sim \mu U h^{-2} \ , \ |\text{Term 6}| \sim \rho g \ . \end{array}\right\} \tag{2.4}$$

The lubrication-flow model. I will use the term *lubrication model* to describe the case when the following idealizations all hold:

$$\frac{h}{\ell} \cdot \frac{\rho U h}{\mu} \ll 1 \quad , \quad \frac{h}{\ell} \ll 1 \quad , \quad \frac{\ell g}{RT} \ll 1 \ . \tag{2.5}$$

Now the quantity RT/g has the dimensions of length. The length RT/g is called the *scale height of the atmosphere*. When the gas is air and T has the value 15° Celsius (the sea-level value for the U.S. Standard Atmosphere) the scale height has a value on the order of 10 km. Thus, as long as the channel length, ℓ, is small compared to 10 km the assumption $(2.5)_3$ will be accurate.

One may justify the neglect of the gravity term in (2.3) (*i.e.* Term 6) by forming the ratio of its order of magnitude to that of another term, say Term 3:

$$\frac{|\text{Term 6}|}{|\text{Term 3}|} \sim \frac{\rho g}{|\nabla p|} \sim \frac{\rho g/(RT)}{p/\ell} = \frac{\ell g}{RT} \ll 1 \ , \tag{2.6}$$

in which I have made use of (2.1) (in the second step) and $(2.5)_2$ (in the last). By similar reasoning (2.4) and (2.5) enable one to derive the following estimates:

$$\frac{|\text{Term 2}|}{|\text{Term 5}|} \sim \frac{h}{\ell} \cdot \frac{\rho U h}{\mu} \ll 1 , \tag{2.7}$$

$$\frac{|\text{Term 4}|}{|\text{Term 5}|} \sim \frac{h}{\ell} \ll 1 . \tag{2.8}$$

At this point, one has reason to neglect all of the terms in momentum equation, (2.3), except Terms 3 and 5. One concludes that these two terms balance each other in the lubrication approximation.

Lubrication flow with purely longitudinal roof motion. Here, and elsewhere, there will a be a velocity vector, $\mathbf{v}_{\text{roof}}$, which represents the motion of the roof of the channel relative to the floor. I will apply the phrase *purely longitudinal roof motion* to the case when the channel is straight and $\mathbf{v}_{\text{roof}}$ is parallel to its long axis. Let (x, y, z) be a set of cartesian coordinates arranged so that the positive z-axis is in the direction of $\mathbf{v}_{\text{roof}}$. Let (u, v, w) be the corresponding cartesian components of the velocity vector, $\mathbf{v}$. Then the form of (2.2) in steady flow is

$$\frac{\partial(\rho u)}{\partial x} + \frac{\partial(\rho v)}{\partial y} + \frac{\partial(\rho w)}{\partial z} = 0 ,$$

or, equivalently,

$$\frac{\partial(\rho w)}{\partial z} = -\frac{\partial(\rho u)}{\partial x} - \frac{\partial(\rho v)}{\partial y} . \tag{2.9}$$

Let V be a scale typical of the cross-channel velocity components, u and v. Then under assumptions stated earlier we have the estimates

$$\left|\frac{\partial(\rho u)}{\partial x} + \frac{\partial(\rho v)}{\partial y}\right| \sim \frac{V}{h} \quad , \quad \left|\frac{\partial(\rho w)}{\partial z}\right| \sim \frac{U}{\ell} .$$

Thus equation (2.9) implies that

$$\frac{U}{\ell} \sim \frac{V}{h} .$$

From this estimate and $(2.5)_2$, one concludes that

$$\frac{V}{U} \sim \frac{h}{\ell} \ll 1 . \tag{2.10}$$

Thus, *in lubrication flow with purely longitudinal roof motion the cross-channel velocity components*, (u, v), *of the velocity are small compared to the longitudinal component*, w.

Consider now the momentum equation, (2.3). If, for reasons stated above, one keeps only Terms 3 and 5, and one resolves the resulting vector equation into cartesian components one gets

$$\left.\begin{aligned} \frac{\partial p}{\partial x} &= \mu\left(\frac{\partial^2 u}{\partial x^2} + \frac{\partial^2 u}{\partial y^2} + \frac{\partial^2 u}{\partial z^2}\right) \\ \frac{\partial p}{\partial y} &= \mu\left(\frac{\partial^2 v}{\partial x^2} + \frac{\partial^2 v}{\partial y^2} + \frac{\partial^2 v}{\partial z^2}\right) \\ \frac{\partial p}{\partial z} &= \mu\left(\frac{\partial^2 w}{\partial x^2} + \frac{\partial^2 w}{\partial y^2} + \frac{\partial^2 w}{\partial z^2}\right) \end{aligned}\right\} . \tag{2.11}$$

In view of (2.10) one may argue that the right members of the first two of these equations are small compared with the right member of the last. In view of the slenderness assumption, $(2.5)_2$, moreover, the second derivative of w with respect to the longitudinal coordinate, z, is small compared to the second derivatives of w with respect to the the cross-channel coordinates, x and y. The system (2.11) thus reduces to

$$\frac{\partial p}{\partial x} = 0 \quad , \quad \frac{\partial p}{\partial y} = 0 \quad , \quad \frac{\partial p}{\partial z} = \mu\left(\frac{\partial^2 w}{\partial x^2} + \frac{\partial^2 w}{\partial y^2}\right) . \tag{2.12}$$

The system (2.12) implies that *the pressure is effectively uniform over the channel*. This cross channel uniformity of the pressure is another feature of lubrication flow with purely longitudinal roof motion. In this context p is a function of the single variable, z, which I will sometimes denote by $p(z)$. The partial derivative $\partial p/\partial z$ thus reduces to an ordinary derivative [which I will sometimes denote by $p'(z)$] and the system (2.12) reduces to the single equation

$$p'(z) = \mu\left(\frac{\partial^2 w}{\partial x^2} + \frac{\partial^2 w}{\partial y^2}\right) . \tag{2.13}$$

Recall, now, the equation of state (2.1), which one may write in the form

$$\rho = \frac{p(z)}{RT} .$$

In the first paragraph of §2, I stated the assumption that T was uniform. In an ideal gas, so is R. One concludes from the above equation that ρ, like p, is a function of the single variable z [which I will sometimes denote by $\rho(z)$] in lubrication flow with purely longitudinal roof motion.

Plane flow. Consider the special case in which $v = 0$ identically and there is no variation of the other two velocity components with respect to the spanwise coordinate, y (*i.e.* the one perpendicular to the plane of Fig. 1.2). Then the fluid velocity vector is everywhere parallel to the z-x coordinate plane. Following custom, I will refer to a flow satisfying this condition as *plane flow*. In plane flow, then, (2.13) reduces to

$$p'(z) = \mu \frac{\partial^2 w}{\partial x^2} .$$

The second antiderivative of this equation with respect to x is

$$p'(z)\tfrac{1}{2}x^2 + C_1(z)x + C_2(z) = \mu w , \qquad (2.14)$$

in which $C_1(z)$ and $C_2(z)$ are arbitrary functions of z. If one applies the boundary conditions

$$w = 0 \quad \text{on} \quad x = 0 ,$$
$$w = W \quad \text{on} \quad x = h$$

(both of which are statements of the *no-slip condition*) to (2.14) one may solve for $C_1(z)$ and $C_2(z)$. If one substitutes these results back into (2.14) one gets

$$\frac{p'(z)}{2}(x^2 - hx) + \frac{\mu W x}{h} = \mu w(x,z) . \qquad (2.15)$$

A brief digression here to introduce the so-called *stream function* will expedite the statement of boundary conditions in the sequel. Under the restriction to plane flow equation (2.9) reduces to

$$\frac{\partial(\rho w)}{\partial z} = -\frac{\partial(\rho u)}{\partial x} .$$

A standard representation of the velocity components (w,u) which is compatible with the above equation is

$$\rho w = \frac{\partial \psi}{\partial x} \quad , \quad \rho u = -\frac{\partial \psi}{\partial z} , \qquad (2.16)$$

in which $(x,z) \mapsto \psi(x,z)$ is any twice differentiable function of the variables (x,z). Following custom, I will refer to such a function, ψ, as a *stream function*.

One may interpret the stream function in terms of mass current (per unit span) across a contour in the plane of the flow. To this end, let (z,x) and $(z+dz, x+dx)$ be the coordinates of two neighboring points in the flow plane and let $\mathcal{C}$ be a contour drawn between them. In steady flow the net rate of transport of mass (per unit span) into or out of a small triangle with $\mathcal{C}$ as the hypotenuse and $(z+dz, x)$, say, as the vertex is zero. Now the expression $(\rho w)dx$ represents the transport across the vertical leg of the triangle (positive for outflow) and the expression $(\rho u)dz$ represents the transport across the horizontal leg of the triangle (positive for inflow). The *net outflow* across the two legs is thus

$$(\rho w)dx - (\rho u)dz ,$$

which must equal the inflow across $\mathcal{C}$. According to (2.16), however, the expression given above for the net rate of outflow across the legs is just

$$\frac{\partial \psi}{\partial x}dx - \left(-\frac{\partial \psi}{\partial z}\right)dz = \frac{\partial \psi}{\partial x}dx + \frac{\partial \psi}{\partial z}dz ,$$

which is the expansion of the total differential, $d\psi$, of the stream function between the two ends of $\mathcal{C}$. One concludes that *the change in stream function between two points in a plane flow equals the rate of transport of mass (per unit span) across any contour drawn between those two points.*

This result is handy in the statement of boundary conditions. Thus, the condition that a wall is impermeable to mass reduces to the statement that *the stream function is constant on the wall.* This concludes the digression regarding the stream function and I now resume the main discussion at the point where I digressed, namely equation (2.15).

If one solves (2.15) for w and substitutes the result into $(2.16)_1$ one gets

$$\frac{\partial \psi}{\partial x} = \rho(z)\left[\frac{p'(z)}{2\mu}(x^2 - hx) + \frac{W}{h}x\right] .$$

The antiderivative of this equation with respect to x is

$$\psi = \rho(z)\left[\frac{p'(z)}{2\mu}(\tfrac{1}{3}x^3 - h\tfrac{1}{2}x^2) + \frac{W}{h}\tfrac{1}{2}x^2\right] + f(z) , \qquad (2.17)$$

in which $f(z)$ is an arbitrary function of z. Since the floor is impermeable, the stream function must be constant on it and it is convenient to choose zero for the value of the stream function on the floor. One thus arrives at the boundary condition $\psi = 0$ on $x = 0$ for all z. If one applies this boundary

condition to (2.17) one concludes that $f(z) = 0$ and (2.17) reduces to

$$\psi = \rho(z)\left[\frac{p'(z)}{2\mu}(\tfrac{1}{3}x^3 - h\tfrac{1}{2}x^2) + \frac{W}{h}\tfrac{1}{2}x^2\right] . \quad (2.18)$$

Since the roof is also impermeable, the stream function must be constant on it as well. Let ψ_h denote the value of the stream function on the roof. If one evaluates (2.18) at $x = h$ (*i.e.* the roof elevation) one gets

$$\psi_h = \rho(z)\left[\frac{p'(z)}{2\mu}h^3(\tfrac{1}{3} - \tfrac{1}{2}) + \frac{W}{h}\tfrac{1}{2}h^2\right] .$$

But $\rho = \rho(z) = p(z)/(RT)$ [*cf.* (2.1) and the discussion following (2.13)], so the last equation implies that

$$\psi_h = \frac{p(z)}{RT}\left[-\frac{p'(z)}{2\mu}\frac{h^3}{6} + \frac{Wh}{2}\right] . \quad (2.19)$$

Equation (2.19) is an ordinary differential equation for the distribution of pressure down the channel. Two special cases serve as useful benchmarks. One may characterize the first special case by the condition $p'(z) = 0$, or $p = p_o$, in which p_o is a constant. This case—which I referred to as COUETTE flow in §1—corresponds to the physical situation when both ends of the channel are vented to the same reservoir. One may characterize the second special case by the condition $\psi_h = 0$. Now ψ_h represents the rate of mass transport per unit span through the channel so the condition $\psi_h = 0$ represents a blocked channel, *i.e.* one with no net mass transport. I will refer to this case as the *dead-head* case.

In the dead-head case the left member of (2.19) is zero by definition. In the mean time, expression outside the square brackets in the right member is nonzero. One concludes that in the dead-head case the expression inside the square brackets must be zero. It follows that

$$\frac{p'(z)}{2\mu}\frac{h^3}{6} = \frac{Wh}{2} ,$$

or

$$p'(z) = \frac{6\mu W}{h^2} . \quad (2.20)$$

Since the right member of (2.20) is constant in z one concludes that the pressure varies linearly along the channel in the dead-head case. Thus, $p'(z) = p_o/\ell_{dh}$, in which p_o is the pressure at the right end and ℓ_{dh} is a length, which I will call the *dead-head* length. If one writes p_o/ℓ_{dh} in place of $p'(z)$ in (2.20) and rearranges, one gets

$$\ell_{dh} = \frac{p_o h^2}{6\mu W} . \quad (2.21)$$

If the given channel length, ℓ, is greater than the dead-head length, ℓ_{dh}, then one may partition the channel into two parts, namely the part where $0 \le z \le \ell - \ell_{dh}$ (and the $p = 0$ identically) and the part where $\ell - \ell_{dh} < z < \ell$ (and the pressure ramps up linearly to the value, p_o, at the right end).

Some abbreviations will be convenient in the sequel. Thus I will denote by q the *pressure-volume* throughput (per unit span) through the channel. Let $\dot\delta$ denote the corresponding volumetric throughput (per unit span). Then the definition of q is $q := p\dot\delta$. According to (2.1), however, $p = \rho RT$. In the mean time, ψ_h is the mass throughput per unit span, so $\psi_h = \rho\dot\delta$. One concludes that

$$\psi_h RT = \rho\dot\delta RT = p\dot\delta = q . \quad (2.22)$$

One should note that q, like ψ_h, is constant in z under assumptions already introduced but $\dot\delta$ is not.

If one writes $\psi_h = q/(RT)$ in (2.19) one may arrange the resulting equation in the equivalent form

$$\frac{1}{6}\frac{d}{(z/h)}\left(\frac{ph}{\mu W}\right) = \frac{\dfrac{ph}{\mu W} - \dfrac{2q}{\mu W^2}}{\dfrac{ph}{\mu W}} , \quad (2.23)$$

in which each of the fractions illustrated is nondimensional. One may characterize three regimes of the flow as summarized in the following table:

$0 < \frac{ph}{\mu W} < \frac{2q}{\mu W^2}$,	favorable pressure gradient
$0 \le \frac{2q}{\mu W^2} < \frac{ph}{\mu W}$,	weak adverse pressure gradient
$\frac{2q}{\mu W^2} \le 0 < \frac{ph}{\mu W}$,	strong adverse pressure gradient

Table 2.1 Regimes of the solutions of (2.23)

I have applied the adjective *favorable* (or *unfavorable*) to the pressure gradient, $p'(z)$, if the pressures on the leading and trailing faces of a fluid element are unequal and urge the element to move *in the same direction as* (or *in the opposite direction*

from) the wall motion, respectively. In flow with a *favorable* pressure gradient ($p'(z) < 0$), there is expansion rather than compression in the direction of wall motion. The case $p'(z) < 0$ is therefore irrelevant to the design of a viscous-drag pump. In flow with an adverse pressure gradient ($p'(z) > 0$), there will be compression in the direction of wall motion if the adverse pressure gradient is not strong enough to cause reversed flow ($\psi_h < 0$, or, equivalently, $q < 0$). Alternatively, if the pressure gradient *is* strong enough to cause reversed flow then the device will not act as a compressor in that case either. One concludes that the weak-adverse-pressure-gradient case in Table 2.1 above is the only one of interest in the design of a viscous drag pump.

One may rearrange (2.23) into a form suitable for solution in the case of a weak pressure gradient, viz.

$$6\frac{d(z/h)}{d\left(\frac{ph}{\mu W}\right)} = 1 + \frac{\frac{2q}{\mu W^2}}{\frac{ph}{\mu W} - \frac{2q}{\mu W^2}},$$

which now treats z/h as the dependent variable and $ph/(\mu W)$ as the independent variable. The antiderivative with respect to $ph/(\mu W)$ is

$$6\frac{z}{h} = \frac{ph}{\mu W} + \frac{2q}{\mu W^2}\ln\left(\frac{ph}{\mu W} - \frac{2q}{\mu W^2}\right) + C_3\,, \quad (2.24)$$

in which C_3 is an arbitrary constant. Let the stations $z = 0$ and $z = \ell$ correspond to the inlet and the outlet of the channel, respectively. Let p_o denote the pressure at the outlet. If one evaluates (2.24) at $p = p_o$ (where $z = \ell$) and subtracts the result from (2.24) one gets

$$6\frac{z-\ell}{h} = \frac{ph}{\mu W} - \frac{p_o h}{\mu W} + \frac{2q}{\mu W^2}\ln\left(\frac{\frac{ph}{\mu W} - \frac{2q}{\mu W^2}}{\frac{p_o h}{\mu W} - \frac{2q}{\mu W^2}}\right). \quad (2.25)$$

Figure 2.1 nearby shows a family of pressure distributions derived from (2.25) in the special case $p_o h/(\mu W) = 1,000$.

Two features of these results merit mention at this point. First, the curve with $q = 0$ is the dead-head case mentioned above. As stated there, the slope, $p'(z)$ is constant and the model predicts a perfect vacuum in the interval $0 \le z \le \ell - \ell_{dh}$. Second, each curve with $q > 0$ tends toward a horizontal asymptote in the upstream direction (see the

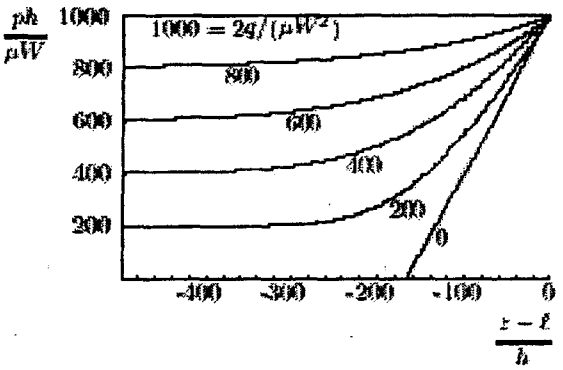

Fig. 2.1 Longitudinal pressure distributions down a channel predicted by (2.25) in the special case $p_o h/(\mu W) = 1,000$ (Plane-flow case).

left margins of the curves). Third, each pressure curve attains a value close to its upstream asymptotic value at a distance two or three dead-head lengths upstream of the outlet. This last observation suggests that any portion of the channel more that two or three dead-head lengths upstream of the outlet does little more than add weight to the pump while playing little or no role in compressing the gas.

That there should be an asymptote on a curve of constant q is apparent from (2.25) since the value of the natural logarithm tends to negative infinity as $ph/(\mu W) \to 2q/(\mu W^2)$. On such an asymptote the pressure is uniform and thus corresponds to the COUETTE state discussed earlier.

One may derive a simple formula formula for the volumetric throughput (per unit span), $\dot{\delta}_C$, on the upstream asymptote. This formula will prove useful in the sequel, so I will derive it now. In the text above equation (2.22), I pointed out that $\psi_h = \dot{\delta}$. If one substitutes this result into the equation just before (2.19) one gets

$$\rho(z)\dot{\delta} = \rho(z)\left[-\frac{p'(z)}{2\mu}\frac{h^3}{6} + \frac{Wh}{2}\right].$$

If one cancels the common factor $\rho(x)$ in the left and right member and evaluates on the remote upstream asymptote (where $p'(z) \to 0$ and $\dot{\delta} \to \dot{\delta}_C$), one gets

$$\dot{\delta}_C = \frac{Wh}{2}. \quad (2.26)$$

As an application of the foregoing formulas to an initial pump design, consider the following specifications:

1. The fluid is air and its temperature inside the pump is 120° F;
2. The volumetric rate of transport, S, of gas into the inlet is 7 L/min [0.247 $ft^3/(min)$].*
3. The volumetric transport rate, S_C, on the remote upstream asymptote of the pressure distribution is such that $S_C = 1.1\,S$.;
4. The aspect ratio of the channel cross section, $\lambda := b/h$, in which b and h are the channel span and thickness, respectively, has the value $\lambda = 5$;
5. The inlet pressure, p_i, and the outlet pressure, p_o, equal 10^{-4} Atm and 1 Atm, respectively;
6. The spin rate of the drum, f, is in the range 30,000 to 90,000 RPM;
7. The radius of the drum, $\mathcal{R}$, is in the range 1–3 cm.

With these specifications, one may calculate various parameters of a pump such as: the channel thickness, h, the channel length, ℓ, the altitude of the drum, L, and the area, $\mathcal{A}$, of the drum (to name four examples). With the aim of calculating these quantities, one must first rewrite some of the equations already in hand to put them into a form convenient in this application.

From the foregoing definitions, we have $S_C = \dot{\delta}_C h$, or, in view of (2.26),

$$S_C = \frac{W h \lambda}{2} . \tag{2.27}$$

Recall, next, that $q = p\dot{\delta}$ [*cf.* the equation before (2.22)]. But q is independent of position along the channel [*cf.* the text after (2.22)], so we may calculate q at any convenient station along it. If one takes the inlet (where $p = p_i$ and $\dot{\delta} = S/b$) as this reference station, one gets

$$q = \frac{p_i S}{b} . \tag{2.28}$$

Now evaluate (2.25) at the inlet (where $p = p_i$ and $z = 0$) and multiply the result by -1:

$$6\frac{\ell}{h} = -\frac{p_i h}{\mu W} + \frac{p_0 h}{\mu W} + \frac{2q}{\mu W^2} \ln\left(\frac{\frac{p_o h}{\mu W} - \frac{2q}{\mu W^2}}{\frac{p_i h}{\mu W} - \frac{2q}{\mu W^2}} \right) .$$

If one eliminates q by means of (2.28) one gets

$$6\frac{\ell}{h} = -\frac{p_i h}{\mu W} + \frac{p_0 h}{\mu W} + \frac{2p_i S}{\mu W^2 b} \ln\left(\frac{\frac{p_o h}{\mu W} - \frac{2p_i S}{\mu W^2 b}}{\frac{p_i h}{\mu W} - \frac{2p_i S}{\mu W^2 b}} \right) .$$

If one eliminates b by means of (2.27) then one may show, after some reductions and rearrangement, that

$$\ell = \frac{p_o h^2}{6\mu W} \left\{ 1 - \frac{p_i}{p_o} + \frac{p_i S}{p_o S_C} \ln\left(\frac{\frac{p_o}{p_i}\frac{S_C}{S} - 1}{\frac{S_C}{S} - 1} \right) \right\} . \tag{2.29}$$

Note that the expression outside the large curly braces in the right member is equals the dead-head length, ℓ_{dh}, defined by (2.21).

If one substitutes $b = \lambda h$ into (2.27), one gets, after rearrangement,

$$h^2 = \frac{2S_C}{\lambda W} . \tag{2.30}$$

In the mean time, we know that.†

$$W = 2\pi \mathcal{R} f . \tag{2.31}$$

If one eliminates W from (2.30) by means of (2.31) one gets

$$h^2 = \frac{2S_C}{\lambda 2\pi \mathcal{R} f} . \tag{2.32}$$

If one substitutes (2.31) and (2.32) into (2.29) to eliminate W and h^2, respectively, one gets

$$\ell = \frac{p_o}{3\mu} \frac{S_C}{\lambda (2\pi \mathcal{R} f)^2} \left\{ 1 - \frac{p_i}{p_o} + \frac{p_i S}{p_o S_C} \ln\left(\frac{\frac{p_o}{p_i}\frac{S_C}{S} - 1}{\frac{S_C}{S} - 1} \right) \right\} . \tag{2.33}$$

From the specification that the gas is air at $T = 120°$ F one can look up the corresponding shear viscosity, μ, from a handbook or calculate it from a standard empirical formula, such as the so-called *Sutherland law* [*cf.* *U.S. Standard Atmosphere 1976*, [1]. The latter gives

$$\mu = 1.91848 \times 10^{-4} \text{ dyne s } (\text{cm})^{-2} . \tag{2.34}$$

* This value corresponds to the rated speed of a scroll pump (Air Squared model number P10H10/N4.0 or Spiradyn-003-DSP) now installed in a prototype gas analyzer (AVEMS) in the Hazardous Gas Detection Lab at KSC.

† Remember that f is in *cycles* per unit time rather than *radians* per unit time. This distinction accounts for the presence of the factor 2π in the result asserted.

With (2.34) and the data in the specifications above, equation (2.33) is in a form suitable for immediate substitution of numerical values, provided one takes due account of necessary unit conversions. As an example of the latter, one may note that

$$p_a = 1 \text{ Atm} = 1.01325 \times 10^6 \text{ dyne (cm)}^{-2}$$

which expedites the computation of the ratio p_a/μ in (2.33). Thus, specifications 3 and 5 above are sufficient to determine the numerical value of the expression in curly braces above (It has the value 1.00096). The closeness of this factor to one is worth noting and is a consequence of the smallness of the factor p_v/p_a.

One may now tabulate the channel length, ℓ, by substituting the foregoing values of the parameters into the right member of (2.33). Table 2.1 furnishes results obtained in this way.

	ℓ (m)		
$\mathcal{R}$ (cm)	$f = 3{\cdot}10^4$ (RPM)	$f = 6{\cdot}10^4$ (RPM)	$f = 9{\cdot}10^4$ (RPM)
1	45.12	11.28	5.01
2	11.28	2.82	1.25
3	5.01	1.25	0.557

Table 2.1 Dependence of channel length, ℓ, upon drum radius, $\mathcal{R}$, and rotation rate, f.

The square root of equation (2.32) furnishes a formula for the h. Table 2.2 furnishes calculated values of h:

	h (mm)		
$\mathcal{R}$ (cm)	$f = 3{\cdot}10^4$ (RPM)	$f = 6{\cdot}10^4$ (RPM)	$f = 9{\cdot}10^4$ (RPM)
1	1.278	0.904	0.738
2	0.904	0.639	0.522
3	0.738	0.522	0.426

Table 2.2 Dependence of channel width, h, upon drum radius, $\mathcal{R}$, and rotation rate, f.

If, as stated earlier, one constructs a viscous drag pump by rotating a cylindrical drum in a stationary cylinder then one may estimate the inside area, A, of the cylinder by the product of the channel length, ℓ with the channel span, $b = \lambda h$. Of course, the cylinder area in a real pump must be larger to allow for the portion of the area taken up by seals between adjacent channels (or threads). Even, so the the product $\ell\lambda h := A$ is interesting since one expects that the mass of a hollow drum to scale with this quantity. Table 2.3 furnishes calculated values of A:

	A (cm)^2		
$\mathcal{R}$ (cm)	$f = 3{\cdot}10^4$ (RPM)	$f = 6{\cdot}10^4$ (RPM)	$f = 9{\cdot}10^4$ (RPM)
1	2884.	509.8	185.0
2	509.8	90.12	32.70
3	185.0	32.70	11.87

Table 2.3 Dependence of cylinder area A, upon drum radius, $\mathcal{R}$, and rotation rate, f.

If one divides the cylinder area, A, by the cylinder circumference, $2\pi\mathcal{R}$, one gets the cylinder altitude, L. Table 2.4 furnishes calculated values of L:

	L (cm)		
$\mathcal{R}$ (cm)	$f = 3{\cdot}10^4$ (RPM)	$f = 6{\cdot}10^4$ (RPM)	$f = 9{\cdot}10^4$ (RPM)
1	459.0	81.14	29.44
2	40.57	7.172	2.603
3	9.815	1.735	0.6296

Table 2.4 Dependence of cylinder altitude L, upon drum radius, $\mathcal{R}$, and rotation rate, f.

I will conclude the discussion of numerical results by noting that the pressure-volume throughput, Q, defined by $Q := p_i S$, is a constant of the problem. Thus, since S and p_i are given by Specifications 2 and 5, respectively, the corresponding value of Q becomes 7×10^{-4} Atm L/min or

$$Q = 1.167 \times 10^{-2} \text{ Atm (cm)}^3/\text{s}) .$$

3. CONCLUSIONS

The present effort supports several conclusions including the following:

1. The assumptions of lubrication theory of a gas enable one to solve for the plane flow down a uniform channel (with roof motion parallel to the long axis of the channel) in terms of elementary functions;

2. One may identify three distinct regimes of the flow, namely favorable pressure gradient, weak adverse pressure gradient, and strong adverse pressure gradient, of which only one is compatible with flow in a compressor;
3. If one can spin the drum up to 9×10^4 RPM, then one can replicate the pumping speed (namely 7 L/min) of existing backing pumps of scroll- and diaphragm-type with a cylindrical drum of surface area less than 12 $(cm)^2$.

4. UNRESOLVED ISSUES; FUTURE OPPORTUNITIES

The foregoing conclusions give cause for optimism that miniaturization of backing and roughing pumps of viscous drag type may be possible. The relative simplicity of the concept also suggests that such a device may be ruggedized.

In the geometry considered thus far the velocity, v_{roof}, of the roof relative to the floor corresponds to the velocity of a stationary cylinder relative to a rotating drum interior to it. If the channel has the shape of a screw-thread then there will inevitably be a component of v_{roof}, say $v^{\perp}_{roof}$, perpendicular to the thread. The effects of a nonzero $v^{\perp}_{roof}$ include a two-dimensional *recirculating flow* in the plane of a typical cross section. The presence of such a recirculating flow may influence the performance of a pump in a number of ways. To discuss them, however, I must first describe the so-called *liftup effect*.

To set the stage for a description of the liftup effect, note that the recirculating flow will move some fluid particles closer to the roof and others closer to the floor. There will be some tendency for such particles to retain their translational momentum (and, hence, their streamwise velocity, w) as they move into a new environment. The velocity distribution given by (2.15) would thus be subject to warping. This warping of the streamwise velocity distribution is the liftup effect, a phenomenon discussed (for example) by LUDWIG PRANDTL in the 1920s. The liftup effect may affect pump performance in number of ways. Thus:

1. The pump performance estimates given above presume that the flow is not turbulent. The liftup effect typically destabilizes a nonturbulent flow and makes it more apt to become turbulent. The question of whether—or if—the flow trips to a turbulent state and, if it does, how the turbulence affects the pump performance, are serious questions worthy of further investigation.
2. Even if there is no turbulence, the redistribution of streamwise momentum in the cross section due to the liftup effect may affect the performance of the pump significantly. The derivation of appropriate formulas or computational models to predict such changes in performance is a important subject for follow-on work.
3. The recirculating flow in the cross section and, for that matter, the flow as a whole may be affected significantly by the leakage of fluid across seals that separate adjacent flow channels on the rotating drum. The derivation of appropriate formulas or computational models to predict such effects of seal leakage—and its effects on pump performance—is a fit subject for further investigation.

ACKNOWLEDGEMENTS

As usual, I am indebted to my NASA colleague RIC ADAMS (of the newly constituted Technology Implementation Branch, YA-C3, of the Spaceport Technology Development Office, YA-C, of the Spaceport Engineering and Technology Directorate, YA), for his suggestion of the problem addressed here, for inspiring conversations pertaining thereto and for continued moral and material support. I am also indebted to Dr. RICHARD ARKIN and GUY NAYLOR of Dynacs, Inc. for showing me their prototype Aircraft Volcanic Emissions Mass Spectrometer (AVEMS) and for furnishing me with technical data for both the scroll pump that the present device features and for a diaphragm pump under consideration as a replacement. I am indebted to Dr. BOB YOUNGQUIST for many useful conversations on technical subjects as well as on the mysteries of working for the government. I am, as usual, indebted to CASSIE SPEARS of the UCF/ASEE Faculty Summer Fellowship office and to Dr. TIM KOTNOUR for his assiduous care in managing of this summer's program.

REFERENCES

[1] ANONYMOUS *U.S. Standard Atmosphere 1976*. U.S. Committee on Extension of the Standard Atmosphere (COSEA). Superintendent of Documents, U.S. Government Printing Office, Washington, D.C.

2002 NASA/ASEE SUMMER FACULTY FELLOWSHIP PROGRAM

JOHN F. KENNEDY SPACE CENTER
UNIVERSITY OF CENTRAL FLORIDA

THE ELECTRONIC NOSE TRAINING AUTOMATION DEVELOPMENT

Nathan Schattke
Research Associate
BCPS Department
Illinois Institute of Technology
Rebecca Young

ABSTRACT

The electronic nose is a method of using several sensors in conjunction to identify an unknown gas. Statistical analysis has shown that a large number of training exposures need to be performed in order to get a model that can be depended on. The number of training exposures needed is on the order of 1000.

Data acquisition from the noses are generally automatic and built in. The gas generation equipment consists of a Miller-Nelson (MN) flow/temperature/humidity controller and a Kin-Tek (KT) trace gas generator. This equipment has been controlled in the past by an old data acquisition and control system. The new system will use new control boards and an easy graphical user interface. The programming for this is in the LabVIEW G programming language. A language easy for the user to make modifications to.

This paper details some of the issues in selecting the components and programming the connections. It is not a primer on LabVIEW programming, a separate CD is being delivered with website files to teach that.

THE ELECTRONIC NOSE TRAINING AUTOMATION DEVELOPMENT

Nathan Schattke

Introduction

Training the electronic nose is a time consuming task. The statistically significant number of training exposures can run into the thousands. In order to get that many tests computer control of the gas generation equipment is required. The Chemical Instrumentation and Processes Lab in the Operations & Controls building at the Kennedy Space Center is an advanced laboratory for evaluating chemical sensors, especially those sensors relating to spaceport related gasses. The most important gas is Hydrazine, an excellent propellant but with a threshold limit value of 10 parts per billion in air. The equipment in the lab for creating a stream of this gas, and others, are several Kin-Tek Span Pac 361 automated gas standards generators. These produce a trace gas by mixing a minute flow of component vapor into a much larger flow of dilution gas.[1] Molecular permeation of vapor through a polymeric membrane is the controlling mechanism. That is, they use a small section of a porous plastic between a very high concentration sample and a gas stream. In order for this to be reproducible the permeation source must have a steady flow of gas across it and a steady temperature. To use the gas one needs to plumb a sample line from the outlet of the unit towards the sensor to be tested. The disadvantage of this is that the gas only comes from three sources, each of a specific concentration. Another piece of equipment in the lab helps to dilute those three concentrations down to a much wider concentration range. This second instrument is the Miller-Nelson Research inc. Flow-Temperature-Humidity control system HCS-301. This has analog control of pure air flow from 5 to 50 liters per minute, Temperature range of 20 to 55 C, and Relative Humidity of 5% or 20 to 90%. A precision mass flow controller, a heated water chamber and a dry heater achieve these parameters.

Training the electronic nose is a time consuming process. It must be trained with many different parameters including all the different gasses at different temperatures, concentrations, and humidity conditions. Previously the control for parts of this was performed with a combination of 15-year-old data acquisition and control and manual operation. This paper describes an implementation of National Instruments' LabVIEW to control these two instruments. Also, future improvements to the system are explained.

[1] Kin-Tek labs Operating Instructions

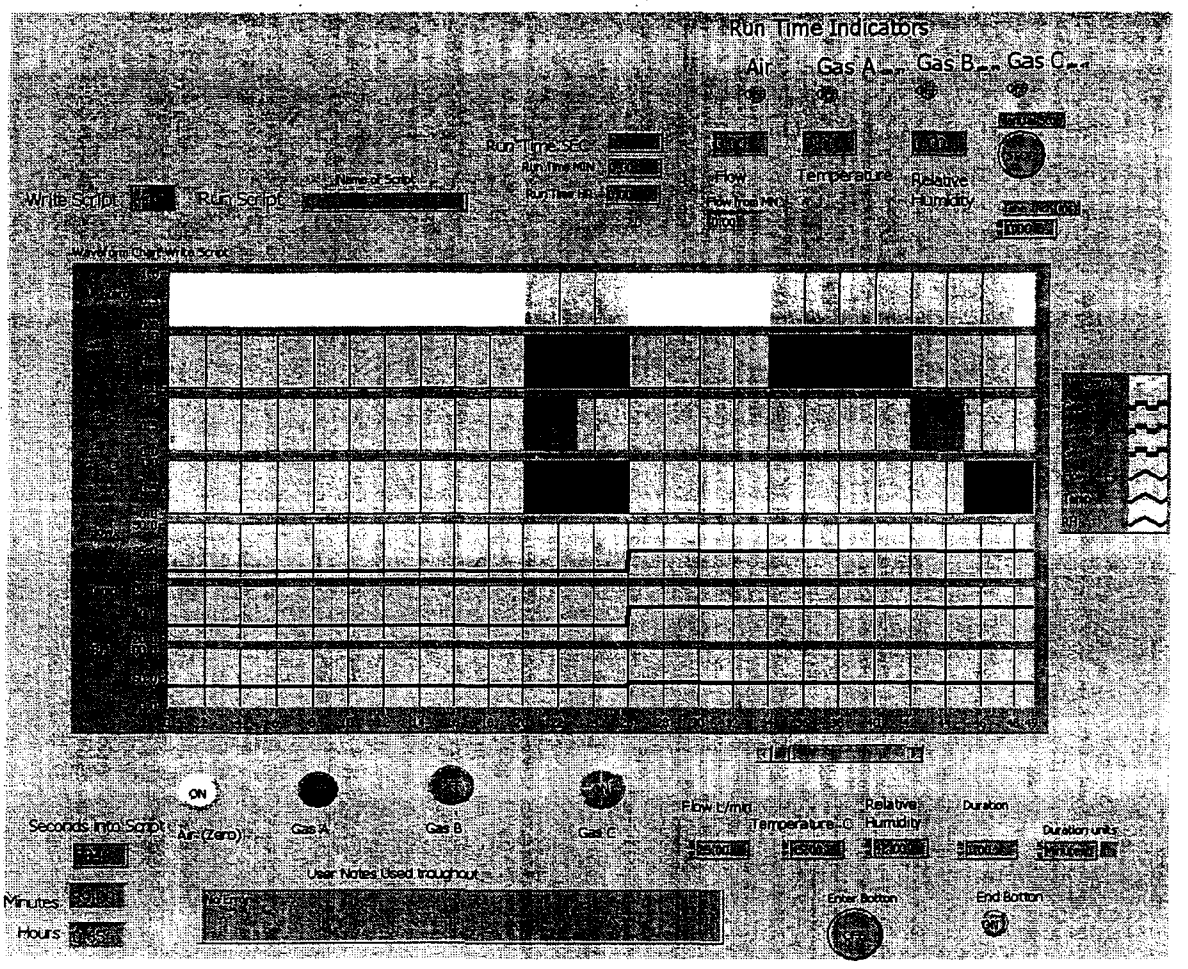

Use

The program is called "Read and Write.vi" in the "KinTek and MN Control folder", it must also have the library file in the same directory. The program is made to build scripts then run them. Choose the "Operate Value" tool, it looks like a hand with the index finger pointing up, from the tools palette. Use this to operate the slide switch in the top left corner of the front panel. The default position is write script, click on the right side to run a script. Start the program by pressing the run button in the lower left of the menu bar on top. The first thing you will be asked is the name and location of the file.

When writing the script, choose the settings for the next step. That is: what gasses will be used, what flow rate, temperature, relative humidity, duration, and duration units. If this is the last step in the script press the End button. Otherwise press the Enter button and continue to make changes after each step. When you are ready for the last step press the End button, then the Enter button twice. The file created is a text tab delimited file with the following columns: Time (starting at 0 sec), Zero/Air (0 or 1), Gas A, Gas B, Gas C, Flow (0-50 L/min), Temperature (0-55C), Relative Humidity (20-90%). There is no header or anything else in the file.

After the program stops, you can change to Run Script. In this case when you run the program with the arrow the computer will ask for a file to run. The progress of the run is shown in the text boxes in the upper right hand corner. I was unable to create a graph that would show this. Time is to the left in Seconds, Minutes and Hours. The LED type indicators light when the particular gas is on, the MN values are below those. A manual stop button is ready to end the program smoothly if a run needs to be aborted prematurely. The time increment button is set in milliseconds. It will almost never be touched, however, if you wished to use shorter files and run each step as minutes or hours you would use 60,000 or 3,600,000 respectively.

Run Script Diagram

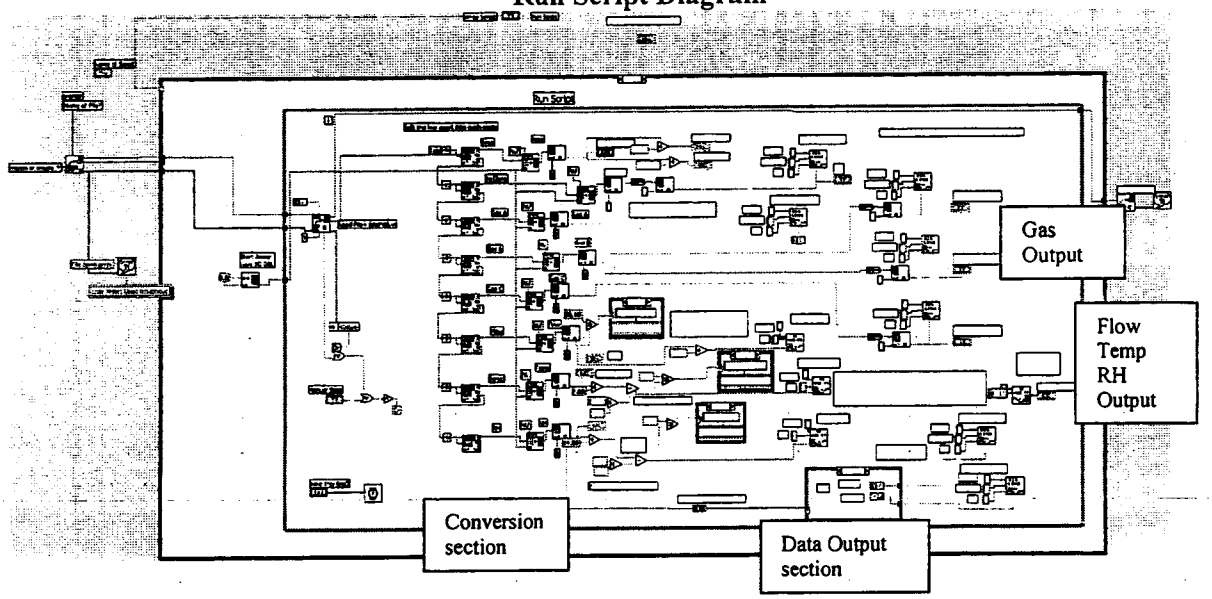

Write Script Diagram

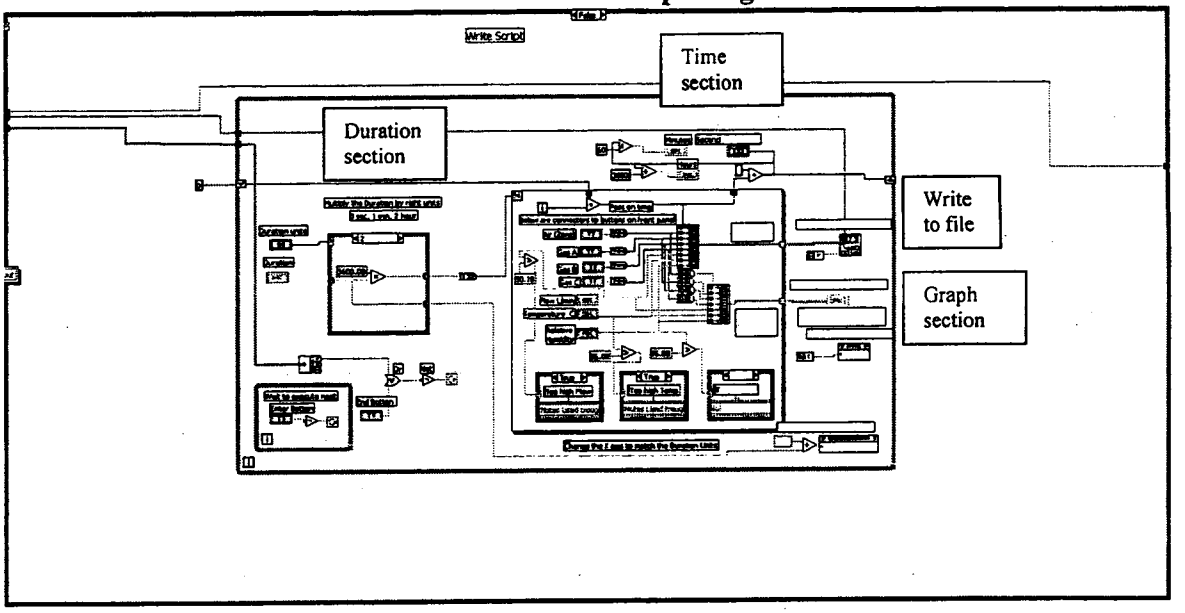

Logic Flow

The program is set up to do a few things then choose which condition to do as this run, either Read or Write. Within each of these cases the program operates on a one second per step basis, either reading or writing the values for the parameters.

The first logical split is whether this run of the program will be Read or Write. The program opens on old tab delimitated text file (Read) or creates a new file (Write).

For Read, also called Run Script, the file is read one line at a time using a While loop, each

iteration of the loop takes 1 second (controlled by the little watch in the lower left corner in the diagram).

A While loop.

The line is translated as follows. It is read as a script, this is split into before and after the tab symbol eight times, anything left after that in a line is ignored. Those sections of the script are each converted into double byte real number 1 dimensional arrays. The first (#0) byte of that is stripped off and translated into the appropriate type of number (Boolean, integer, or real). This number is finally presented to the DAQ system.

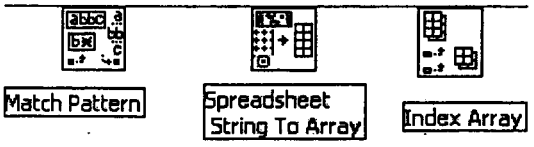

These blocks are used for this translation.

The data acquisition and control (DAQ) system control is performed in the program by the black and white square block with either "Dig Line" or "AO One Pt" written inside.

Digital out

Analog out

This is the heart of the program and deserves a bit of explanation. Besides the data feeding it there are three parameters: Device, Channel, and Line. Device can be found by running either NI-DAQ or "Measurement & Automation " programs in the National Instruments directory. When that program is run, the current DAQ boards in the computer are found and identified (you can even test them from this program). For all the outputs currently device 2 is used which is a National Instruments Co. NI 6711 (pn 777740-01). This is an Analog Output – 1 MS/S/Channel, 12-Bit, 4 Analog output channels. There are also 8 bits of digital data that can be either input or output. A line is the value of a singe bit of that word. We will use the analog controls to change the flow, temperature and relative humidity. We will use the digital controls to turn the gasses on and off and change all the relays.

A few more sections of the Read need to be explained. The relays for Zero/Air are controlled near the top. Relay A is always on; relay B is turned on when air is on, otherwise it is off. Both relays off control Standby but that is it is not desired. The relay control for the Wet/Split/Dry control is in the bottom right of the run script while loop. This is a conditional control with the relays set depending on the requested RH. The hardware is not ready for this yet. The relays inside the humidifier are 24 volts actuated and the highest these types of boards give is 10 volts.

The Writer Script section is easier. This section builds the file using iterations of a While loop with a nested For loop.

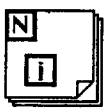

A For loop.

A Conditional structure

The choice of what state to have the buttons at, is done by the front panel controls. I'll explain about the front panel in the next paragraph. After the state of each part is chosen the Enter button is pressed on the front panel and the while loop iterates once. The duration units control a Conditional structure that multiplies the Duration by 1, 60 or 3600 for seconds, minutes, or hours respectively. This feeds the number of times to do the For loop to iterate and converts everything down to seconds. Within the For loop the blue line (integer) on top brings in the last time written and adds the current iteration number of

the For loop (0 to start). This value is the first of several numbers put into an array. For the Air and Gas buttons note that the boolean (green) values have been converted to integer (blue) and further down another part of that line has been converted to real (orange). This data is grouped together into two arrays. The top array is for writing the data file; the bottom is for the graph. The graph needs to be fed all real numbers but the writing file can take reals or integers but not booleans. The one-dimensional array forms a two-dimensional array at the border of the For loop by "indexing" (right click on the little box at the edge to activate). Outside the For loop the two-dimensional array is fed to a sub program called "write to spreadsheet file.vi". This converts all the values into their text equivalents with tabs separating all the numbers and an end of line symbol at the end. Then the while loop waits until the Enter button is pressed before doing it all again, giving you time to change any parameters on the front panel. The while loop ends when the End button is pressed. This part of the program is not performing as I would like and the while loop executes one more time because the Enter button is then pressed and then the false state ending command is given to the while loop end condition.

The front panel is the user interface. The "Diagram" is the program. For each element on the front panel a block is put in the diagram and wires of data are fed to it or come from it. The connection between the two can be found by: using the arrow tool, selecting the front or diagram part, right clicking and choosing "find terminal". The properties of the chart are controlled from the front panel, unless a "property node" is created in the diagram. These property nodes allow you to control or read parts of the graph from the diagram. In this program the X-axis scale is set with the duration units.

Hardware connections. The DAQ boards are plugged into the computer slots. Cables go from there to a connector block. The wires from the cables connect to certain pins on this connector block as defined in the drawing below. Device 1 is the 6023, device 2 is the 6711. The other end of the cable is plugged into the appropriate machine.

Opportunities for improvement

The graph for running the script was attempted. I tried to put a waveform chart within the while loop. This caused a fault in the program that shut the program down with a note to call National Instruments.

There must by a way to select portions of the write graph then copy and paste them. I was not able to find it. Also in the write section the ending switch needs to be more immediate, the file is written to one more time, this could cause problems. Perhaps one fix is to force the feed to N of the For loop to zero when the end button is pressed.

For both I would add more comments going to the front dialog box.

The relays for the MN wet/dry/split are 24 volt actuated. The LEDs for the KT zero/span/standby start at 53 volts. The rest of the controls for KT start at 3 volts. All these need relays to accurate. It would be more straightforward to have these in the machine than in an external relay system. The external system may be less expensive. Perhaps KT and MN could refurbish the machines to handle modern computer controls.

Outputs from the MN are available. There should be a way to use that and give a control saying change this parameter and wait until it stabilizes.

The control of the equipment becomes strange and wanders around when data is not being given to the instruments. A first fix would be to create a continuous loop with just inputs for the MN and KT values and outputs to those instruments. Run this program get things stable, then quickly shut it down and start the run script. A better fix would be the one mentioned above about waiting until stable. This may be related to not knowing the size of the array before hand.

It would be nice to wait until a user defined time of day to start.

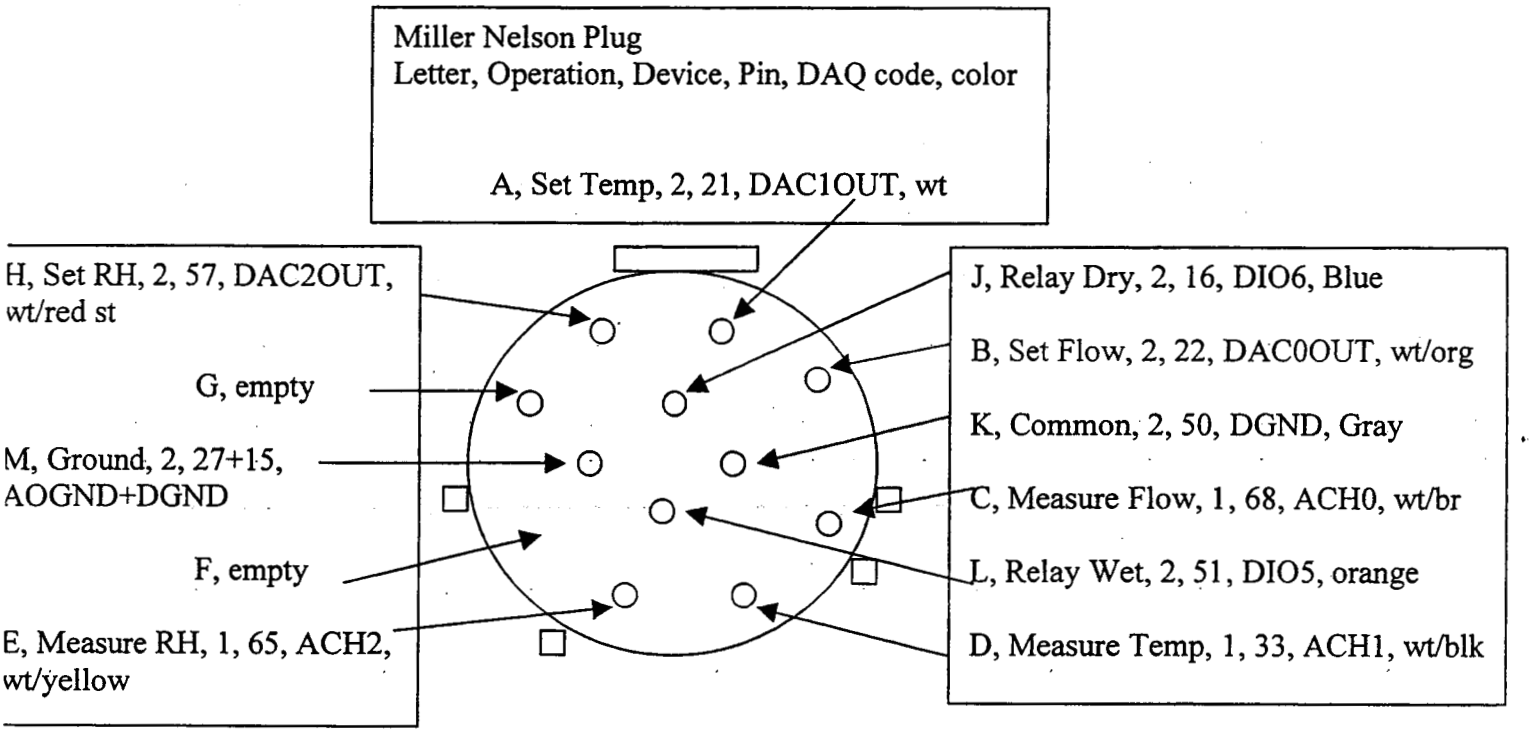
Miller Nelson Plug
Letter, Operation, Device, Pin, DAQ code, color
A, Set Temp, 2, 21, DAC1OUT, wt
H, Set RH, 2, 57, DAC2OUT, wt/red st
G, empty
M, Ground, 2, 27+15, AOGND+DGND
F, empty
E, Measure RH, 1, 65, ACH2, wt/yellow
J, Relay Dry, 2, 16, DIO6, Blue
B, Set Flow, 2, 22, DAC0OUT, wt/org
K, Common, 2, 50, DGND, Gray
C, Measure Flow, 1, 68, ACH0, wt/br
L, Relay Wet, 2, 51, DIO5, orange
D, Measure Temp, 1, 33, ACH1, wt/blk

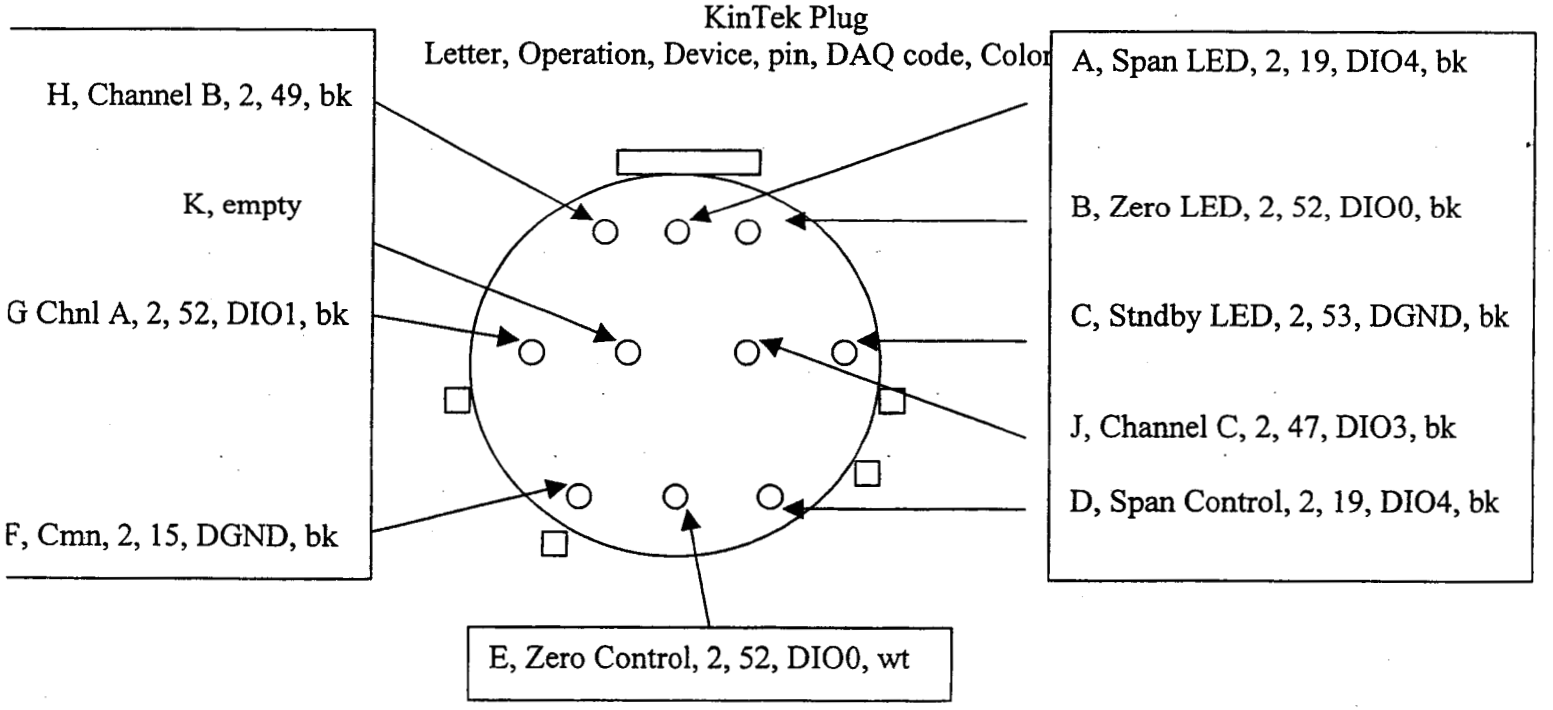
KinTek Plug
Letter, Operation, Device, pin, DAQ code, Color
H, Channel B, 2, 49, bk
K, empty
G Chnl A, 2, 52, DIO1, bk
F, Cmn, 2, 15, DGND, bk
A, Span LED, 2, 19, DIO4, bk
B, Zero LED, 2, 52, DIO0, bk
C, Stndby LED, 2, 53, DGND, bk
J, Channel C, 2, 47, DIO3, bk
D, Span Control, 2, 19, DIO4, bk
E, Zero Control, 2, 52, DIO0, wt

2002 NASA/ASEE SUMMER FACULTY FELLOWSHIP PROGRAM

JOHN F. KENNEDY SPACE CENTER
UNIVERSITY OF CENTRAL FLORIDA

AN INVESTIGATION OF THE REVERSE WATER GAS SHIFT PROCESS AND OPERATING ALTERNATIVES

Dr. Jonathan E. Whitlow
Associate Professor
Department of Chemical Engineering
Florida Institute of Technology
NASA COLLEAGUE: Clyde Parrish

ABSTRACT

The Reverse Water Gas Shift (RWGS) process can produce water and ultimately oxygen through electrolysis. This technology is being investigated for possible use in the exploration of Mars as well as a potential process to aid in the regeneration of oxygen from carbon dioxide. The initial part of this report summarizes the results obtained from operation of the RWGS process at Kenned y Space Center during May and June of this year. It has been demonstrated that close to complete conversion can be achieved with the RWGS process under certain operating conditions. The report also presents results obtained through simulation for an alternative staged configuration for RWGS which eliminates the recycle compressor. This configuration looks promising and hence seems worthy of experimental investigation.

1. INTRODUCTION

The human exploration of Mars will require the utilization of resources present in the Martian environment in order to minimize the payload mass imported from Earth. Reverse Water Gas Shift (RWGS), which reacts carbon dioxide and hydrogen to form water and carbon monoxide, when coupled with water electrolysis is a candidate technology for oxygen production on Mars. The use of the RWGS process for In-Situ Resource Utilization, (ISRU) was originally studied by Pioneer Astronautics, who determined the RWGS process to be a viable candidate for oxygen production. [1-2]

An RWGS system has been operated at Kennedy Space Center (KSC) on an intermittent basis over the past 15 months. Although the operating time has been limited, several conclusions on the RWGS operation have been made and problem areas identified as discussed in this report. An overview of the process components for RWGS is given below followed by a discussion of the results obtained from operation of the system. This report also includes a description of an alterative RWGS configuration, which is being presented in this report for the first time. An evaluation of this new configuration is also included along with a discussion of the modeling equations used to simulate the system.

2. AN OVERVIEW OF THE EXISTING REVERSE WATER GAS SHIFT PROCESS

RWGS uses carbon dioxide and hydrogen as reactants to produce oxygen and carbon monoxide with a copper on alumina catalyst. Prior to operating the RWGS system the copper catalyst, which s produced from copper oxide reduction, must be conditioned to insure no oxygen is present in the system. Operating temperatures for processes on Mars are constrained and in general designs are not being considered which exceed 500 Celsius. At such temperatures, the RWGS reaction equilibrium is limited and does not favor the production of water. Thus in order to improve the overall conversion a separation step is required to allow the non reacted hydrogen and n dioxide to be recycled. This is achieved by passing the exit gases to a condenser to remove most of the water and then to a hollow fiber polymeric membrane, which preferentially permeates hydrogen and carbon dioxide. From the membrane, the reactants can be recycled while the byproduct carbon monoxide can be vented. The water produced is stored in a vessel and used as feed to an electrolysis unit, which produces oxygen as product and hydrogen, which can also be recycled to the reaction process. A simple RWGS process flow schematic is presented in Figure 1 below.

As stated above the RWGS process has been operated on an intermittent basis over the last 15 months. One of the largest problems in performing an analysis of the process has been associated with the composition analysis using the gas chromatograph (GC). The GC used for the process also is used in other laboratory projects and hence scheduling conflicts exist. In addition, the column has required frequent recalibration and in some cases changes in the methods used to perform the analysis (eg retention time and temperature ramp slope). As a result many days the system has been operated in which a lack of composition data exists.

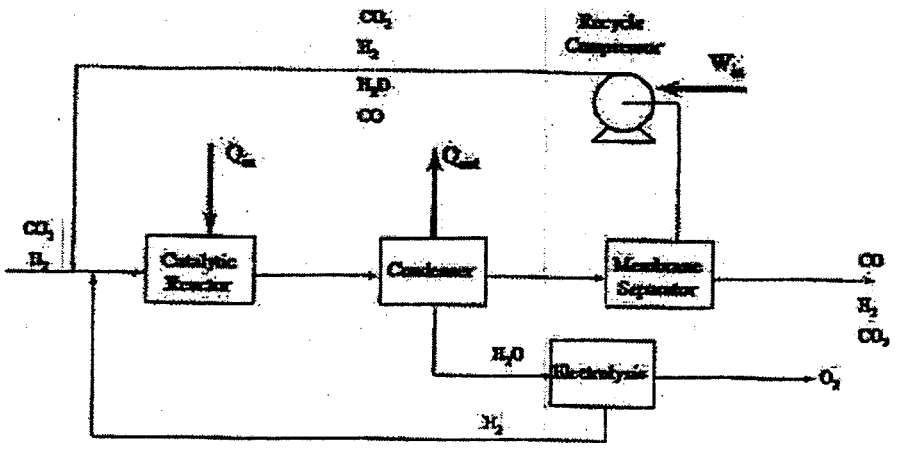

Figure 1 Current RWGS Process Flow Diagram

A summary of the operational data which has included an analysis of the discharge from the process is shown below in Tables 1 and 2. Table 1 is a summary of single pass operations while Table 2 gives the results from operating with the use of a recycle compressor. Both tables include data taken from the first few weeks of the summer but also some taken in February of this year. It can be observed from Table 1 that in February the single pass data showed in general an approach to theoretical equilibrium (calculated from equations 1 & 2) of greater than 90%. The data taken in May did not show the same approach to equilibrium and hence additional data is needed. Due to the operational problems associated with the GC as discussed above, it is likely that the May data is invalid. The data in Table 2 shows that under conditions of low feed rate (0.5 slpm H_2 & CO_2) and the recycle valve being 0% closed (ie 100% open) that essentially complete conversion can be achieved. More operating data is needed and will be collected with subsequent operation of the RWGS system over the next several months.

3. STAGED RWGS PROCESS MODELING

In the current RWGS configuration, the recycle compressor is used to push the equilibrium constrained reaction toward completion by recycling the un-reacted H_2 and CO_2 multiple times with the aid of the separation membrane. The compressor is a component in the system which is costly in terms of both mass and energy. In addition, the mechanical nature of the component brings in to question reliability and the need for redundancy for actual flight. If this component could be eliminated without sacrificing the goal of the system which includes conversion of hydrogen with minimal loss in the reject, it would be a substantial process improvement. Figure 2 shows a staged configuration with no recycle stream that has been evaluated with simulation as a part of this work. Each stage of the alternative RWGS Process consists of a series of three components namely a reactor, condenser and membrane. The idea is to take the reaction products and with the condenser remove most of the water and then with the membrane reject the CO thus leaving reactant CO_2 and H_2 permeate to serve as feed to the next reactor stage.

Table 1 Analysis of Single Pass RWGS Operation

Date	H2 Flow slpm	CO2 Flow slpm	Temp Celsius	Pressure psia	Actual CO2 Conversion	Theoretical Conversion	Equilibrium Approach
2/22/2002	0.5	0.5	400	45	20.82	22.71	0.917
2/15/2002	0.5	0.5	400	45	20.30	22.71	0.894
2/22/2002	1.0	1.0	400	45	22.05	22.71	0.971
2/22/2002	3.0	3.0	400	45	19.98	22.71	0.880
2/15/2002	3.0	3.0	400	45	19.54	22.71	0.861
2/20/2002	1.0	2.0	400	45	15.00	15.77	0.951
2/22/2002	2.0	1.0	400	45	30.21	31.55	0.958
2/20/2002	1.0	1.0	350	45	16.94	18.24	0.929
2/20/2002	1.0	1.0	375	45	19.82	20.47	0.968
2/25/2002	1.0	1.0	425	45	23.68	24.91	0.951
2/25/2002	1.0	1.0	450	45	24.71	27.08	0.913
2/26/2002	1.0	1.0	400	19	22.16	22.71	0.976
2/26/2002	1.0	1.0	400	30	22.33	22.71	0.984
5/28/2002	3.0	1.0	400	45	29.03	37.59	0.772
5/29/2002	1.0	1.0	400	45	17.84	22.71	0.786
5/29/2002	2.0	2.0	400	45	16.89	22.71	0.744
5/30/2002	0.5	0.5	400	45	17.272	22.71	0.761
5/30/2002	1.2	1.2	400	45	17.52	22.71	0.772

Table 2 Analysis of RWGS Recycle Operation

Date	H2 Flow slpm	CO2 Flow slpm	Temp Celsius	Pressure psia	CO2 Conversion	Recycle Valve
2/21/2002	1.0	1.0	400	45	52.52	(100% closed)
2/21/2002	1.0	1.0	400	45	63.31	(66% closed)
2/21/2002	1.0	1.0	400	45	95.81	(33% closed)
2/21/2002	1.0	1.0	400	45	99.05	(0% closed)
2/27/2002	0.5	0.5	400	45	66.63	(100% closed)
2/27/2002	0.5	0.5	400	45	99.98	(0% closed)
6/3/2002	1.0	1.0	400	45	45.87	(100% closed)
6/4/2002	1.0	1.0	400	45	98.48	(0% closed)
6/5/2002	0.5	0.5	400	45	99.37	(0% closed)
6/7/2002	0.5	0.5	400	45	99.99	(0% closed)
6/10/2002	1.5	1.5	400	45	82.92	(0% closed)

A brief description of the equations used to model the RWGS system is provided in this section. A more detailed description of the modeling equations and associated theory can be found in the 1999 NASA/ASEE Summer Faculty Program Research Report [3]. While the basic modeling equations are the same as in the 1999 report some modifications to the membrane model have been made and are discussed below.

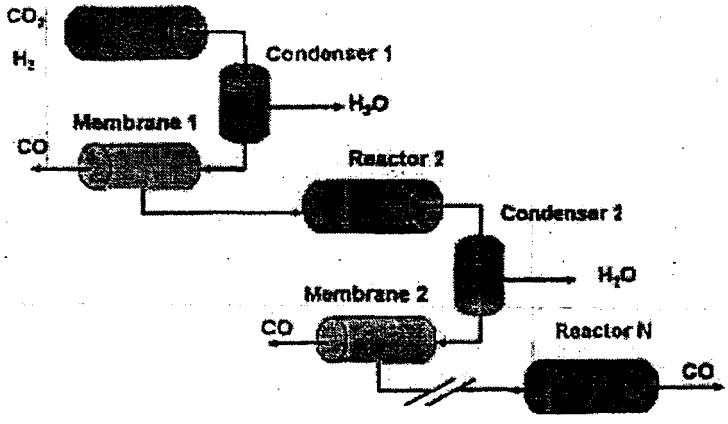

Figure 2 Alternative Staged RWGS Process Flow Diagram

The chemical equilibrium constant K for the reaction is given as a function of temperature by the expression: [4]

$$K = e^{13.148\frac{5639.5}{T}\ 1.077\ \ln T\ 5.44\times10^{-4}T + 1.125\times10^{-7}T^2 + \frac{49170}{T^2}} \qquad (1)$$

The equilibrium constant is also written in terms of product and reactant concentrations which subsequently can be expressed in terms of conversion of the limiting reactant hydrogen by the expression:

$$K = \frac{[CO][H_2O]}{[CO_2][H_2]} = \frac{(\Theta_{CO} + x_{eq})(\Theta_{H_2O} + x_{eq})}{(\Theta_{CO_2} - x_{eq})(1 - x_{eq})} \qquad (2)$$

The values of Θ_{CO}, Θ_{H2O}, Θ_{CO2} represent the molar ratios of those components to the limiting reactant hydrogen in the inlet to the reactor. Given a reaction temperature, the value of K can be determined from equation 1 and the equilibrium conversion, x_{eq} determined by solving equation 2. The equilibrium conversion is the maximum conversion, which can be achieved, in a single pass through the reactor. For the simulation models it is assumed that equilibrium is reached for simplicity. The experimental results given in Table 1 have shown the single pass approach to equilibrium to be in the range between 86 and 97 % depending on the total feed flow rate. While it may not be feasible to reach total equilibrium in practice, proper design of the reactor bed should allow the system to come close based on the experimental findings.

The exit gases from the reactor are sent to a condenser where most of the water is removed. For modeling purposes, the compositions of the liquid and vapor streams leaving the condenser are determined by employing Raoult's Law to determine the amount of water in the vapor phase and Henry's Law to determine the solubility and hence concentration of the gasses dissolved in the condensed phase.

The gases leaving the condenser are fed into a hollow fiber polymeric membrane which separates the components of a gas mixture based on a given components permeability to the polymer. The membrane operates in a countercurrent fashion, and is modeled based on a 1998 publication, [5] which depicts the membrane as an N stage process as shown in Figure 3. Here, $L_{,k}$ and $x_{j,k}$ are the total molar flow and mole fraction of component j in the feed/reject leaving stage k, while $V_{,k}$ and $y_{j,k}$ are the total molar flow and mole fraction of j in the permeate leaving stage k. For each stage the mass transferred of a component j on a given stage $m_{j,k}$ is given by the permeability coefficient of that component times the difference in partial pressures in component j across the membrane. For N stages, a system of N nonlinear simultaneous equations is yielded for each component j requiring an iterative solution.

The permeability coefficients in the membrane model for each component (excluding water) were refined based on a set of RWGS operating data from July 18,2001. [6] Although the actual dimensions and data associated with the membrane are unknown and proprietary, the permeability coefficients were forced to fit the data and hence the values used have good predictive capabilities.

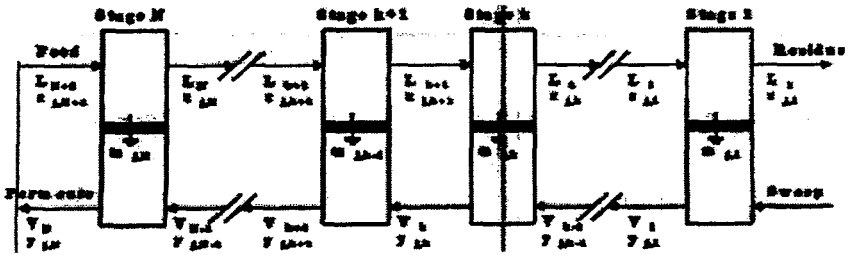

Figure 3 Flow Diagram for an N Stage Counter-Current Membrane

The membrane model has been modified from the model used in previous work to allow the introduction of a sweep stream into the system as shown in Figure 3. In addition the pressure drop across stage k on the permeate side of the membrane has been accounted for by using the Hagen-Poiseuille equation for laminar flow of an incompressible fluid in an impermeable tube:

$$\Delta P_k = \frac{8\mu_{mix} V_k R T \Delta z}{\Pi R_i^4 P_{Vk}} \qquad (3)$$

Here μ_{mix} is the viscosity of the gas mixture, Δz is the length of the fibers for the given stage, Ri is the inner radius of the fibers, V_k is the permeate flow on stage k, R is the universal gas constant, T is the absolute temperature and P_{Vk} is the permeate pressure on stage k.

4. SIMULATION RESULTS AND DISCUSSION

For a given stage there are many variables which affect the operation and hence the simulation results These variables include reaction temperature, condenser temperature, pressure drop across the membrane, absolute pressure in the membrane, membrane area, CO_2 and H_2 feed rates, CO_2 to H_2 ratio and sweep flow rate. Since each of these can be altered in each subsequent stage the task of finding optimum operating conditions is difficult at best. After multiple simulation runs a base case was determined which gave good results in terms of overall H_2 utilization and conversion as well as met the hypothetical design constraints for the system in terms of limiting operating pressure and number of overall stages. The base case which is presented in Table 3 was used to evaluate the sensitivity of the overall H_2 conversion to the system variables listed above. As can be observed from the base case results an overall H_2 conversion including loss in the membrane reject, equal to 99.5% can be achieved in only 5 stages. An inlet pressure

of only 80 psia is needed for a 6 stage configuration to achieve a 99.8% conversion of H_2.

By performing additional simulations and comparing them to the base case the following information was obtained. The overall H_2 conversion increases with increasing reaction temperature as expected however increasing the temperature above the base case value of 400 C gives limited improvement as shown in Figure 4. This is significant in that it may be possible to use a single heating zone and temperature controller for all reactors with appropriate geometrical configuration with limited consequences. Increasing the condenser temperature above 5 C decreases the overall conversion as expected but it is not until values greater than 40 C are used that a substantial drop in conversion is seen leading to the conclusion that a single condensation zone may be employed for all stages with again, a single temperature control point. It also indicates that the condensers may be able to operate at temperatures higher than originally believed thus resulting in energy savings.

The introduction of a CO_2 sweep into the permeate side of the membrane had the greatest positive effect on the simulations in terms of increasing the conversion while both reducing stages and system pressure requirements. It can be seen in Figure 5 that as the flow of sweep increases the overall conversion generally increases, however an optimum is reached near the base flow rate of 3 slpm. Another variable observed to have a significant optimum is the ratio of CO_2 to H_2 in the initial feed as shown in Figure 6.

Table 3 Base Case for Six Stage RWGS Alternative Configuration

	Stage 1	Stage 2	Stage 3	Stage 4	Stage 5	Stage 6	Exit
Reactor Temperature (C)	400	400	400	400	400	400	
Condenser Temperature (C)	5	5	5	5	5	5	
Reactor Pressure (psia)	80	64	48	32	20	12	
Membrane Delta P (psia)	16	16	16	12	8	8	
Permeate Delta P (psia)	0.15	0.21	0.36	0.70	1.31	3.28	
Membrane Area (m^2)	27	27	27	27	27	27	
Permeate CO2 Sweep (slpm)	3	3	3	3	3	3	
H2 Reactor Feed (slpm)	4	2.50	1.38	0.60	0.16	0.01	0.00
CO2 Reactor Feed (slpm)	12.00	13.24	14.87	16.83	19.01	21.21	23.27
CO Reactor Feed (slpm)	0.000	0.147	0.101	0.053	0.012	0.002	0.000
H2 in Reject (slpm)	0.00006	0.00007	0.00013	0.00358	0.00212	0.00008	
CO in Reject (slpm)	1.35638	1.15943	0.83380	0.47623	0.15234	0.01543	
Reactor H2 Conversion	37.59	44.60	56.81	72.97	89.87	98.21	
Overall H2 Conversion	37.44	65.28	84.92	95.90	99.50	99.84	

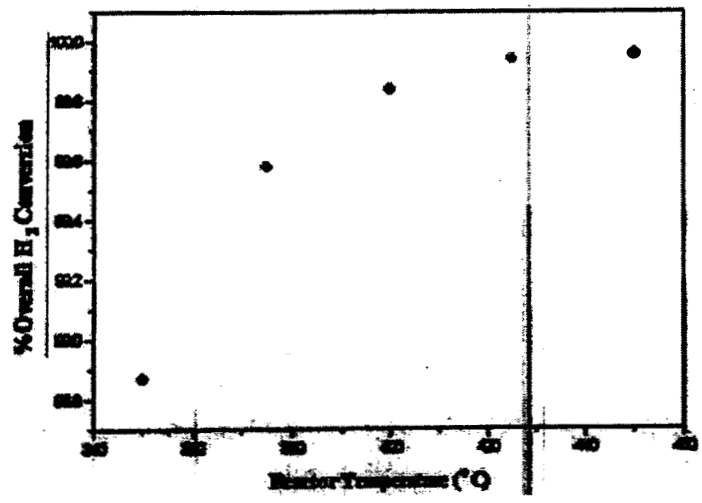

Figure 4 Simulation Results for Overall H_2 Conversion versus Reaction Temperature

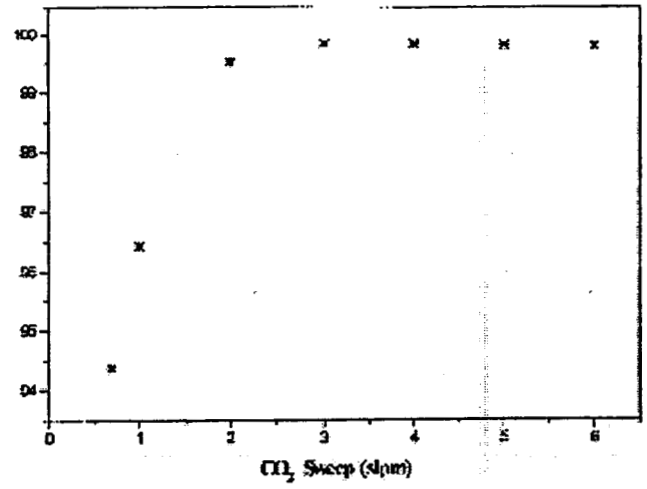

Figure 5 Simulation Results for Overall H_2 Conversion versus CO_2 Sweep

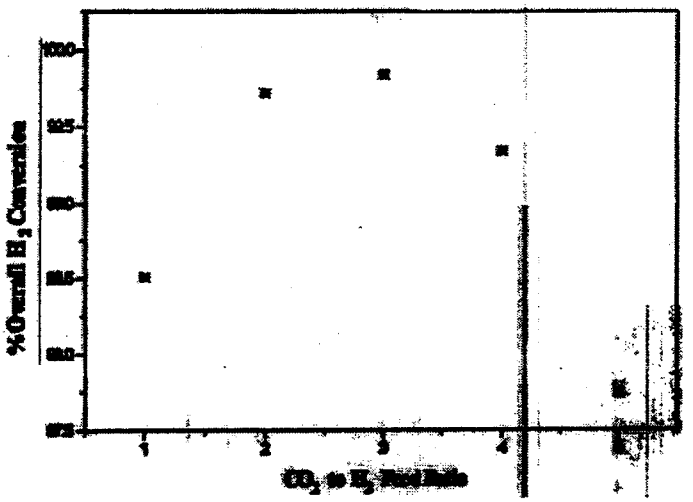

Figure 6 Simulation Results for Overall H_2 Conversion versus Feed Ratios

Although additional figures could not be included due to space limitations, it was also found that an optimum exists in the membrane area used close to the value used in the base case simulations. It was also found that as membrane pressure drop is reduced to a fractional value of 0.8 to 0.9 of the values used for each stage in the base case an optimum is found. If this was done the overall system pressure could be reduced even further.

While the simulation results have shown that using the alternative staged configuration of RWGS has much promise, experimental verification is needed. Hopefully additional funds will be obtained to perform the experimental work and validate the modeling results.

4. REFERENCES

[1] Zubrin R., Kito, T. and B. Frankie, "Report on the Construction of a Mars Methanol In- Situ Propellant Production Unit", NASA Contract NAS9-97082, Sept., 1997.
[2] Frankie, B. and R. Zubrin, "Mars Reverse Water Gas Shift Unit Design Manual", Delivered to Dynacs Engineering and The Embedded Technology Development Group, June30, 1999.
[3] Whitlow, J.E., "Modeling and Analysis of the Reverse Water Gas Shift Process for In-Situ Propellant Production", NASA/ASEE Summer Faculty Program Research Report, NASA CR-1999-208586, 1999.
[4] Bissett, L. "Equilibrium Constants for Shift Reactions", Chemical Engineering, October 24,1977.
[5] Coker, D.T. , Freeman, B.D. and G.K. Fleming, "Modeling Multicomponent Gas Separation Using Hollow-Fiber Membrane Contactors, AICHE Journal, V. 44 , N 6, June - 1998.
[6] Whitlow, J .E., "Operation, Modeling and Analysis of the Reverse Water Gas Shift Process for In-Situ Propellant Production", NASA/ASEE Summer Faculty Program Research Report, NASA CR-2001-210265, 2001.

REPORT DOCUMENTATION PAGE

Form Approved
OMB No. 0704-0188

1. AGENCY USE ONLY (Leave blank)	2. REPORT DATE	3. REPORT TYPE AND DATES COVERED
	December 2002	Contractor Report - Summer 2002

4. TITLE AND SUBTITLE

2002 Research Reports
NASA/ASEE Summer Faculty Fellowship Program

5. FUNDING NUMBERS

NASA Grant
NAG10-315

6. AUTHOR(S)

See attached list

7. PERFORMING ORGANIZATION NAME(S) AND ADDRESS(ES)

University of Central Florida
Orlando, Florida 32816-2450
John F. Kennedy Space Center
Kennedy Space Center, Florida 32899

8. PERFORMING ORGANIZATION REPORT NUMBER

NASA CR-2002-211181

9. SPONSORING/MONITORING AGENCY NAME(S) AND ADDRESS(ES)

National Aeronautics and Space Administration
Washington, D.C. 20546

10. SPONSORING/MONITORING AGENCY REPORT NUMBER

11. SUPPLEMENTARY NOTES

12a. DISTRIBUTION/AVAILABILITY STATEMENT

Unclassified - Unlimited
Subject Category 99

12b. DISTRIBUTION CODE

13. ABSTRACT *(Maximum 200 words)*

This document is a collection of technical reports on research conducted by the participants in the 2002 NASA/ASEE Faculty Fellowship Program at the John F. Kennedy Space Center (KSC). This was the 18th year that a NASA/ASEE program has been conducted at KSC. The 2002 program was administered by the University of Central Florida (UCF) in cooperation with KSC. The program was operated under the auspices of the American Society for Engineering Education (ASEE) and the Education Division, NASA Headquarters, Washington, D.C. The KSC Program was one of nine such Aeronautics and Space Research Programs funded by NASA Headquarters in 2002. The KSC Faculty Fellows spent ten weeks working with NASA scientists and engineers on research of mutual interest to the university faculty member and the NASA colleague. The editors of this document were responsible for selecting appropriately qualified faculty to address some of the many research areas of current interest to NASA/KSC. The NASA/ASEE program is intended to be a two-year program to allow in-depth research by the university faculty member.

14. SUBJECT TERMS	15. NUMBER OF PAGES
Research and Technology	165
	16. PRICE CODE

17. SECURITY CLASSIFICATION OF REPORT	18. SECURITY CLASSIFICATION OF THIS PAGE	19. SECURITY CLASSIFICATION OF ABSTRACT	20. LIMITATION OF ABSTRACT
Unclassified	Unclassified	Unclassified	UL